University of Leeds

School of Civil Engineering

Behaviour of Long Span Composite Beams with Precast Hollow-Core Slabs

By

Ali Murad

BEng MSc

Submitted in accordance with the requirements for the degree of

Doctor of Philosophy

November 2007

The candidate confirms that the work submitted is his own and that appropriate credit has been given where reference has been made to the work of others

Acknowledgements

I would like to thank my supervisors, Dr. Dennis Lam and Dr. Jianqiao Ye, for their guidance and support throughout the course of this research.

I would also like to acknowledge the technical staff in the School of Civil Engineering for their expertise during experimental work. Assistance from all other staff in the Department is also acknowledged.

Thanks are due to Bison Concrete Limited for providing the hollow-core slabs and Fabsec Ltd for providing the steel sections.

Thanks to my family and friends for their support during this time of study and also thanks Hoare Lea Fire Group for allowing time off to conduct this research.

Abstract

The use of precast hollow-core concrete slabs with Fabsec steel beams in composite construction has had little research conducted in this area. The main purpose of the research is to develop an understanding into the behaviour of this form of construction and to demonstrate the advantages of using Fabsec beams with precast hollow-core concrete slabs.

To achieve this, five full scale bending tests were carried out supplemented by horizontal push tests. In addition to the experimental work described, an analytical study is conducted and design recommendations are made. The main issues were the compression behaviour of the hollow-core slabs and the transfer of the horizontal shear forces between the steel beam and the concrete slab.

The aim of the research is to investigate the performance of composite beams with the position of the neutral axis in the concrete and also establish the effective width. By varying the beam size, span of beam, shear connection and slab depth in five full-scale experiments, the behaviour of the composite beam will be established.

Contents

Chapter 4: Test Results and Discussion

Chapter 5: Analytical Study

Chapter 6: Design of Composite Beam

Chapter 7: Conclusions and Future Work

List of Figures

Chapter 3

Chapter 4

List of Tables

Notations

A_s	Cross-sectional area of steel
a_o	width of opening
B_{eff}	Effective width
b_r	Half the transverse spans of slab on the right of the steel beam
b_l	Half the transverse spans of slab on the left of the steel beam
C	Compression
CB	Composite beam
CC	Concrete crushing
D	Beam depth
D_o	Diameter of web openings
D_s	Slab depth
d	Depth of concrete from neutral axis
d_c	Distance from concrete force to neutral axis
d_{bf}	Distance from bottom flange force to neutral axis
d_{bw}	Distance from bottom web force to neutral axis
d_{tf}	Distance from top flange force to neutral axis
d_{tw}	Distance from top web force to neutral axis
E_s	Modulus of elasticity of steel
e	Eccentricity
F	Shear force
FSC	Full shear connection
F_c	Force in concrete
F_s	Force in steel
F_{bf}	Force in bottom flange

F_{bw}	Force in bottom web
F_{tf}	Force in top flange
F_{tw}	Force in top web
F_{con}	Force in shear connection
F_{twc}	Force in top web in compression
F_{twt}	Force in top web in tension
F_{yr}	Reduced axial stress within web
f_{cu}	Strength of concrete
f_t'	Effective tensile strength
F_{flange}	Force in steel flange
g	Gap between ends of precast slabs
HCU	Hollow-core unit
h_o	Height of opening
I	Second moment of area of the combined section
I_{com}	Second moment of area of the composite section
k	Shear connector modulus
L	Span of beam
LVDT	Linear variable displacement transformer
M	Moment
M_{comp}	Composite moment
M_m	Maximum moment
M_n	Nominal moment
M_p	Bending moment capacity without opening
n	Number of shear connector in half span
P	Point load

PSC	Partial shear connection
PT	Push test
P_b	Axial force in bottom tee
P_c	Axial force in concrete
P_t	Axial force in top tee
S	Distance between web openings
SC	Shear connection
SF	Stud failure
SG	Strain Gauge
s	Reinforcement bar spacing
T	Tension
T16	16mm diameter transverse reinforcing bars
t_s	Thickness of slab
V	Shear force acting on opening
V_m	Maximum shear capacity
V_n	Nominal shear capacity
Z	Elastic section modulus
z	Distance between points about which secondary bending moments are calculated
β	gap width factor and is given as 0.5
δ	Deflection of beam
σ_{max}	Maximum stress
ϕ	Effective tensile strength
ω	Transverse joint factor
τ	Web shear stress

Chapter 1

Introduction

Chapter 1: Introduction

1.1 Background

Composite beams with web openings are frequently used these days in multi-storey buildings. Designers of multi-storey buildings are often faced with height limitations imposed by zoning, economic requirements, aesthetics, or the need to match floor heights of existing buildings. The use of web openings in composite steel members is a powerful tool for obtaining shallow floor systems that can be used to reduce storey heights (Darwin and Donahey 1986). Web openings in steel members are useful for passing utilities (sprinkler pipes and air-conditioning ducts etc.) through, and also the reduction in building height can provide major cost savings.

Fabsec beams are steel I-sections with web openings, but they are fabricated differently to cellular beams. They are fabricated by automatic welding of profiled steel plates used to form the flanges and web of the section, i.e. the web of the beam has the openings cut into it, and then the flanges are welded to the web to make the I-section. Figure 1.1 shows a multi-storey steel frame structure using Fabsec beams.

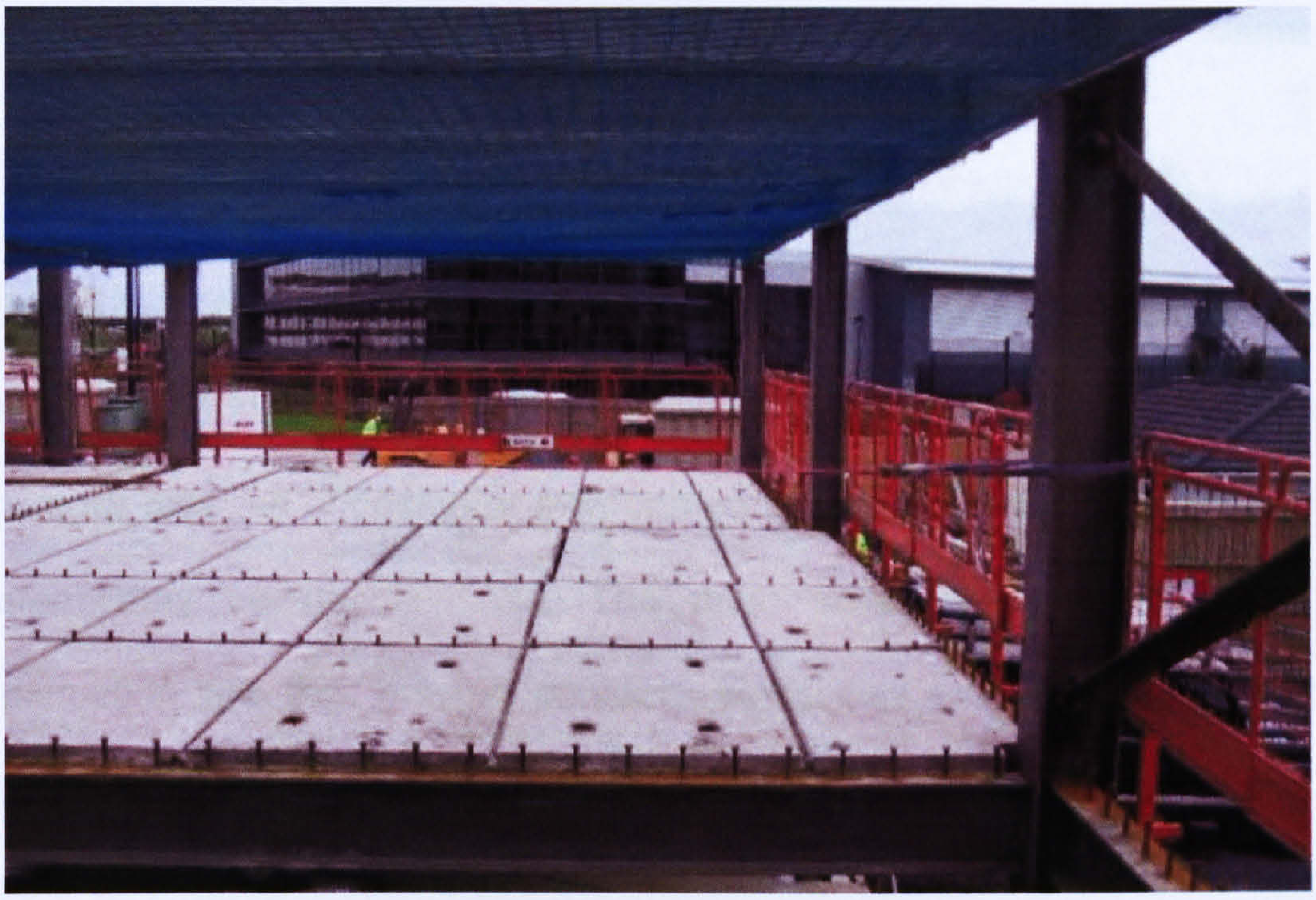

Figure 1.1: Multi-Storey building using Fabsec Beams

The benefits of using Fabsec beams for long span construction are:

- Savings in cladding costs, when the floor to floor height is reduced.
- Reduction in the number and total weight of steel columns and their foundations.
- Greater usable area of space, due to fewer (or no) internal columns.
- Fewer steel elements leading to faster speed of erection of the primary structure.

The success of Fabsec beams in the commercial building sector is implicitly related to the notion that long span construction in buildings leads to greater use of internal space, to facility for service integration, and to ease of future adaptability. All these benefits are part of the philosophy of 'sustainable' construction (Fabsec Limited 2002).

Composite construction using hollow-core slabs is intended to complement the now traditional steel frame/steel decking method and to offer advantages where for reasons of design or environmental considerations a steel decking system may be unacceptable. The main advantages of this form of construction are that precast concrete slabs can span up to 15 metres without propping. The erection of 1.2 metre wide precast concrete units is simple and quick. Shear studs are pre-welded on the steel beams before delivery to site, thereby offering additional savings associated with shorter construction times. Because no return is received from money invested in the construction of a multi-storey building until the building is occupied, the loss of income from capital may be 10% of the total cost of the building for a construction time of two years, which is about one-third of the cost of the structure (Lam 1998).

Although tests have been conducted in the past with cellular and castellated steel beams, no experimental tests have been conducted using Fabsec steel beams with web openings together with precast hollow-core concrete slabs. An experimental program is to be setup using five Fabsec beams spanning between 9m and 12m with varying shear connection and depth for the hollow-core slab. An analytical study is conducted and design requirements will be established.

1.2 Objectives of Research

The use of precast hollow-core concrete slabs with Fabsec steel beams in composite construction has had little research conducted in this area. The main purpose of the research is to develop an understanding into the behaviour of this form of construction and to demonstrate the advantages of using Fabsec beams with precast hollow-core concrete slabs. The objectives of the research are:

1. To study the interaction between the hollow-core concrete slabs and Fabsec steel beam with the neutral axis in the concrete slab.
2. To establish the effective width of such composite beams.
3. To propose design recommendations for Fabsec beams with precast hollow-core concrete slab.

1.3 Scope of Thesis

The scope of this research is to study the behaviour of long span composite beams with precast hollow-core slabs. To achieve this, five full scale bending tests were carried out supplemented by horizontal push tests. In addition to the experimental work described, an analytical study is conducted and design recommendations are made. The main issues were the compression behaviour of the hollow-core slabs and the transfer of the horizontal shear forces between the steel beam and the concrete slab.

Chapter 2 presents a literature review of work related to composite beams with solid and metal decking construction, also presented is a review of current work on composite beams with hollow-core slabs. Full scale tests are reported in Chapters 3 and 4. Chapter 3 covers the beam specimen design and test set up and Chapter 4 contains the test results and discussion. In Chapter 5 an analytical study is conducted, from the study a comparison with design calculations is made in Chapter 6. Finally conclusions and recommendations are given in Chapter 7.

Chapter 2

Literature Review

Chapter 2: Literature Review

2.1 Introduction

Composite beams with web openings are frequently used these days in multi-storey buildings. Experimental and analytical research has been conducted into web openings in steel beams, but limited effort has been made to investigate the behaviour of composite beams with precast hollow-core slabs.

In this chapter, a literature review on composite beams with web openings is presented covering the following topics:

- Steel-Concrete Composite Beams
- Shear Connection of Composite Beams
- Effective Width of Composite Beams
- Steel Beams with Web Openings
- Behaviour of Steel Beams with Web Openings
- Composite Beams with Precast Concrete Hollow-Core Slabs

2.2 Steel-Concrete Composite Beams

Composite steel-concrete structures are widely used in modern day building construction. A composite member is formed when a steel component, an I-section beam is attached to a concrete component, such as a floor slab. Shown in Figure 2.1, is a composite beam, the high compression strength of the concrete compliments the high strength of the steel in tension.

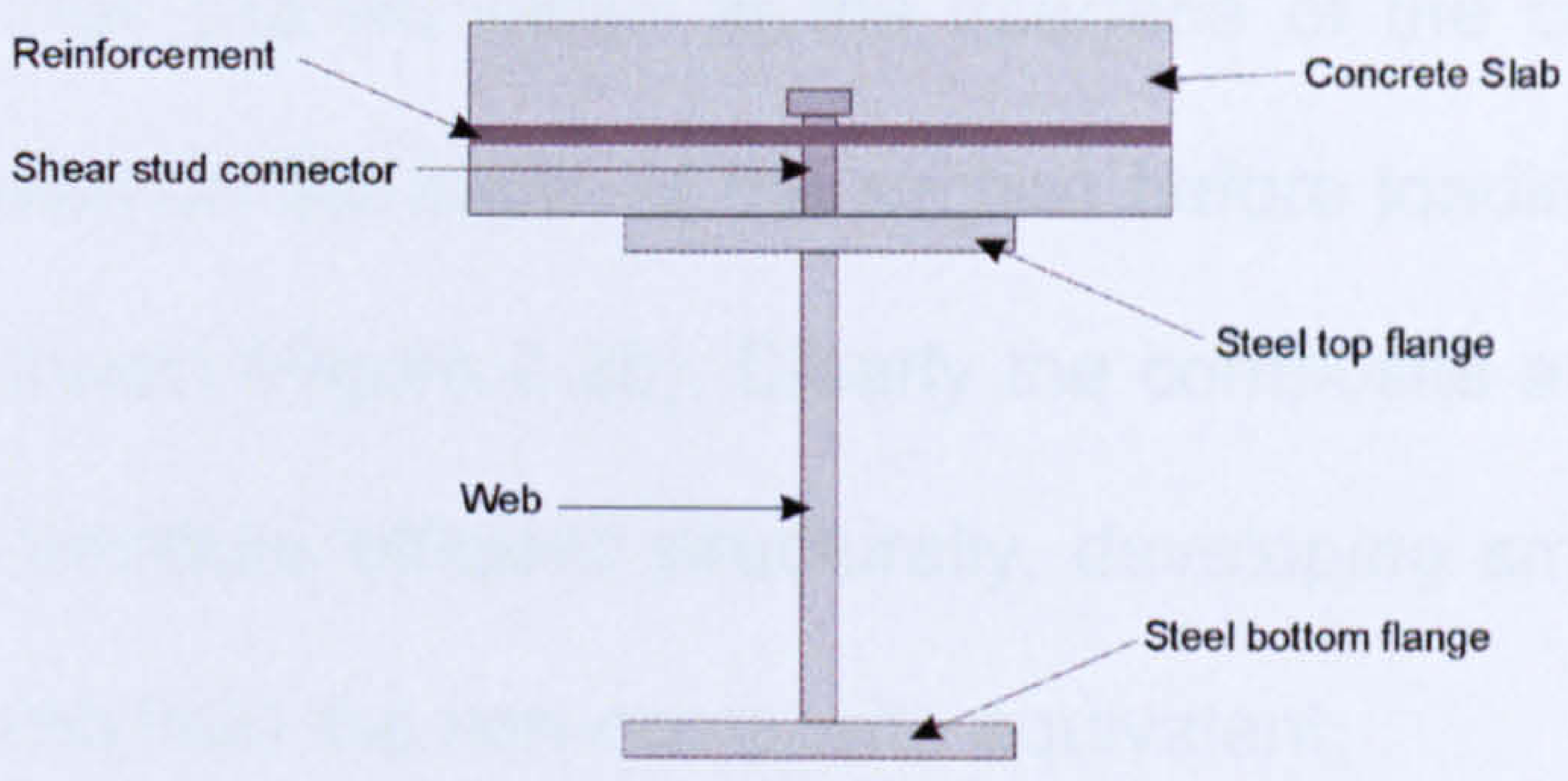

Figure 2.1: Composite T-beam

Each material (steel or concrete) in composite structures is used to take advantage of the materials best attributes; therefore composite steel-concrete construction is very efficient and economical. The real attraction of composite construction is based on having an efficient connection of the steel to the concrete, and it is this connection that allows a transfer of forces and gives composite members their unique behaviour (Bradford and Oehlers 1999).

Figure 2.2 shows the concept of a beam consisting of two constituent parts acting either separately or compositely. For the non-composite arrangement the load will be shared between the two parts, each deforming in bending separately. While for the composite arrangement the load will act on the beam with continuity preserved along the horizontal interface, so both parts of the beam respond as a unit (Nethercot 2001).

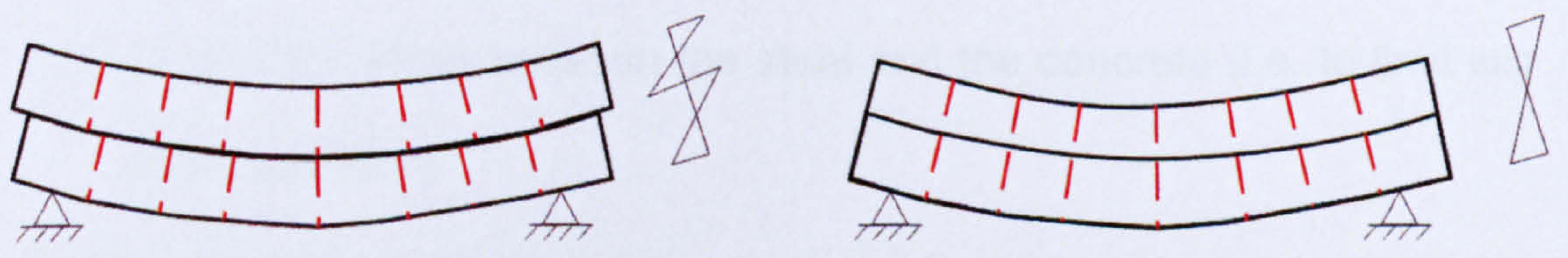

Figure 2.2: Mechanics of Composite Beam

Since no horizontal slip will occur at the interface of the composite beam, vertical lines drawn on the depth of the section before loading will remain as single lines as shown (Figure 2.2b). Clearly the composite arrangement may be expected to be more efficient structurally, developing smaller deflections and smaller strains than the non-composite equivalent.

The advantages of composite beams compared with normal steelwork beams are the increased moment capacity and stiffness, or alternatively the reduced steel sizes for the same moment capacity. Apart from saving in material, the reduced construction depth can be worthwhile in multi-storey buildings. The main disadvantage of composite beams is the need to provide shear connectors to ensure interaction between the steel and concrete (Morris and Plum 1996).

2.3 Shear Connection of Composite Beams

In composite beams, the steel beams are designed to act with a part of the concrete slab, so they act compositely. For this to happen it is necessary to prevent slip at the interface. This is achieved by the use of shear connectors (Nethercot 2001). A shear connector must perform two functions:

(a) To transfer shear between the steel and the concrete (i.e. to limit slip at the interface).
(b) To prevent separation of the steel and the concrete at right angles to the interface (i.e. to prevent uplift).

The welded shear stud connector (Figure 2.3) is currently the most commonly used for composite beams. The transfer of shear initially occurs at the area of the weld and the remainder of the connector, the head of the stud provides anchorage against uplift (Davies 1975).

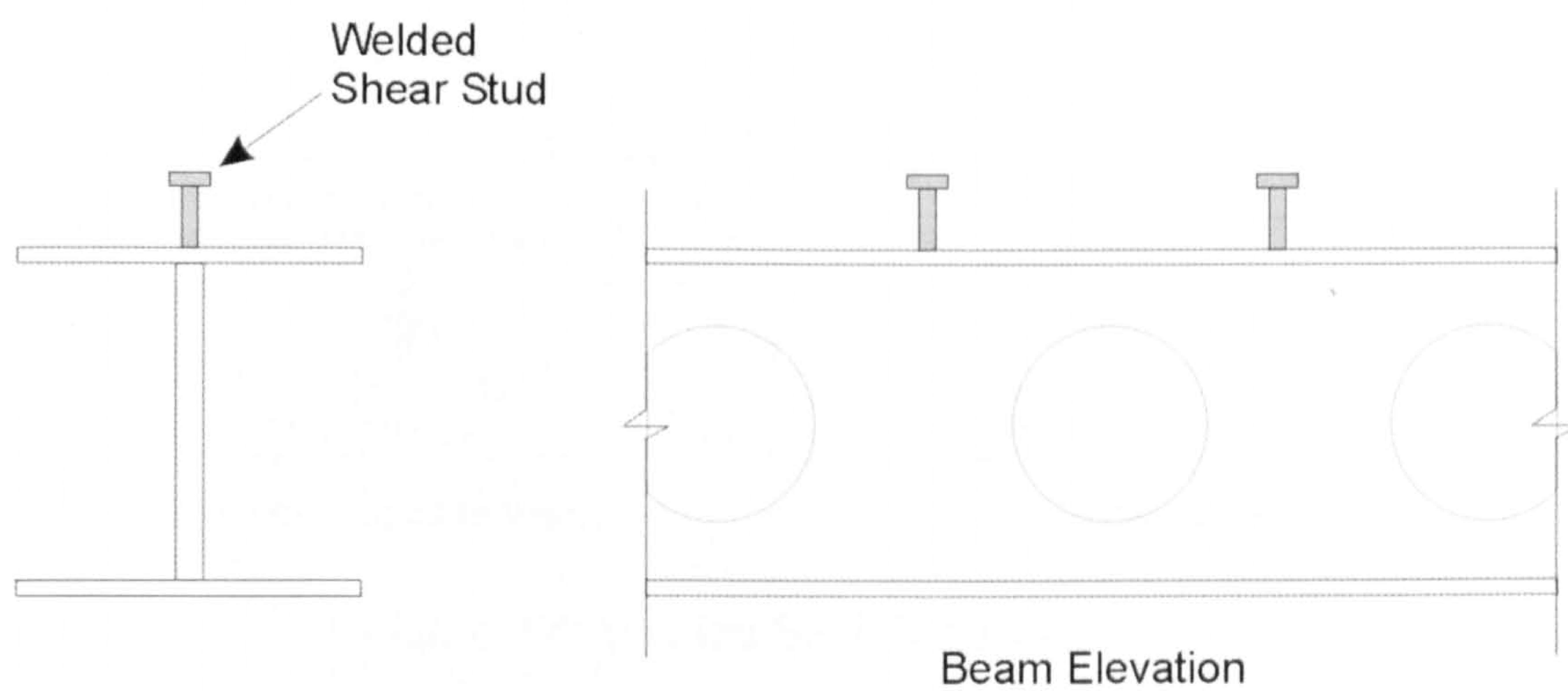

Figure 2.3: Welded Stud Shear Connector

2.3.1 Purpose of Shear Connectors

Designers assume that the sole purpose of the shear connectors is to resist longitudinal slip (Figure 2.4). This action causes the concrete slab and steel beam to interact, and resultant longitudinal compressive and tensile forces to develop in the slab and steel beam, when the beam is loaded and bends. At any location along the beam, the resultant compressive force in the slab, **C**, is assumed to be evenly distributed across the effective width of the beam (OneSteel Market Mills 2001).

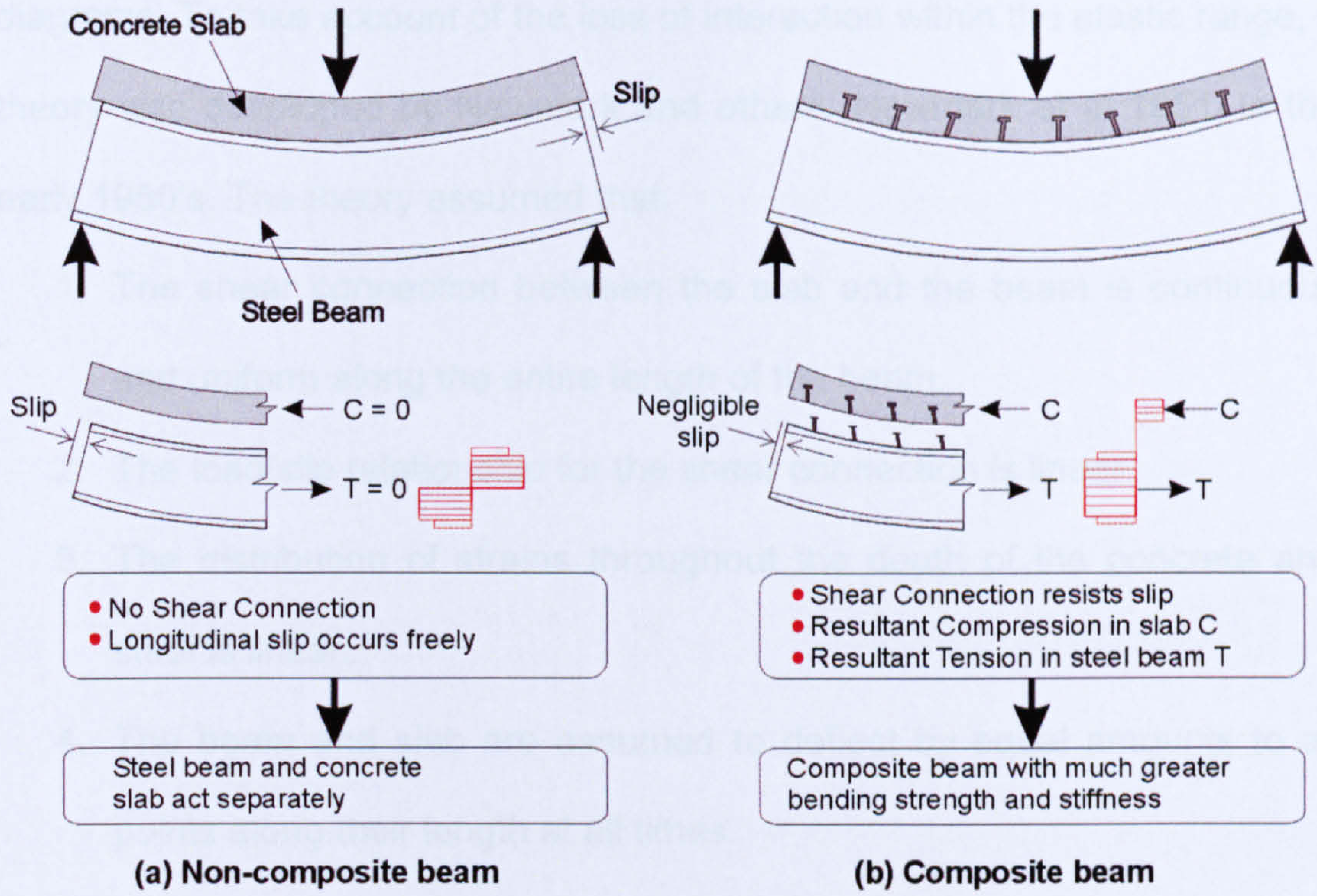

Figure 2.4: Welded Stud Shear Connector

Tensile forces develop in the shear connectors when they resist vertical separation between the steel beam and the concrete slab. Therefore, shear connectors must be provided with some sort of tie-down feature such as the head on a stud. Normally, the effect that these tensile forces has on the shear capacity of the types of connectors can be ignored in design. In Eurocode 4, Part 1.1 this is assumed to be the case in design provided the tensile force per connector is less than 10 per cent of the shear capacity of a connector (OneSteel Market Mills 2001).

Because of the flexibility of the shear connectors and the compressibility of the concrete, horizontal slip at the interface cannot be completely prevented. Therefore the interaction between the steel and the concrete is incomplete and the effect of slip at the interface is to produce a discontinuity in the strain diagrams. To take account of the loss of interaction within the elastic range, a theory was developed by Newmark and others (Newmark et al 1951) in the early 1950's. The theory assumed that:

1. The shear connection between the slab and the beam is continuous and uniform along the entire length of the beam.
2. The load/slip relationship for the shear connection is linear.
3. The distribution of strains throughout the depth of the concrete and steel is linear.
4. The beam and slab are assumed to deflect by equal amounts to all points along their length at all times.

The theory defined the load required per connector to produce unit slip as the 'shear connector modulus' k and this was assumed to be constant for the 'elastic' range considered. In fact, shear connectors do not behave elastically, and the load/slip curve for a shear connector is actually similar to the stress/strain relationship for concrete. In practice the 'shear connector modulus' (that gradient of the load/slip curve) is not constant but depends on the magnitude of the applied load (Davies 1975).

2.3.2 Partial Shear Connection

Two terms that describe composite behaviour are partial-shear-connection and partial interaction, and these relate to the behaviour of the connection between the steel and concrete components. Partial-shear-connection concerns equilibrium of forces within a composite member, while partial interaction concerns compatibility of deformations at the steel/concrete interface. Therefore, partial-shear-connection represents a strength criterion, while partial interaction represents a stiffness criterion (Bradford and Oehlers 1999).

The effect of partial interaction on the full-shear-connection strength of a composite beam is described by Ahmed et al (Ahmed et al 1997). It was shown that for composite beams in buildings, where the axial strength of the concrete section is usually much larger than that of the steel section, partial interaction has virtually no effect on the strength. Conversely, partial interaction can reduce the strength of composite beams with very strong steel sections.

2.3.3 Load-Slip Behaviour of Shear Connectors

In steel and composite design, the longitudinal shear flow in a composite steel and concrete beam is transferred across the steel flange-concrete slab interface by the mechanical action of the shear connectors. The ability of the shear connector to transfer longitudinal shear forces therefore depends on the strength of the shear connector, and also on the resistance on the concrete slab against longitudinal cracking induced by high concentration of shear force (Lam 2002).

For composite beam members with web openings, shear connectors above the opening, between the openings and the support strongly affect the capacity of the section. As the capacity of the shear connector increase, the strength of the opening increases. This increased capacity can be obtained by either increasing the number of shear connectors or by increasing the capacity of the individual connectors (Darwin and Donahey 1986, 1988).

Composite sections are also subject to bridging, the separation of the slab from the steel section. Bridging occurs primarily in beams with transverse ribs and occurs more as the slab thickness increases (Darwin and Donahey 1988).

The load-slip curve of a shear connector is determined from push-out tests, the load acting as the combined shear force applied to the connectors. Ductile and brittle behaviour of shear connectors, as well as the assumed model for design, are shown diagrammatically in Figure 2.5.

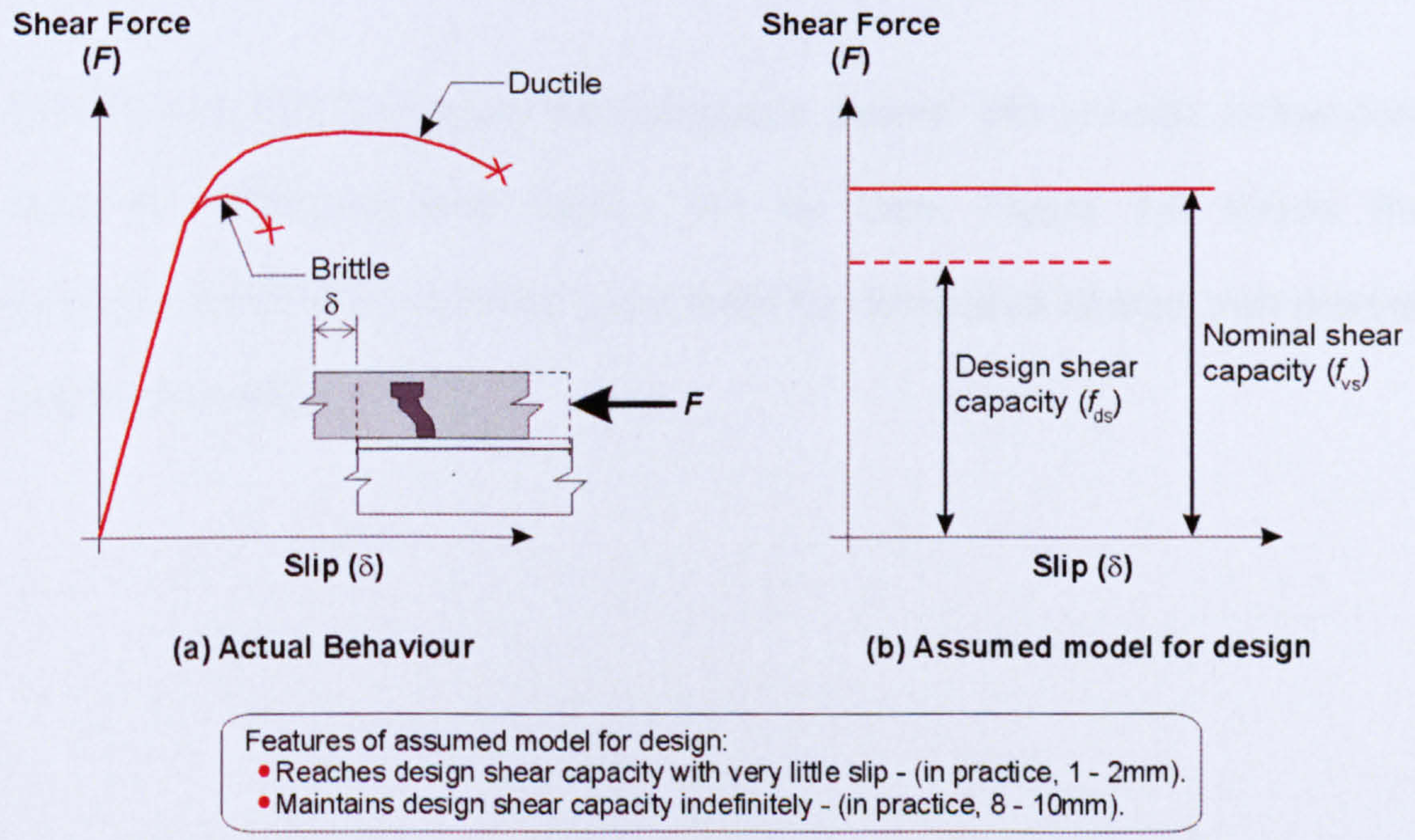

Figure 2.5: Load-Slip Behaviour of Shear Connectors

When shear connection is provided between the steel member and concrete slab, the two act together to span as a composite beam. The main function of the steel beam at mid-span is to resist tension, and the compression is assumed to be resisted by an 'effective' breadth of slab (Johnson 1994).

2.3.4 Push Test for Hollow-Core Slabs

In steel-concrete composite design, the longitudinal shear flow in a composite steel and concrete beam is transferred across the steel flange and concrete slab interface by the mechanical action of the shear connectors. The ability of the shear connector to transfer longitudinal shear forces therefore depends on the strength of the shear connector, and also on the resistance of the concrete slab against longitudinal cracking induced by the high concentration of shear force (Lam 2007). In order to determine the strength of shear connection in composite construction, push tests need to be performed.

A new push test procedure for composite beams with precast hollow-core slabs is introduced and carried out by Lam. Figure 2.6 shows the arrangement of the horizontal push tests for composite beams with precast hollow-core slabs.

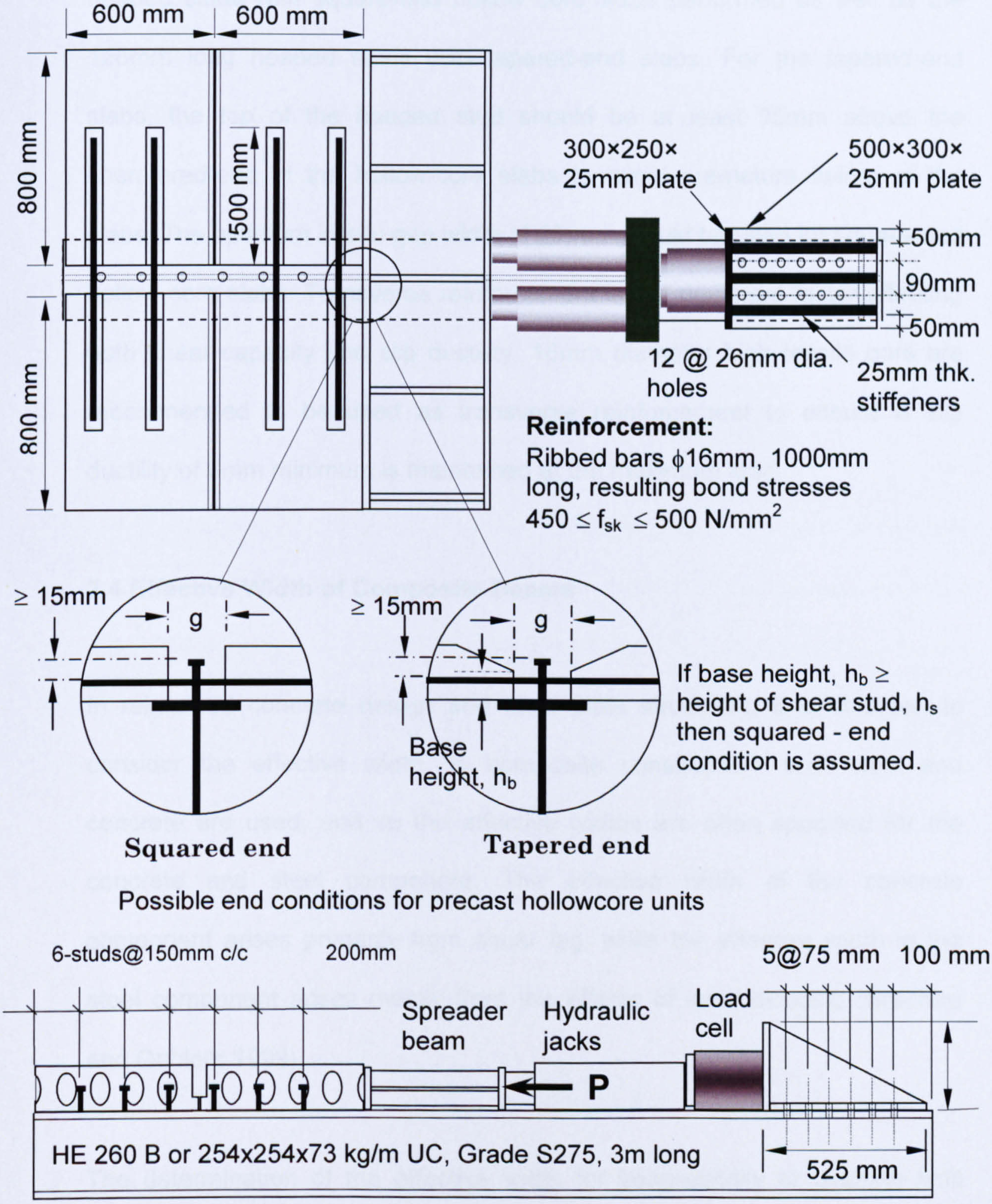

Figure 2.6: General arrangement for horizontal push test (Lam 2007)

From the push tests carried out by Lam, the results showed 100mm long headed studs with square-end hollow core slabs performed as well as the 125mm long headed studs with tapered-end slabs. For the tapered-end slabs, the top of the headed stud should be at least 35mm above the chamfered-end of the hollow-core slabs to avoid premature failure of the slabs. The optimum in-situ gap width of 80mm should be used for square-end hollow core slabs. Transverse reinforcement is the dominant factor affecting both shear capacity and slip ductility. 16mm diameter high tensile bars are recommended to be used as transverse reinforcement to ensure a slip ductility of 6mm minimum is maintained at the maximum load.

2.4 Effective Width of Composite Beams

In reinforced concrete design and steel plate structures, it is common to consider the effective width. In composite construction, both steel and concrete are used, and so the effective widths are often specified for the concrete and steel component. The effective width of the concrete component arises primarily from shear lag, while the effective width in the steel component arises mainly from the effects of local buckling (Bradford and Oehlers 1999).

The determination of the effective width for serviceability or ultimate limit states analysis is the basis for the design of steel-concrete composite beams. Shear strains play an important role for an elastic analysis of composite beams. The shear strains cause a non-uniform distribution of the normal stresses and the non-planarity of the slab cross-section; this is known as shear lag (Amadio and Fragiacomo 2002). The term shear lag is used to describe the discrepancies between the approximate engineering theory and the real behaviour of the composite beam. There are increases in the stresses in the concrete component adjacent to the steel I-section component in a composite T-beam and decreases in stresses in the concrete component away from the steel.

2.4.1 Effective Cross-Section

Longitudinal shear in the slab causes shear strain in its plane. When the composite beam is loaded the vertical cross-sections through the beam do not remain plane. At a cross-section, the mean longitudinal bending stress through the thickness of the slab varies, as shown in Figure 2.7.

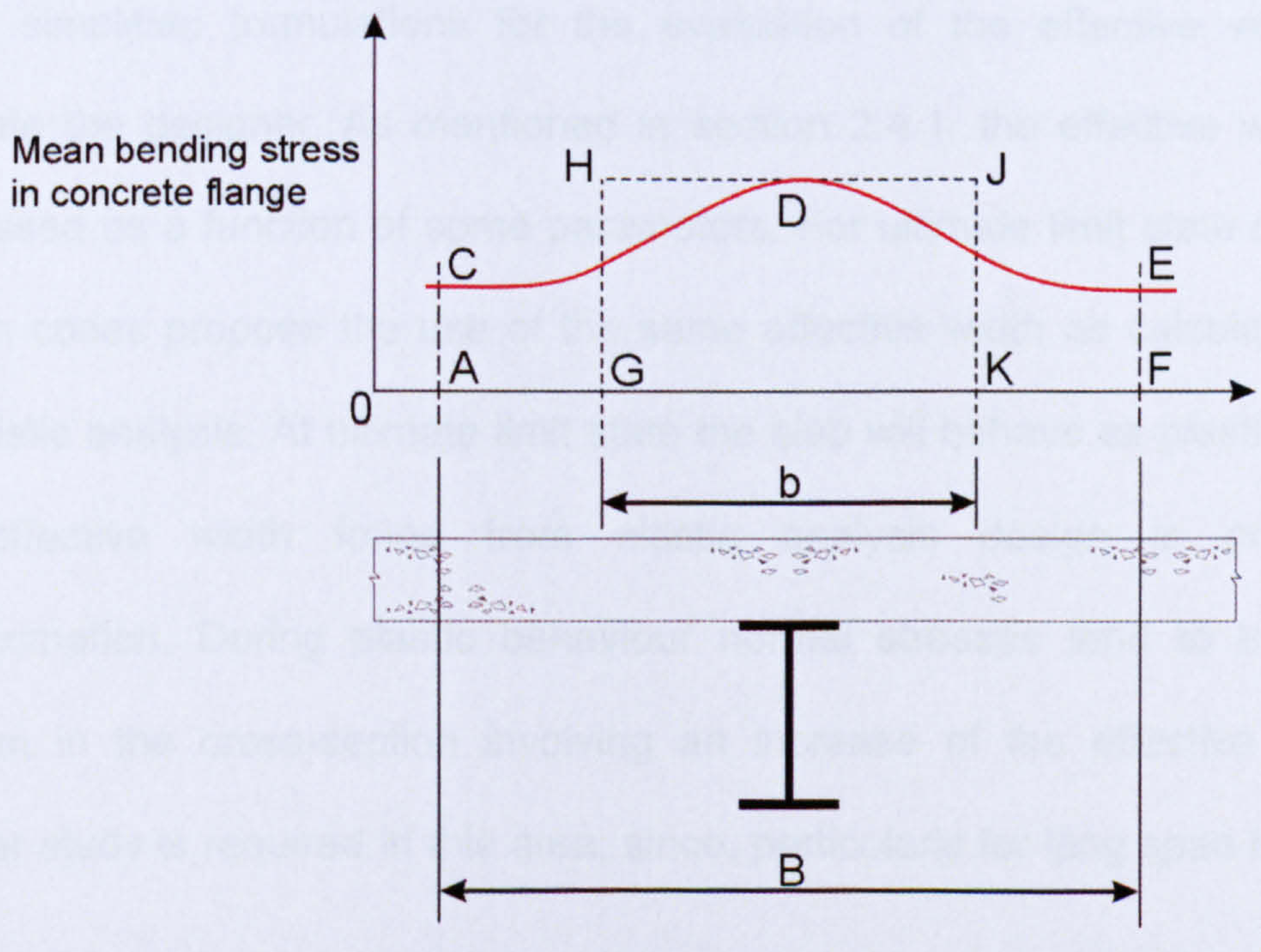

Figure 2.7: Use of Effective Width to allow for shear lag (Johnson 1994)

Simple bending theory can give the correct value for maximum stress (at point *D*) if the true flange breadth *B* is replaced by an effective breadth, *b*. Therefore, the area *GHJK* equals the area *ACDEF*. Research based on elastic theory has shown that the ratio b/B depends in a complex way on the ratio of *B* to the span *L*, the type of loading, the boundary conditions at the supports, and other variables. For beams in buildings, it is assumed that the effective width is $l_o/8$ on each side of the steel web, where l_o is the distance between points of zero bending moment. For a simply supported beam, l_o is equal the span *L*, so $b_{eff} = L/4$, provided that the width of the slab $L/8$ is present at each side of the slab (Johnson 1994).

2.4.2 Effective Width Evaluation

Due to the difficulty of the complex analytical evaluation to calculate the effective width (Allen et al 1961, Bild and Sedlacek 1993), design codes adopt simplified formulations for the evaluation of the effective width to facilitate the designer. As mentioned in section 2.4.1, the effective width is expressed as a function of some parameters. For ultimate limit state design, design codes propose the use of the same effective width as calculated for an elastic analysis. At ultimate limit state the slab will behave as plastic, thus the effective width found from elastic analysis design is only an approximation. During plastic behaviour normal stresses tend to become uniform in the cross-section involving an increase of the effective width. Further study is required in this area, since, particularly for long span beams, an increase of the effective width can imply a significant increase of load capacity.

A factor that controls the stress in the serviceability condition is the connection between the concrete and steel. This is generally neglected in a correct evaluation of the effective width. The effective width calculated in the hypothesis of rigid connection is in fact larger than the one evaluated with a deformable connection. This occurs in both cases of partial and full shear connection (Amadio and Fragiacomo 2002). Amadio and Fragiacomo carried out a numerical study using Abaqus finite element analysis, in which they found that the connection deformability plays an important role in evaluation of the effective width for stress elastic analysis of steel-concrete composite beams.

For a non-linear analysis, cracking of concrete and plastic behaviour of steel should be taken into account. The effective width proposed by design codes are based on elastic analysis and do not take plastic behaviour into account. For both cases of sagging and hogging moment the plastic zone is extended in almost the whole concrete slab in compression and the whole reinforcement distributed into the slab in tension respectively.

2.5 Steel Beams with Web Openings

Web openings provide an economical means for reducing the depth of floor systems in steel buildings. In the majority of these structures, the concrete slab is designed to act compositely with the steel. The design of regions around web openings has been looked at as four separate problems, with the beam treated as composite in positive/sagging moment regions and non-composite in negative/hogging moment regions. During the past decade design techniques (Darwin and Donahey 1988, Cho and Redwood 1993, Darwin and Lucas 1990) for openings in composite members have reached a level of maturity (Darwin 2000).

The conventional steel beams with web openings are known as cellular or castellated beams, they are manufactured by using a solid steel beam and burning along the web. Then the two parts of the separated web are welded together to form to deeper beam, as shown below:

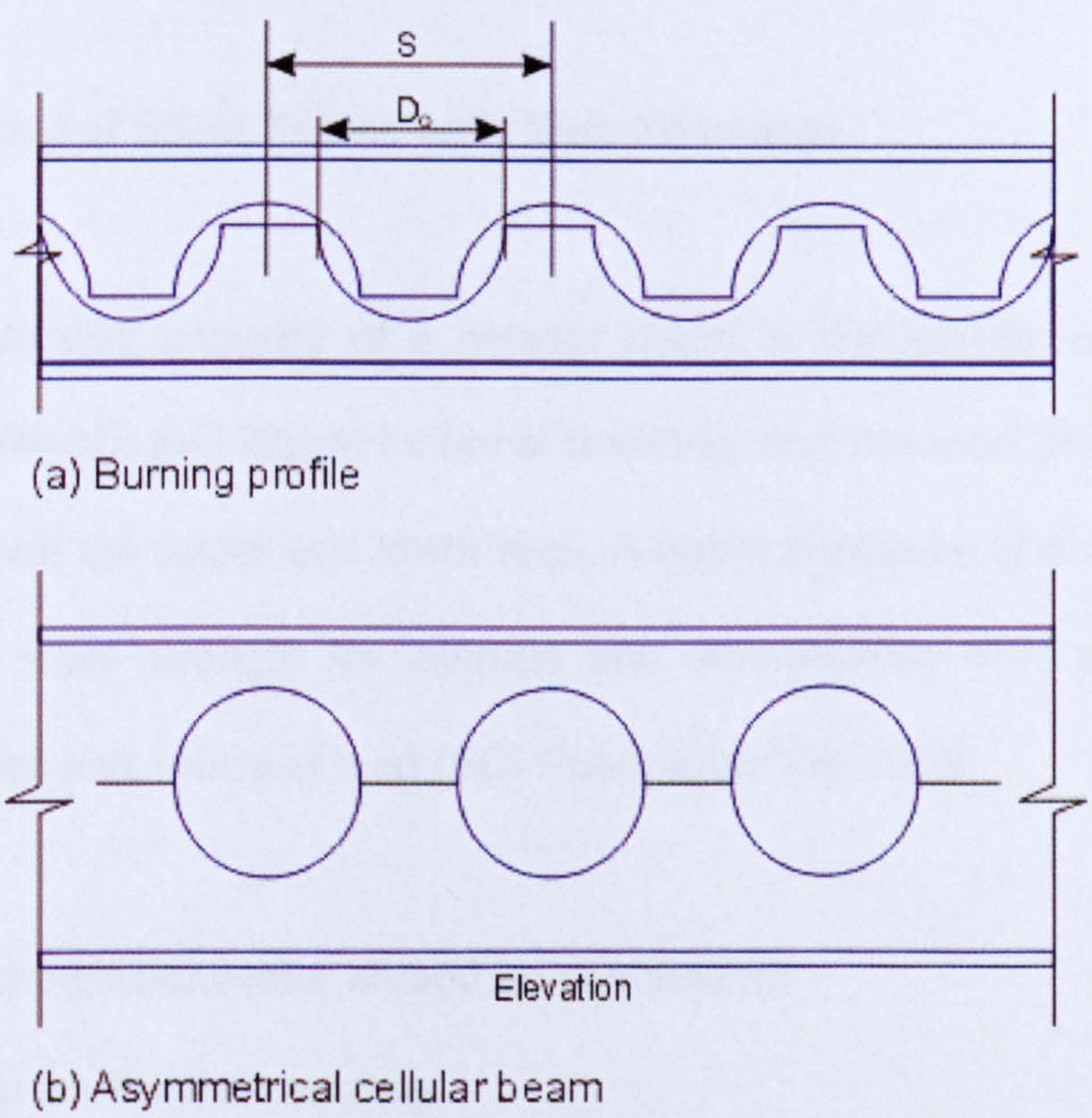

Figure 2.8: Cellular beam burning profile

Cellular beams have limited shear capacity and are best used as long-span secondary beams where loads are low or where concentrated loads can be avoided. The height of the opening should not be more than 70% of the beam depth, and the length should not be more than twice the beam depth. The best location for web openings is in the low shear zones of the beam; this is because the web does not contribute much to the moment resistance of the beam (Liew and Uy 2003).

Fabsec beams are also steel beams with web openings, but they are fabricated differently to cellular beams. They are fabricated by automatic welding of profiled steel plates used to form the flanges and web of the section, i.e. the web of the beam has the openings cut into it, and then the flanges are welded to the web to form the I-section beam.

2.6 Behaviour of Steel Beams with Web Openings

The load carrying capacity of a cellular beam is the smaller of its overall strength in flexure and lateral torsional buckling, and the local strength of the web posts and the upper and lower tees. A beam should be checked for both overall and local strength for ultimate and serviceability limit states under factored dead and imposed load (SCI Publication 100 1990).

The overall beam behaviour should be checked for:

- Beam flexural capacity
- Beam shear capacity

- Overall beam buckling

The overall flexural capacity is assessed by considering the plastic moment of the cross section through the centre line of the opening. The maximum moment in the beam should not exceed the plastic moment capacity of the reduced section of the beam which is normally based on the tensile capacity of the lower web tee.

The vertical shear capacity of the beam is also governed by the cross section through the centre line of the circular opening. The shear capacity is equal to the sum of the shear capacities of the upper and lower tees. The horizontal shear capacity depends on the minimum cross-sectional area of the web post. In areas of high shear, under point loads and at the supports, the required shear capacity may only be achieved by infilling the openings and adding stiffeners, as shown in Figure 2.9.

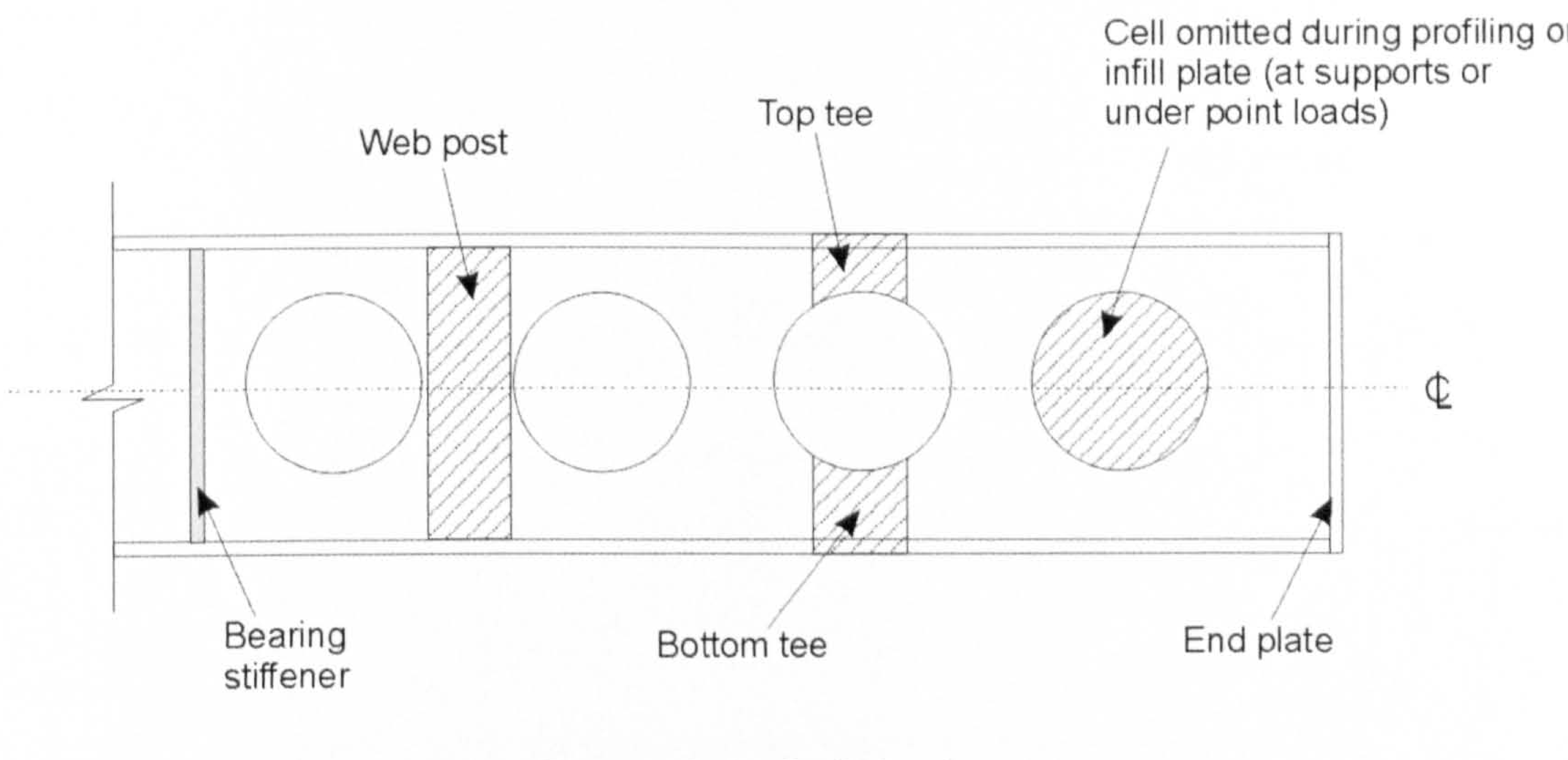

Figure 2.9: Cellular beam

Cellular beams without lateral restraint are likely to fail by lateral torsional buckling. In comparison to solid web beams, cellular beams are prone to buckle laterally because of their relatively deep and slender section and the reduced torsional stiffness of the web (SCI Publication 100 1990).

The forces that act at web openings are shown in Figure 2.10. In the figure, a composite beam is illustrated, but the equations that follow are valid equally well to steel members. For positive bending, the section below the opening, or bottom tee, is subjected to a tensile force, P_b, shear, V_b, and secondary bending moments, M_{bl} and M_{bh}. The section above the opening, or top tee, is subjected to a compressive force, P_t, shear, V_t, and secondary bending moments, M_{bl} and M_{bh} (Darwin 1990).

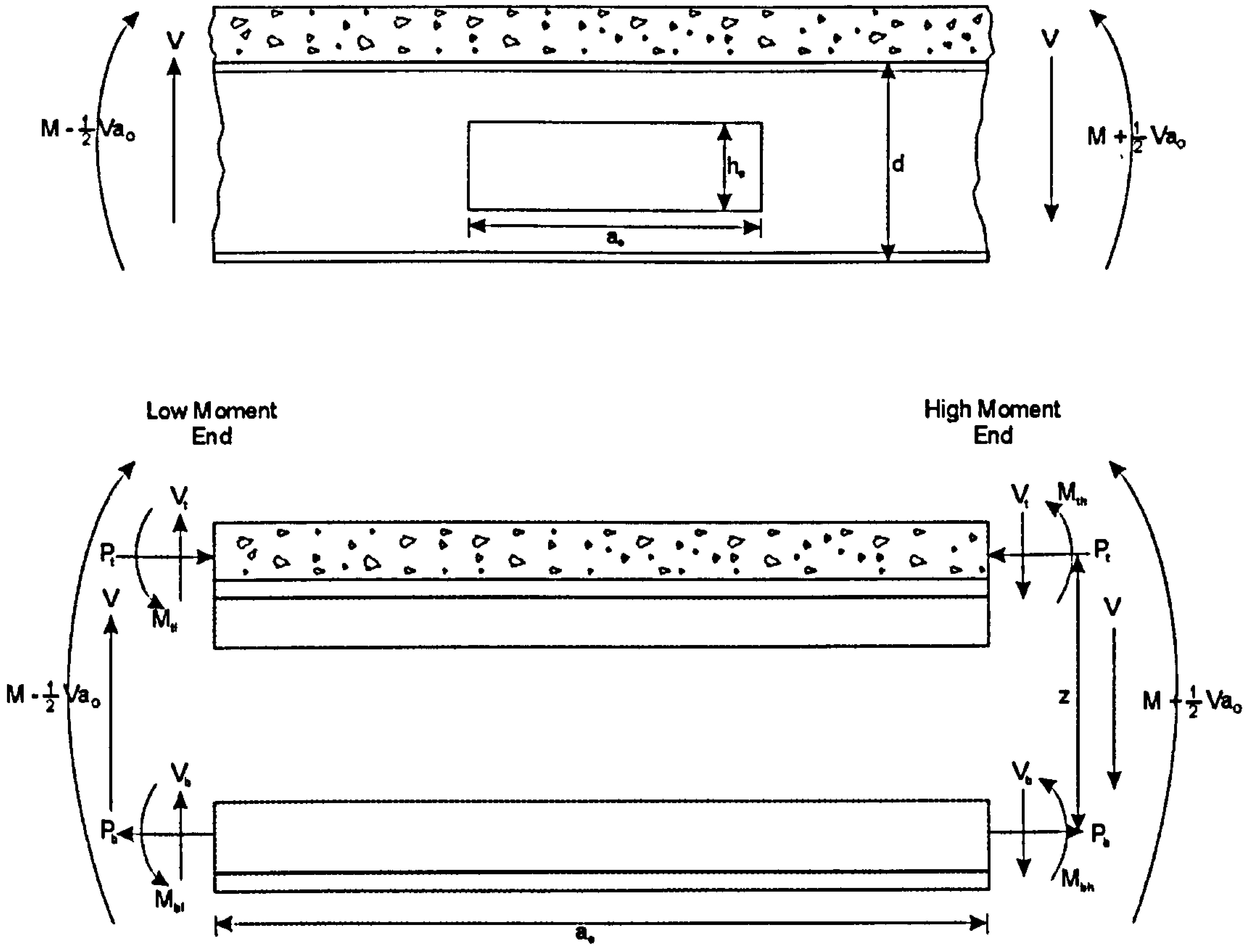

Figure 2.10: Forces acting at web opening

Based on equilibrium:

$$P_b = P_t = P \tag{2.1}$$

$$V = V_b + V_t \tag{2.2}$$

$$V_b a_o = M_{bl} + M_{bh} \tag{2.3}$$

$$V_t a_o = M_{tl} + M_{th} \tag{2.4}$$

$$M = Pz + M_{th} + M_{bh} - \frac{V a_o}{2} \tag{2.5}$$

Where:

V = total shear acting at an opening

M = primary moment acting at opening centre line

a_o = length of opening

z = distance between points about which secondary bending moments are calculated

2.6.1 Modes of Failure

The deformation and failure modes for beams with web openings are illustrated in Figure 2.11. Figures 2.11(a) and (b) illustrate steel beams, while Figures 2.11(c) and (d) illustrate composite beams with solid slabs.

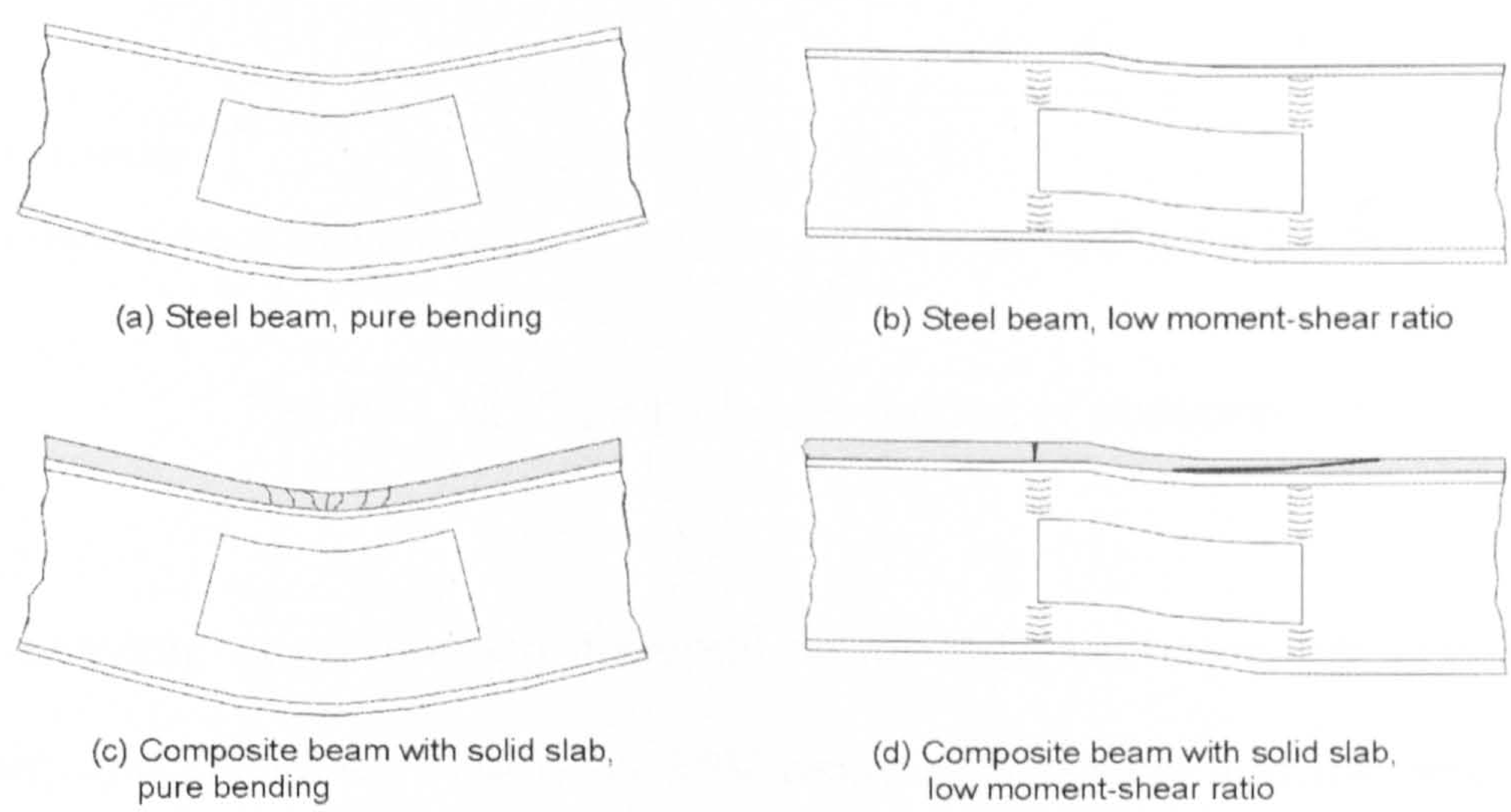

Figure 2.11: Failure modes at web openings (Darwin 1990)

Vierendeel bending is caused by the need to transfer shear force across the web openings to be consistent with the rate of change of bending across the beam. The flexural capacity of the upper and lower tees under Vierendeel bending is critical. In the absence of local or overall instability, cellular beams have two basic modes of collapse (SCI Publication 100 1990). They are:

- Plastic tension and compression stress blocks in the lower and upper tees in regions of high overall bending, shown in Figure 2.12(a).

- Parallelogram or Vierendeel action due to the formation of plastic hinges at the four corners of the opening in regions of high shear, shown in Figure 2.12(b).

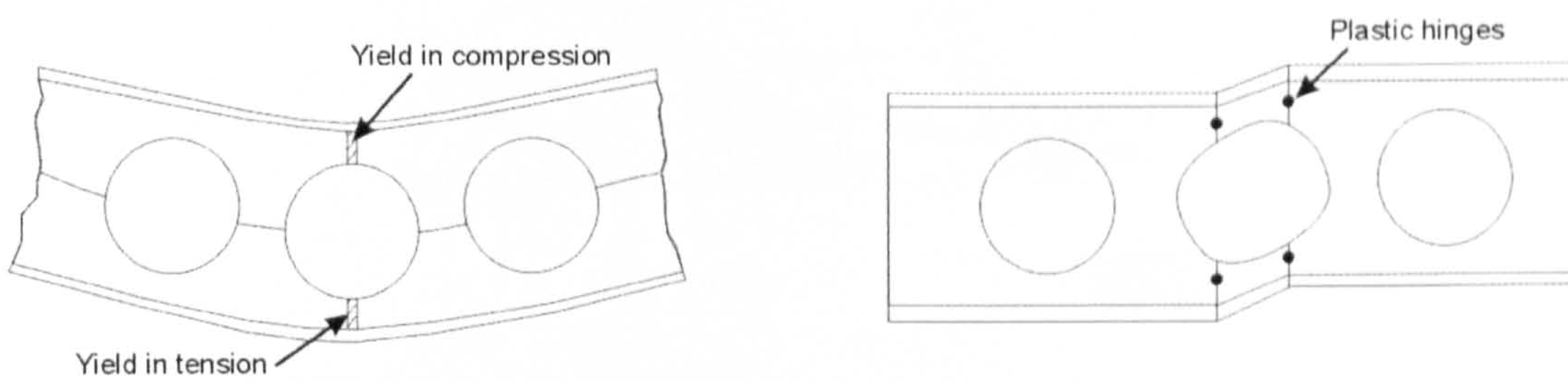

(a) Yielding due to high bending

(b) Yielding due to high shear

Figure 2.12: Cellular beam modes of collapse

The behaviour at an opening depends on the ratio of moment to shear, *M/V* (Darwin and Donahey 1988). As *M/V* decreases, shear and the secondary bending moments increase, causing increasing differential, or Vierendeel deformation to occur at the opening [Figures 2.11(b) and (d)]. The bottom and top tees display a well defined shape in curvature (Darwin and Lucas 1990).

For steel beams, failure occurs with the formation of plastic hinges at all four corners of the web opening [Figure 2.12(b)]. The yielding first occurs within the webs of the tees. For composite beams the formation of plastic hinges is accompanied by a diagonal tension failure within the concrete due to prying action across the opening. For members with ribbed concrete slabs, the diagonal tension failure is noticed as a rib separation and a failure of the concrete around the shear connectors (Figure 2.13). Also for composite members with ribbed slabs in which the rib is parallel to the beam, failure is accompanied by longitudinal shear failure in the slab (Figure 2.14).

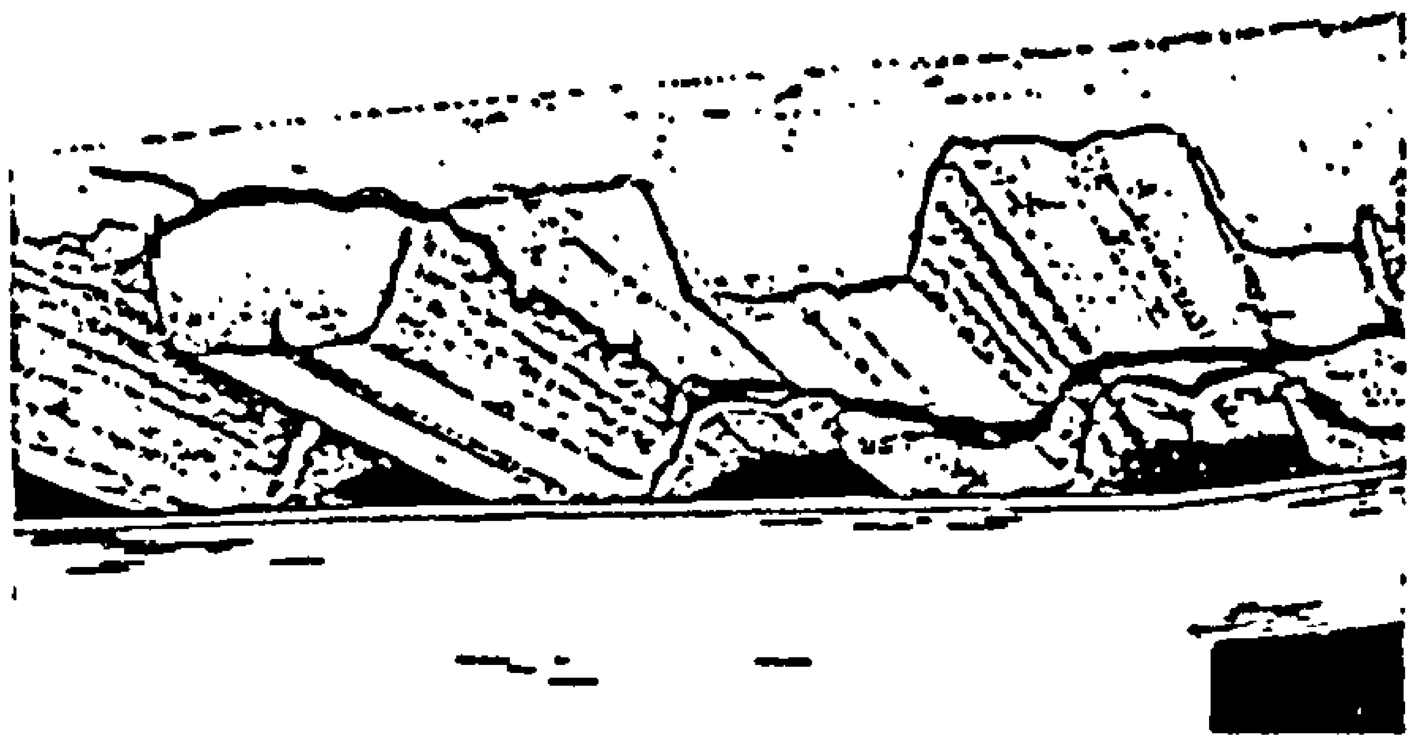

Figure 2.13: Rib failure and failure of concrete around shear connectors in slab with transverse ribs (Darwin and Lucas 1990)

Figure 2.14: Longitudinal rib shear failure (Darwin and Lucas 1990)

For members with low moment-shear ratios, the effect of secondary bending can be quite striking, as illustrated by the stress diagrams for a steel member in Figure 2.15 and the strain diagrams for a composite member with a ribbed slab in Figure 2.16. Secondary bending can cause portions of the bottom tee to go into compression and portions of the top tee to go into tension, even though the opening is subject to a positive bending moment. In composite beams, large slips take place between the concrete slab and the steel section over the opening (Figure 2.16). The slip is enough to place the lower portion of the slab in compression at the low moment end of the opening, although the adjacent steel section is in tension. Secondary bending also results in tensile stress in the top of the concrete slab at the low moment end of the opening, which results in transverse cracking.

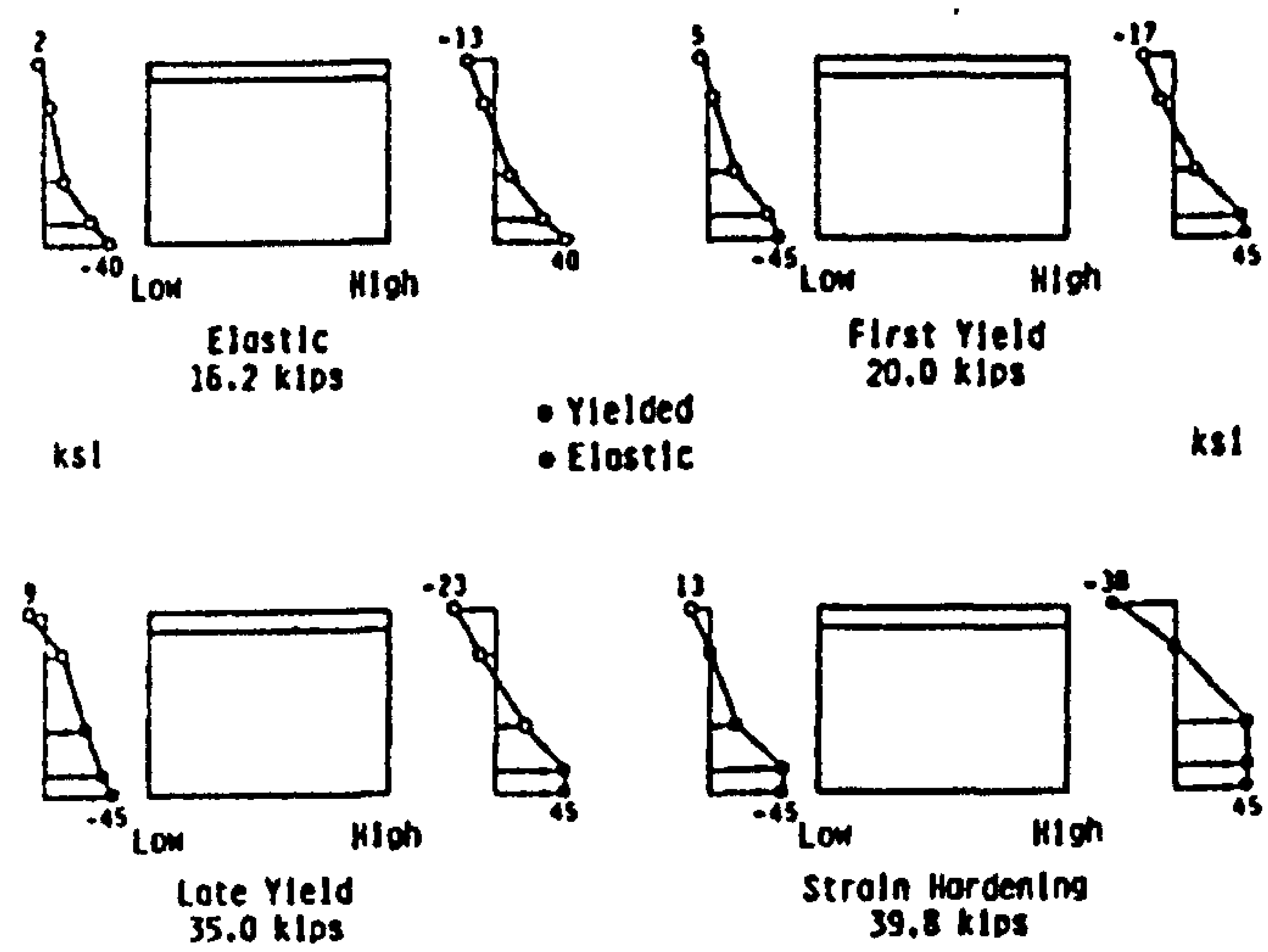

Figure 2.15: Stress diagrams for opening in steel beam with low moment-shear ratio (Bower 1968)

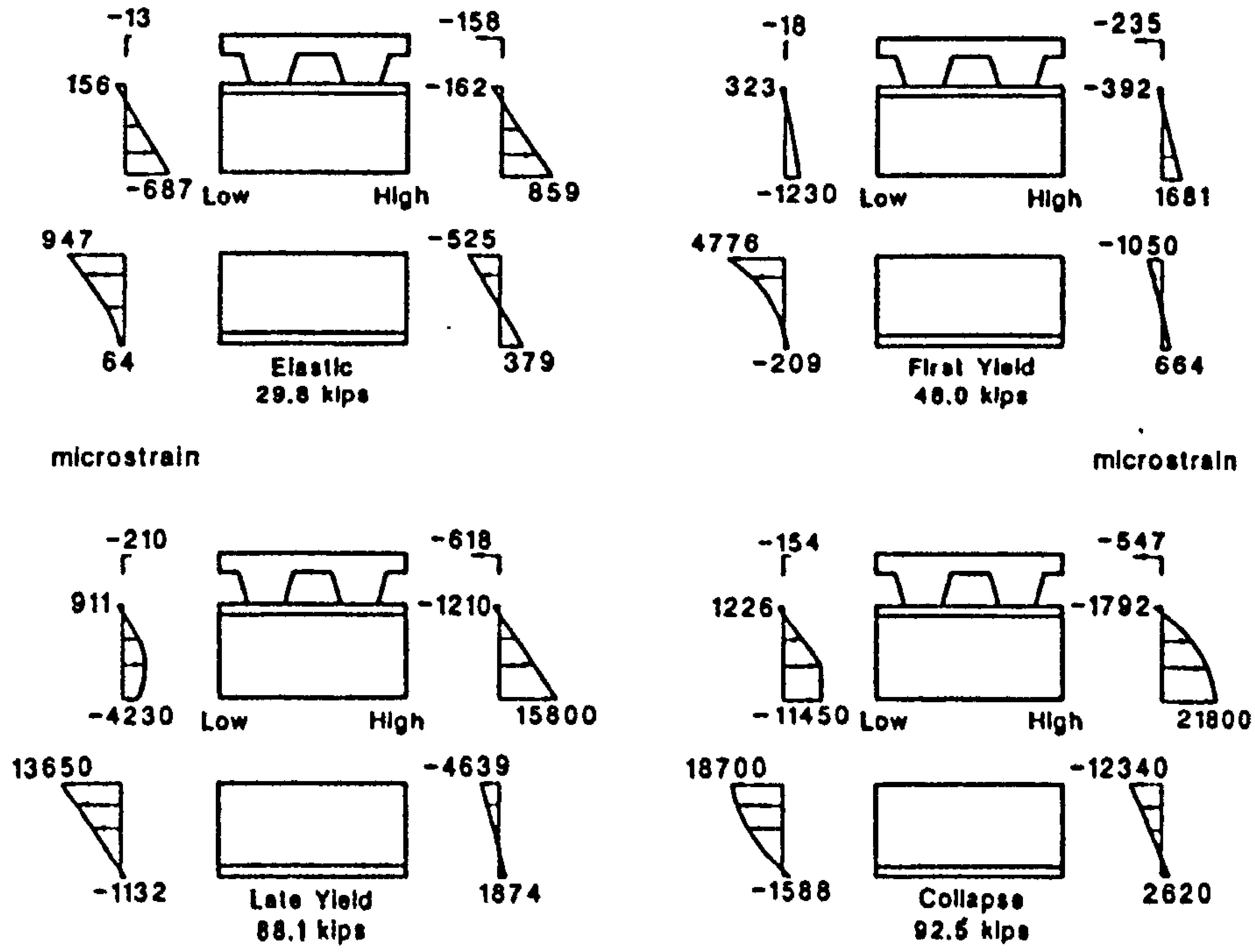

Figure 2.16: Strain distributions for opening in composite beam with low moment-shear ratio (Darwin and Donahey 1988)

Summarising the failure of steel beams with web openings, failure occurs at openings due to stress concentrations at the corners of the openings. For steel beams, depending on the proportions of the top and bottom tees and the proportions of the opening with respect to the member, failure can be manifested by general yielding at the corners of the opening. This is followed by web tearing at the high moment end of the bottom tee and the low moment end of the top tee (Bower 1968). Strength may be reduced or governed by web buckling in more slender members (Lupien and Redwood 1978). In high moment regions, compression buckling of the top tee is a concern for steel members (Redwood and Shrivastava 1980).

For composite beams, stresses remain low in the concrete until well after the steel has begun to yield (Darwin and Donahey 1988). The concrete contributes significantly to the shear strength, as well as the flexural strength of these beams at web openings. This contrasts with the standard design practice of composite beams, in which the concrete deck is used only to resist the bending moment, and shear is assigned solely to the web of the steel section (Darwin 1990).

If multiple web openings are used in a single steel beam, strength can be reduced if the openings are placed too closely together (Redwood and Shrivastava 1980, Aglan and Redwood 1974). The following failures can occur if web openings are placed to closely together; (1) a plastic mechanism may form, which involves interaction between the openings, (2) the portion of the member between the openings, or web post, may become unstable, or

(3) the web post may yield in shear. The close proximity of web openings in composite beams may also be detrimental due to bridging of the slab from one opening to another (Darwin 1990).

For both steel and composite sections, failure at web openings is quite ductile. For steel sections, failure is preceded by large deformations through the opening and significant yielding of the steel. For composite members, failure is preceded by major cracking in the slab, yielding of the steel and large deflections in the member.

First yielding in the steel does not give a good presentation of the strength of either steel or composite sections. Tests show that the load at first yield can vary from 35 to 64 percent of the failure load in steel members (Bower 1968) and from 17 to 52 percent of the failure load in composite members (Darwin and Donahey 1988).

It has been found that circular openings perform better than rectangular openings of similar size (Redwood and Shrivastava 1980). This improved performance is due to the reduced stress concentrations in the region of the opening and the relatively larger web regions in the tees that are available to carry shear.

2.6.2 Design of Beams with Web Openings

The interaction between the moment and shear strengths at a web opening is generally quite weak for both steel and composite sections. That is, at openings, beams can carry a large percentage of the maximum moment capacity without a reduction in the shear capacity and vice versa (Darwin 1990).

The design of web openings has historically consisted of the construction of a moment-shear interaction diagram of the type shown in Figure 2.17. Models have been developed to generate the moment-shear diagrams point by point, illustrated in Figure 2.18. However these models were developed for research. For design it is preferable to generate the interaction diagram more simply. This is done by calculating the maximum moment capacity, M_m, the maximum shear capacity, V_m, and connecting theses points with a curve or series of straight line segments. This has resulted in a number of different shapes for interaction diagrams, as shown in Figures 2.17 and 2.18. To construct a curve the end points, M_m and V_m, must be determined for all models. Some other models require an additional calculation for M_v, which represents the maximum moment that can be carried at the maximum shear [Figures 2.18(a) and (b)].

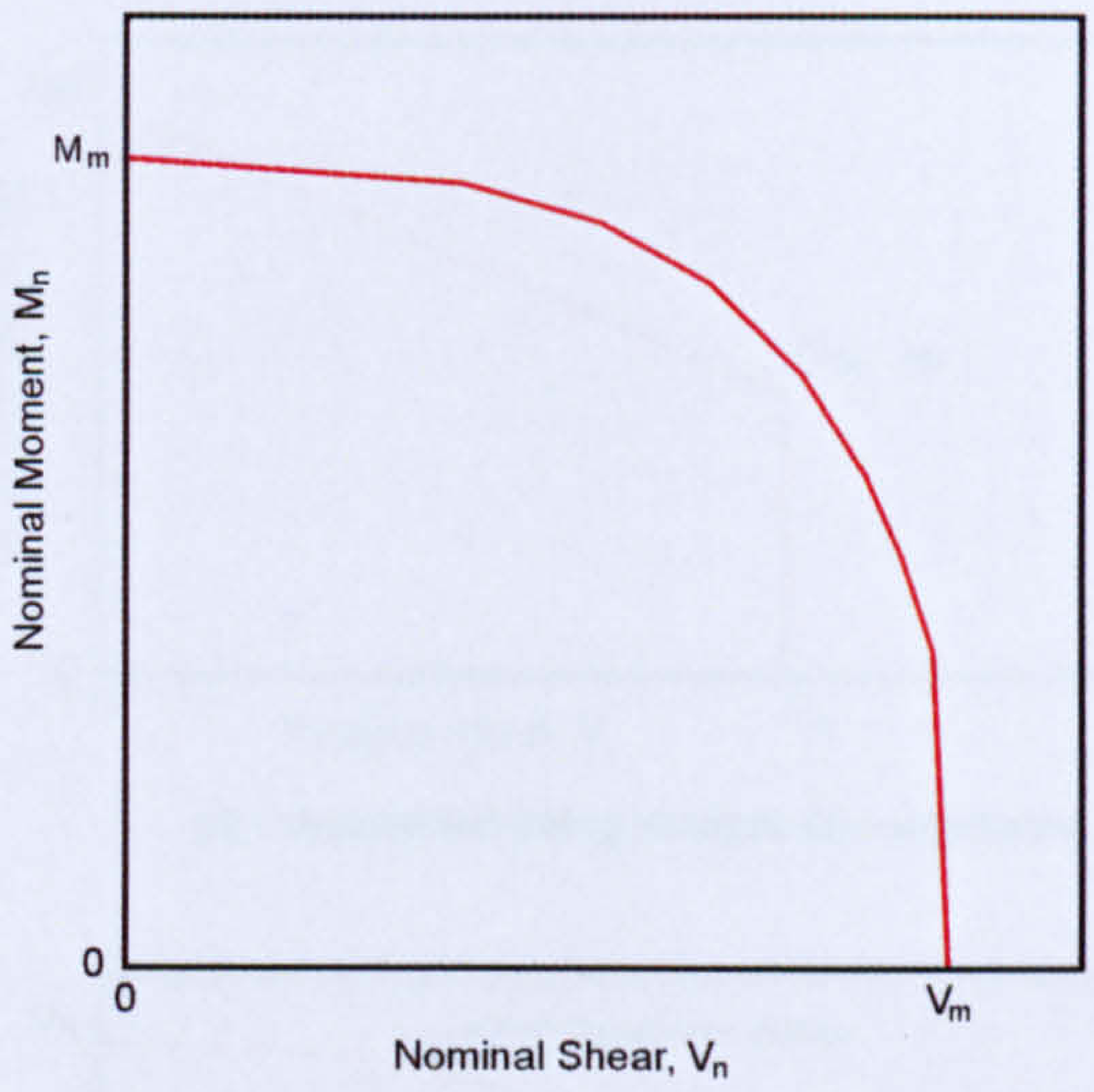

Figure 2.17: General Moment-Shear interaction diagram (Darwin and Donahey 1988)

All procedures agree on the maximum moment capacity, M_m. This represents the bending strength at an opening subjected to zero shear. The methods differ in how they calculate the maximum shear capacity and what curve shape is used to complete the interaction diagram. Models which use straight line segments for all or a portion of the curve have an apparent advantage in simplicity of construction. However, models that use a single curve [Figure 2.18(c)] generally prove to be the easiest to apply in practice (Darwin 2001).

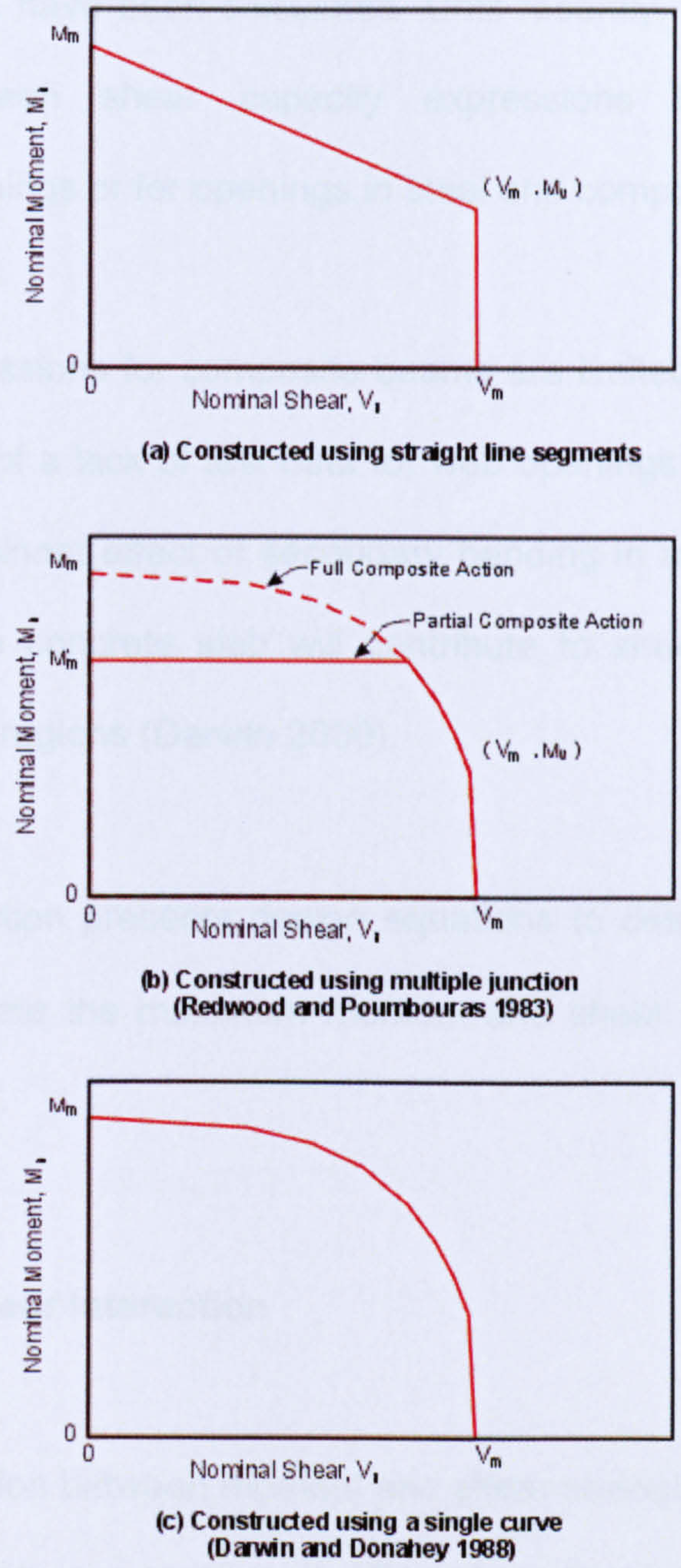

(a) Constructed using straight line segments

(b) Constructed using multiple junction (Redwood and Poumbouras 1983)

(c) Constructed using a single curve (Darwin and Donahey 1988)

Figure 2.18: Moment-Shear interaction diagrams

In the past the maximum shear capacity, V_m, has been calculated for specific cases, such as concentric unreinforced openings, eccentric unreinforced openings, and eccentric reinforced openings (Redwood and Shrivastava 1980) in steel beams. Also concentric and eccentric unreinforced openings (Darwin and Donahey 1988) and reinforced openings (Donoghue 1982) in composite beams have been calculated. Until recently, there has been little correlation between shear capacity expressions for reinforced and unreinforced openings or for openings in steel and composite beams.

The design expressions for composite beams are limited to positive moment regions because of a lack of test data for web openings in negative moment regions. The dominant effect of secondary bending in regions of high shear suggests that the concrete slab will contribute to shear strength, even in negative moment regions (Darwin 2000).

The following section presents design equations to describe the interaction curve, and calculate the maximum moment and shear capacities, M_m and V_m.

2.6.3 Moment-Shear Interaction

The weak interaction between moment and shear strengths at a web opening has been dealt with in a number of different ways, as illustrated in Figures 2.17 and 2.18. Darwin and Donahey observed that this weak interaction can be represented using a cubic interaction curve to relate the nominal bending and shear capacities, M_n and V_n, with the maximum shear capacities, M_m and V_m (Figure 2.19).

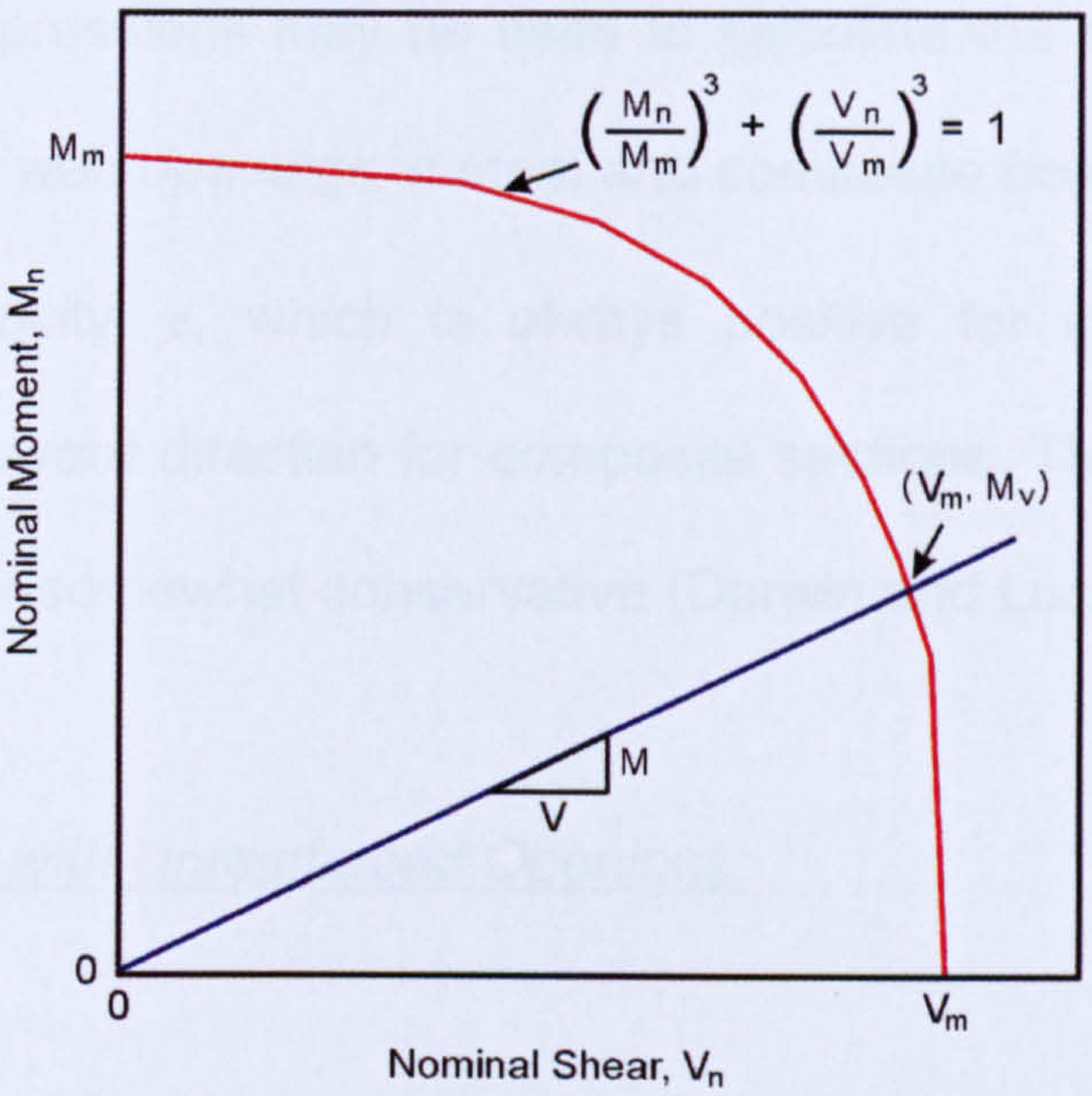

Figure 2.19: Cubic Interaction diagram (Darwin and Donahey 1988)

The solutions for M_m and V_m are shown below. These solutions are based on equilibrium, assumed stresses at failure, and selected simplified assumptions.

$$\left(\frac{M_n}{M_m}\right)^3 + \left(\frac{V_n}{V_m}\right)^3 = 1 \qquad (2.6)$$

Equation 2.6 accurately represents the weak interaction between flexure and shear, provides good agreement with test results (Darwin and Donahey 1986), and allows M_n and V_n to be easily calculated for any segment of factored moment to factored shear.

Maximum Moment Capacity

The following expressions may be used to calculate the maximum moment capacity, M_m, at web openings in steel and composite beams. The openings have an eccentricity, e, which is always positive for steel sections and positive in the upward direction for composite sections. The expressions are generally exact or somewhat conservative (Darwin and Lucas 1990).

For Steel Beams with Unreinforced Openings:

$$M_m = M_p \left[1 - \frac{\Delta A_s \left(\frac{h_o}{4} + e \right)}{Z} \right] \tag{2.7}$$

Where M_p = bending capacity without opening $= F_y Z$; $\Delta A_s = h_o t_w$; e = eccentricity of opening $= |e|$; and Z = plastic section modulus of member without opening.

For Steel Beams with Reinforced Openings:

$$M_m = M_p \left[1 - \frac{t_w \left(\frac{h_o}{4} + h_o e - e^2 \right) - A_r h_o}{Z} \right] \le M_p \quad \text{for} \quad t_w e < A_r \tag{2.8}$$

$$M_m = M_p \left[1 - \frac{\Delta A_s \left(\frac{h_o}{4} + e - \frac{A_r}{2t_w} \right)}{Z} \right] \leq M_p \quad \text{for} \quad t_w e \geq A_r \tag{2.9}$$

Where $\Delta A_s = h_o t_w - 2A_r$.

For Composite Beams:

When the Plastic Neutral Axis (PNA) in the composite beam is located at or above the top of the flange:

$$M_m = M_{pc} \left(\frac{A_{sn}}{A_s} + \frac{F_y \Delta A_s e}{M_{pc}} \right) \leq M_{pc} \tag{2.10}$$

Where M_{pc} = nominal capacity of the composite section at the location of the opening; A_s = cross-sectional area of steel with web openings in the member; A_{sn} = net area of steel section with opening and reinforcement $= A_s - h_o t_w + 2A_r = A_s - \Delta A_s ; \Delta A_s = h_o t_w - 2A_r$; and e = eccentricity of opening, positive upward. Equation 2.10 is always conservative for $A_{sn} \leq A_s$.

When the PNA in the composite beam is located below the top of the flange and $P_c \geq P_{c\min} = F_y \left[\left(3/4 \right) t_w d - \Delta A_s \right]$

$$M_m = F_y A_{sn} \frac{d}{2} + F_y \Delta A_s e + P_c \left(t_s - \frac{\bar{a}}{2} \right) \leq M_{pc} \tag{2.11}$$

Where t_s= thickness of slab; $\bar{a}$= depth of concrete stress block $= P_c/(0.85f'_c b_e)$; P_c= force in the concrete $[P_c \le 0.85 f'_c b_e t_e; P_c \le NQ_n; P_c \le F_y A_{sn}]$.

Equation 2.11 is also accurate when the PNA in the section with web openings is above the top of the flange and provide realistic results if the PNA is in the flange. However, if P_c is small it may provide an unrealistic high prediction of M_m (Darwin and Lucas 1990).

Maximum Shear Capacity

The maximum shear capacity, V_m, is obtained by considering the load condition in which the axial forces in the top and bottom tees, P_t and P_b, equal zero Figure 2.20. This gives a very close approximation of the true pure shear capacity but is not precisely pure shear. While the secondary bending moments at each end of the bottom tee are equal, the secondary bending moments at each end of the top tee are not equal. Therefore, the moment at the opening centreline has a small but finite volume (Darwin and Donahey 1988).

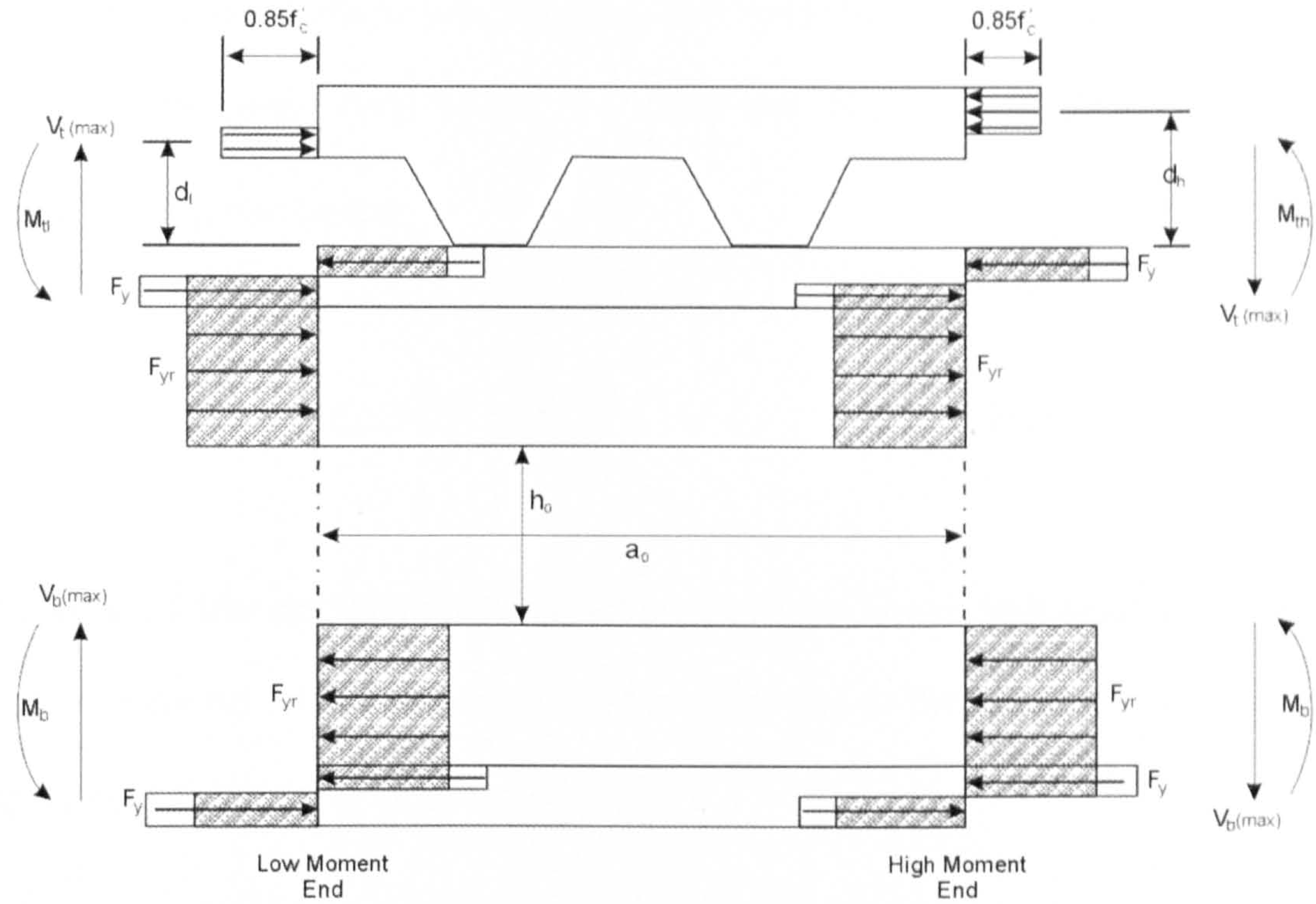

Figure 2.20: Stresses at Maximum Shear (Darwin and Donahey 1988)

V_m is equal to the sum of individual shear capacities of the top and bottom tees:

$$V_m = V_b(\max) + V_t(\max) \qquad (2.12)$$

$V_b(\max)$ and $V_t(\max)$ are calculated using the moment equilibrium equations for the tees (Equations 2.3 and 2.4) and the appropriate representations for the stresses in the steel and concrete. Since $V_b(\max)$ and $V_t(\max)$ are obtained under the combined effects of shear and secondary bending, the interaction between shear and axial stresses must be considered. The greatest proportion of the shear is carried by the steel webs of the tees.

For simultaneous shear and bending, the reduced axial stress within a web, F_{yr}, and the web shear stress, τ, using the Von Mises yield criterion, the equation is given below:

$$F_{yr} = \left(F_y^2 - 3\tau^2\right)^{1/2} \qquad (2.13)$$

To simplify the calculations, interaction between shear and axial stresses is not considered for the concrete, and axial stress in the concrete is assumed to be $0.85f_c^{'}$ when V_m is attained.

The moment capacity of reinforced openings is limited to the plastic bending capacity of the section with web openings (Redwood and Shrivastava 1980).

2.7 Precast Hollow-Core Slabs

Hollow-core floor slabs are used in all building types. The section profile incorporates hollow cores (Figure 2.21) to reduce the self-weight without significant reduction in section stiffness. Hollow core units typically range in depth from 150mm to 450mm. The majority of manufacturers produce units with a nominal width of 1200mm. Reinforcement is provided by high tensile prestressing strand or wire that has an ultimate strength of more than three times that of conventional high tensile reinforcement. The structural performance that results from the combination of these features produces a slab that is highly efficient and economic for a wide range of load/span situations.

Figure 2.21: Precast Hollow-Core Slabs

The edges of hollow core units are profiled to provide an effective shear key so that when the joints between units are grouted (Figure 2.22) the individual units behave as a system acting together. The grout is commonly a C20/25 or C25/30 concrete with 10mm aggregate.

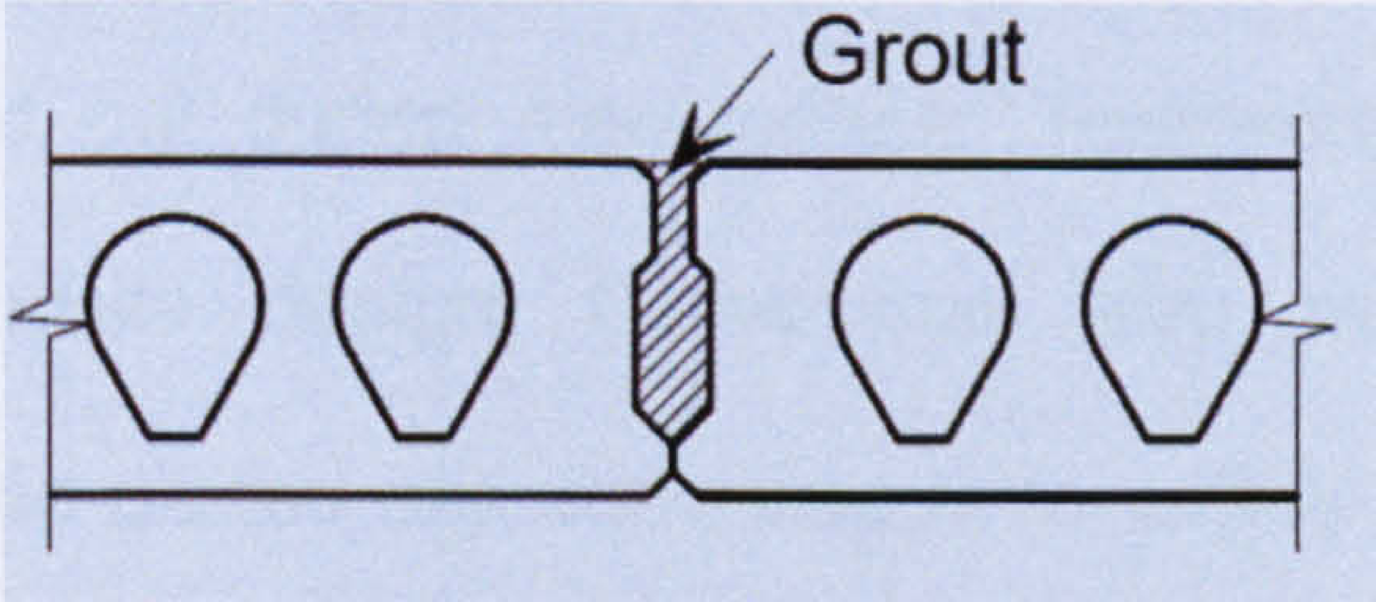

Figure 2.22: Grouted joint between Hollow-Core Slabs

The shape of the cores varies according to the manufacturer and the depth of the unit. Core profiles can be circular, square, elongated circles and bulb shaped. Typical cross-sections of hollow core units are shown in Figure 2.23.

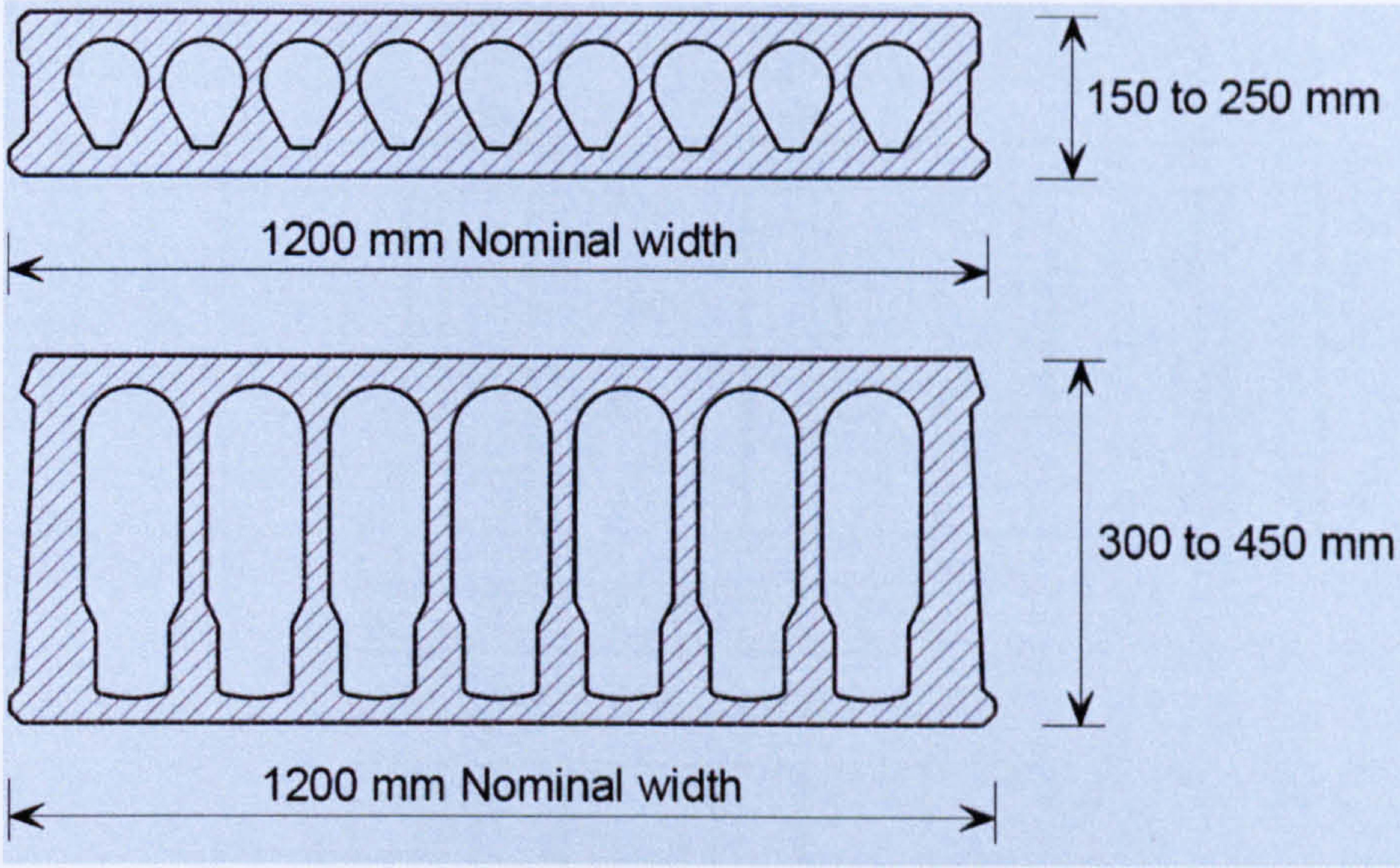

Figure 2.23: Typical cross-sections of Precast Hollow-Core Slabs (SCI Publication P351 2007)

2.7.1 Opened Hollow-Cores

One of the advantages of hollow core units is that some cores can be opened out to receive transverse (transverse to beam) reinforcement. The tops of a specified number of hollow cores (usually two, three or four per unit end, as shown in Figure 2.24) may be opened up. Typically, this opening up operation is carried out during manufacture. Transverse reinforcement is required for composite design. Cores may also be opened so that reinforcement can be placed and concreted in to satisfy tying requirements, with slots typically 500mm long.

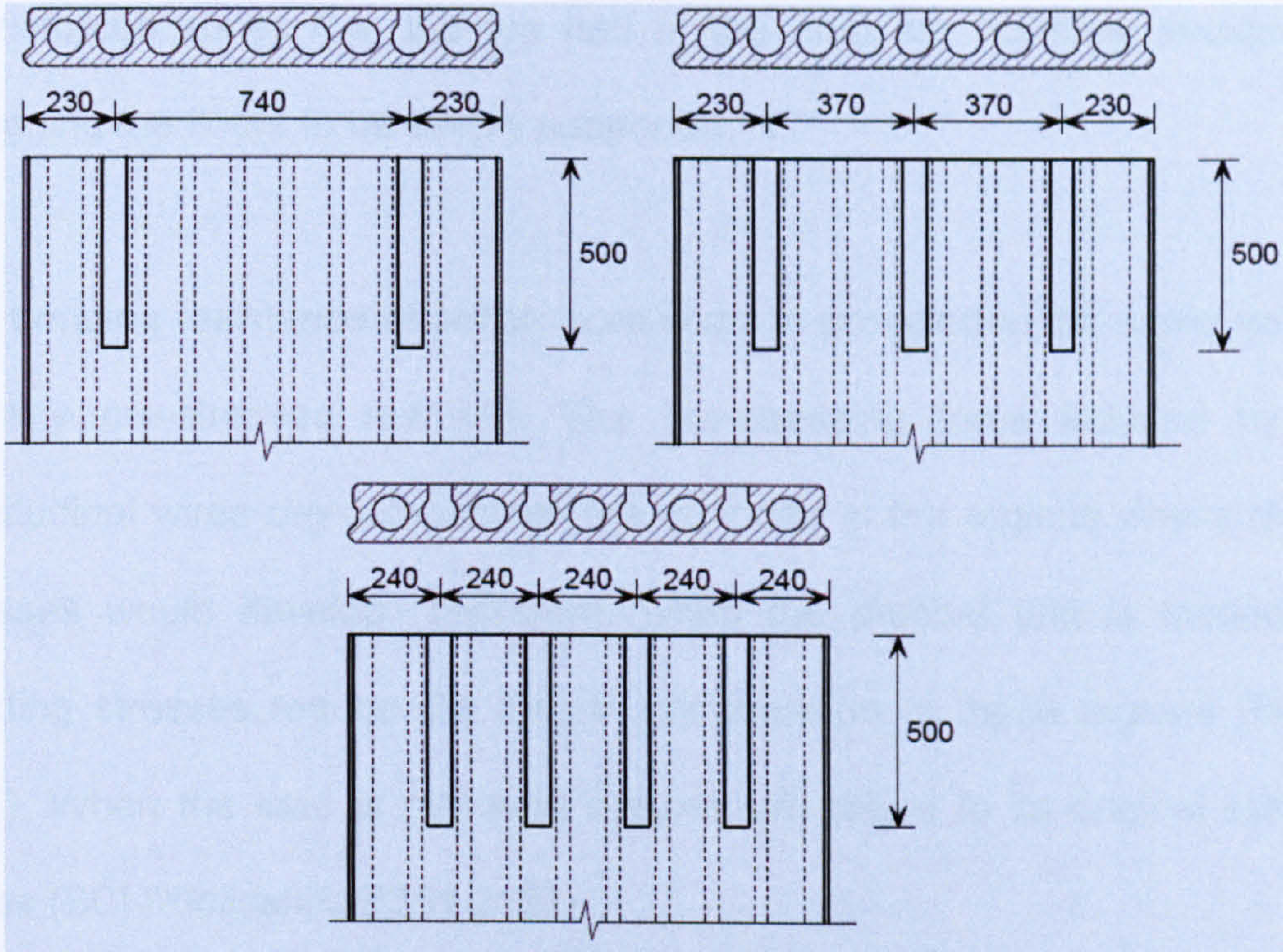

Figure 2.24: Typical details of opened cores

The void at the back of each opened core is blocked with concrete during manufacture; the other cores are normally blocked using a polystyrene bung.

2.7.2 Precast Slab Design

The design of precast units is a traditional pre-stressed concrete analysis with some well established considerations appropriate to its geometrical profile.

The only reinforcement in hollow-core slabs is the longitudinal pre-stressing tendons located in the lower half. The tendons are anchored by their bond with the concrete. Consequently, whenever possible, tensile stresses in unreinforced zones (i.e. the top half of the unit) are normally avoided by designing the floors to be simply supported.

The bending resistance of hollow-core slabs is provided in the same way as for any pre-stressed member. The pre-stressing force induced by the longitudinal wires pre-compresses the concrete in the regions where tensile stresses would develop. Therefore, when the precast unit is loaded the bending stresses reduce the built-in compression in those regions (Figure 2.25). When the load is removed the unit will return to its original state of stress (SCI Publication P351 2007).

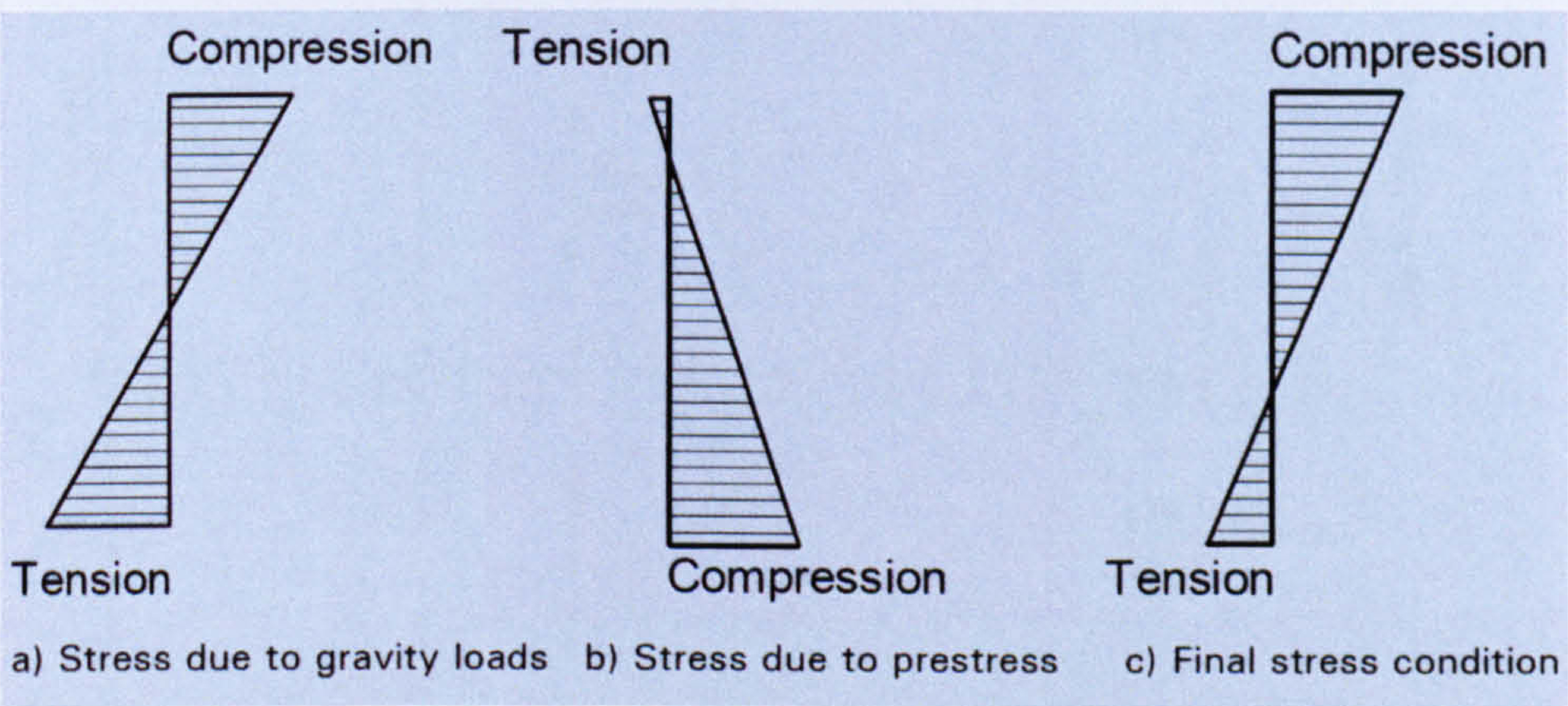

Figure 2.25: Precast slab stresses

2.7.3 Floor Diaphragm Action

The floor is often required to provide diaphragm action in order to transfer wind loads to braced walls or concrete core walls (Figure 2.26). In a steel frame building with precast unit floors, the diaphragm action can be achieved through a combination of the following measures:

- Utilisation of the shear resistance of the grouted joints between the precast units.
- Provision of a continuous in-situ reinforced topping to enhance the diaphragm action provided by the grouted joints (a topping is recommended for larger floors or taller buildings).
- Ties between the perimeter members and the floor units.
- Ties between the floor units and the shear walls or reinforced cores.
- Encasement of columns into the floor.

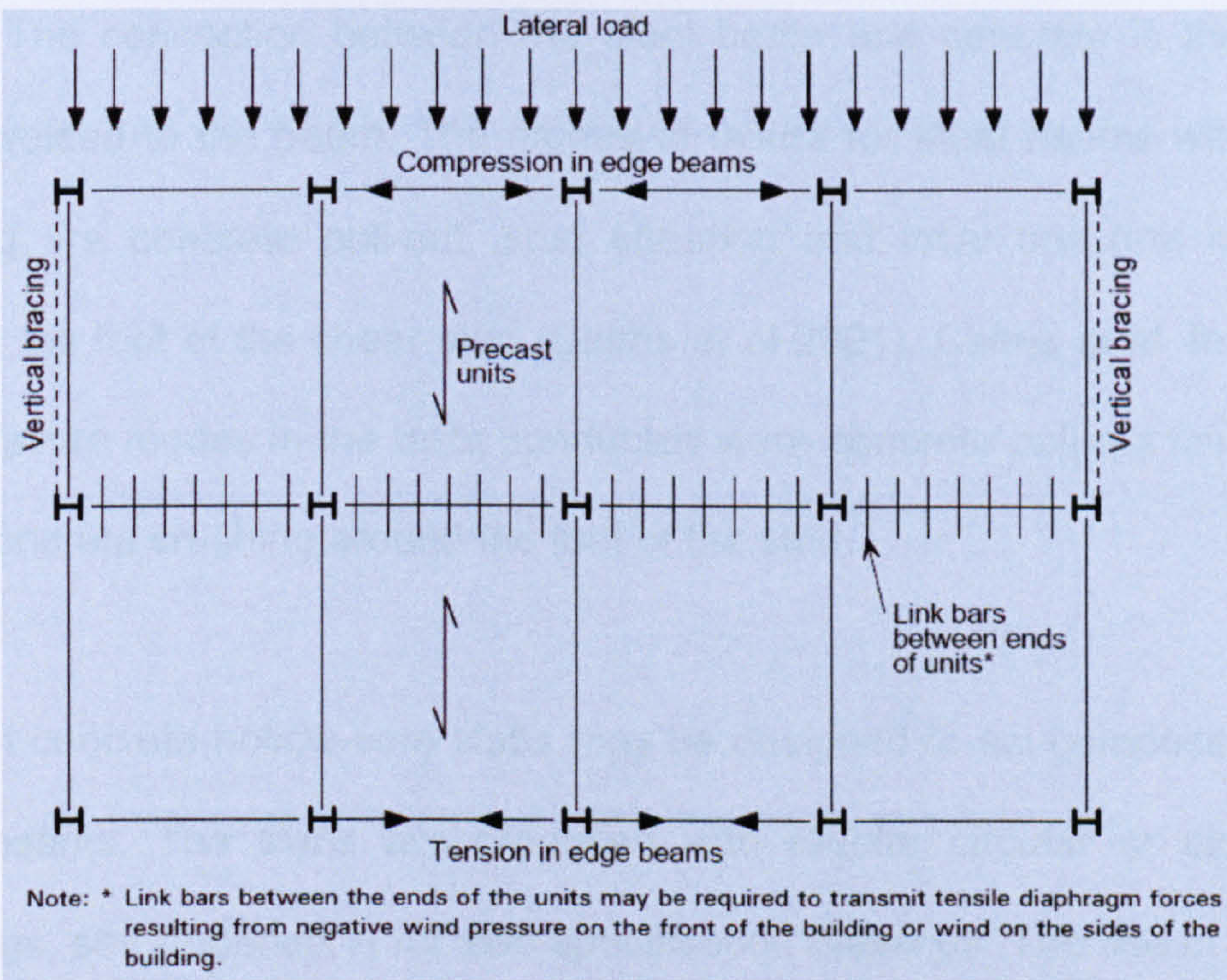

Figure 2.26: Diaphragm action in a precast slab floor (SCI Publication P351 2007)

To ensure that the whole floor acts together, the longitudinal joints between the slabs must be grouted and allowed to cure before an in-situ concrete topping is poured. When a structural topping is provided with precast floors acting compositely with steel beams using shear studs, floor diaphragm action is generally adequate for buildings with regular rectangular floors of normal proportions without large openings (SCI Publication P351 2007).

2.8 Composite Beams with Precast Concrete Hollow-Core Slabs

The most common form of composite beams in buildings, use steel beams with metal decking. The metal decking is placed on the beam as a form of permanent formwork for the concrete which is poured once the decking is in place. The connection between the steel beam and concrete is the shear studs welded to the beam. The modes of failure for steel beams with metal decking are concrete pull-out, stud shearing and local concrete crushing around the foot of the shear stud (Cairns et al 2001). Cairns et al. found the major failure modes in the tests conducted were concrete pull-out failure and local concrete crushing around the foot of the stud.

Precast concrete hollow-core slabs may be designed to act compositely with steel beams. The slabs are produced with regular circular or elongated openings, see Appendix A for slab specification drawings. The use of precast concrete hollow-core slabs uses the same principle as metal decking. But there is no metal deck and pouring of the concrete floor. The slabs are cast from the factory, and can be placed on delivery to site. The only in-situ concrete needed is to cast the joint between the steel beam, precast concrete slab and transverse reinforcement (Figure 2.27).

Composite steel beams with precast concrete hollow-core slabs, as shown in Figures 2.27 and 2.28 are commonly used in long span multi-storey steel framed buildings. The slabs are placed on the top flanges of universal beams (UBs). The main advantages of this form of construction are that precast concrete slabs can span up to 15m without propping and the erection of 1.2m wide precast concrete units is simple and quick. Shear studs are pre welded onto beams before delivery to site, thereby offering the savings associated with shorter construction times (Lan 2002).

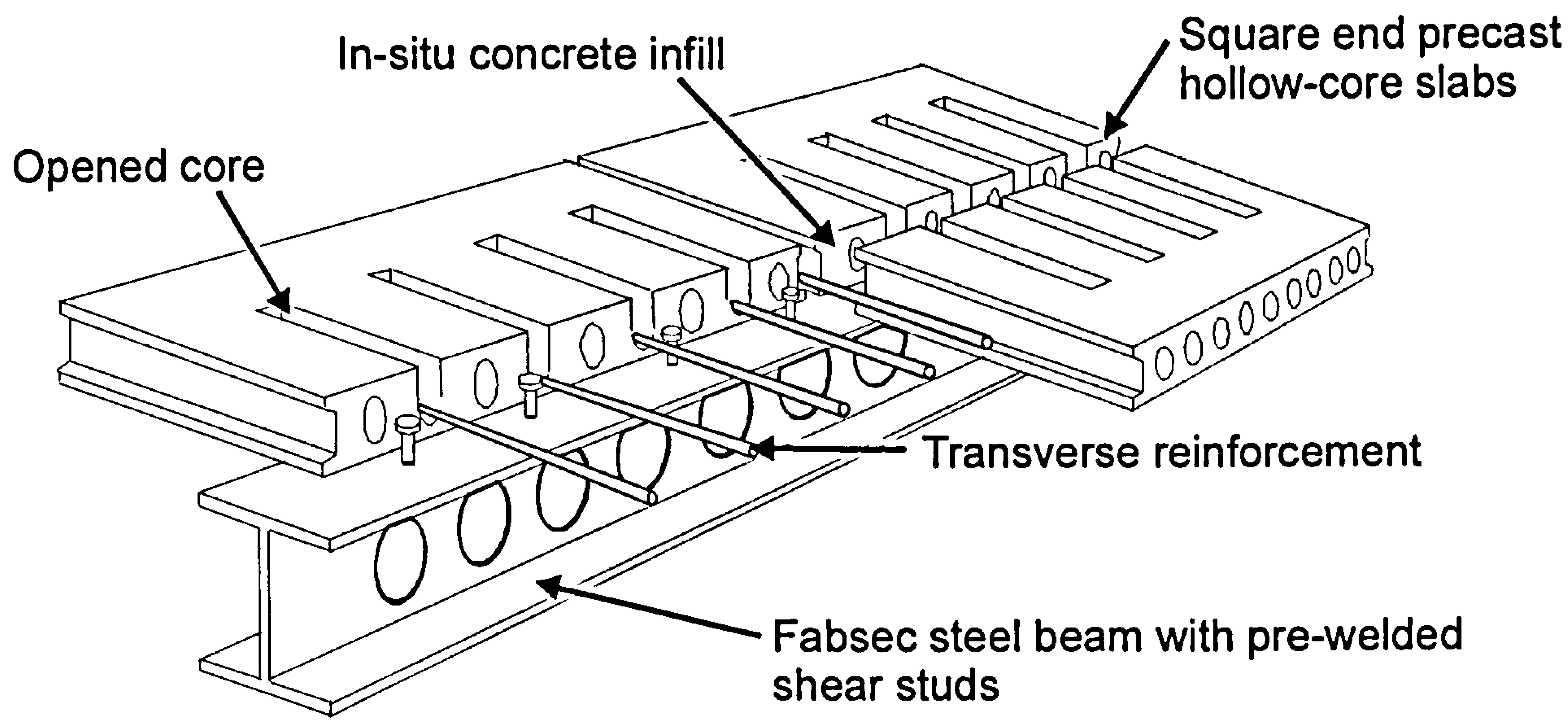

Figure 2.27: Composite Beam with Precast Hollow-Core Slabs

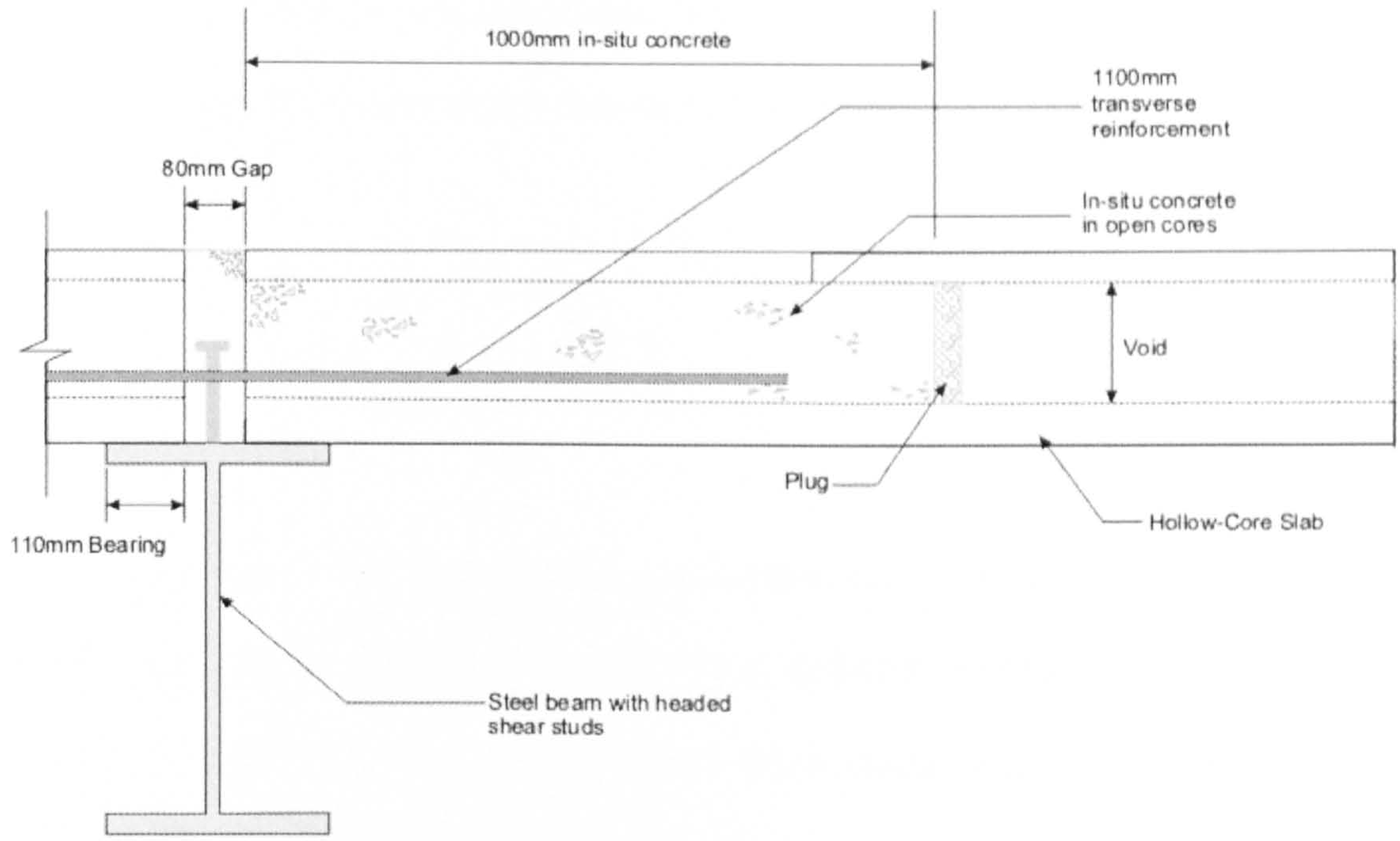

Figure 2.28: Cross-section of Beam with Precast Hollow-Core Slabs

Hollow-core slabs have longitudinal voids, and are produced on a long pre-stressing bed, either by slip form or extrusion, and are then saw-cut to length. The slabs depth ranges from 150 to 400mm, with the performance limited to a maximum span/depth ratio of around 50, although 35 is more usual for office loading conditions. The horizontal compressive forces are transferred through the slab the joint between the units being filled with in-situ concrete (Figure 2.20). The compressive strength of the infill may vary from 20-40N/mm^2, although 30N/mm^2 is normally used in design (Lam 2002).

Experimental tests (Lam 1998), together with a parametric study conducted by Elliott et al. found that an increase in transverse reinforcement significantly increases the moment capacity but, as ductility is reduced, a brittle failure of the composite beam is found due to crushing failure of the concrete slab. In addition, increases in slab thickness lead to increases in moment capacity, though slab failure might occur due to direct tensile force in the slab (Elliott et al 2000).

2.9 Summary

There has been a lot of research conducted into steel-concrete composite beams, most of which is concerning metal decking. Research conducted by Lam et al. show that the use of hollow-core slabs with steel beams is as competent as metal decking used with steel beams for multi-storey buildings. But, little research has been carried out into the use steel beams with web openings and precast concrete slabs to form long span composite beams. The concept of using steel beams with web openings and precast hollow-core slabs could have potential benefits in the design of multi-storey buildings. Therefore, this project is designed to investigate the behaviour of composite steel beams with web openings and precast hollow-core slabs. The aim of the research is to investigate the performance of composite beams with the position of the neutral axis in the concrete and also establish the effective width. By varying the beam size, span of beam, shear connection and slab depth in five full-scale experiments, the behaviour of the composite beam will be established.

Chapter 3

Beam Design and Test Setup

Chapter 3: Beam Design and Test Set-up

3.1 Introduction

Five full scale long span composite beams consisting of steel I-sections and precast hollow-core concrete slabs were tested. The main variables for this research were the stud spacing (degree of shear connection), span of beam and depth of hollow-core slab. Prior to testing the composite beams, six push tests were performed to establish the capacity of 19mm x 125mm headed shear studs in square end hollow-core slabs. This chapter describes the test specimen design, testing arrangement, instrumentation used for the experiment, loading procedure and material testing.

3.2 Push Test for Hollow-Core Slabs

The push tests were set up as proposed by Lam (Lam 2006); with test specimens each consisting of four 600mm wide x 800mm long pre-stressed hollow-core units connected to a 254 x 254 x 73 UC with a single row of 6 pre-welded headed studs at 150mm centres. The first stud is located 200mm from the end of the slabs as suggested in the Eurocode 4. Cores of 500mm long were left open to allow placement of the transverse reinforcement. The 600mm slab width was chosen instead of the common 1200mm width so that the effect of the transverse joint could be observed. Figure 3.1 shows the general arrangement of the horizontal push test and Figure 3.2 shows the push test specimen before casting of in-situ concrete. LVDT's are used to measure longitudinal slip at the end of the slabs until the load has dropped to 20% below the maximum load reached. This enables the load and slip capacity to be determined and the results are shown in Chapter 4.

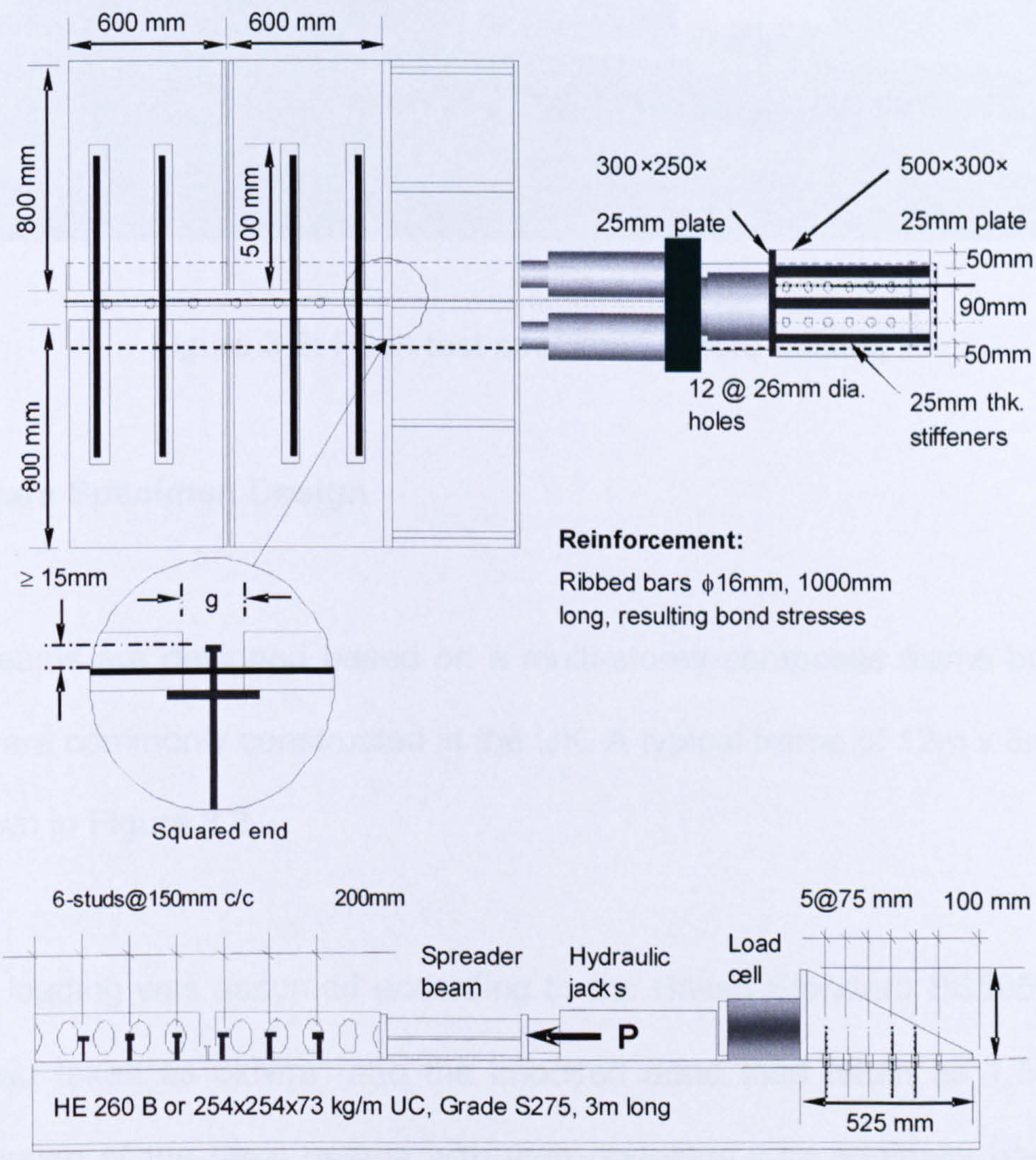

Figure 3.1: General arrangement for horizontal push test

Figure 3.2: Push test specimen before casting

3.3 Beam Specimen Design

The beams are designed based on a multi-storey composite frame building, which are commonly constructed in the UK. A typical frame of 12m x 8m bays is shown in Figure 3.3.

Office loading was assumed according to the British Standard BS5950, with live load taken as $5kN/m^2$ and the imposed dead load taken as $1.5kN/m^2$. The design of the steel beams with web openings was originally based on SCI Publication 100. The SCI design code gave the size of beam as UB610x305x238 with 400mm web openings for a castellated steel beam. Using the beam size from the castellated design, the steel beams were specified for fabrication by Fabsec Ltd (See Appendix A for beam specification drawings). The equivalent steel beams fabricated were 640x300

Fabsec beams (30mm flanges with a 20mm web) with varying shear connection, also fabricated was a 457x191x89UB for the 9m span test.

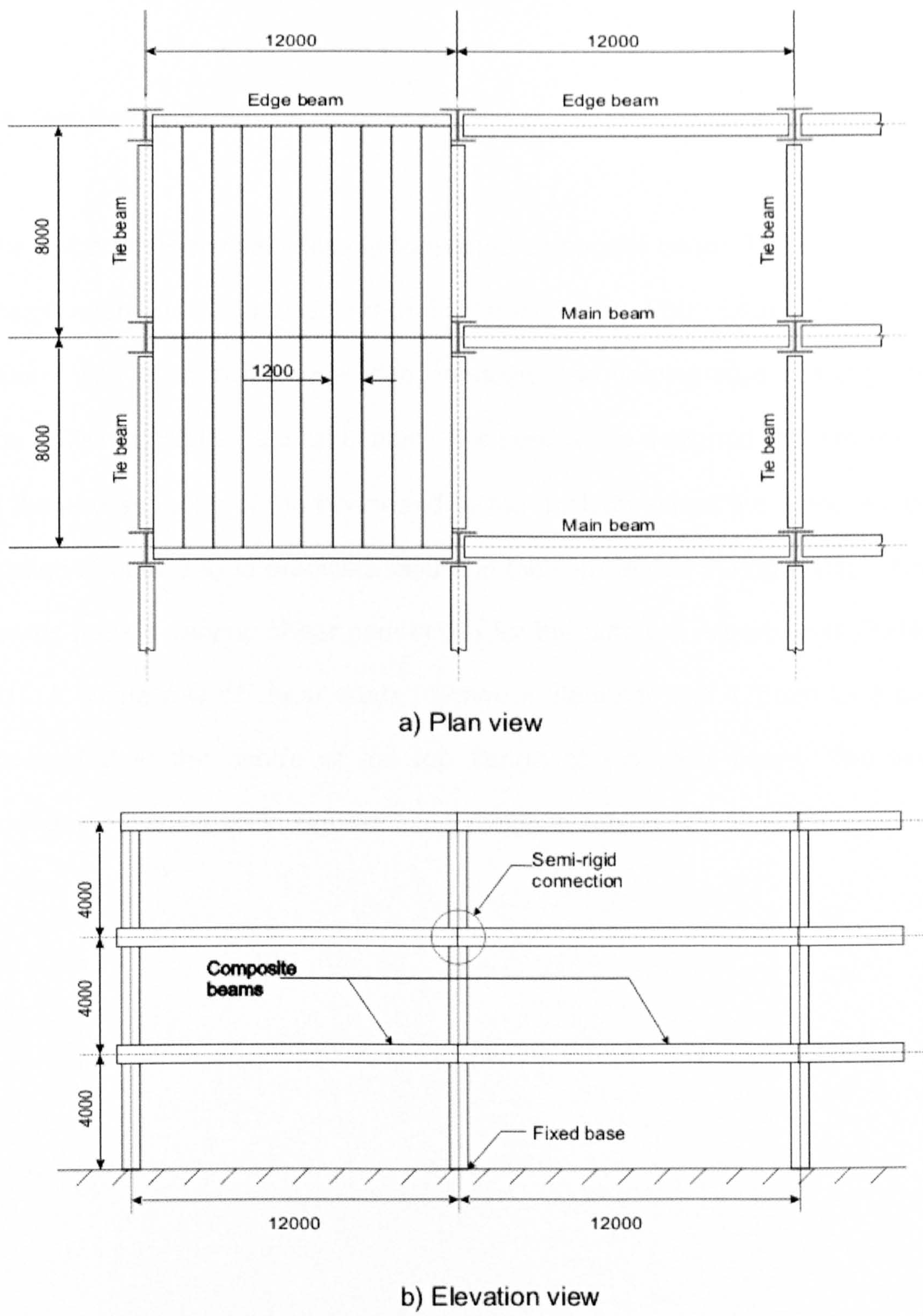

Figure 3.3: Typical floor arrangement of steel/hollow-core slab structure

The precast hollow-core concrete slabs were manufactured by Bison Concrete Products Ltd. The slab depth (200 and 400mm) is the only variable for the concrete in the tests conducted. Appendix A shows the specification of the precast concrete slabs and technical information.

3.4 Test Setup

The test arrangement is a simply supported composite beam. The steel beam specification drawings are shown in Appendix A. Four 640x300 Fabsec beams with 400mm diameter web openings and varying stud spacing and one 457x191x89UB were fabricated. The beams are designed with stiffeners at the end supports of the beam and at the position where the loads will be applied (Figure 3.4) to eradicate failure in the web region during testing. The beams have a varying shear connection for the different experiments (Table 3.1). A single row of shear studs, 19mm in diameter and 125mm long are pre-welded in the centre of the top flange of the steel beam. The test arrangement is shown in Figures 3.5, through to 3.10.

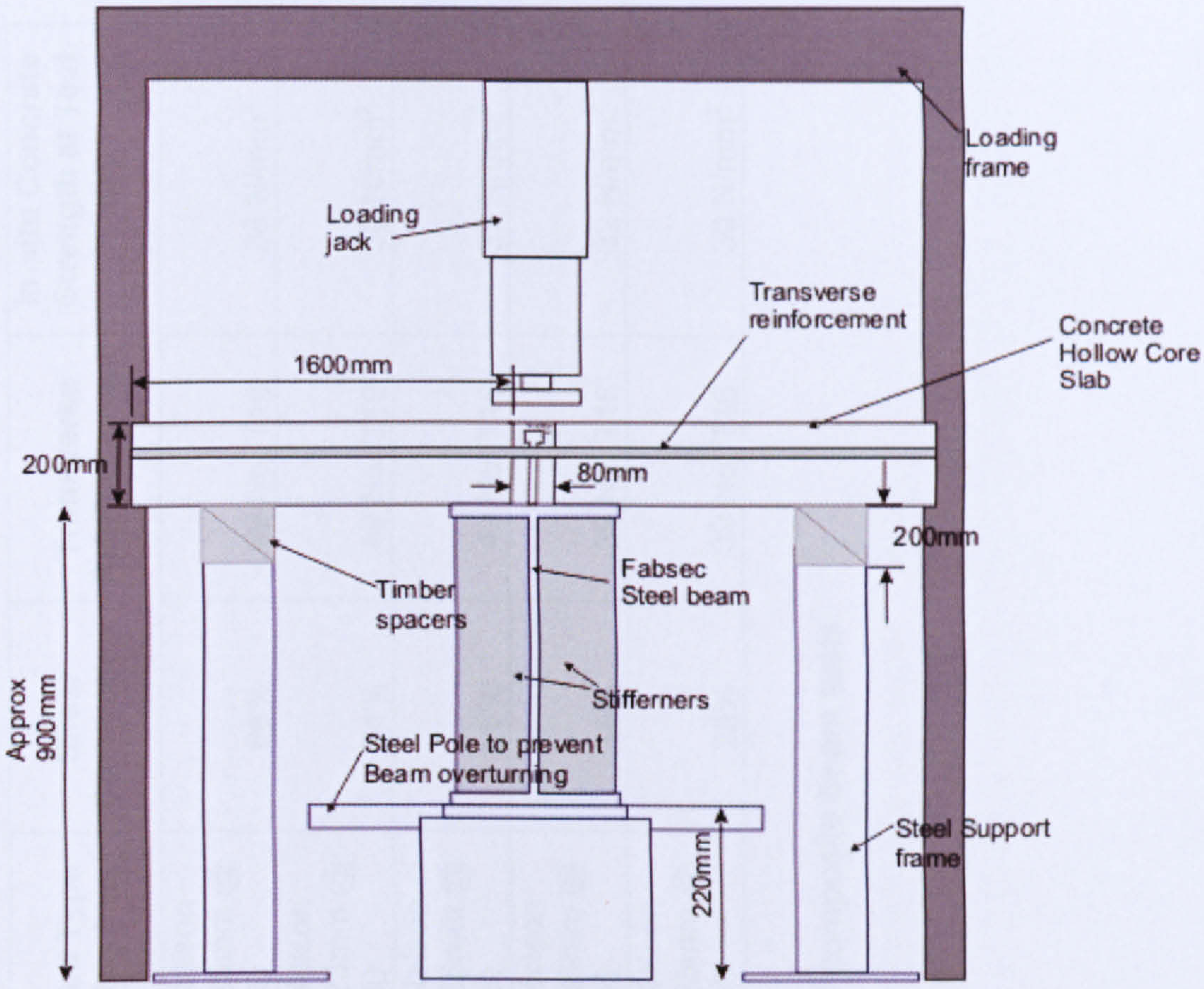

(a) Elevation beam test specimen setup

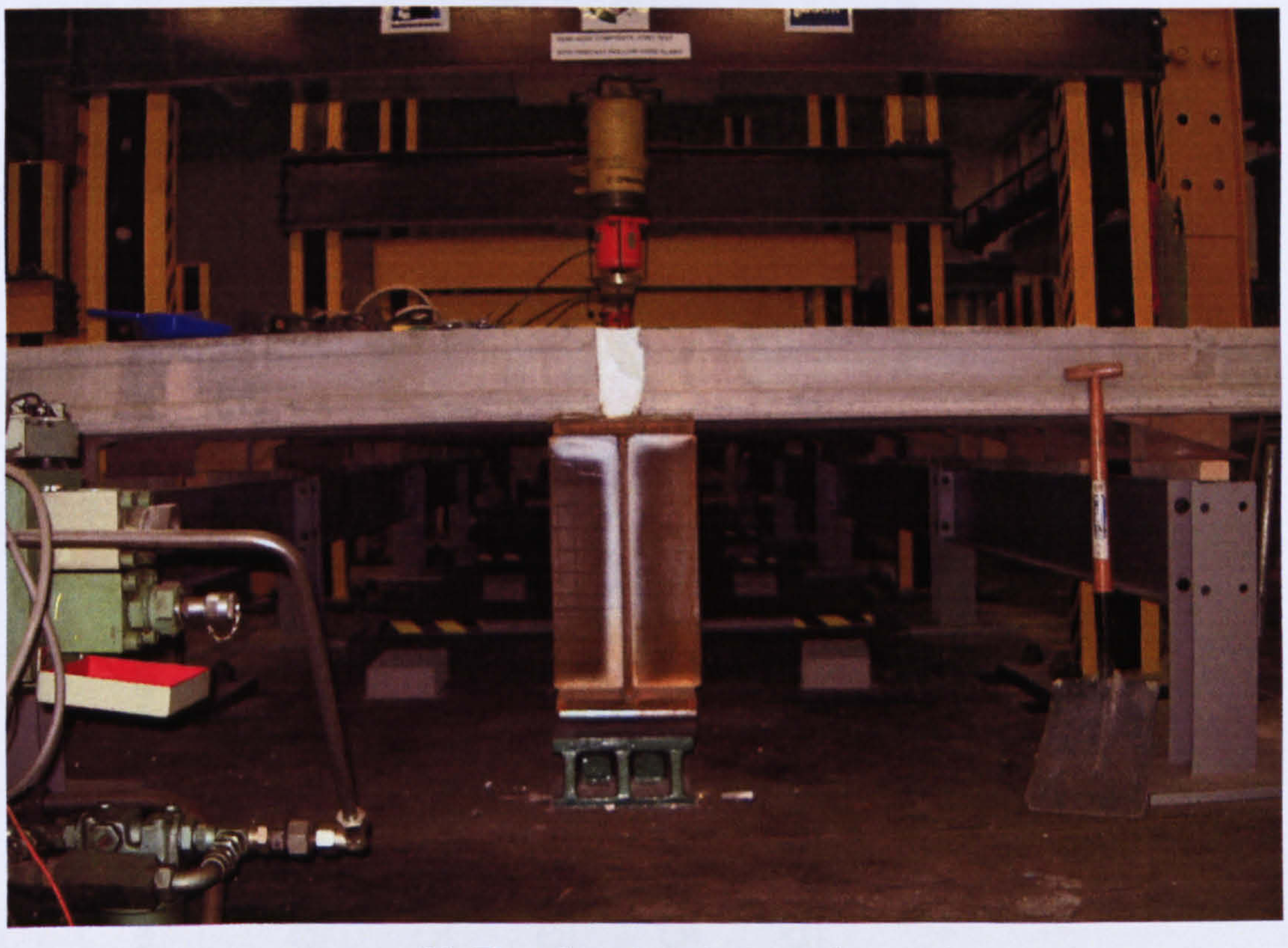

(b) Elevation photo test specimen setup

Figure 3.4: Elevation of composite beam test specimen

Test No.	Beam Size	Hollow-core Slab Depth	Span	Shear Stud Type and Spacing (mm)	Shear Connection	Transverse Reinforcement	In-situ Concrete Strength at Test day
CB-1	640x300 Fabsec	Bison 200mm HCU	12m	TRW-Nelson 19mmx125mm @ 150	68%	49 No. T16	38 N/mm^2
CB-2	640x300 Fabsec	Bison 200mm HCU	12m	TRW-Nelson 19mmx125mm @ 300	34%	49 No. T16	30 N/mm^2
CB-3	640x300 Fabsec	Bison 200mm HCU	12m	TRW-Nelson 19mmx125mm @ 400	26%	49 No. T16	35 N/mm^2
CB-4	437x191x89UB	Bison 200mm HCU	9m	TRW-Nelson 19mmx125mm @ 200	38%	39 No. T16	32 N/mm^2
CB-5	640x300 Fabsec	Bison 400mm HCU	12m	TRW-Nelson 19mmx125mm @ 400	26%	39 No. T16	30 N/mm^2

Table 3.1: Test parameters of composite beam tests

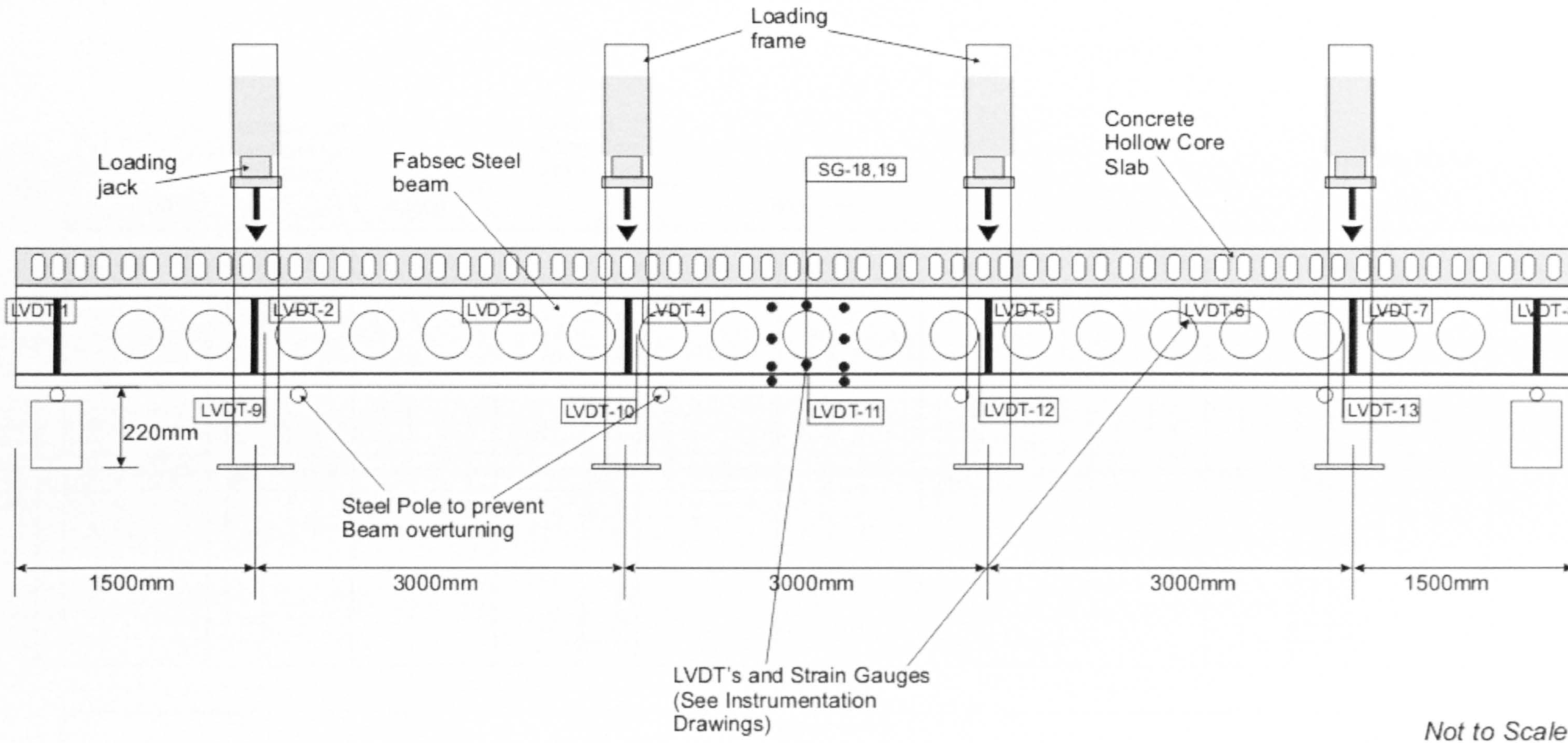

Figure 3.5: General arrangement of test set-up

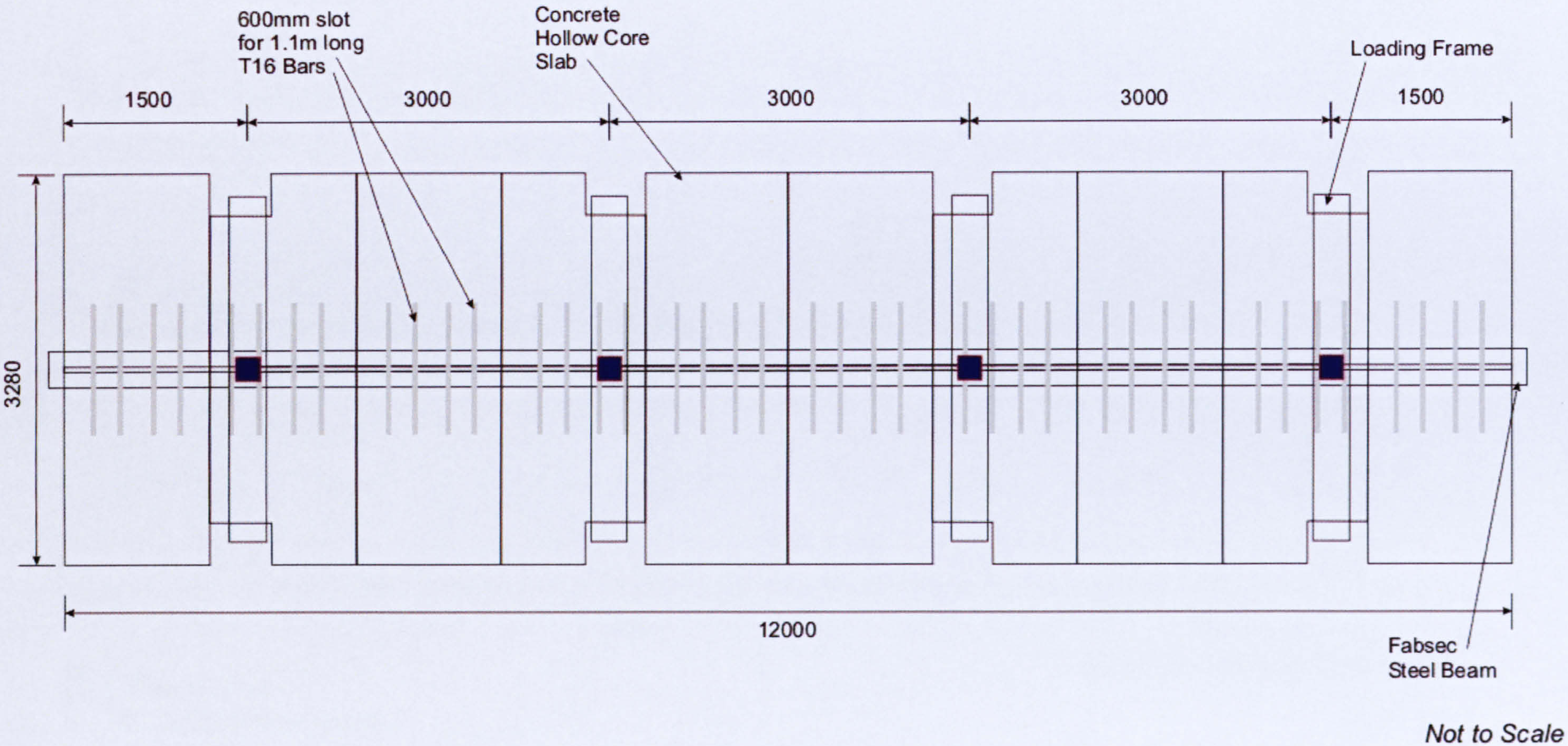

Figure 3.6: Plan view of test set-up

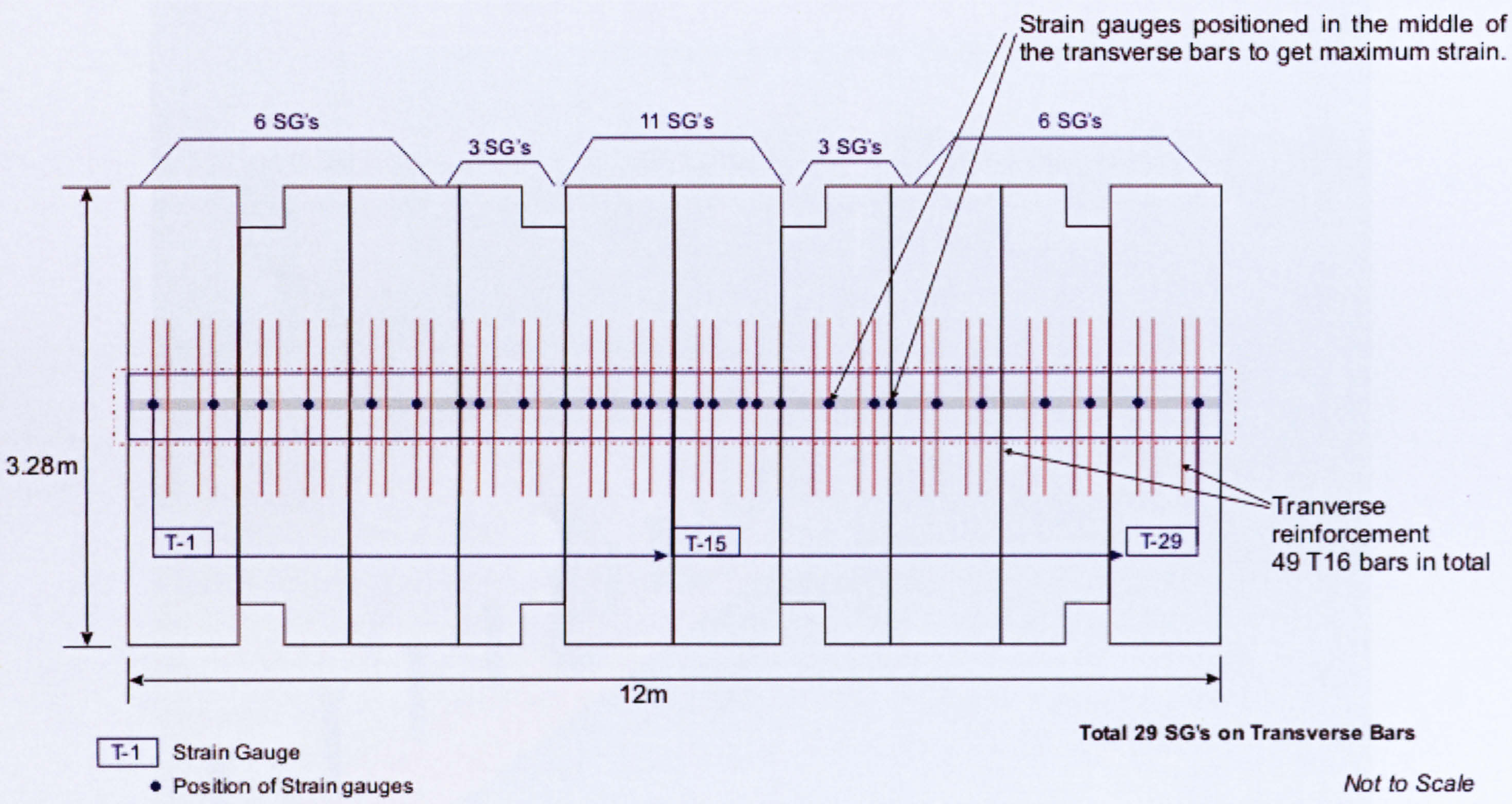

Figure 3.7: Plan view of test set-up with strain gauge positions

Figure 3.8: Placement of slabs on steel beam

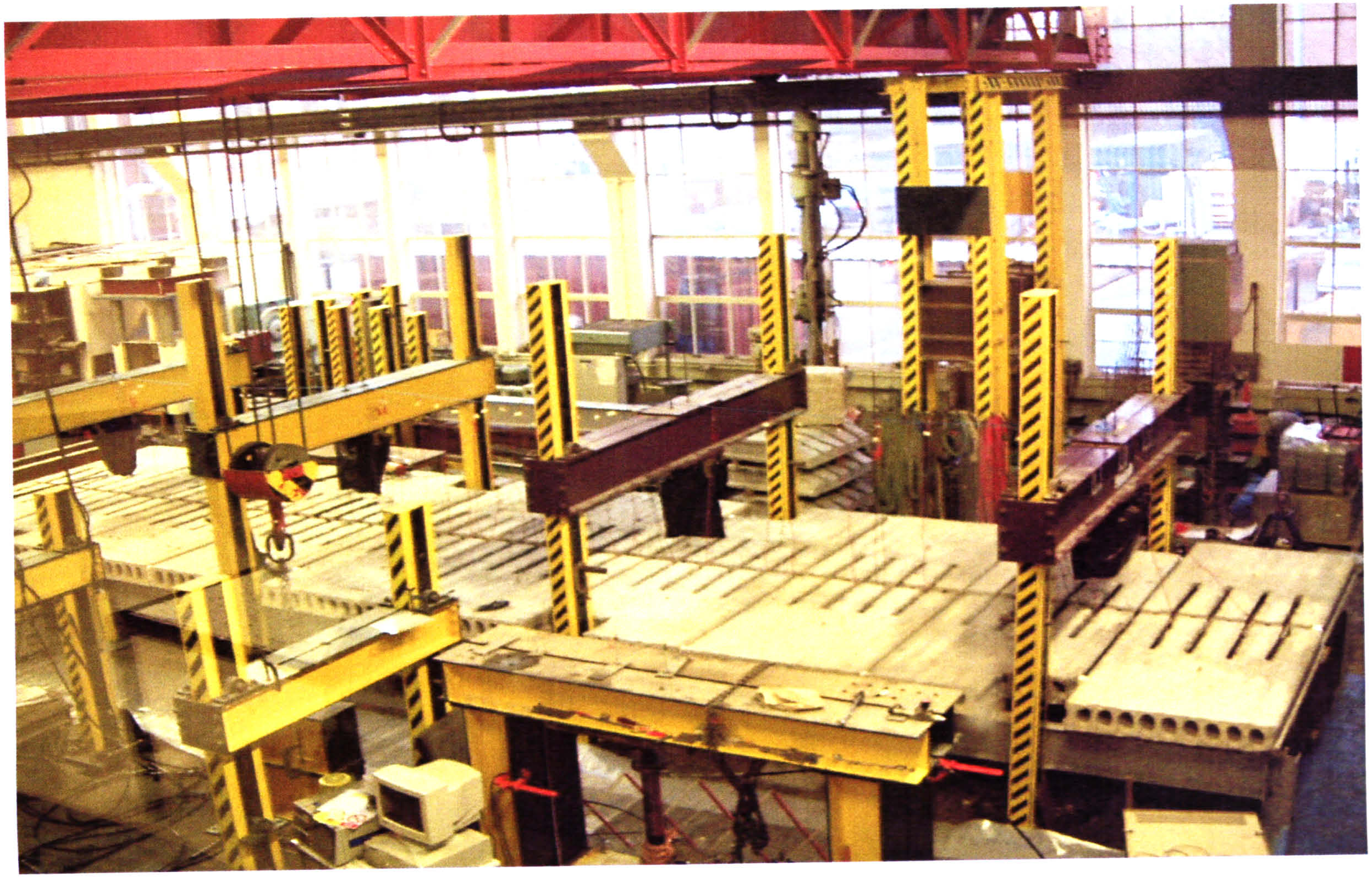

Figure 3.9: General arrangement of test set-up prior in-situ cast

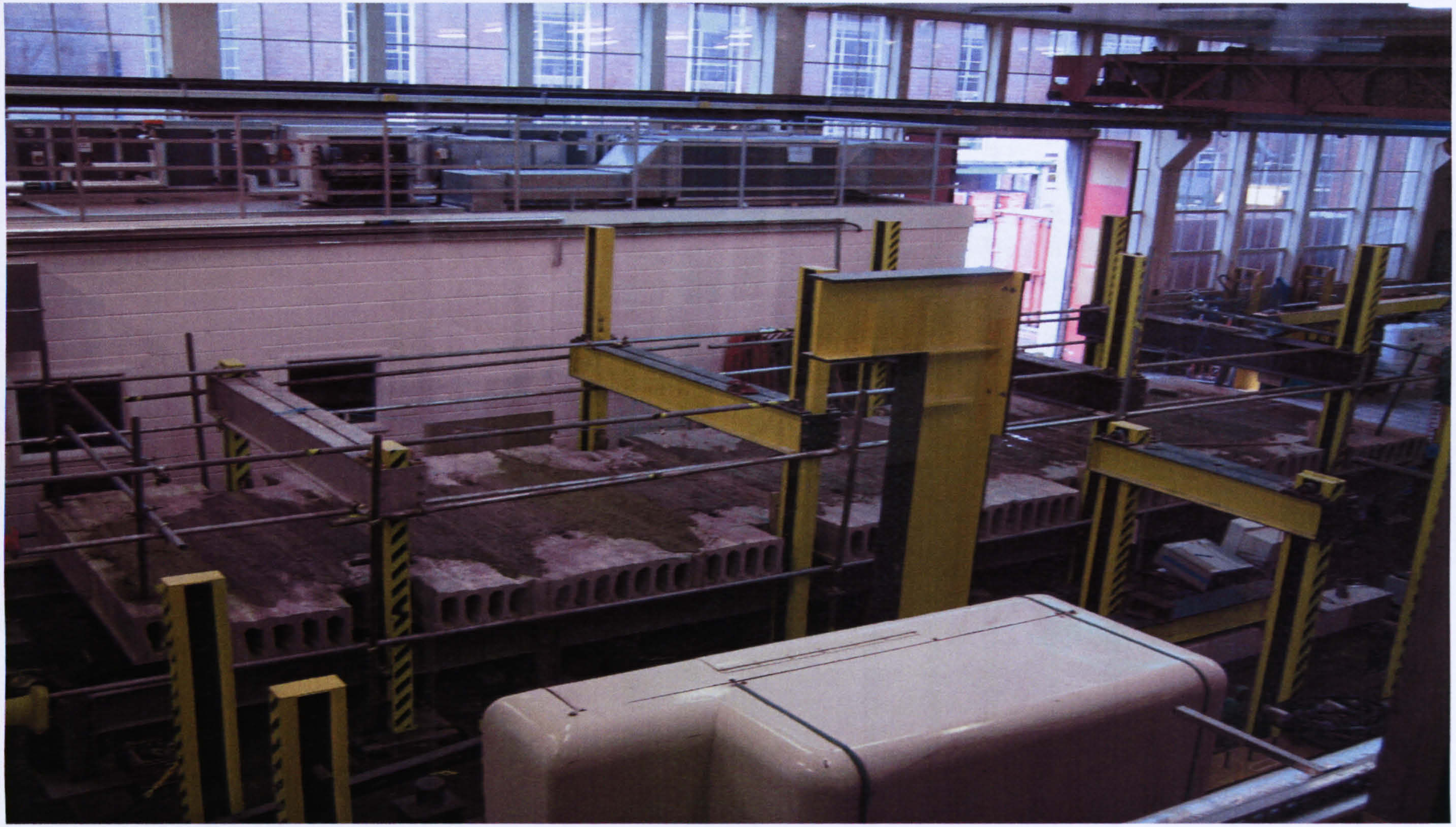

Figure 3.10: General arrangement of test set-up after in-situ cast

Placed on the Fabsec steel beam were Bison precast hollow-core slabs. A total of twenty slabs was used for each 12m span test (ten slabs placed on either side of the beam), and eighteen slabs for the 457UB 9m spanning test. The hollow-core units are 1600mm wide and 1200mm long with three or four 600mm opening slots for the placement of the transverse reinforcement. The depth of the slab used was 200mm and 400mm for the different experiments (Table 3.1). The hollow-core units were connected transversely by reinforcing bars across the slots and between the units. The transverse reinforcement was 1100mm long and 16mm diameter (T16) reinforcing bars placed in the 600mm slots within the slabs. In-situ concrete was poured into the 80mm gap between the slabs and into the slots once the transverse bars were placed.

The top cover to the transverse reinforcement was approximately 150mm for the 200mm deep slabs and 350mm for the 400mm slabs. Once the composite beam test was set up, the specimen was cast with the in-situ concrete. The in-situ concrete had a concrete slump of a minimum 75mm (workability), so the concrete could fill the gaps in the connection of the composite beam. The in-situ concrete of a strength grade C30 (30N/mm^2 at 28 days) was aimed for all tests.

When casting the in-situ concrete, two 30mm vibrating pokers were used to ensure the concrete flowed into all the openings in the slabs to form the composite connection. The core openings at the edge of the slabs were filled with paper/polystyrene (Figure 3.11) up to 1m from the centreline of the beam, so that during casting the concrete would not pour out of the sides.

After casting the connection, the top of the composite beam was covered with polythene sheeting and left to cure (Figures 3.12 and 3.13). The cylinders, prisms and cubes for each cast were cured under the same conditions as the specimen and were tested at 7, 14 and 28 days.

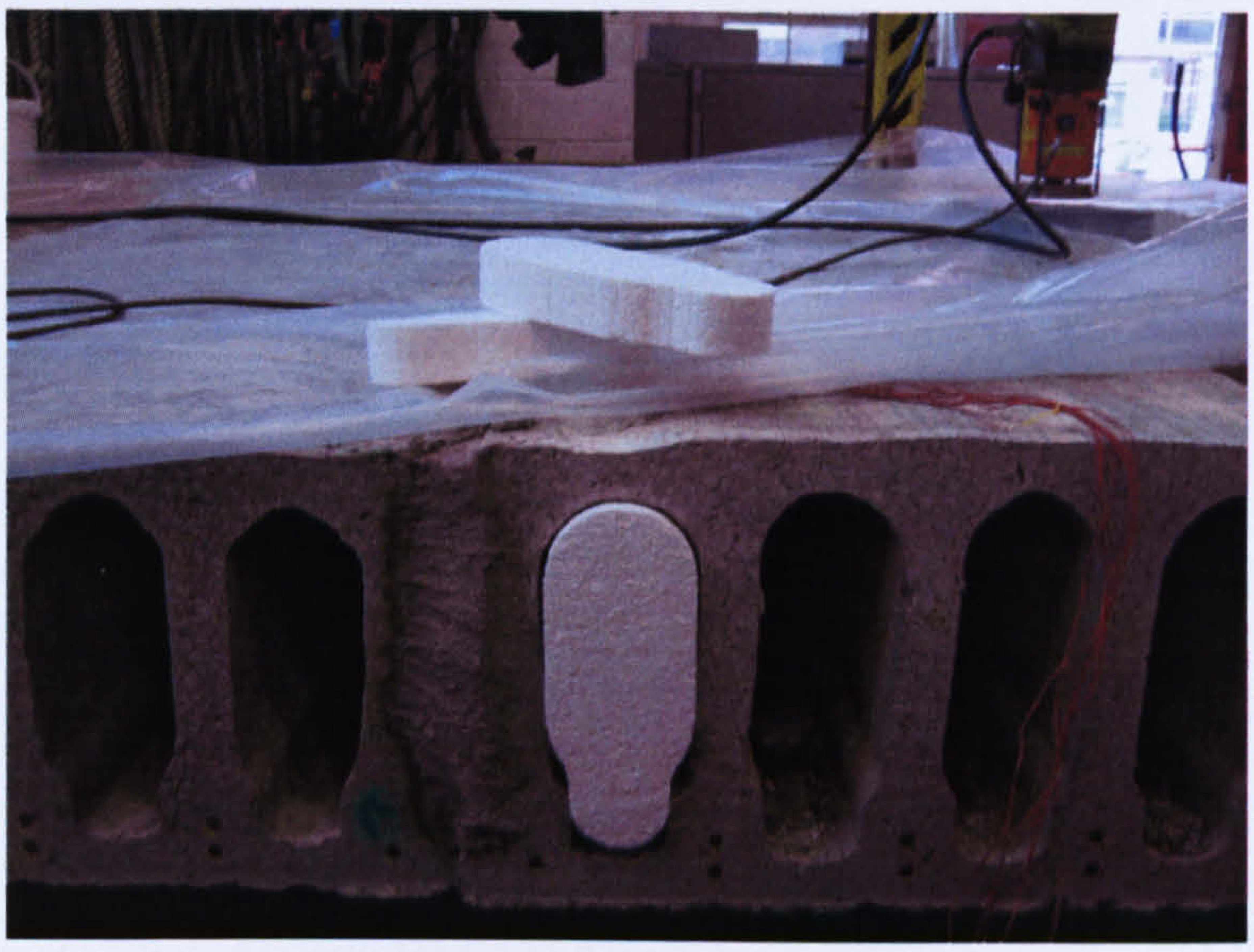

Figure 3.11: Polystyrene bung

Figure 3.12: Composite beam covered for curing

Figure 3.13: Composite beam covered for curing (end view)

A steel support frame was designed to support the slabs while the test specimen was being put together. Also, scaffolding poles are attached to the bottom flange of the beam, to prevent the beam from overturning. The support frame and poles were used as safety apparatus and these were removed before testing.

The main components of the test rig consisted of four 500kN hydraulic jacks on the 12m span tests and two 500kN jacks on the 9m test with load cells placed between the jacks and the top slab surface to record the load during testing. A single manual pump was used for all jacks so loading was applied simultaneously to the composite beam. To improve distribution of load, square steel plates of size 300x300mm in area and 50mm in depth were placed between the hydraulic jacks and precast concrete surface.

Figures 3.4 to 3.13, shows the experimental setup for the test of the composite beam. Table 3.1 shows the variations in the testing of the composite beam.

3.5 Instrumentation

Instrumentation included linear voltage displacement transducers (LVDT's) and electrical resistance strain gauges (ERSG's). The LVDT's were used for measuring vertical deflection and horizontal slip of the composite beam specimen, while ERSG's were used on the steel beam, shear studs and transverse reinforcing bars to measure strain.

3.5.1 Strain Gauges

Strain gauges (ERSG's) were used on the steel beam (web, flanges and shear studs) and the transverse reinforcement. The gauges used were of type FLA-5-11 with a length of 5mm, the resistance of the gauge was $120 \pm 0.3\Omega$ with a gauge factor of 2.13. Strain gauges were placed around the centre web opening of the beam (Figures 3.14, 3.15 and 3.16) and on the top and bottom flanges. The readings from the gauges placed on the flanges, would allow the strain profile to be plotted, and the position of neutral axis will be obtained.

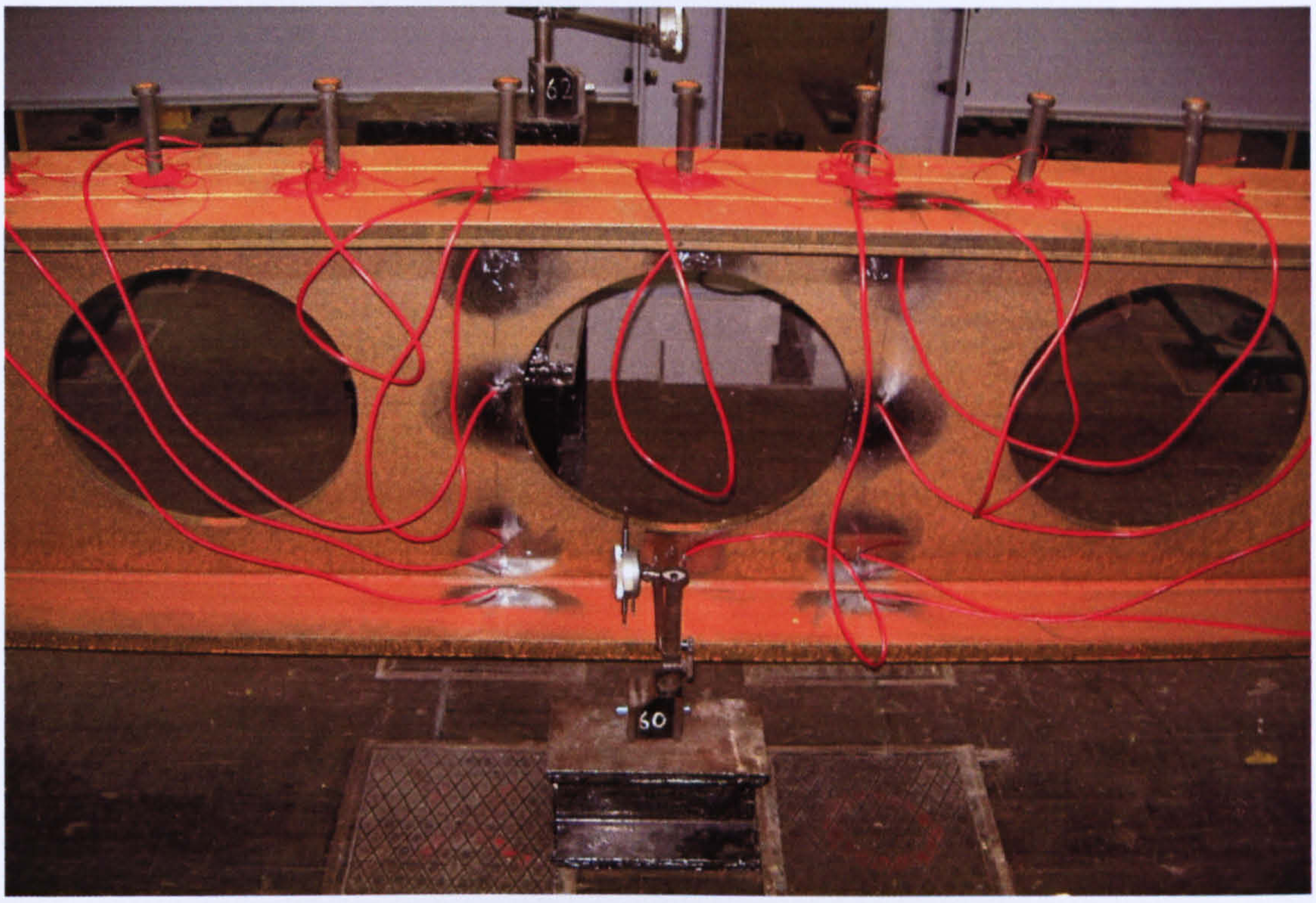

Figure 3.14: Location of strain gauges around centre opening

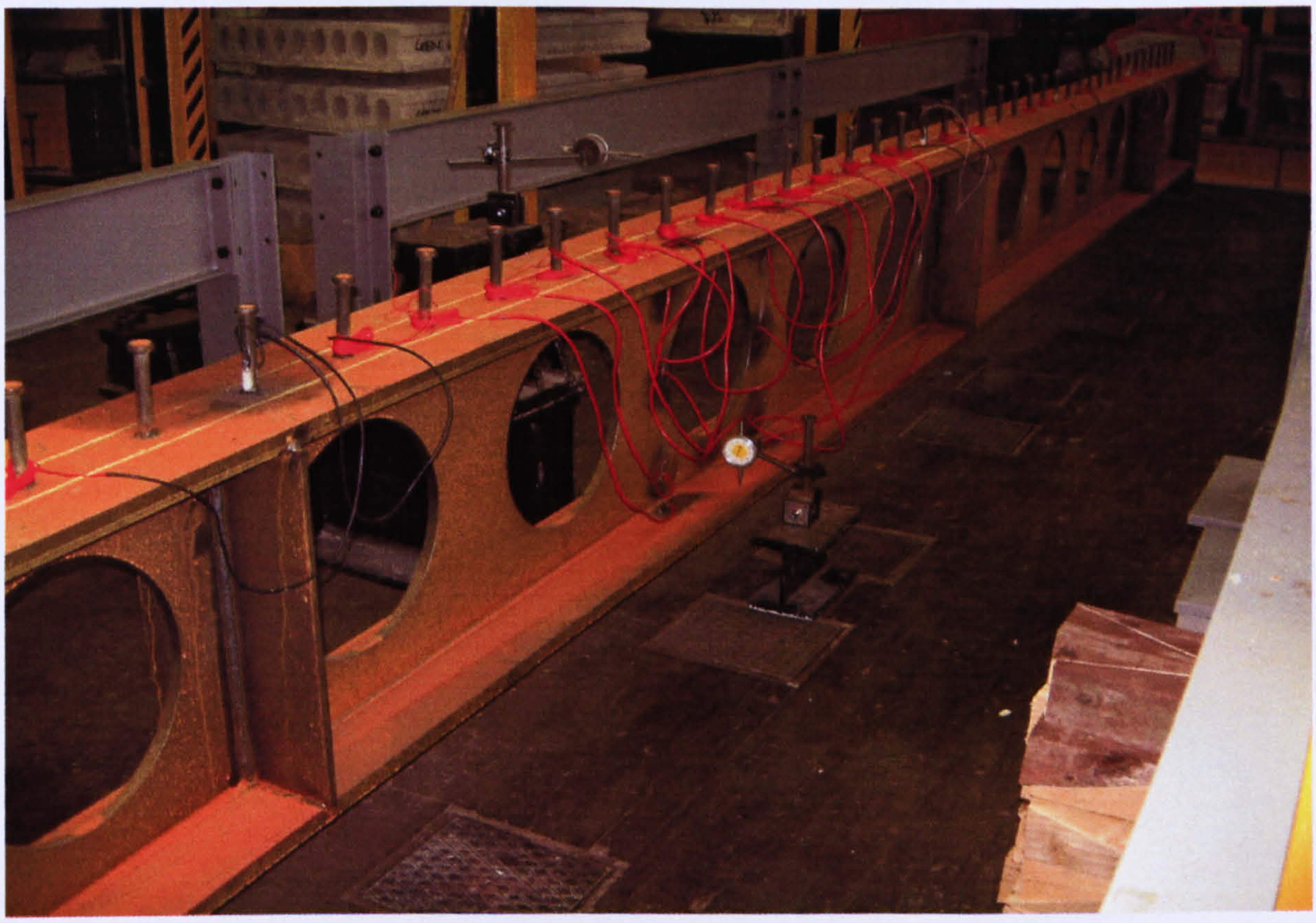

Figure 3.15: Strain gauges along steel beam

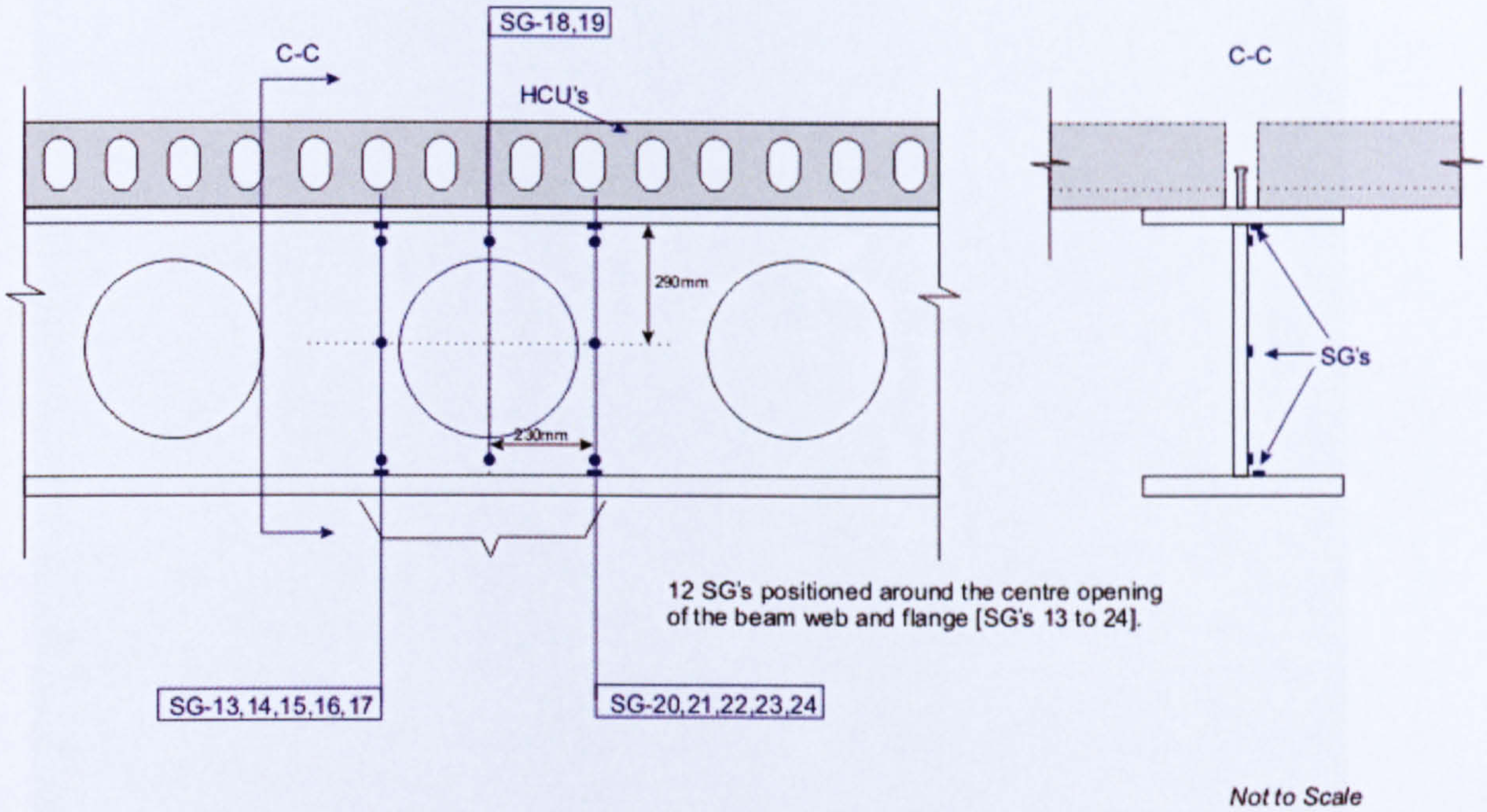

Figure 3.16: Position of strain gauges around centre opening

Gauges were also placed on shear studs and in the centre of the transverse reinforcing bars and were protected with heated shrink wrap (Figure 3.17). Twelve studs were gauged with a gauge placed on either side of the stud, in order to establish the behaviour of the stud during testing. These gauges (on studs and reinforcing bars) were coated with an epoxy resin to protect them from the in-situ concrete (Figure 3.18).

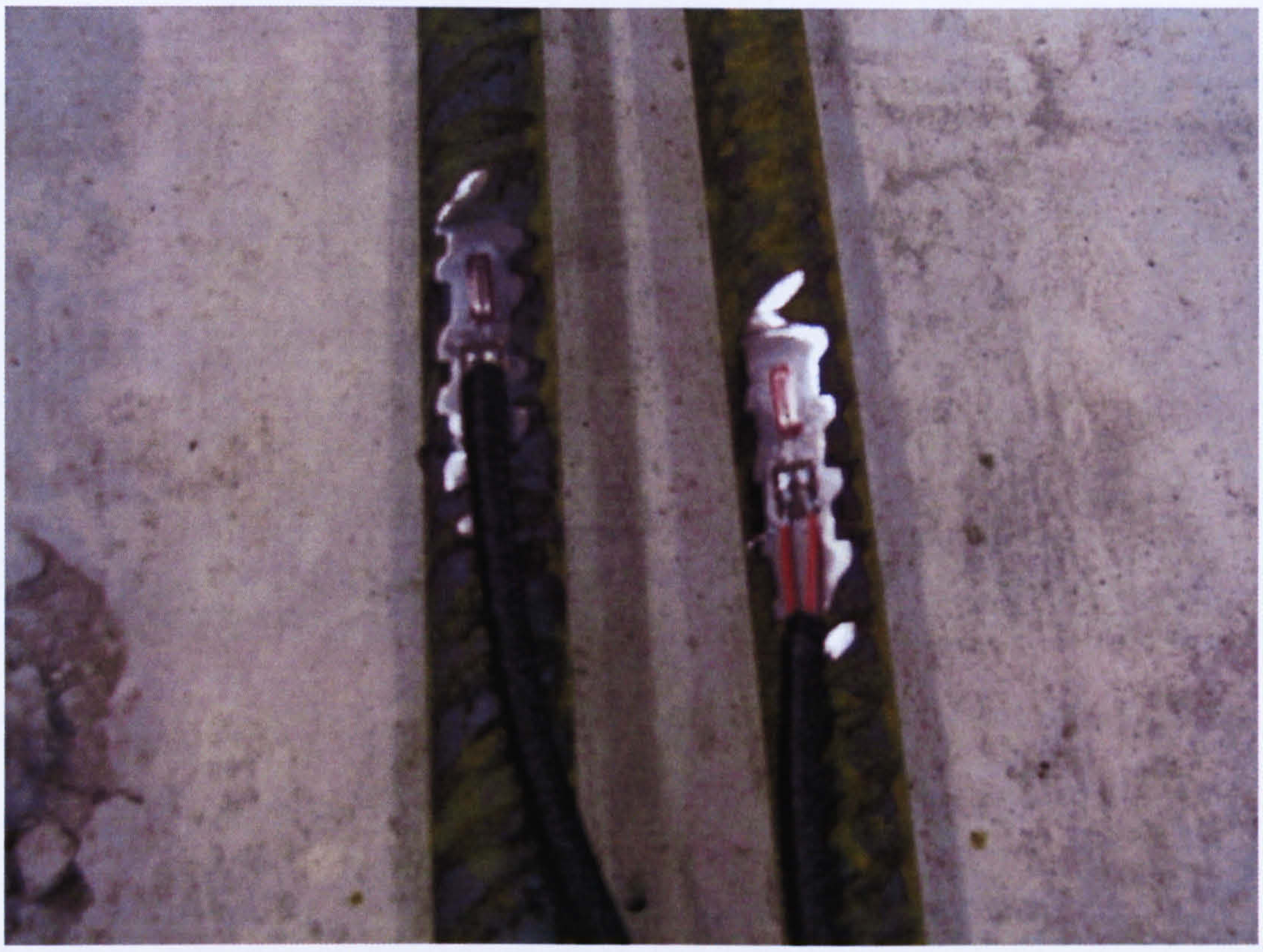

(a) Strain gauges placed at centre of transverse reinforcement

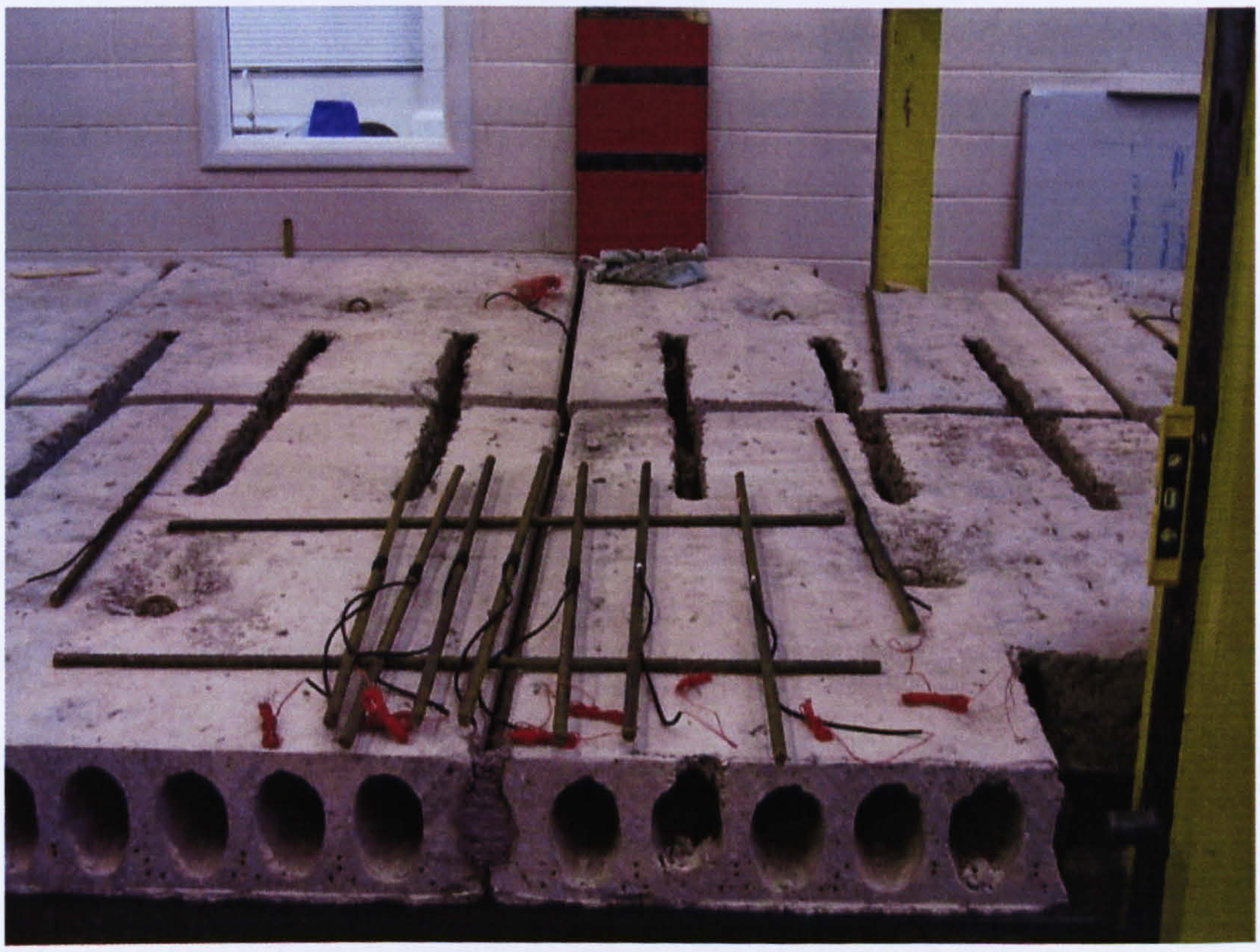

(a) Transverse reinforcement ready for placement in slabs

Figure 3.17: Transverse reinforcement ready for placement in slabs

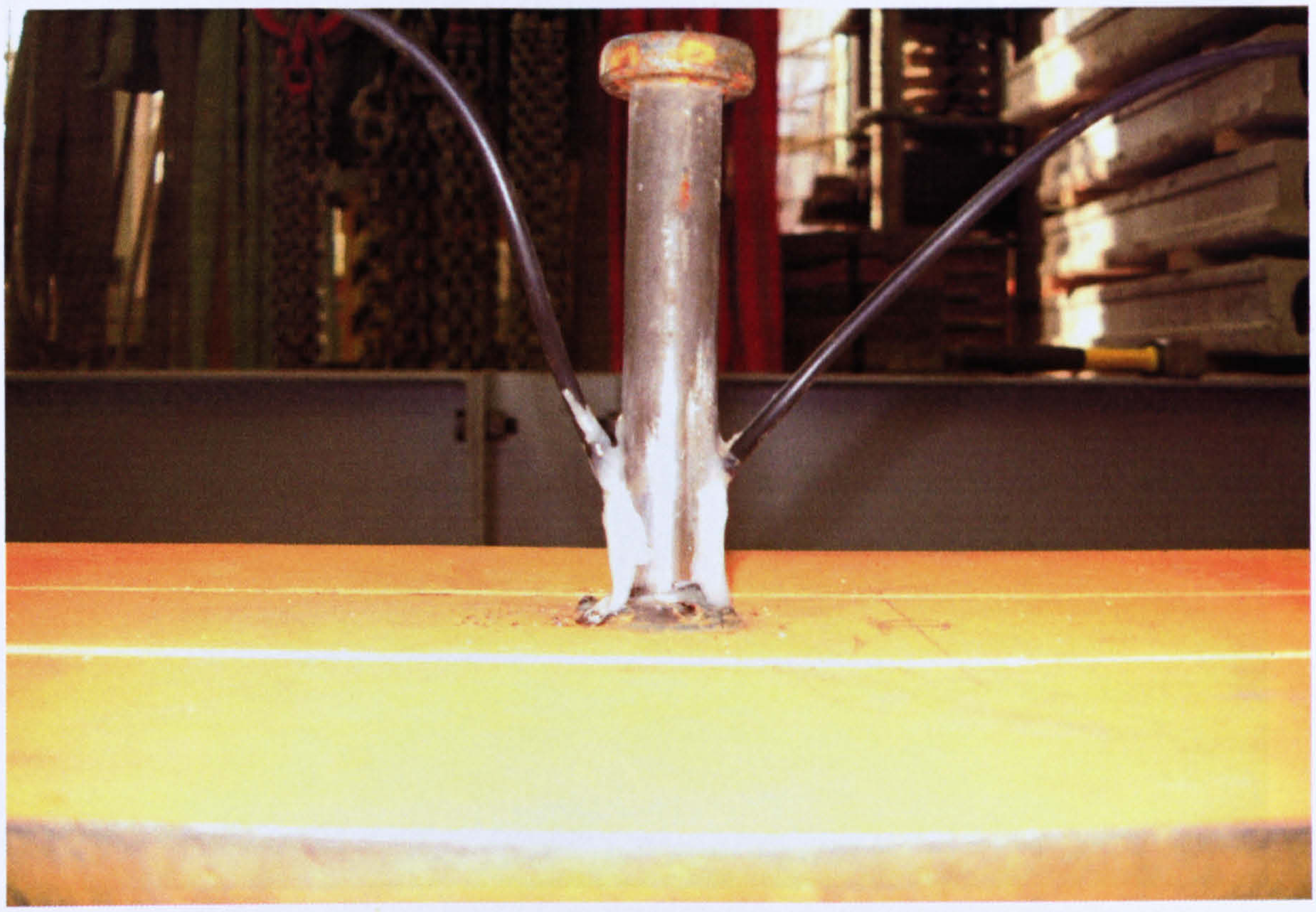

Figure 3.18: Location of strain gauges on shear stud coated in resin

3.5.2 Displacement Transformers

LVDT's (Linear Variable Differential Transformers) were used to measure the slip between the concrete slab and steel beam as well as the bending deflection. To measure horizontal slip, eight LVDT's were placed the concrete/steel interface under the bottom surface of the slab, and to measure the vertical deflection of the beam, five LVDT's were placed on the top surface of the bottom steel flange. LVDT's were positioned using magnetic clamps and brackets to measure movement (Figures 3.19 and 3.20).

Figure 3.19: LVDT's positioned using magnetic clamps and brackets

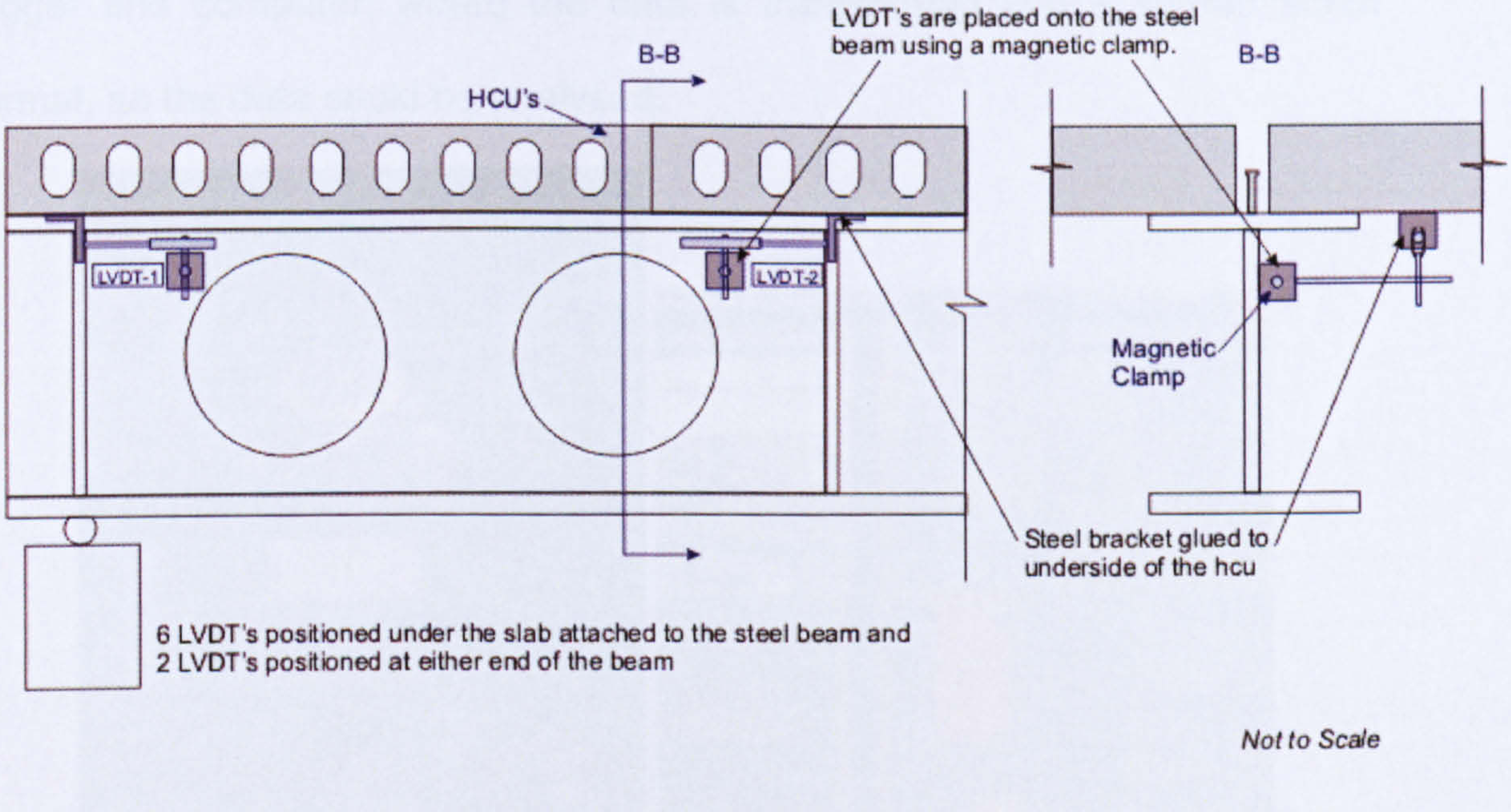

Figure 3.20: Position of LVDT's on test specimen

3.5.3 Loading Procedure

The load was applied manually by a hydraulic pump simultaneously to all jacks. Elastic tests were run before testing to check instrumentation and the loading system. The load was applied in 20kN intervals with unloading cycles at about 200 to 300kN dependant on the test specimen. The loading intervals were decreased to 10kN and 5kN as the test specimen got close to failure. Loading was applied to the specimen until failure was reached, i.e. excessive slip, failure of shear connection or severe cracking was observed. After testing, the specimen was dismantled in order to investigate the condition of the shear studs, concrete and possible failure of the steel beam.

Figure 3.21 shows the hydraulic pump, load cell and jack. All the data from the instrumentation was simultaneously collected and stored by the data logger and computer, where the data is transformed into a spread sheet format, so the data could be analysed.

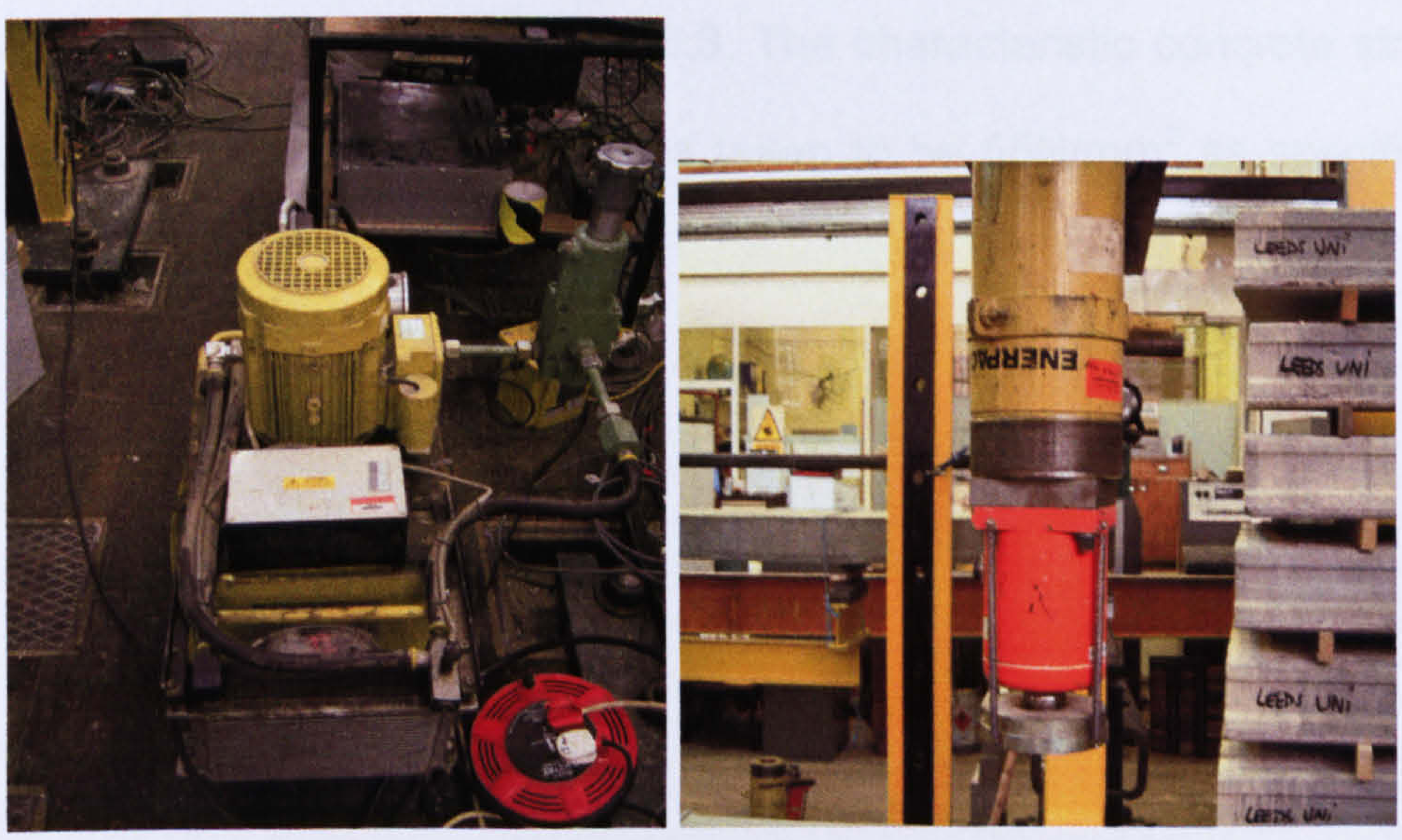

a) Hydraulic pump b) Load cell and jack

Figure 3.21: Hydraulic pump, load cell and jack used in tests

3.6 Material Testing

Material testing was performed on all materials that formed the composite beam. The following sections describe how the material testing was carried out for the in-situ concrete, steel coupons from the beam and transverse reinforcing bars.

3.6.1 In-Situ Concrete

In-situ concrete is used for the infill between the concrete slab and steel beam. To monitor the in-situ concrete strength, concrete cubes (100x100x100mm) and concrete cylinders (150mm diameter x 300mm long) were sampled and cured in the same conditions as the test specimen. The concrete samples were tested at 7, 14, 21 and 28 days in accordance with BSI 1881. The compressive and tensile strength of the in-situ concrete were derived from the compressive test and the Brazilian splitting test, results of which are shown in Tables 3.2 and 3.3. The characteristic concrete strength for the precast hollow-core slabs was taken to be 55N/mm^2 as specified by the manufacturer.

Specimen	Compressive Strength (N/mm^2)								
	7 days			Test days			28 days		
	1	2	Average	1	2	Average	1	2	Average
CB-1	24.60	25.10	24.85	42.10	41.80	**41.95**	42.10	41.80	41.95
CB-2	19.40	19.20	19.30	32.40	32.80	**32.60**	32.40	32.80	32.60
CB-3	16.20	16.40	16.30	34.20	34.60	**34.40**	28.30	27.90	28.10
CB-4	16.60	16.20	16.40	35.10	34.90	**35.00**	28.60	29.10	28.85
CB-5	17.60	17.10	17.35	30.10	31.20	**30.65**	30.10	31.20	30.65

Table 3.2: In-situ concrete infill compressive strength

Specimen	Tensile Strength (N/mm^2)								
	7 days			Test days			28 days		
	1.00	2.00	Average	1.00	2.00	Average	1.00	2.00	Average
CB-1	2.33	2.34	2.34	2.64	2.68	**2.66**	2.64	2.68	2.66
CB-2	1.62	1.65	1.64	2.05	2.10	**2.08**	2.05	2.10	2.08
CB-3	1.51	1.55	1.53	2.89	2.94	**2.92**	2.70	2.64	2.67
CB-4	1.48	1.51	1.50	2.94	2.84	**2.89**	2.94	2.84	2.89
CB-5	1.61	1.64	1.63	2.08	2.10	**2.09**	2.08	2.10	2.09

Table 3.3: In-situ concrete infill tensile splitting strength

3.6.2 Steel Coupons and Transverse Reinforcing Bars

Steel coupons were cut from the flanges and web of the beam after each test, so they can be tensile tested. The steel coupons (Figure 3.22) were taken from the areas where the stresses are low, i.e. at supports for the flanges and between stiffeners for the web. In addition, tensile tests will be carried out on a sample of transverse reinforcing bars to measure the tensile strength of the bars. Tensile tests of the coupons were conducted using the Instron testing machine according to BS EN 10002 – Part 1. From the tensile tests conducted on the steel coupons and reinforcing bars, the yield strength, ultimate strength and ultimate strain were obtained. Test results are shown in Tables 3.4, 3.5 and 3.6.

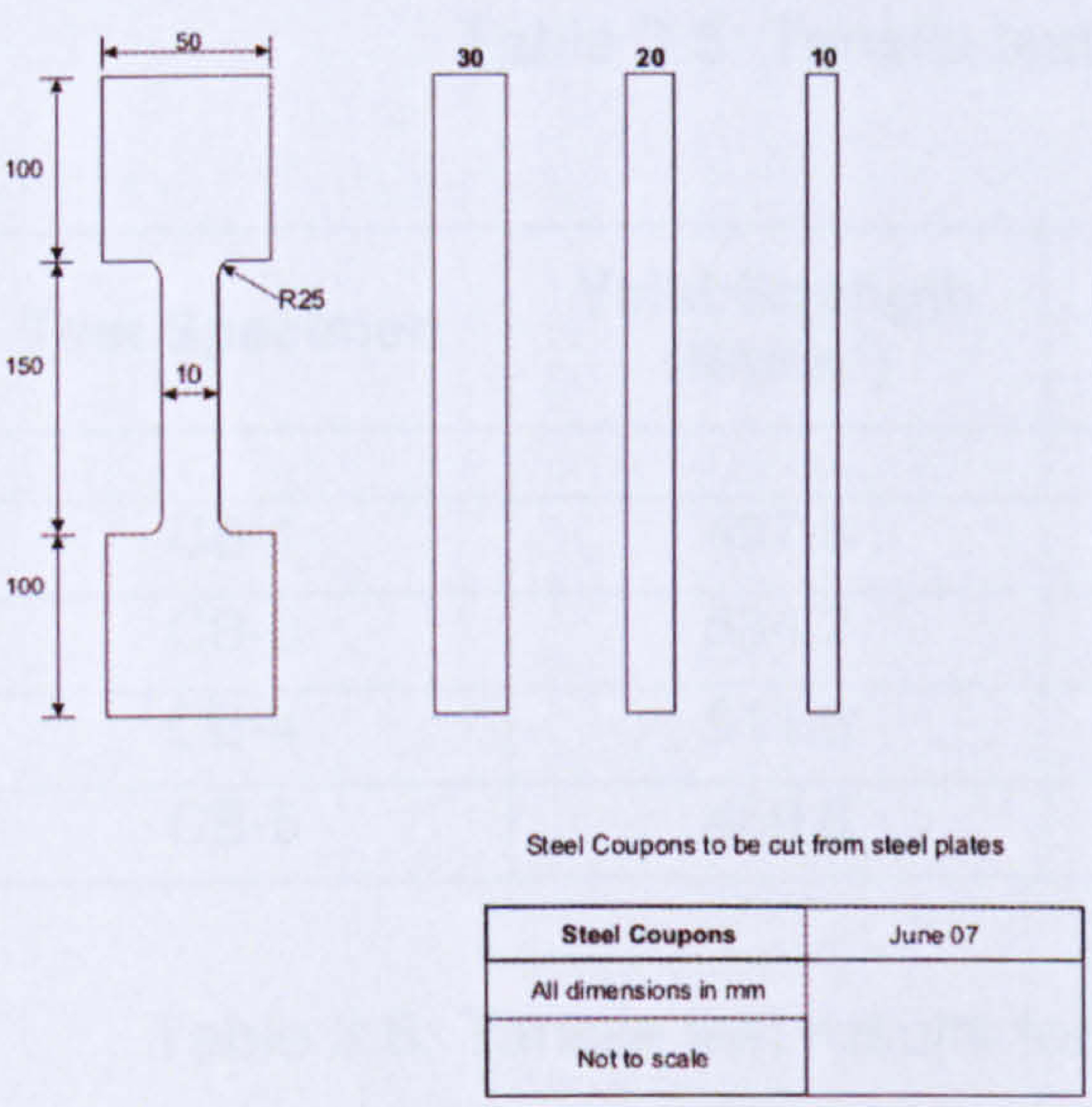

a) Dimensions for coupon test specimen

b) Coupon test specimen

Figure 3.22: Steel coupons form cut from beam

Specimen	Yield Strength (N/mm^2)	Ultimate Strength (N/mm^2)	Ultimate Strain (με)
CB-1	378.1	542.8	199465.5
CB-2	385.2	545.1	206579.4
CB-3	402.6	564.6	212185.8
CB-4	360.3	518.5	196668.7
CB-5	391.4	545.4	200964.5

Table 3.4: Tensile test results for steel flange

Specimen	Yield Strength (N/mm^2)	Ultimate Strength (N/mm^2)	Ultimate Strain (με)
CB-1	362.1	506.7	199465.6
CB-2	365.2	502.3	206079.3
CB-3	362.1	489.5	189187.8
CB-4	350.5	468.7	193368.4
CB-5	375.4	510.2	189961.7

Table 3.5: Tensile test results for steel web

Test Specimen	Yeild Strength (N/mm^2)	Ult. Strength (N/mm^2)	Cross-Sectional Area (mm^2)
CB-1	497.5	645.3	195.5
CB-3	534.2	643.2	195.4
CB-4	511.6	634.5	195.5
CB-5	489.8	632.1	195.5

Table 3.6: Tensile test results for T16 transverse reinforcing bars

3.7 Composite Test Arrangement

All the beam test specimens were setup as described in section 3.4. In order to investigate different variables, different test arrangements were adopted for each test. For the first three tests (CB-1, 2 and 3), the main variables investigated were the shear stud spacing of the shear connection. In test CB-4, the variable was the span of beam, which was reduced to 9m and CB-5 had the variable of using 400mm deep slabs. The test parameters of the five composite beam tests are shown in Table 3.1.

3.7.1 Test CB-1

CB-1 was designed with a 68% shear connection, with a stud spacing of 150mm on the steel beam. Figure 3.23 shows the general arrangement and the position of LVDT's and strain gauges on the steel beam. LVDT's are placed in five locations on the bottom flange of the beam to measure vertical deflection and eight LVDT's are placed at the concrete/steel interface to measure slip. Gauges are placed along the flanges, around the centre web opening of the beam and on studs. Figure 3.24 shows the general arrangement of the transverse reinforcing bars, with twenty nine of the forty nine bars having gauges placed in the centre of the bars.

3.7.2 Test CB-2

The purpose of this test is to study the effect on the shear connection with a reduced number of studs, giving half the connection of CB-1. CB-2 was designed with a 34% shear connection, with a stud spacing of 300mm on the steel beam. Figures 3.25 and 3.26 show the general arrangement and the position of LVDT's and strain gauges on the composite beam. All instrumentation is similar to CB-1, with only a reduction in the number of strain gauges used on the transverse reinforcement (Figures 3.26).

3.7.3 Test CB-3

CB-3 was designed with a 26% shear connection, with a stud spacing of 400mm on the steel beam. Again, the purpose of this test is to study the effect on the shear connection with a reduced number of studs compared to CB-1 and CB-2. All instrumentation is similar to CB-2, as shown in Figures 3.27 and 3.28.

3.7.4 Test CB-4

CB-4 was designed to span 9m with a 50% shear connection, the beam size was 457x191x89UB used with 200mm hollow-core slabs. The purpose of this test was to study the effect of beam span in comparison to the other tests which were all spanning 12m. All instrumentation is similar to previous tests, with a reduction of LVDT's and strain gauges due to the shorter span. Another difference is the number of slots in the hollow-core slabs (three slots instead of four as in previous tests), therefore a reduction in transverse reinforcement. Figures 3.29 and 3.30 show the general arrangement and the position of LVDT's and strain gauges on the composite beam.

3.7.5 Test CB-5

The purpose of this test was to study the effect of the hollow-core slab depth in comparison to the other tests which all used 200mm deep units. The hollow-core slabs used in this test were 400mm for a 12m spanning composite beam. CB-5 was designed with a 25% shear connection, with a stud spacing of 400mm on the steel beam. As with CB-4, the number of slots in the hollow-core slabs was reduced (three slots instead of four). Figures 3.31 and 3.32 show the general arrangement and the position of LVDT's and strain gauges on the composite beam.

3.8 Conclusion

In this chapter, the test setup, material tests, instrumentation and loading system of five full scale composite beam tests consisting of steel I-sections with precast hollow-core slabs are described in detail. The test observations and test results are presented in Chapter 4.

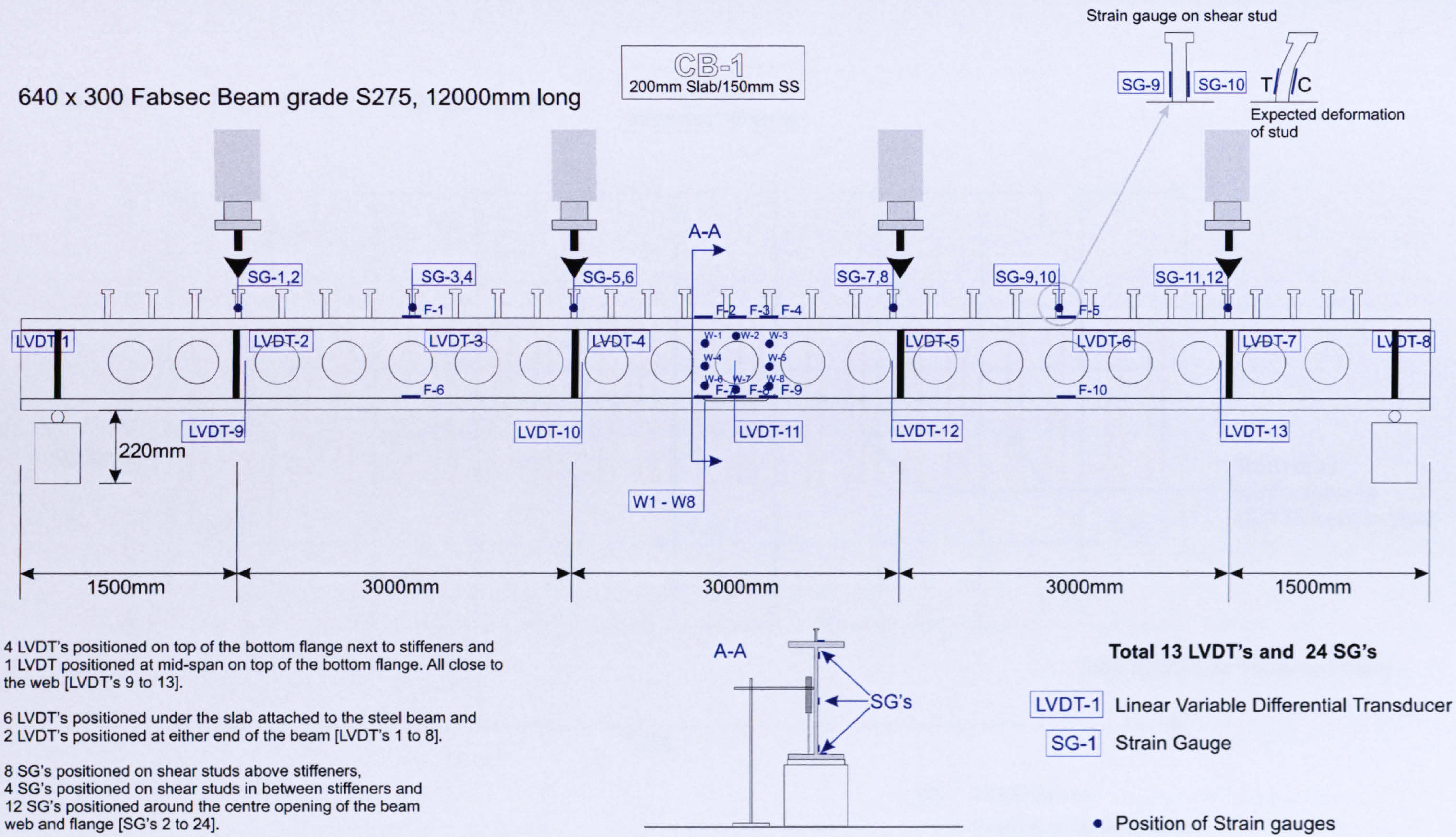

4 LVDT's positioned on top of the bottom flange next to stiffeners and 1 LVDT positioned at mid-span on top of the bottom flange. All close to the web [LVDT's 9 to 13].

6 LVDT's positioned under the slab attached to the steel beam and 2 LVDT's positioned at either end of the beam [LVDT's 1 to 8].

8 SG's positioned on shear studs above stiffeners,
4 SG's positioned on shear studs in between stiffeners and
12 SG's positioned around the centre opening of the beam web and flange [SG's 2 to 24].

Total 13 LVDT's and 24 SG's

LVDT-1 Linear Variable Differential Transducer

SG-1 Strain Gauge

• Position of Strain gauges

Not to Scale

Figure 3.23: Strain gauge positions on Fabsec steel beam (CB-1)

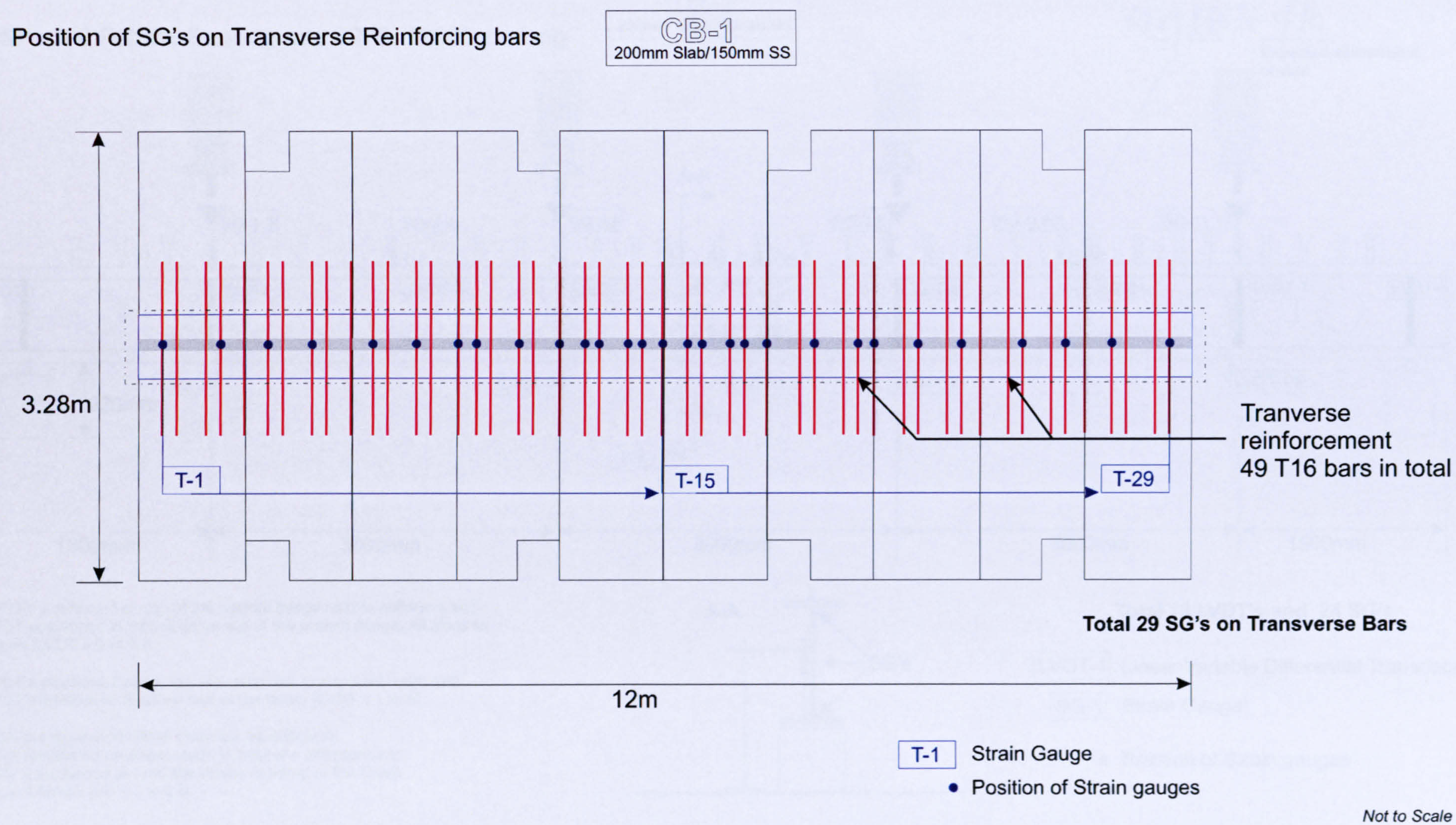

Figure 3.24: Strain gauge positions on transverse reinforcement (CB-1)

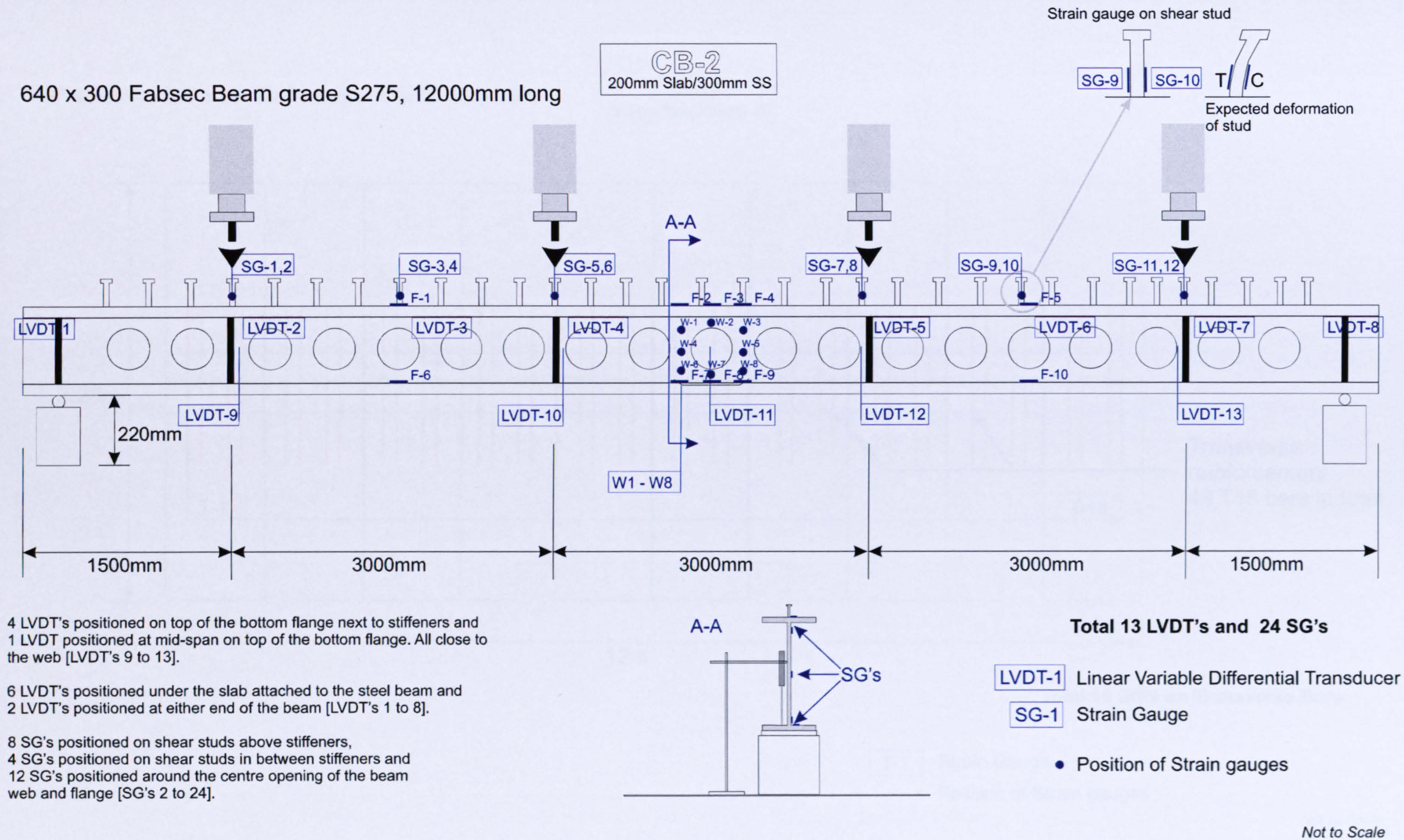

Figure 3.25: Strain gauge positions on Fabsec steel beam (CB-2)

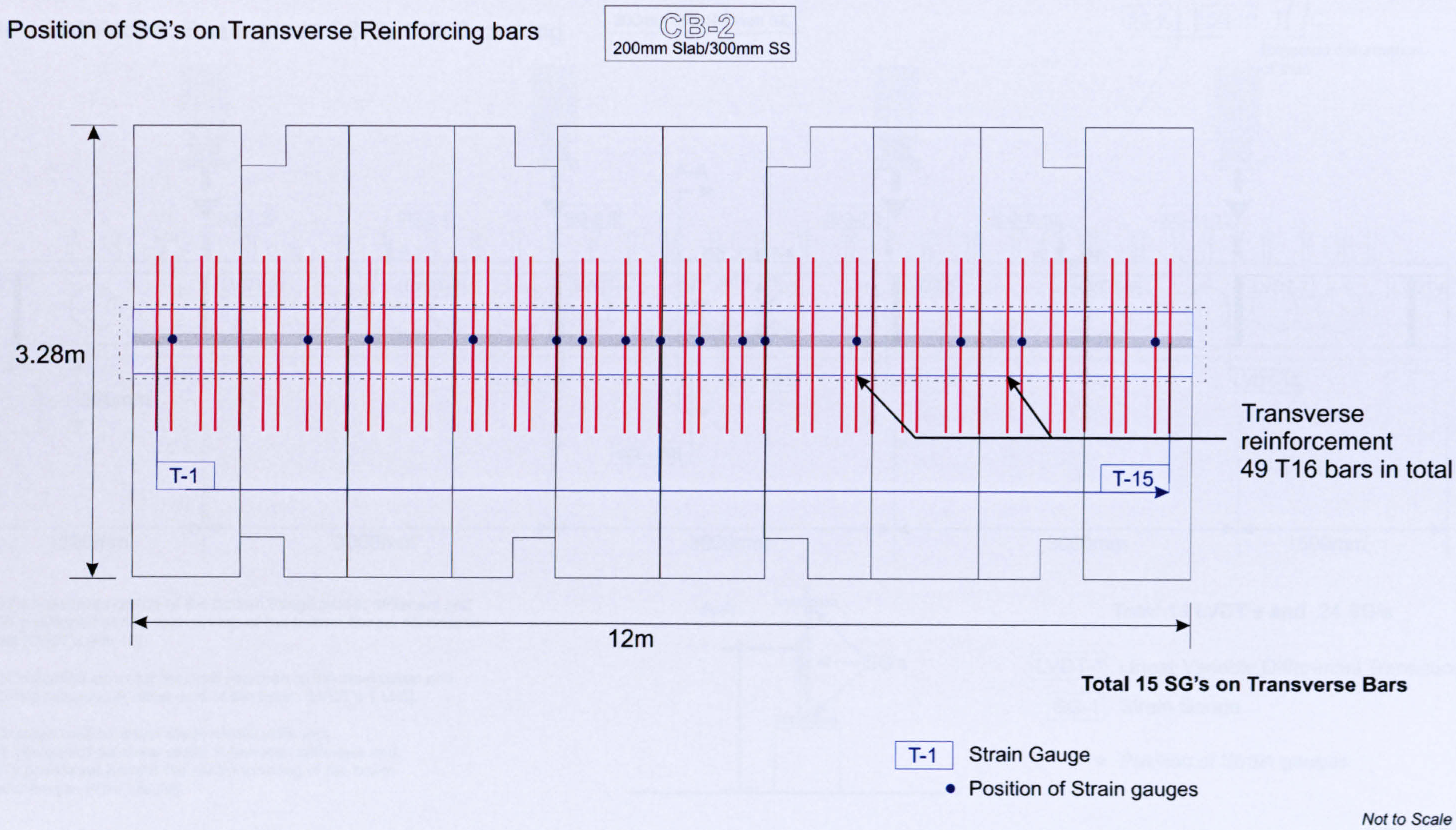

Figure 3.26: Strain gauge positions on transverse reinforcement (CB-2)

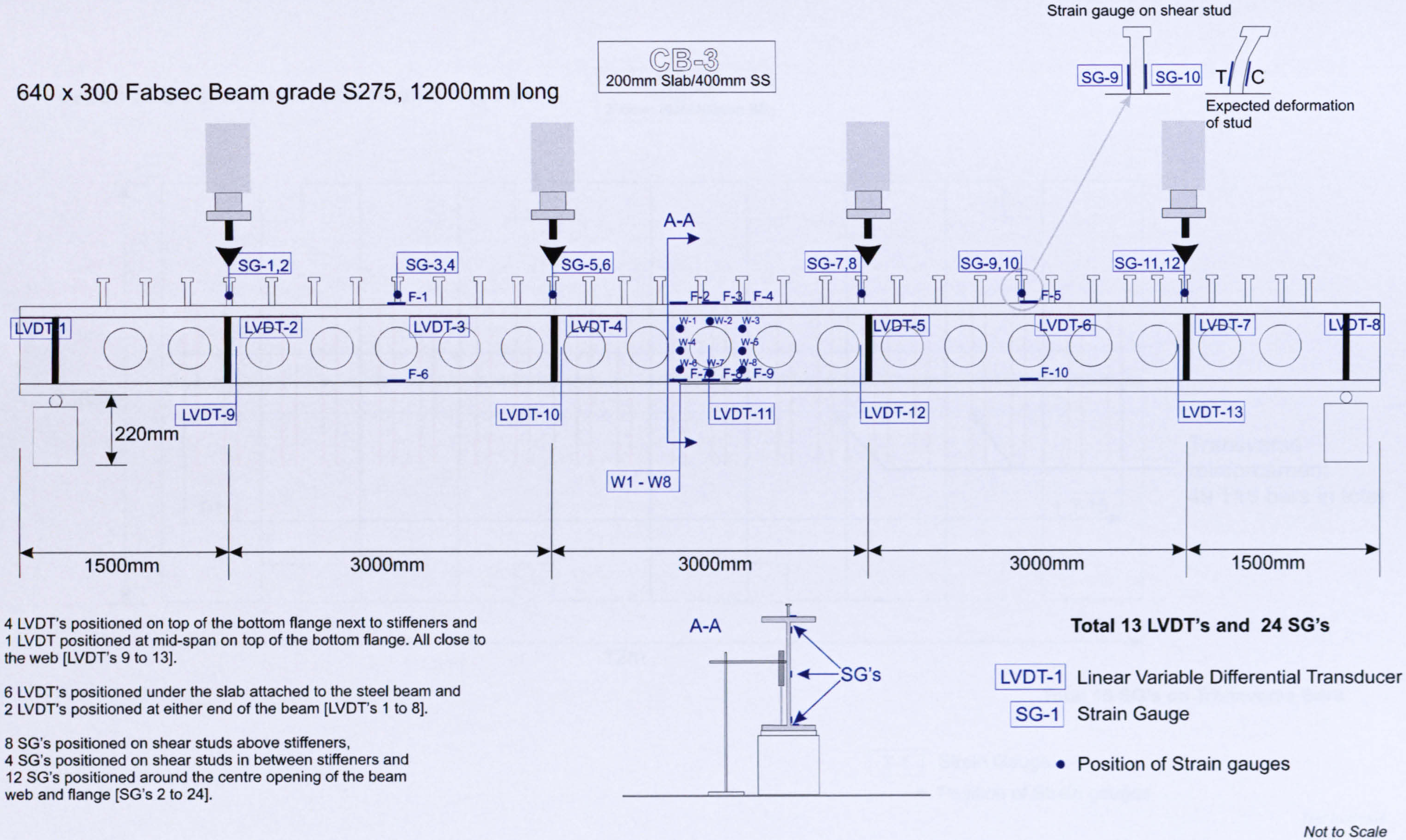

Figure 3.27: Strain gauge positions on Fabsec steel beam (CB-3)

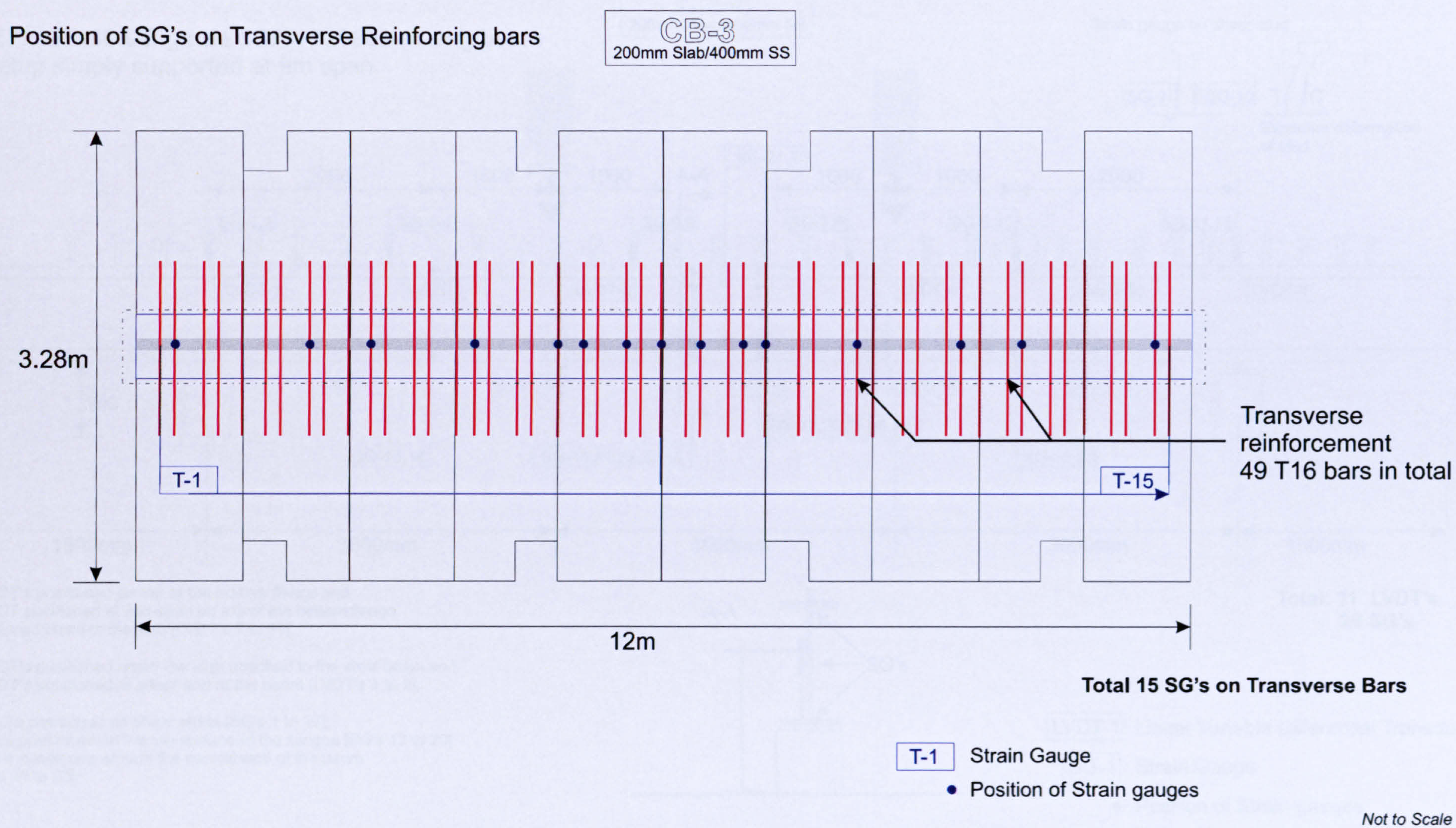

Figure 3.28: Strain gauge positions on transverse reinforcement (CB-3)

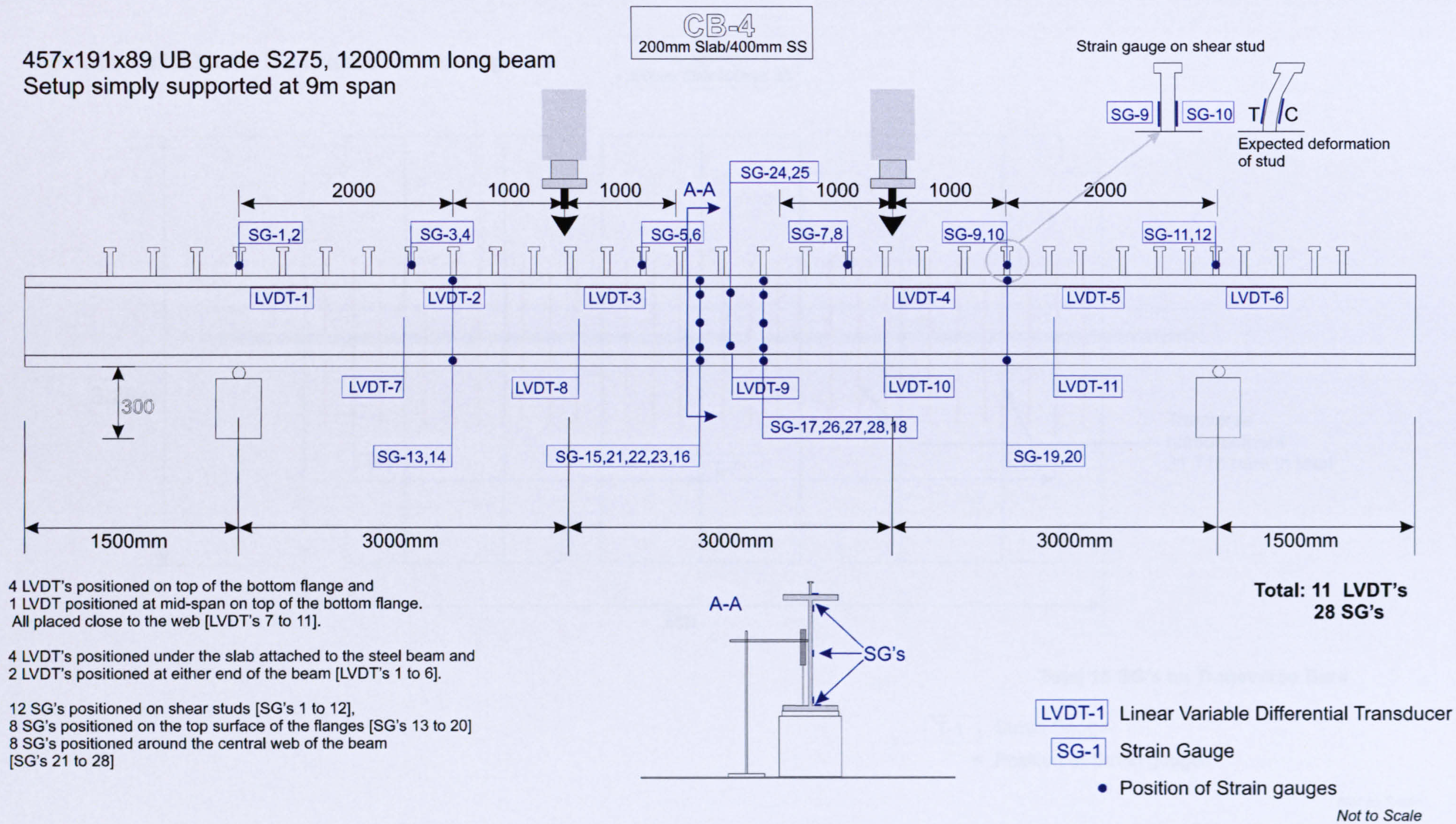

Figure 3.29: Strain gauge positions on 457UB steel beam (CB-4)

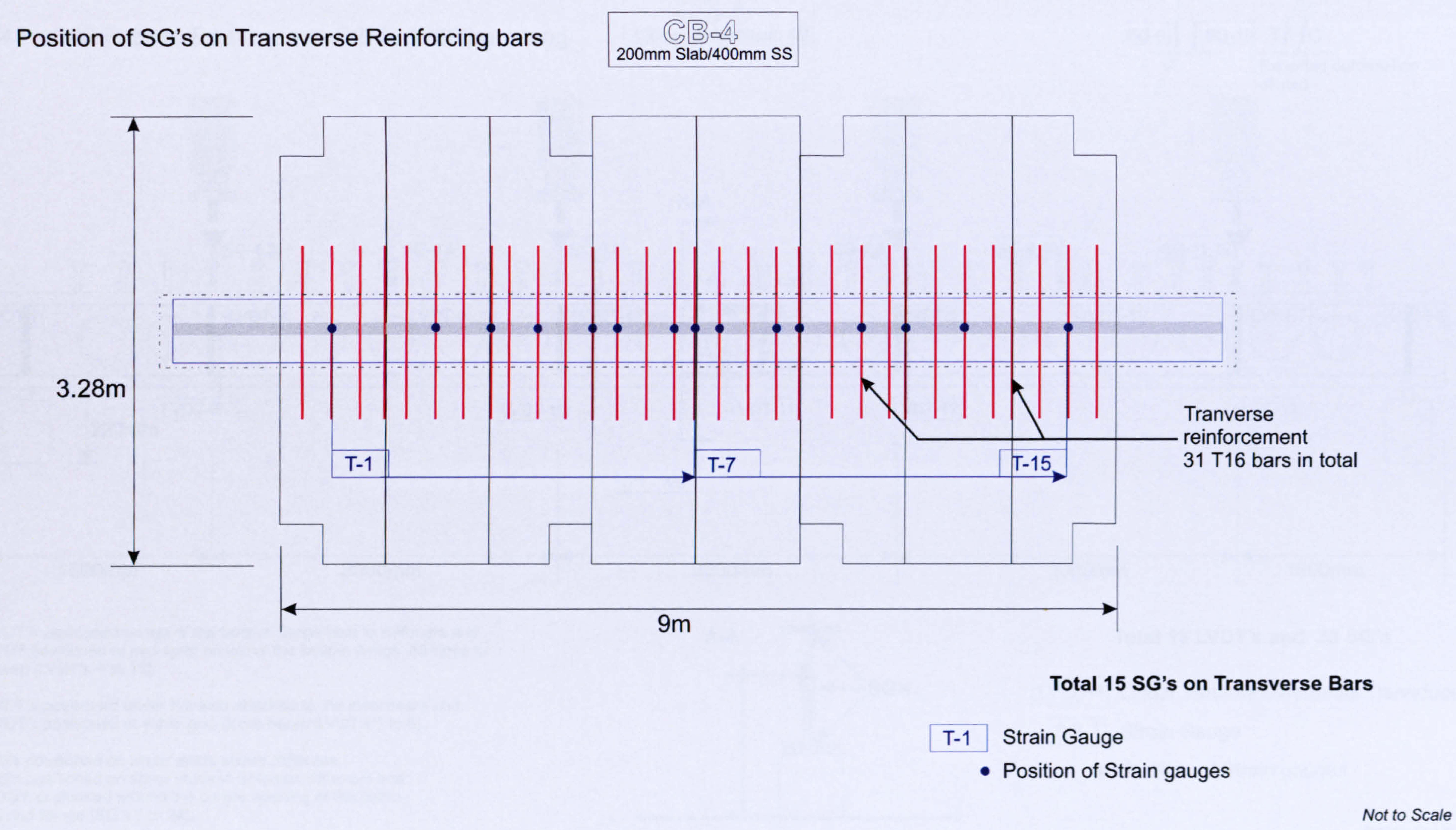

Figure 3.30: Strain gauge positions on transverse reinforcement (CB-4)

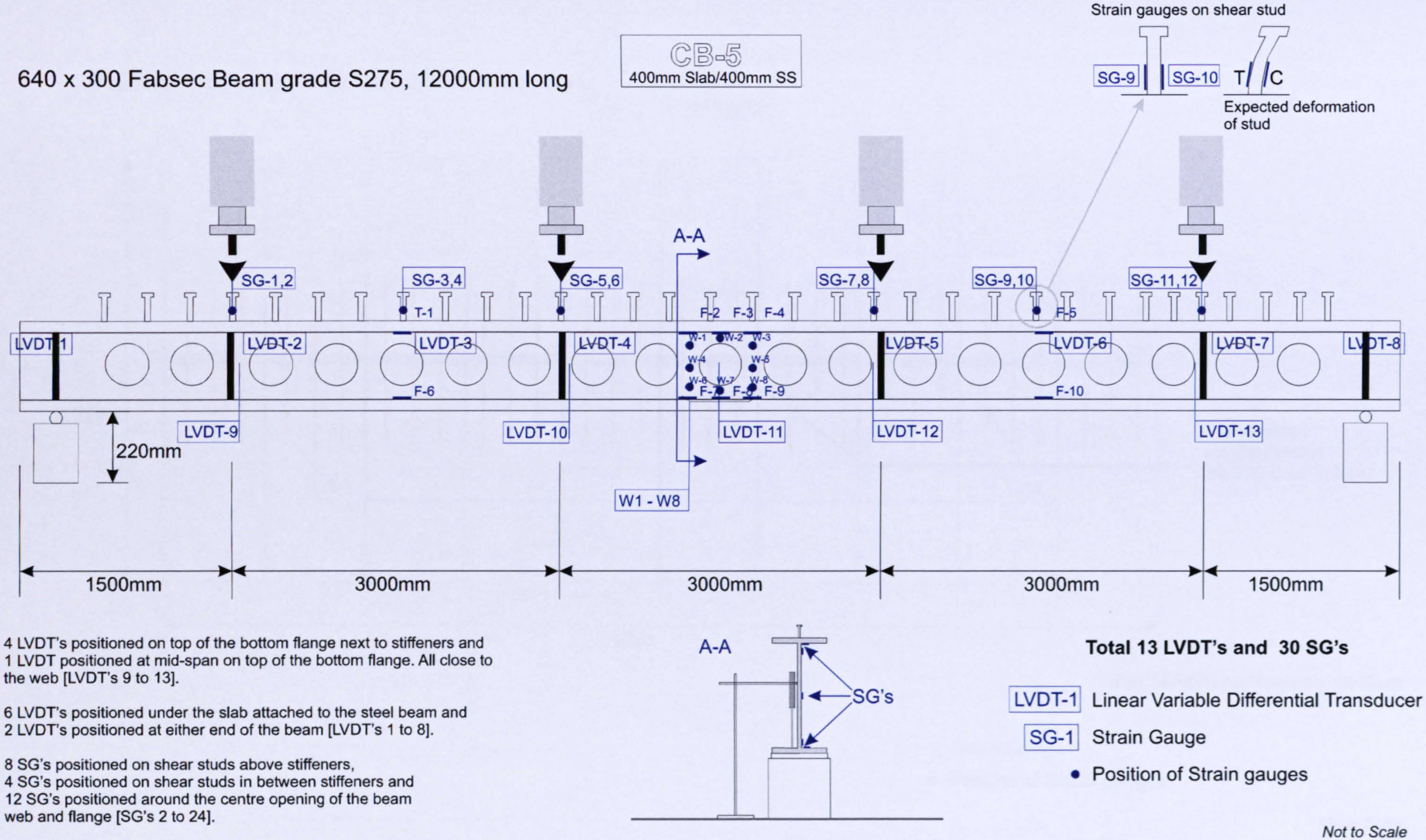

Figure 3.31: Strain gauge positions on Fabsec steel beam (CB-5)

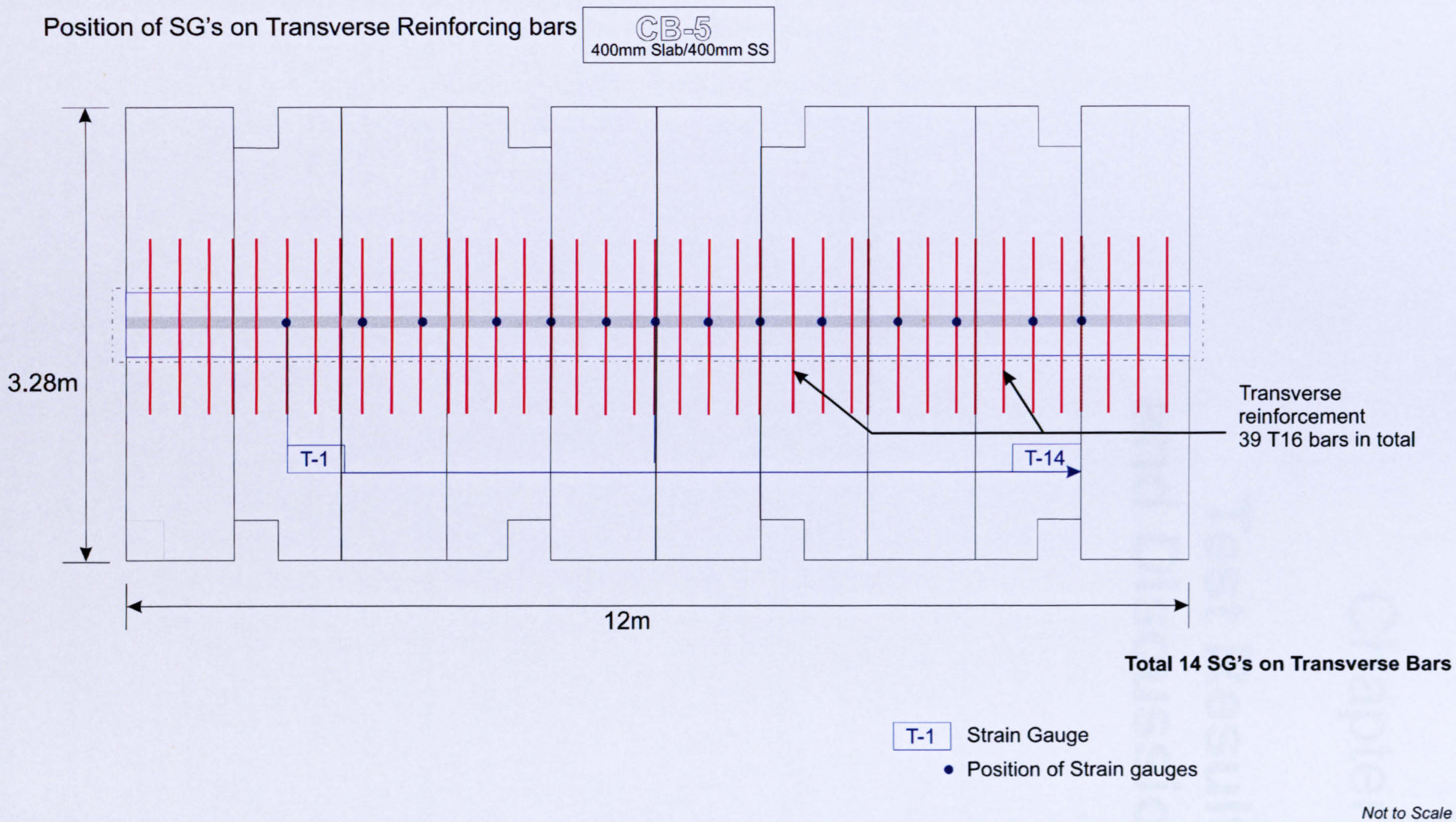

Figure 3.32: Strain gauge positions on transverse reinforcement (CB-5)

Chapter 4

Test Results and Discussion

Chapter 4: Test Results and Discussion

4.1 Introduction

Extensive analysis is conducted on the test results in this chapter, the test observations, results and the modes of failure for push tests and five full scale composite beam tests are presented in detail. Also presented in this chapter is a comparison between the five beam tests conducted and the effects of the different parameters of the specimen on the behaviour of the composite beam. Based on the analysis of the test results, the structural behaviour of the beam is discussed and recommendations for the design purpose have been made.

4.2 Push Test Results

Using the push test proposed by Lam in 2006 for hollow-core slabs, push tests were performed to determine shear capacity of the shear stud. By determining the slip and load per stud a comparison could be made with the beam test results. Six full-scale push tests were carried out, with 19x125mm studs, hollow-core slabs of 150-250mm in depth, T16 reinforcing bars and square end hollow-core slabs.

Results in Table 4.1 include the maximum capacity per stud, the amount of slip when maximum load is achieved and crucially, the stud's capacity at

6mm slip. In accordance to Eurocode 4, shear connectors should have sufficient deformation capacity to justify any inelastic redistribution of shear assumed in design. Ductile connectors are those with sufficient deformation capacity to justify the assumption of ideal plastic behaviour of the shear connection in the structure considered when the characteristic slip is at 6mm. Hence, it is recommended by Lam that the stud capacity at 6mm slip should be used to specify the characteristics capacity of the shear connectors.

In all tests carried out, only 0.1mm of slip was noticed at 40% of the expected failure load. All tests were loaded until failure is reached, the specimens were then dismantled to investigate the condition of the studs after the tests. Tensile strength of the reinforcing bars was determined in accordance with BS 4449. The T16 bars were found to have a yield strength between 535-545N/mm^2 and ultimate tensile strength between 627-633N/mm^2.

Push Test	In-situ concrete strength (N/mm^2)	Rebar @ 300mm c/c and length (N/mm^2)	HC slab depth (mm)	Gap (mm)	Max. Load per stud (kN)	Slip at Max. Load (mm)	Load at 6mm slip (kN)
PT-1	29.17	T16/1000	200	80	102.7	4.71	102
PT-2	29.20	T16/1000	200	80	102.7	4.71	102
PT-3	29.23	T16/1000	150	80	82.6	2.91	78
PT-4	29.15	T16/1000	150	80	89.2	3.67	86
PT-5	25.09	T16/1000	250	80	86.5	5.70	85
PT-6	25.09	T16/1000	250	80	97.4	2.77	85

Table 4.1: Push test results

4.2.1 Push Test Mode of Failure

Three modes of failure were observed during the testing of the push tests. The first mode was crushing of concrete, forming concrete cone failure where no shearing off of headed studs is observed. For this mode of failure, the concrete around the stud started to fail in compression before the stud yielded; the compression failure progressed through the thickness of the concrete forming a conical shape around the stud. Figure 4.1 shows the push test specimen failed in this mode of failure.

Figure 4.1: Crushing of concrete/conical failure

The second mode of failure is when the stud was fully yielded and no concrete failure is observed. This mode of failure is identified as stud failure mode where the yield stress of the headed stud is reached while maximum concrete stress of the concrete element is not reached. Figure 4.2 shows the push test specimen with this failure mode.

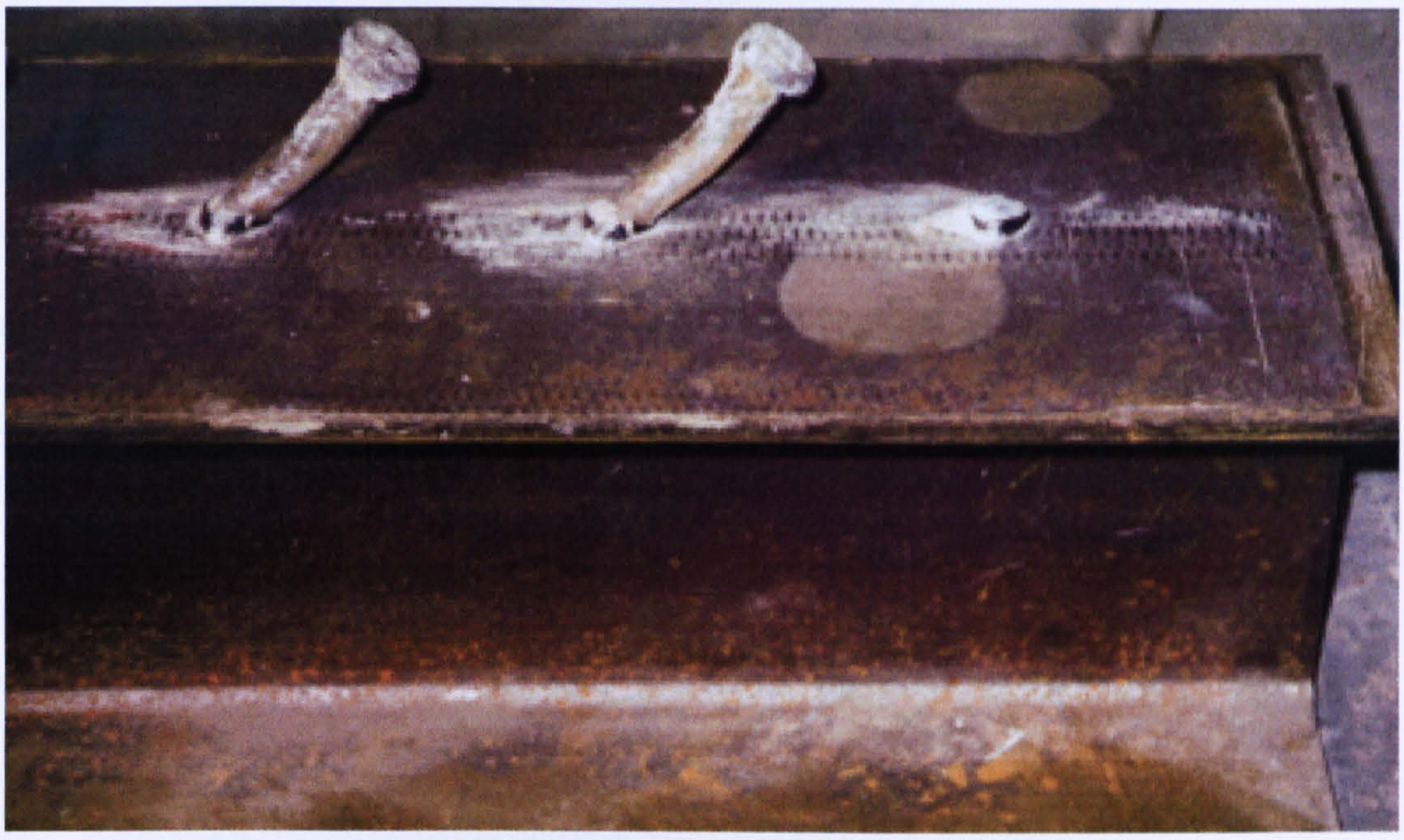

Figure 4.2: Yielding of shear studs

The third mode of failure is the combined failure of stud and concrete slab when maximum stresses are reached in the stud and concrete elements. All three modes of failure were observed in the experimental push tests.

4.2.2 Push Test Discussion

The behaviour of the shear connection in the composite beam with precast hollow-core slabs depends mainly on the load – slip characteristic of the shear connectors at the interface between the top flange of the steel sections and the concrete slabs. This load – slip behaviour (Figure 4.3), usually found from the push-off tests depends on the type of connectors, their sizes and dimensions, the amount of transverse reinforcement, their spacing and the gap and strength of the in-situ concrete infill. Early work by Lam et al (1998) showed that for the beam with full shear connection, a slip of only 2mm was observed in the full-scale beam tests at the ultimate load; therefore the effects of slip can be ignored. However, for this research, the composite beams with hollow-core slabs are designed with partial shear connection, hence the effects of slip cannot be neglected. The ability of the shear studs to maintain the maximum capacity with slip, i.e. the ductility of the shear connector, became a very important issue.

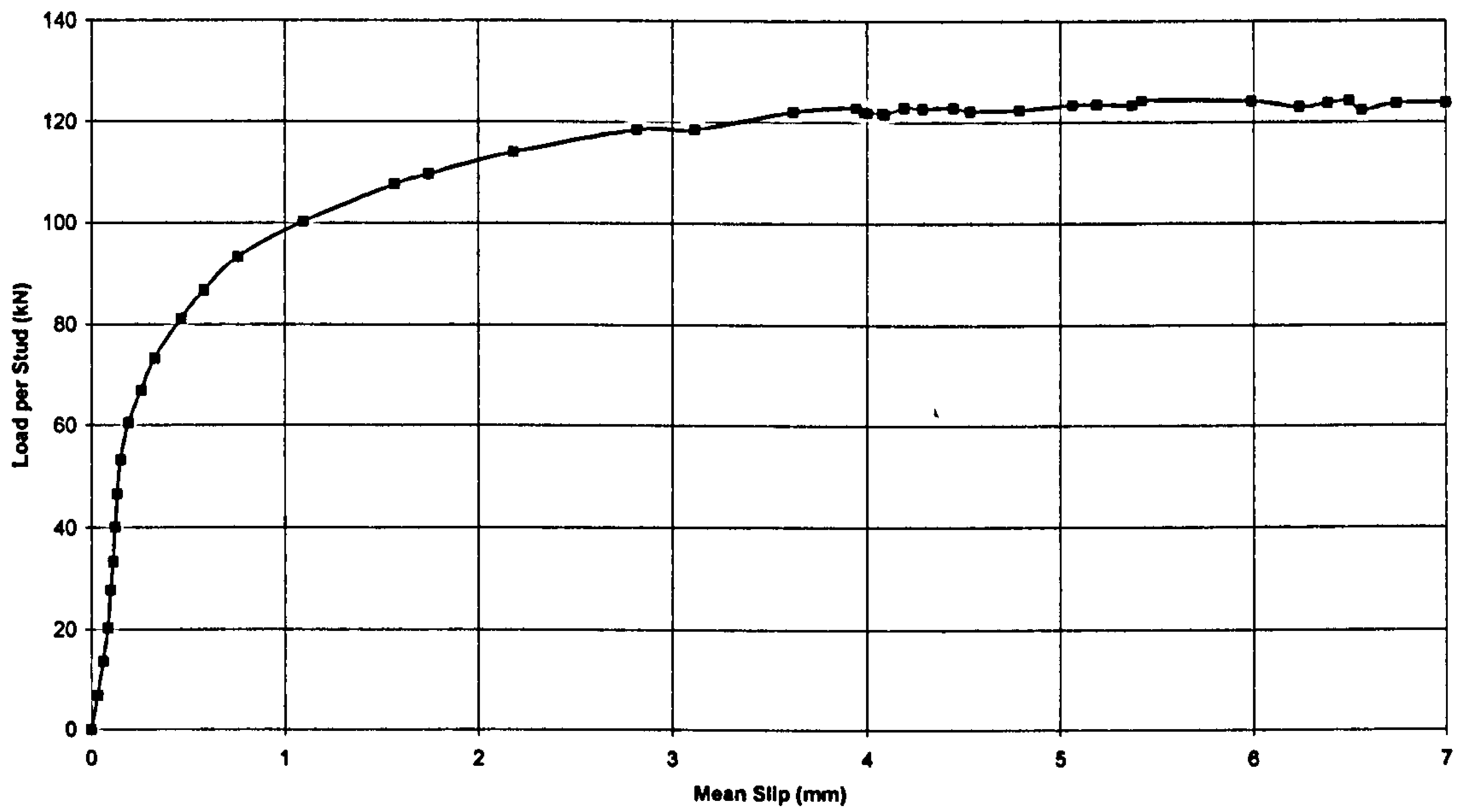

Figure 4.3: Load-Slip curve of shear connector

The results of these push tests showed that the in-situ concrete strength affected the shear capacity of the headed studs in the hollow-core slabs. Increases in in-situ concrete strength lead to increases in the shear stud capacity and the rates of increase were similar for all tests.

The effect of hollow-core slab thickness was investigated. Table 4.1 shows the summary of test results. The results showed that the effect of slab thickness to the capacity of the shear studs was not significant. For all composite beam tests conducted, 125mm long headed studs with hollow-core slabs of depths 200mm and 400mm are used.

4.3 Beam Test Observations and Results

This section describes the five full scale tests (CB-1 to CB-5) individually. All the notations, which include LVDT's on the test specimens and strain gauges placed on the steel beam, studs and transverse reinforcement are in accordance with Chapter 3. Table 3.1 show the test results for all composite beam specimens tested.

4.3.1 General Flexural Behaviour of Composite Beam

For the composite beam, the elastic neutral axis is usually close to the interface between the steel and the concrete. As the moment acting on the composite section is increased, the bottom flange of the steel beam begins to yield and the neutral axis moves towards the compression zone, causing tensile cracking at the underside of the slab.

As bending is further increased in the section, the load carried remains approximately constant and crushing of the slab might occur. The steel section strength is increase by using large steel sections so yielding is unlikely to occur in the steel, forcing the shear connection between the steel beam and concrete to control failure. Crushing of the concrete slab and failure of the shear connectors may occur which will reduce the composite action and thus the load carrying capacity of the section. Tables 4.2 and 4.3, show test results of beam tests and bending results of composite beams.

The purpose of the tests carried out was to investigate the effect of the elastic neutral axis lying in the concrete and to establish if composite beams can induce ultimate moment capacity prior to failure. By using large steel I-sections with precast concrete hollow-core slabs and partial shear connection, the behaviour of the composite beam is established.

4.3.2 End Slip

When the load is applied to the beam, there is a tendency for slip to occur between the slab and the beam to which the connector is attached. This is partly due to the deformation of the concrete surrounding the shear connector and partly due to bending of the shear connector. Observations show that little or no slip occurred at the serviceability load. Slip is not uniform along the length of a beam, even when the external shear force is uniform. The largest slip occurs near the end of the beam and is generally also the region in which slip begins. From the observation of the bending tests, the effect of slip in the working range is unlikely to be sufficiently great to be considered in design. However, slip does have considerable influence on the development of the ultimate moment capacity.

Test Specimen	Max. Load in Test (kN)	Max. Moment in Test (kNm)	Max. Deflection in Test (mm)	Max. Recorded slip (East) (mm)	Max. Recorded slip (West) (mm)	Failure Mode	Effective Width (mm)
CB-1	400	2400	85	4.6	4.2	CC	732 (L/16)
CB-2	367	2200	131	4.5	3.7	CC	910 (L/13)
CB-3	350	2100	126	5.0	13.1	CC/SF	629 (L/19)
CB-4	310	930	121	6.0	15.0	CC/SF	910 (L/10)
CB-5	390	2340	150	8.7	5.8	CC/SF	1319 (L/9)

CC = Concrete Crushing
CC/SF = Concrete Crushing/Shear Failure

Table 4.2: Test Results of composite beam tests

	AT FIRST YIELD				AT MAXIMUM LOAD			
Test Specimen	Max. Moment in Test (kNm)	Mid-span Deflection (mm)	Stiffness $[M_y/\delta]$ (mm)	Recorded slip (mm)	Max. Moment in Test (kNm)	Mid-span Deflection (mm)	Stiffness $[M_y/\delta]$ (kNm/mm)	Recorded slip (mm)
CB-1	2160	54.6	39.6	2.2	2400	84.8	28.2	4.6
CB-2	1920	66.5	28.9	4.2	2200	131.2	16.8	4.5
CB-3	1800	62.9	28.6	4.8	2100	126.0	16.7	13.1
CB-4	750	41.3	18.2	4.0	930	121.3	7.7	15.0
CB-5	2200	55.0	40.0	5.3	2340	150.0	15.6	8.7

Table 4.3: Bending Test Results of composite beams

4.3.3 Test CB-1

This beam test had a shear stud spacing of 150mm and an in-situ concrete strength of 41.95N/mm^2. The composite beam behaved elastically up to about a load of 250kN with a mid-span deflection of 34mm; at this point tensile cracks were observed on the underside of the hollow-core slabs. The first cracks were observed at an applied load of 240kN in the central region of the slab. At the applied load of 340kN (Bending moment = 2040kNm), excessive cracking in the concrete slabs was observed. The bottom flange of the steel started to yield and sudden failure occurred at a moment of 2280kNm, this was due to crushing of concrete around the shear studs in the mid-span region with no yielding in the steel beam.

The maximum load was reached at 400kN (Bending moment = 2400kNm), with a mid-span deflection of 85mm. Figure 4.4 shows the deflection of the beam after testing; the failure mode was due to crushing of concrete around the shear studs in the mid-span region of the beam (Figure 4.5). Once concrete failure occurred the cracks propagated along the connection of the slabs. The maximum recorded slip was 4.6mm on the South side and 4.2mm on the North side. Prior to failure of the concrete, a small amount of slip was observed, but once crushing of the concrete occurred there were larger slips due to the reduced interaction between the steel and concrete, this lead to a reduction in the capacity of the beam. Figure 4.9 shows the moment vs. slip curve, due to the high shear connection the slip at both ends of the beam were less than 6mm as expected.

After the experiment, the beam specimen was dismantled to investigate the mode of failure. This was found to be concrete crushing around the mid-span region of the beam with all shear studs on the steel beam remaining intact. Figures 4.6 and 4.7 show regions of the slab dismantled along the beam with exposed shear studs still intact.

Figure 4.8 shows the moment vs. deflection curve of test CB-1, the beam remained elastic up to 1440kNm, after this the stiffness of the beam decreased when the load was increased. Figure 4.10 shows the strain measured on studs along the beam, although the studs on the beam remained intact, there was an increase in strain on the studs in the central region of the beam after first cracks were observed. The strain measured on the transverse reinforcement (Figure 4.11) was relatively small, suggesting the transverse bars were not fully mobilised. Although as with the studs the transverse bars placed in the centre of the composite beam had an increase in strain once the beam became plastic.

The cracking near the rib of the hollow-core slab is a consequence of crushing of concrete in the concrete section. This causes the neutral axis to move towards the compression zone, allowing tensile force to develop in the hollow-core slab. The position of neutral axis and strain distribution for test CB1 is shown in Figures 4.12 and 4.13.

Figure 4.4: Bending of Test CB-1 after testing

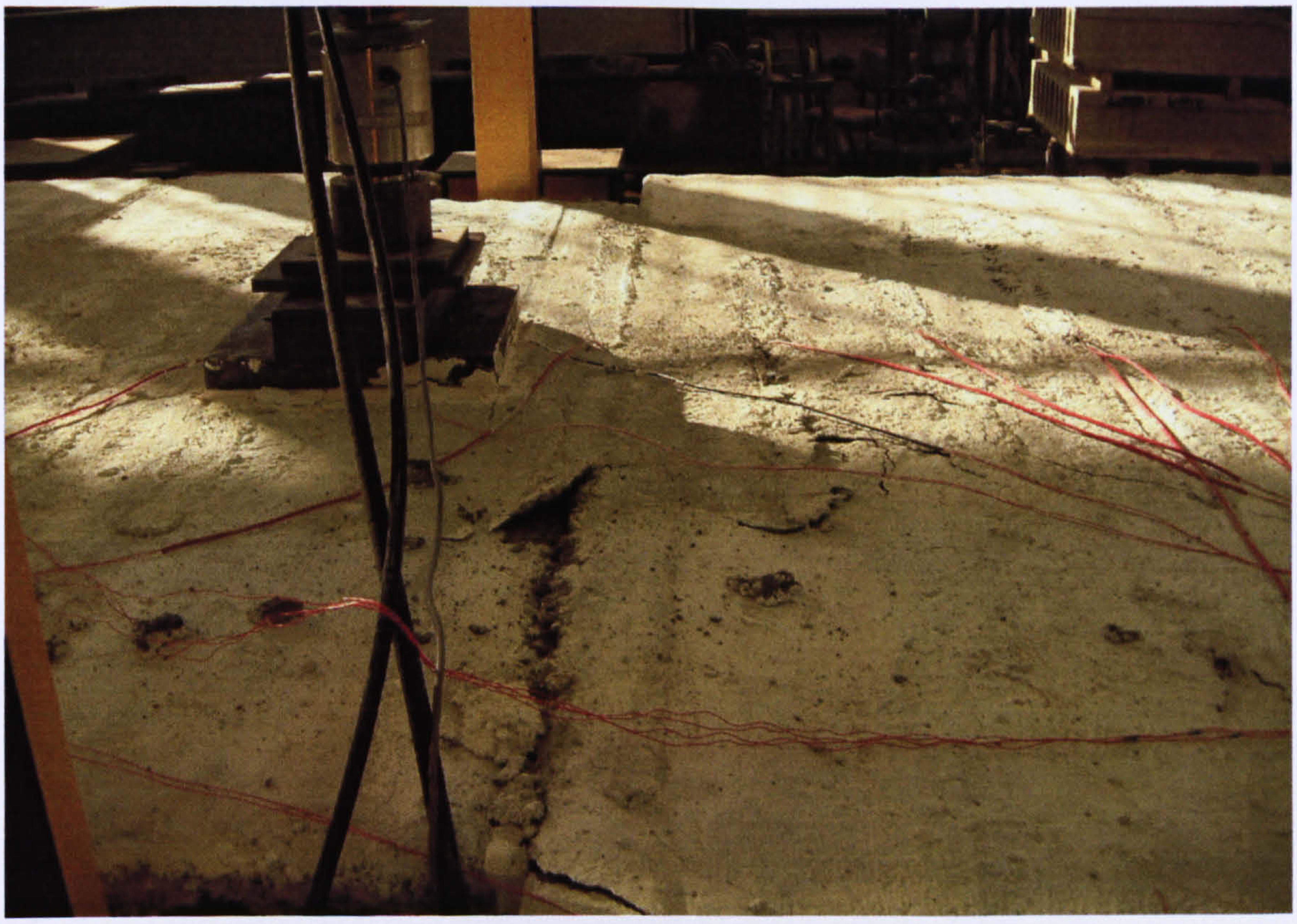

Figure 4.5: CB-1 Transverse cracking along joint between slabs at mid-span

Figure 4.6: Exposed studs on North side of CB-1

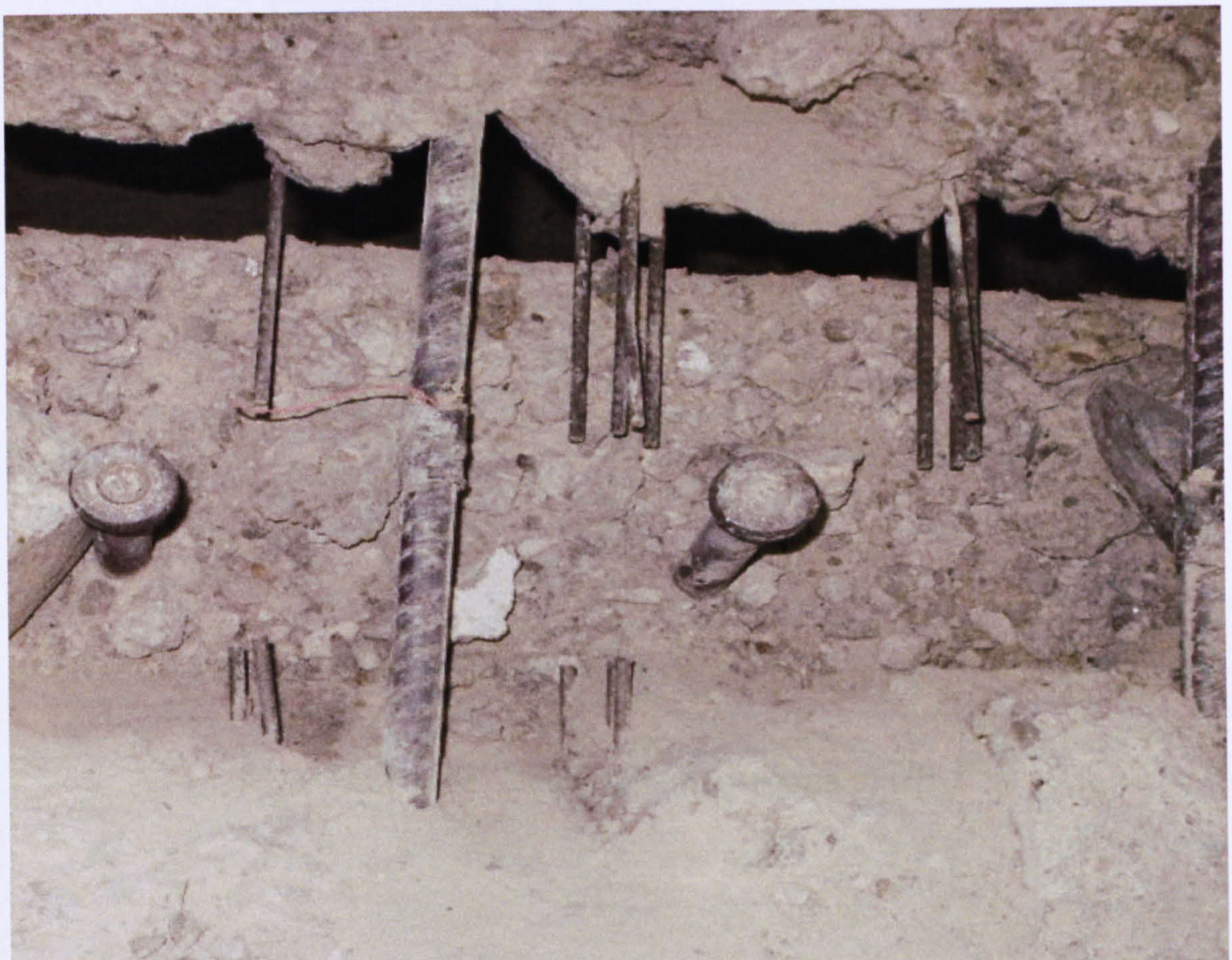

Figure 4.7: Exposed studs on South side of CB-1

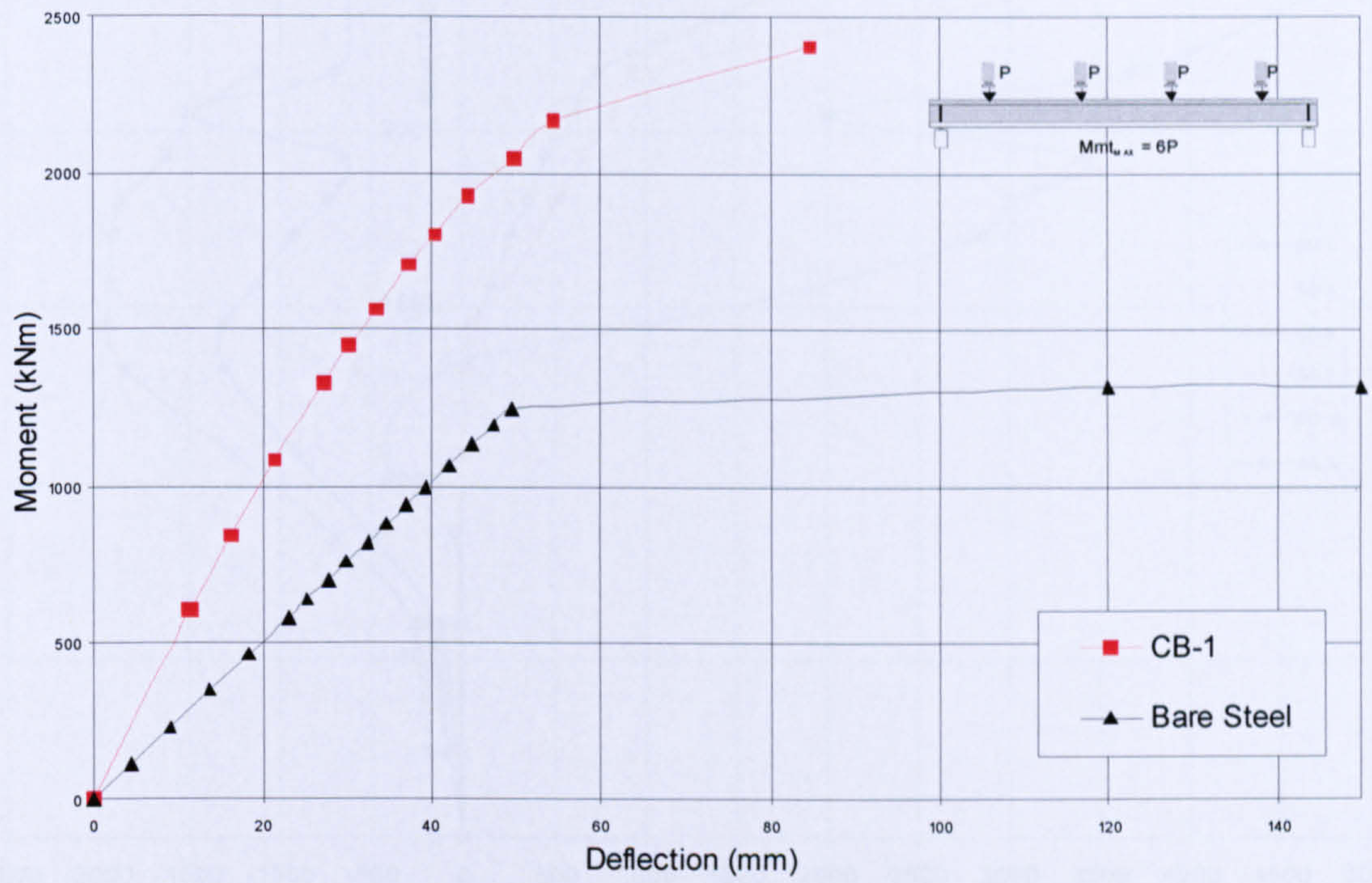

Figure 4.8: Moment vs. Mid-span deflection of CB-1

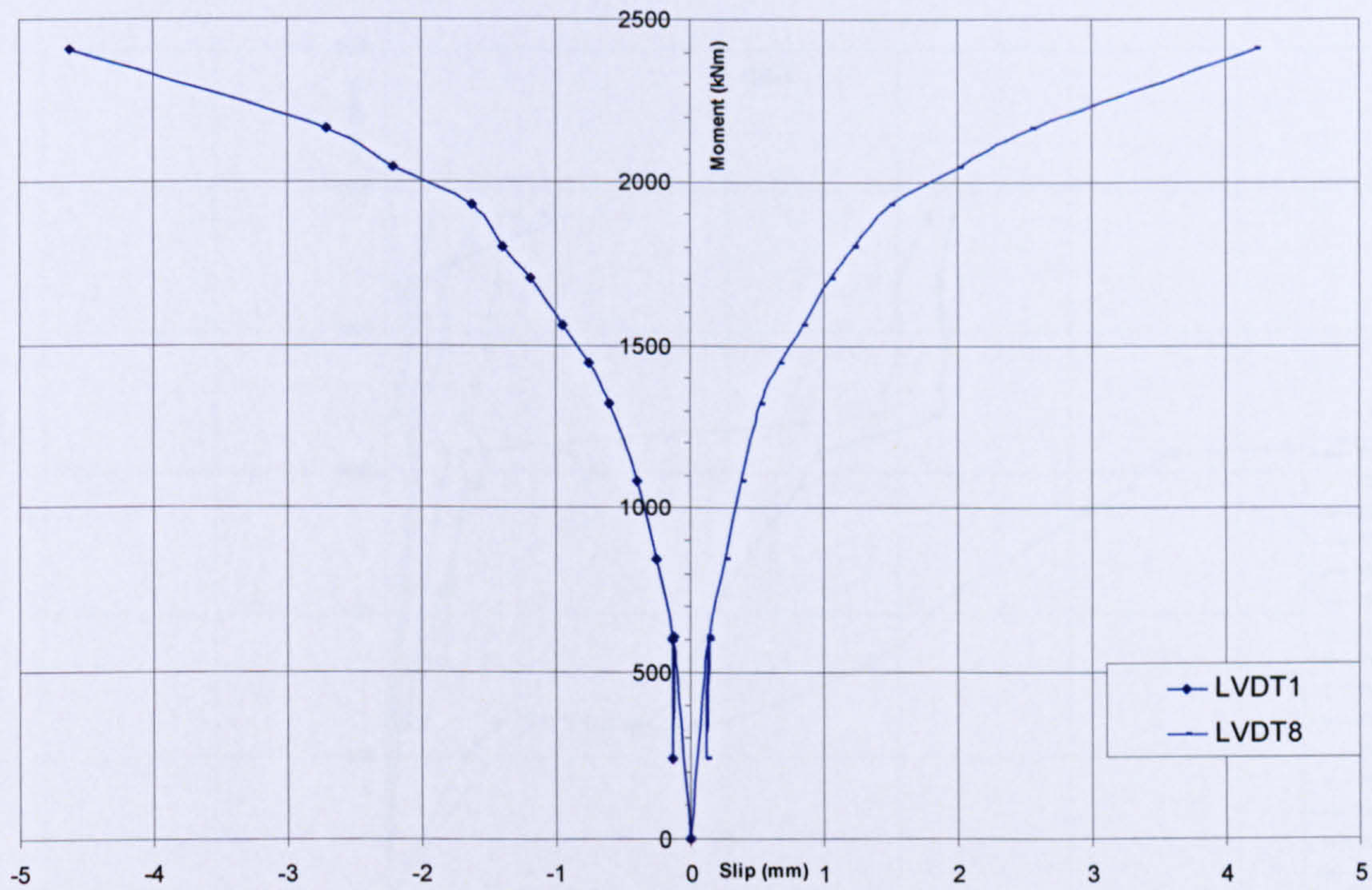

Figure 4.9: Moment vs. Slip at Interface of CB-1

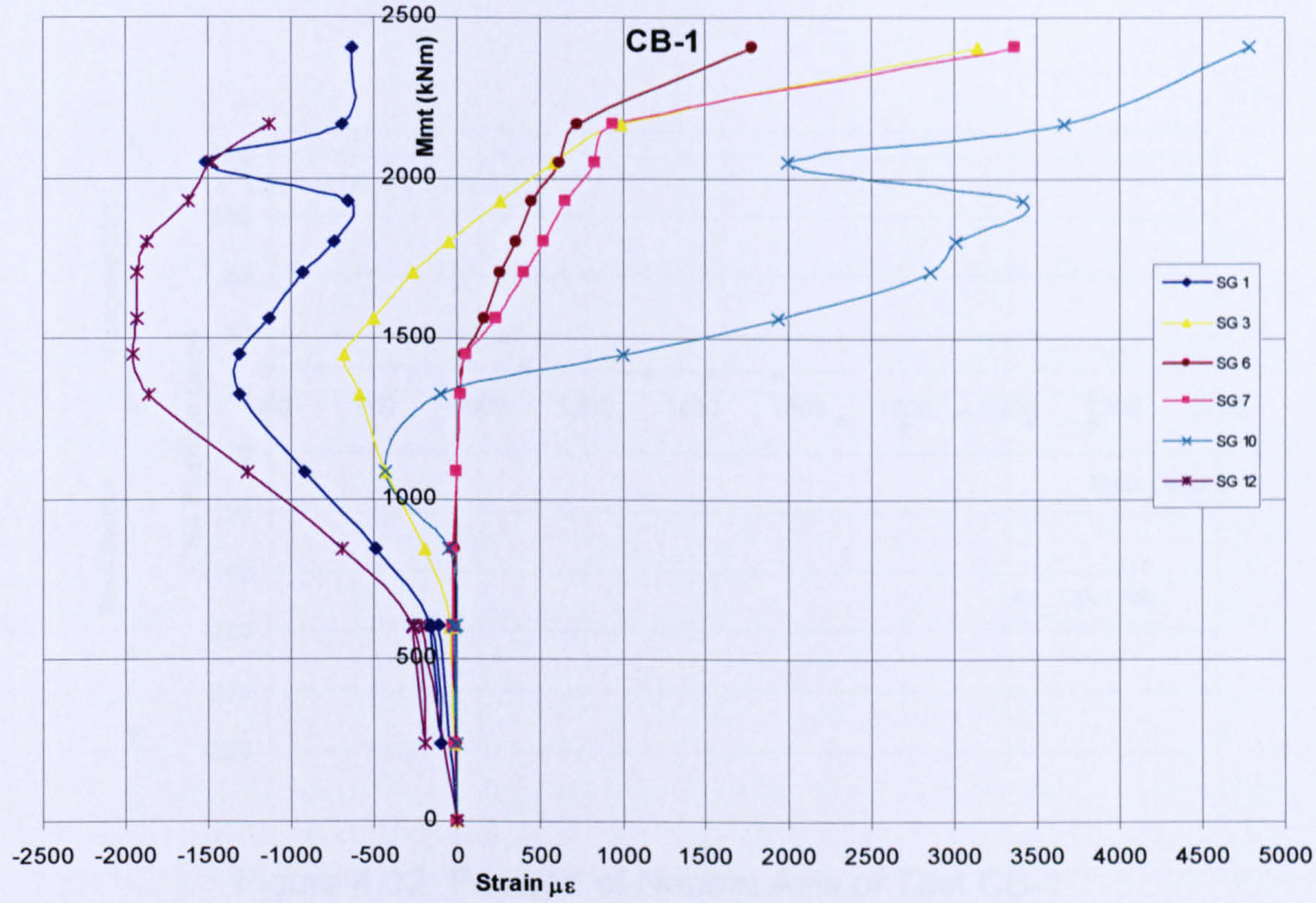

Figure 4.10: Moment vs. Strain on Shear Studs of CB-1

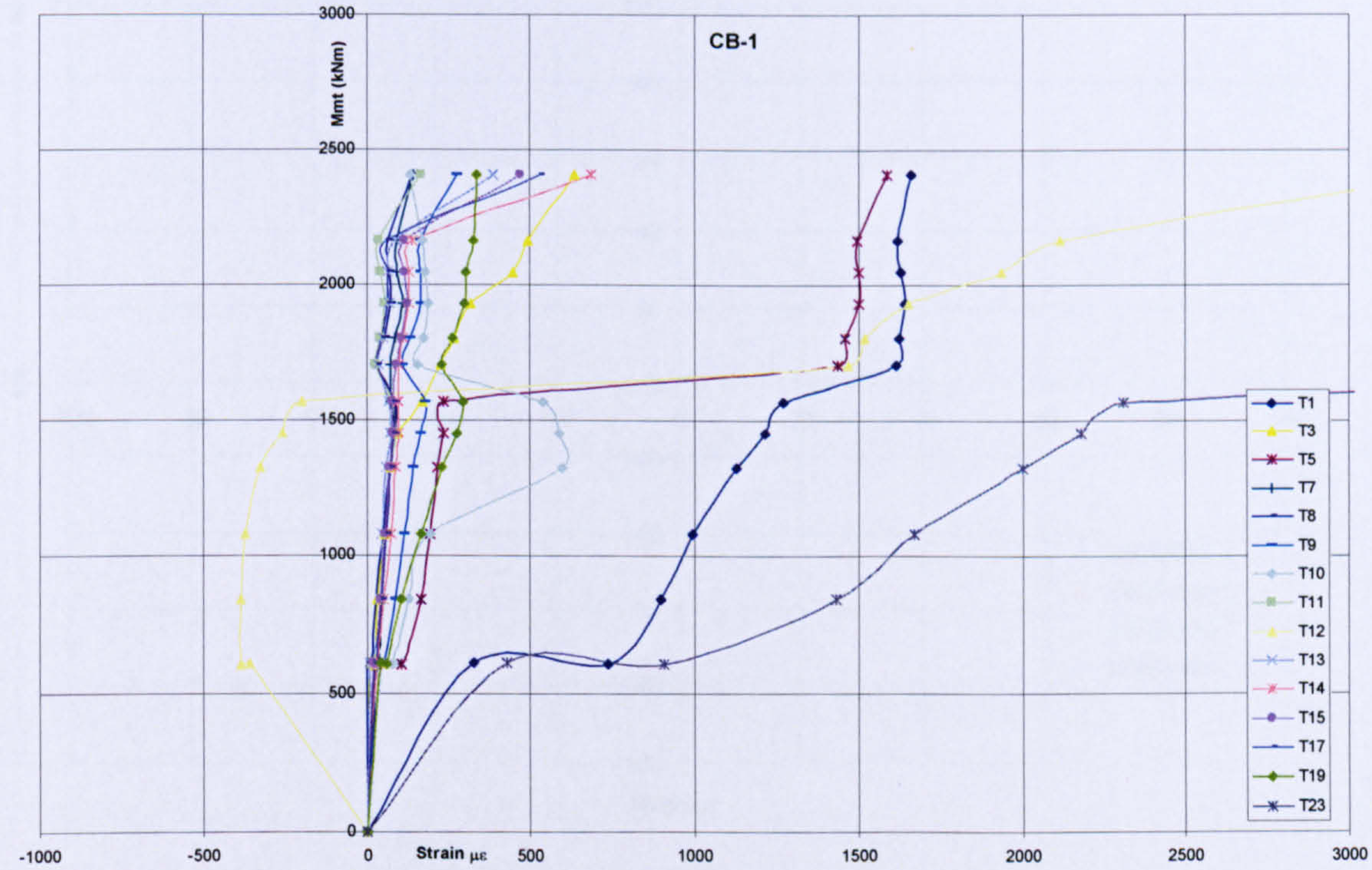

Figure 4.11: Moment vs. Strain on Transverse Reinforcement of CB-1

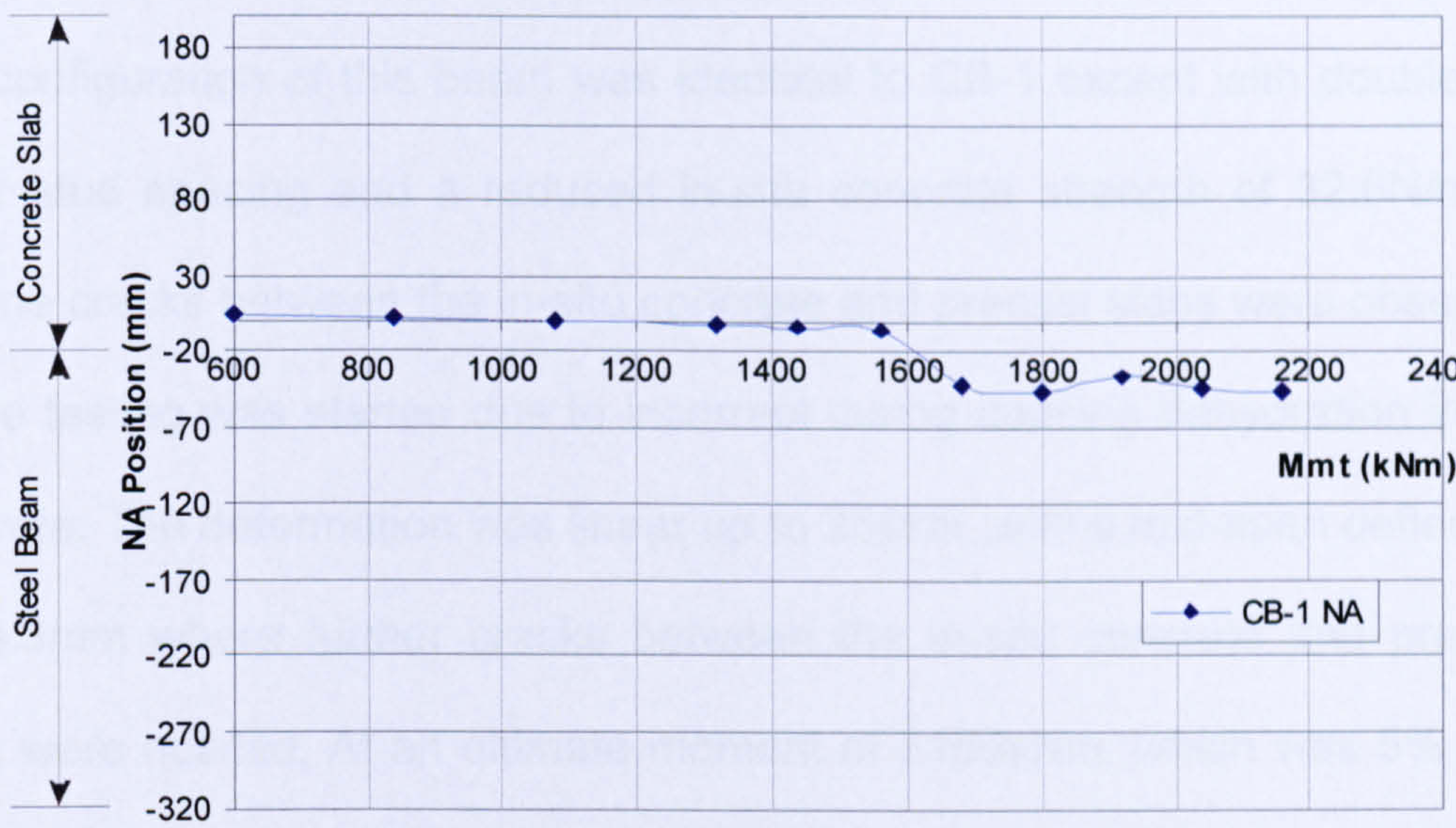

Figure 4.12: Position of Neutral Axis of Test CB-1

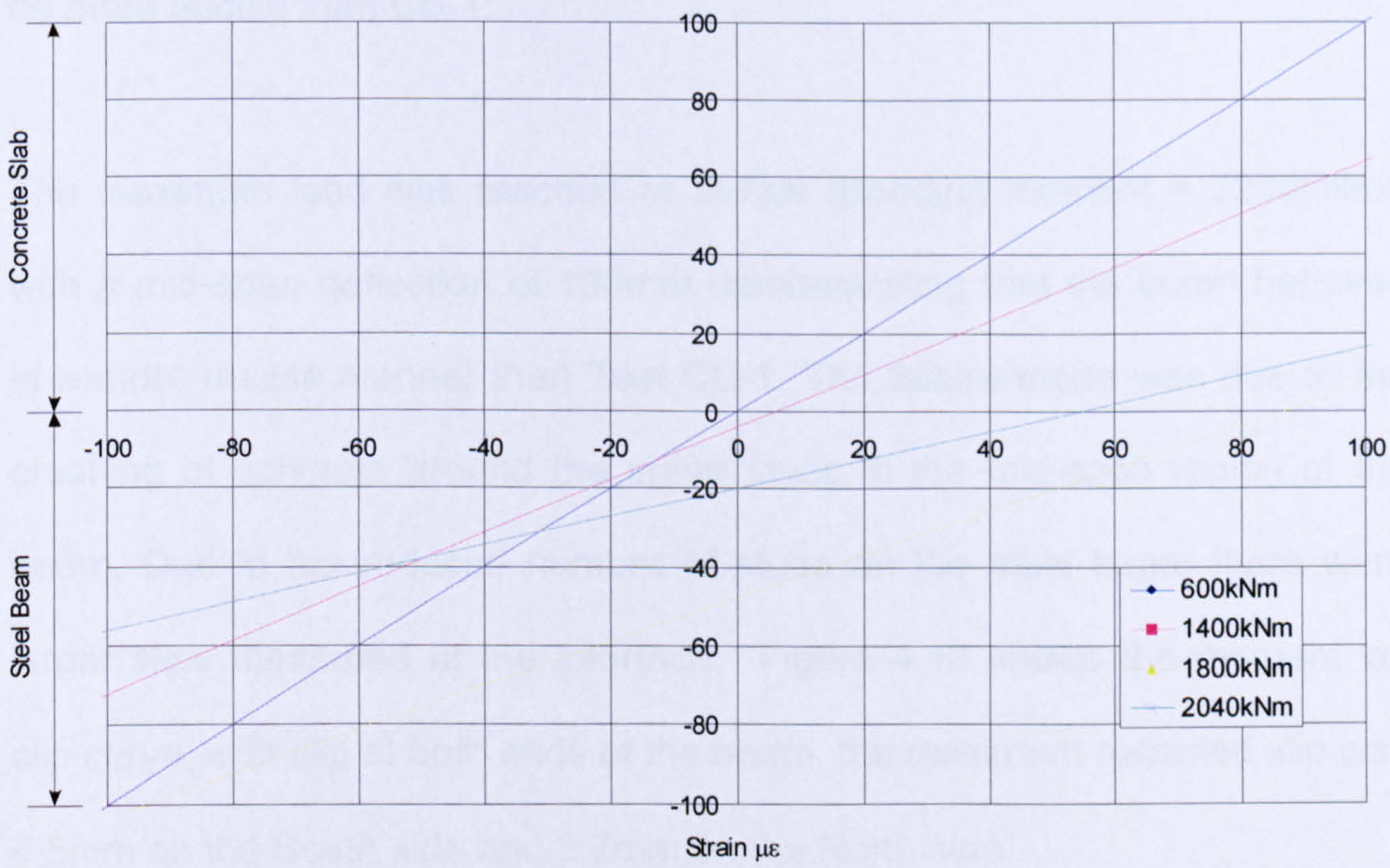

Figure 4.13: Strain Distribution for Test CB-1

4.3.4 Test CB-2

The configuration of this beam was identical to CB-1 except with double the shear stud spacing and a reduced in-situ concrete strength of 32.6N/mm^2. Hairline cracks between the in-situ concrete and precast slabs were observed before testing was started due to incorrect curing causing dehydration in the concrete. The deformation was linear up to 250kN, with a mid-span deflection of 46.3mm where further cracks between the in-situ concrete and precast slabs were noticed. At an ultimate moment of 2150kNm, which was 5% less than reached in test CB-1, crushing of the concrete in the mid-span region occurred and spalling of concrete from the precast slab was observed. The steel beam did not yield and the failure of this beam specimen was found to be more ductile than CB-1.

The maximum load was reached at 367kN (Bending moment = 2200kNm), with a mid-span deflection of 130mm demonstrating that the beam behaved in a more ductile manner than Test CB-1. The failure mode was due to the crushing of concrete around the shear studs in the mid-span region of the beam. Due to the reduced number of studs on the steel beam there were larger slips measured at the interface. Figure 4.18 shows the moment vs. slip curve, with slip at both ends of the beam, the maximum recorded slip was 4.5mm on the South side and 3.7mm on the North side.

The beam specimen was then dismantled to investigate the mode of failure, which was found to be concrete crushing in the mid-span region of the beam with shear studs on the steel beam remaining intact. Figures 4.14 and 4.15 show regions of the slab dismantled along the beam with shear studs still intact. Also observed was the shear failure of the precast slab which occurred at a moment of 1950kNm (Figure 4.16).

Figure 4.17 shows the moment vs. deflection curve of test CB-2, the beam remained elastic up to 1400kNm; further moment caused an increase in strain on the studs and first cracks were observed. Figure 4.19 shows the strain measured on studs increased after cracks were observed in the concrete, although the studs on the beam remained intact. The strain measured on the transverse reinforcement (Figure 4.20) was relatively small, although as with the studs, the transverse bars placed at the central region of the slab had an increase in strain once the beam became plastic.

As crushing in concrete occurred the neutral axis moved towards the tension zone of the beam, finishing in the web of the steel section. Figure 4.21 shows the position of neutral axis and the strain distribution for test CB2 is shown in Figure 4.22.

Figure 4.14: Exposed stud on North side of CB-2

Figure 4.15: Exposed studs on South side of CB-2

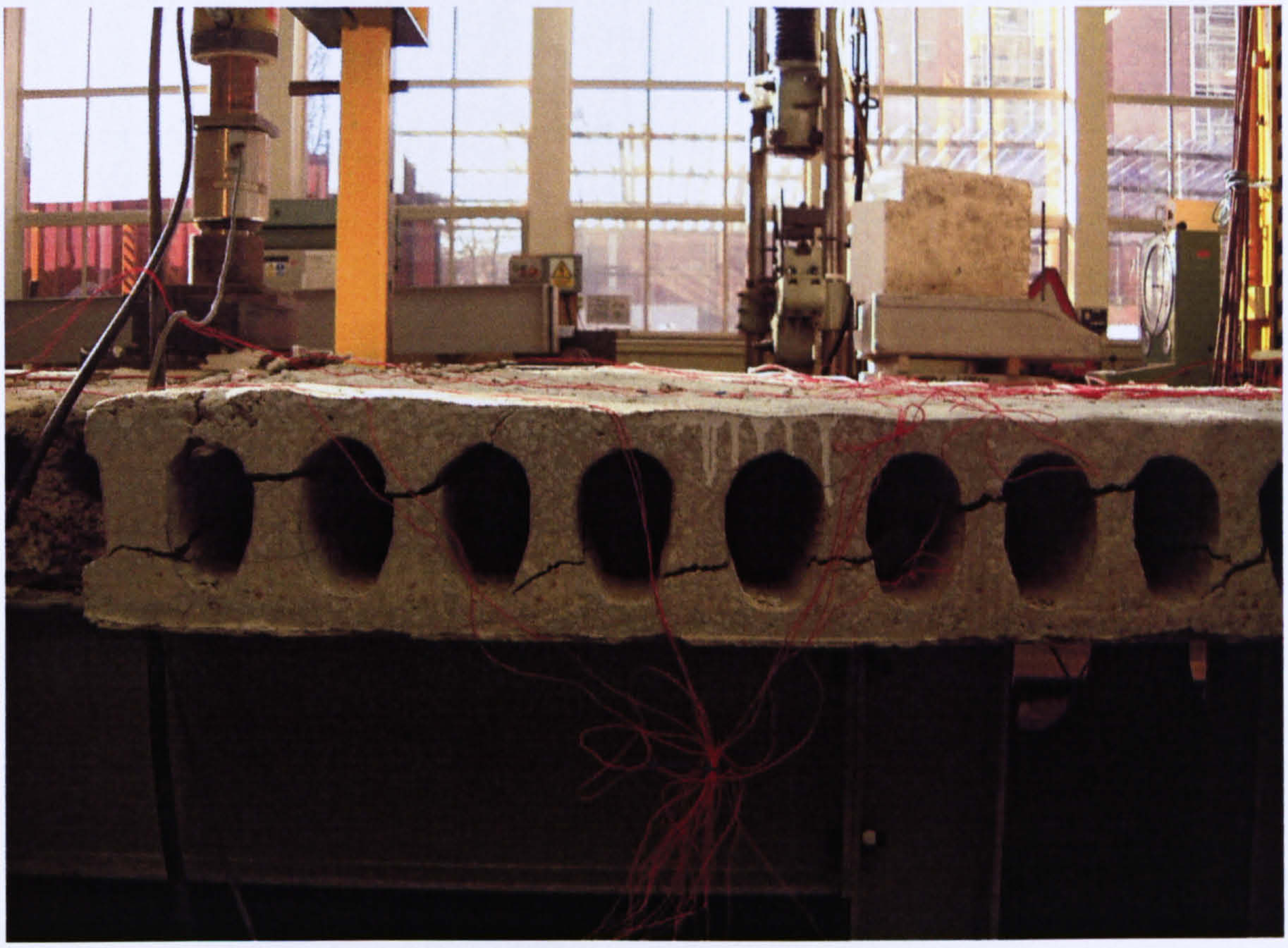

Figure 4.16: Shear failure in central slab of CB-2

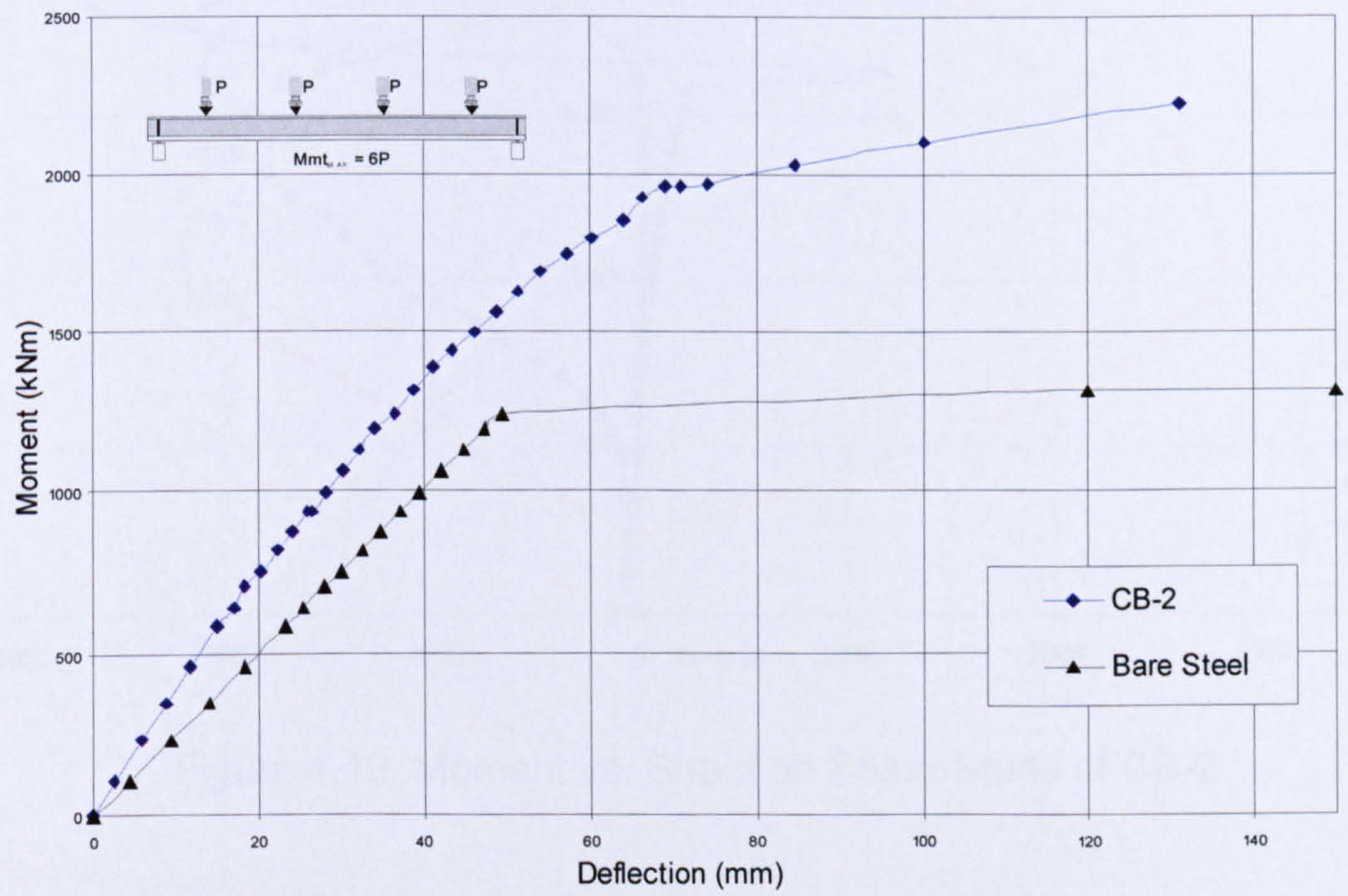

Figure 4.17: Moment vs. Mid-span deflection of CB-2

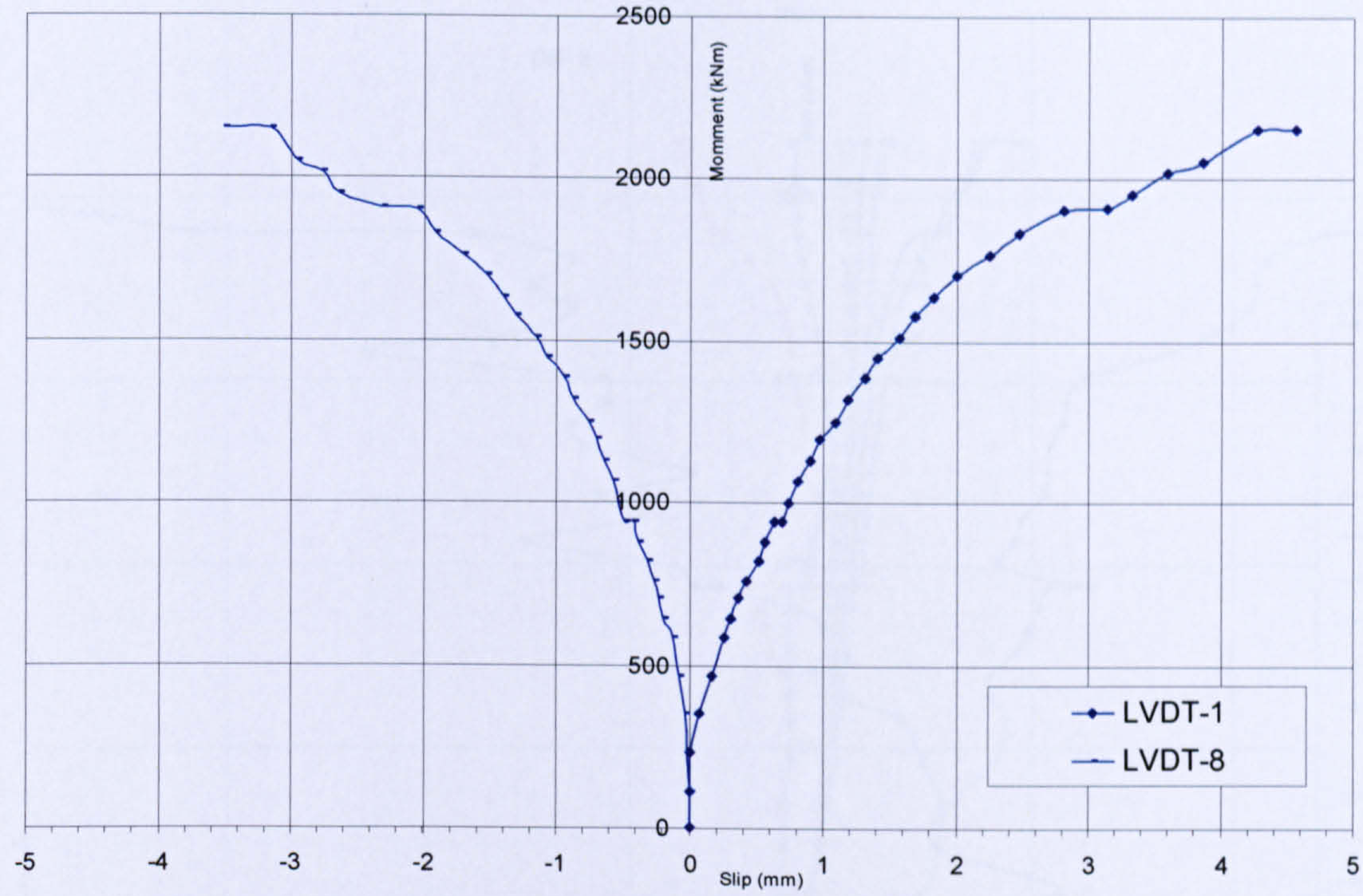

Figure 4.18: Moment vs. Slip at Interface of CB-2

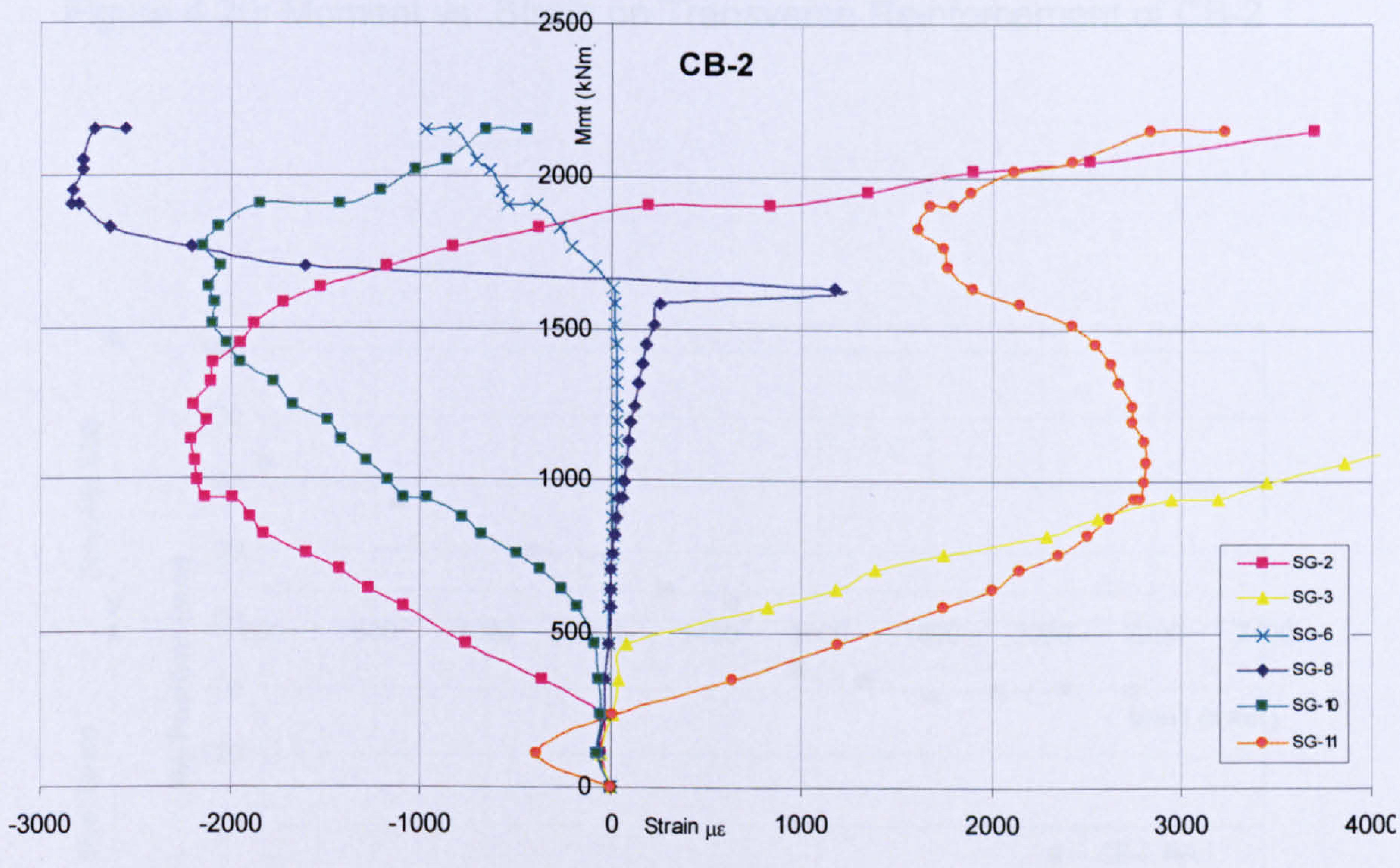

Figure 4.19: Moment vs. Strain on Shear Studs of CB-2

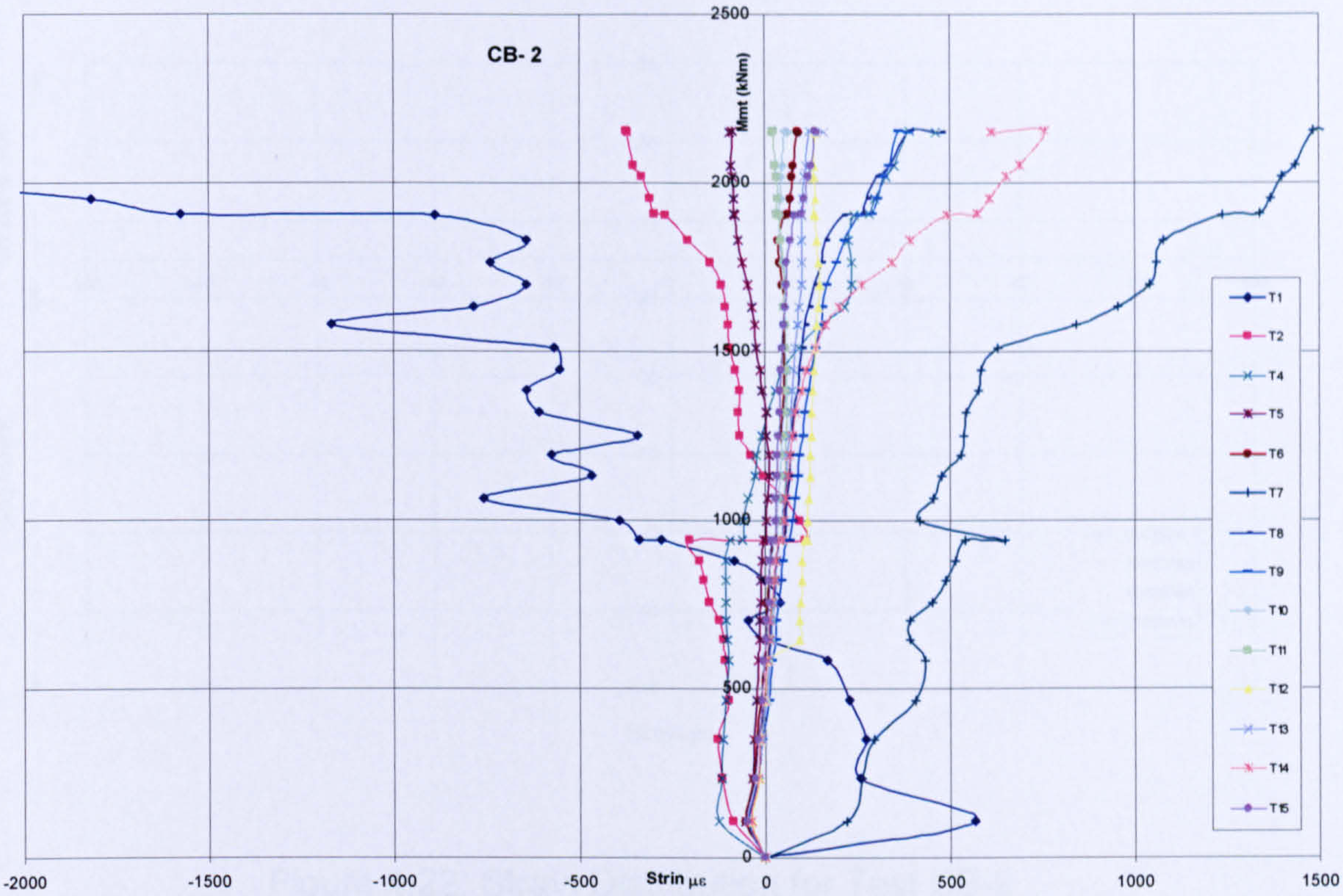

Figure 4.20: Moment vs. Strain on Transverse Reinforcement of CB-2

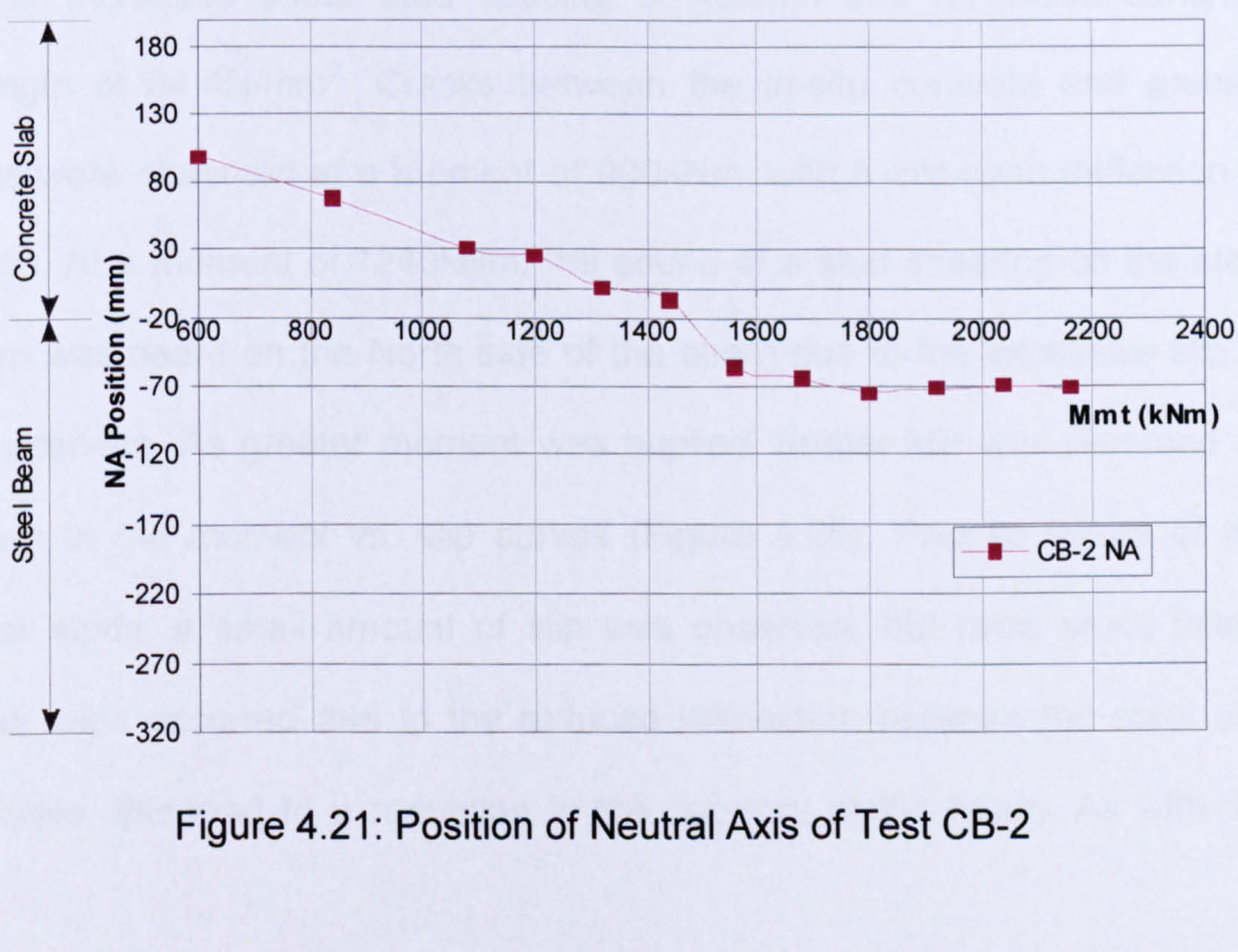

Figure 4.21: Position of Neutral Axis of Test CB-2

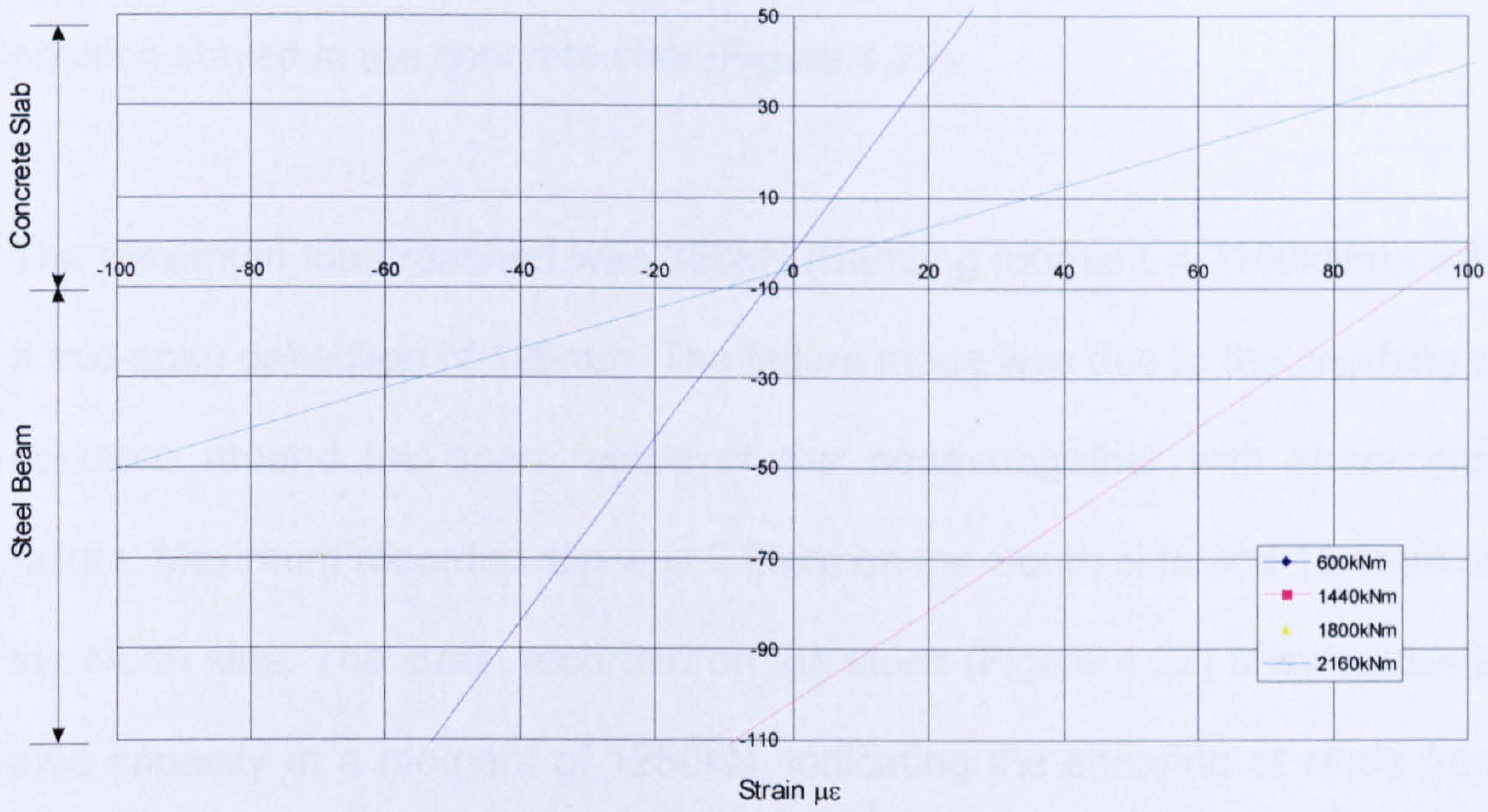

Figure 4.22: Strain Distribution for Test CB-2

4.3.5 Test CB-3

The configuration of this beam was identical to CB-1 and CB-2 except with a further increased shear stud spacing of 400mm and an in-situ concrete strength of 34.4N/mm^2. Cracks between the in-situ concrete and precast slabs were observed at a moment of 900kNm, with a mid-span deflection of 30mm. At a moment of 1240kNm, the sound of a stud shearing off the steel beam was heard on the North side of the beam due to the excessive slip at the interface. As greater moment was applied, further slip was recorded as shown in the moment vs. slip curves (Figure 4.26). Prior to failure of the shear studs, a small amount of slip was observed, but once studs failed, larger slips occurred due to the reduced interaction between the steel and concrete, this lead to a reduction in the capacity of the beam. As with the previous test there was no yielding in the steel beam, as the neutral axis position stayed in the concrete slab (Figure 4.29).

The maximum load reached was 350kN (Bending moment = 2100kNm), with a mid-span deflection of 126mm. The failure mode was due to the crushing of concrete around mid-span region of the beam together with shear stud failure. Maximum recorded slip was 5.0mm on the South side and 13.1mm on the North side. The strain recorded on the studs (Figure 4.27) show a loss in stud capacity at a moment of 1250kN, indicating the shearing of studs from this point onwards.

The beam specimen was then dismantled to investigate the mode of failure, which was found to be concrete crushing in the mid-span and shear stud failure along the beam, with studs shearing off and excessive slip taking place on the North side. Figures 4.23 and 4.24 shows the region of the slab dismantled along the beam with failed shear stud, where separation between the concrete and steel was observed after failure occurred.

Figure 4.25 shows the moment vs. deflection curve of test CB-3, the beam remained elastic up to 1250kNm, after this point there was an increase in strain on the studs and transverse reinforcement. Figure 4.28 shows the strain on the transverse reinforcement with increased strain as studs are lost from the shear connection. Transverse reinforcing bars placed behind the studs in the direction of bending had an increased strain measured. As the stud deformed/rotated due to interface slip, the transverse reinforcing bar provided resistance to rotation of the stud (Figure 4.31).

The neutral axis remained in the concrete throughout testing, dropping lower in the slab as failure occurred (Figure 4.29). Figure 4.30 shows the strain distribution for test CB3. As expected the test was found to be more ductile than CB-1 and CB-2, due to the reduced shear connection of the composite beam.

Figure 4.23: Exposed stud at mid-span region in slab of CB-3

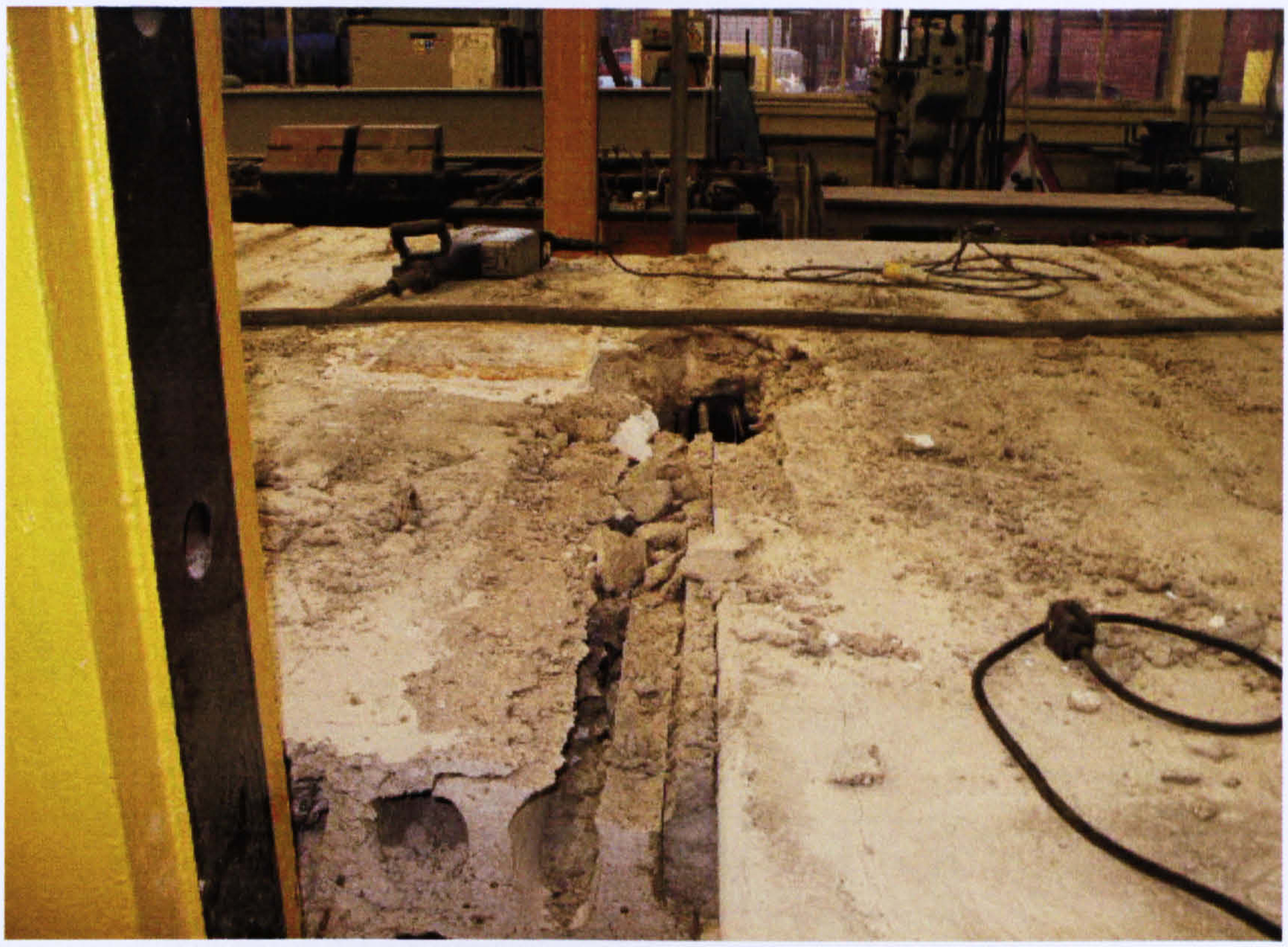

Figure 4.24: Propogated cracking along joint of mid-span region in slab of CB-3

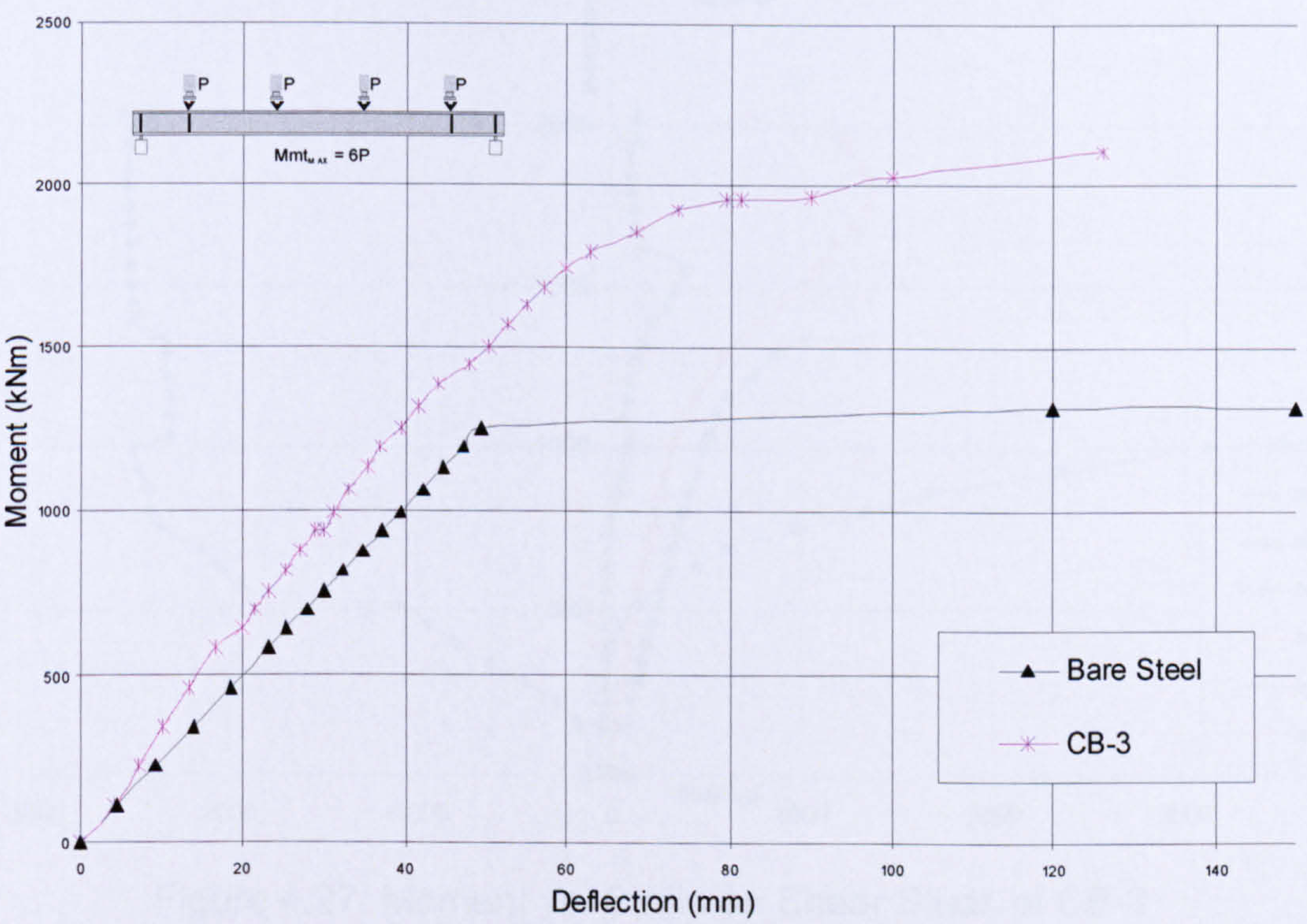

Figure 4.25: Moment vs. Mid-span deflection of CB-3

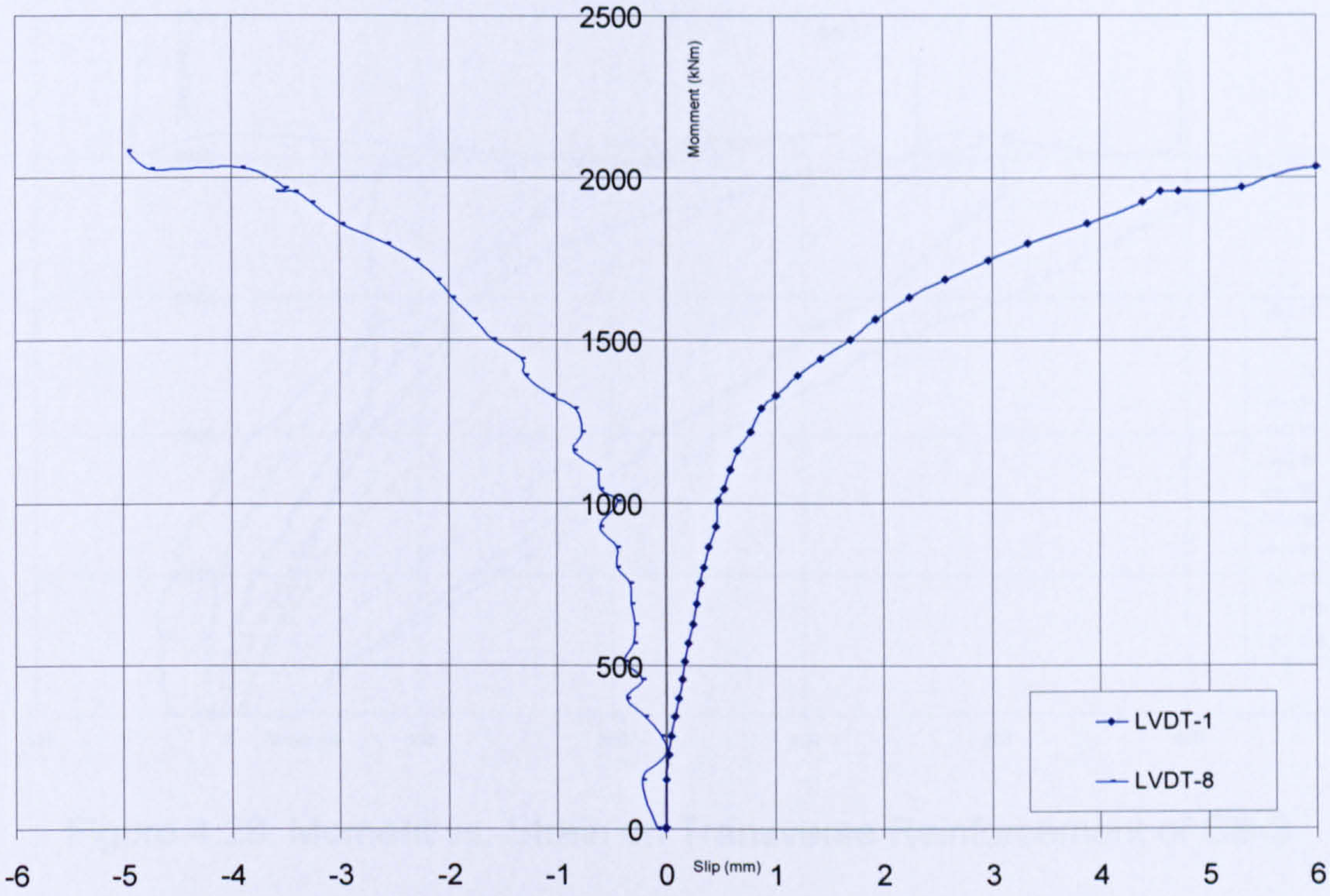

Figure 4.26: Moment vs. Slip at Interface of CB-3

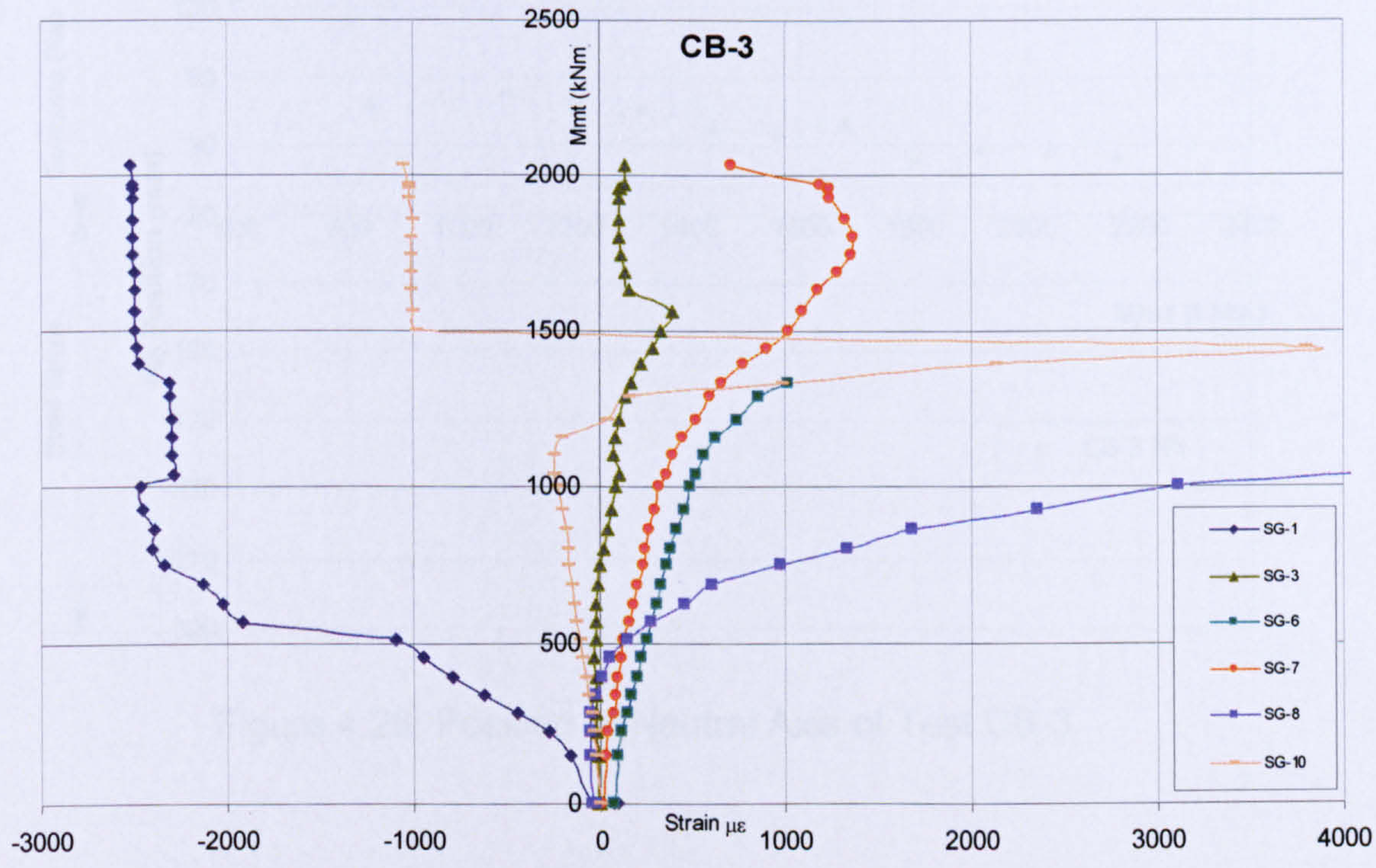

Figure 4.27: Moment vs. Strain on Shear Studs of CB-3

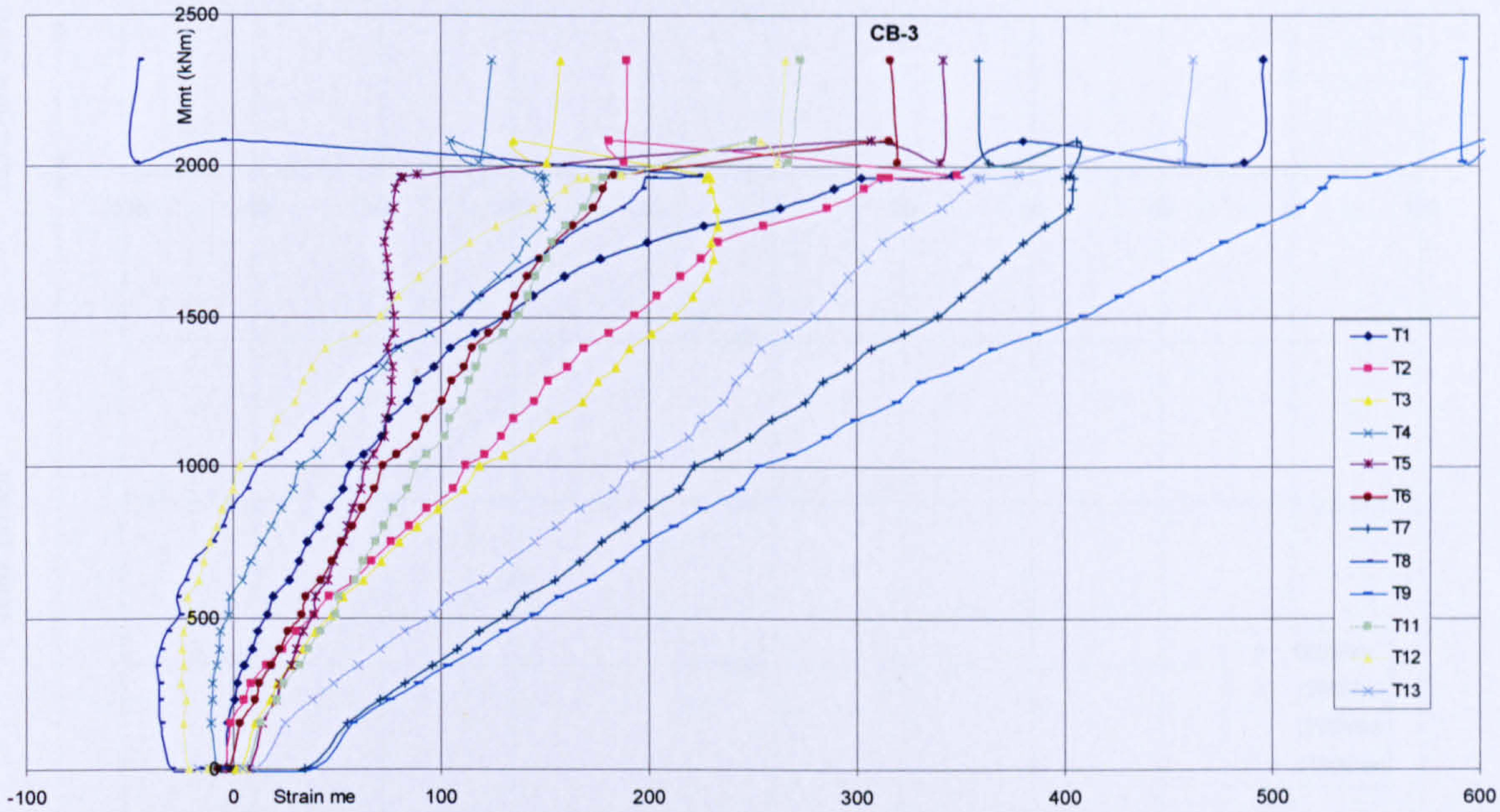

Figure 4.28: Moment vs. Strain on Transverse Reinforcement of CB-3

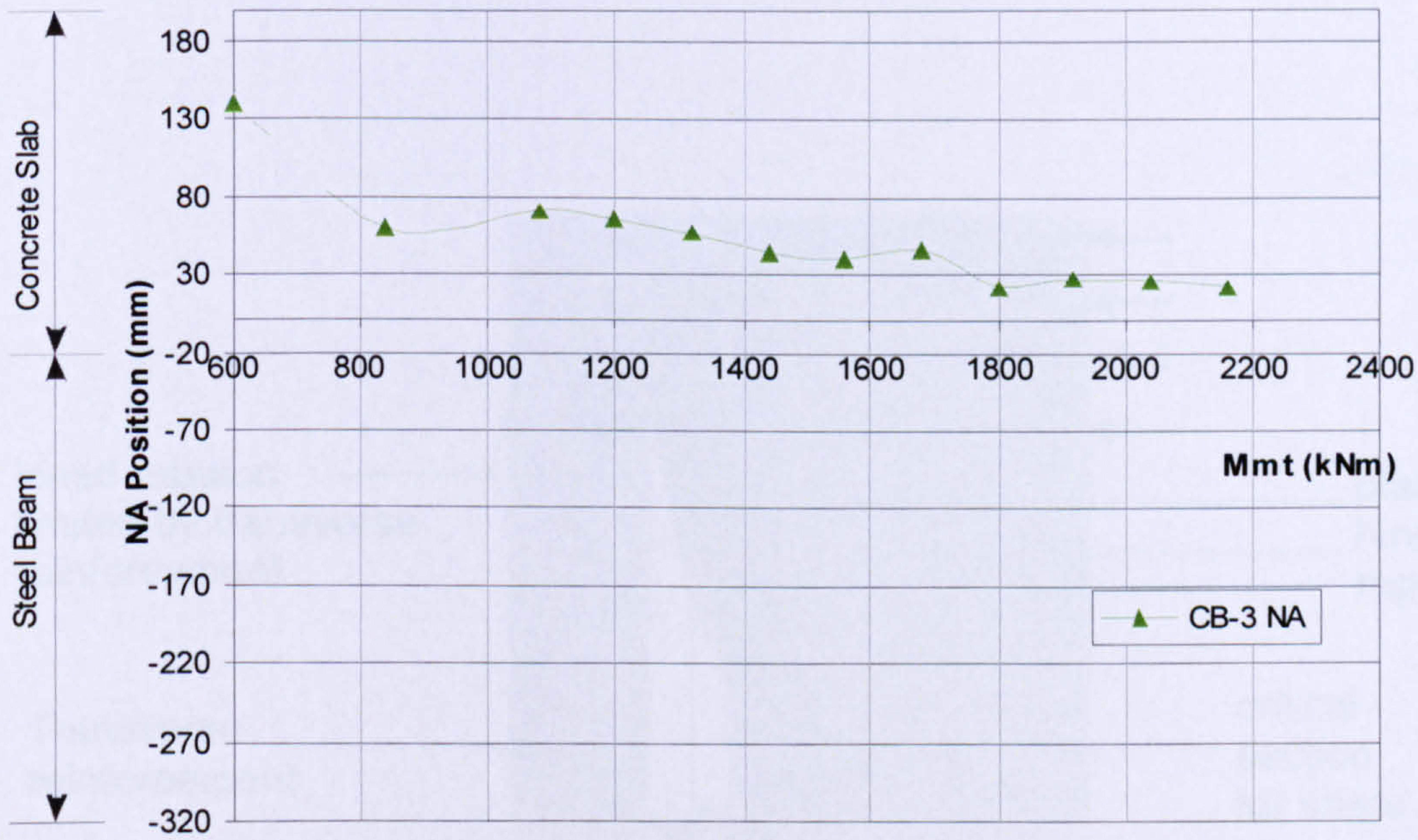

Figure 4.29: Position of Neutral Axis of Test CB-3

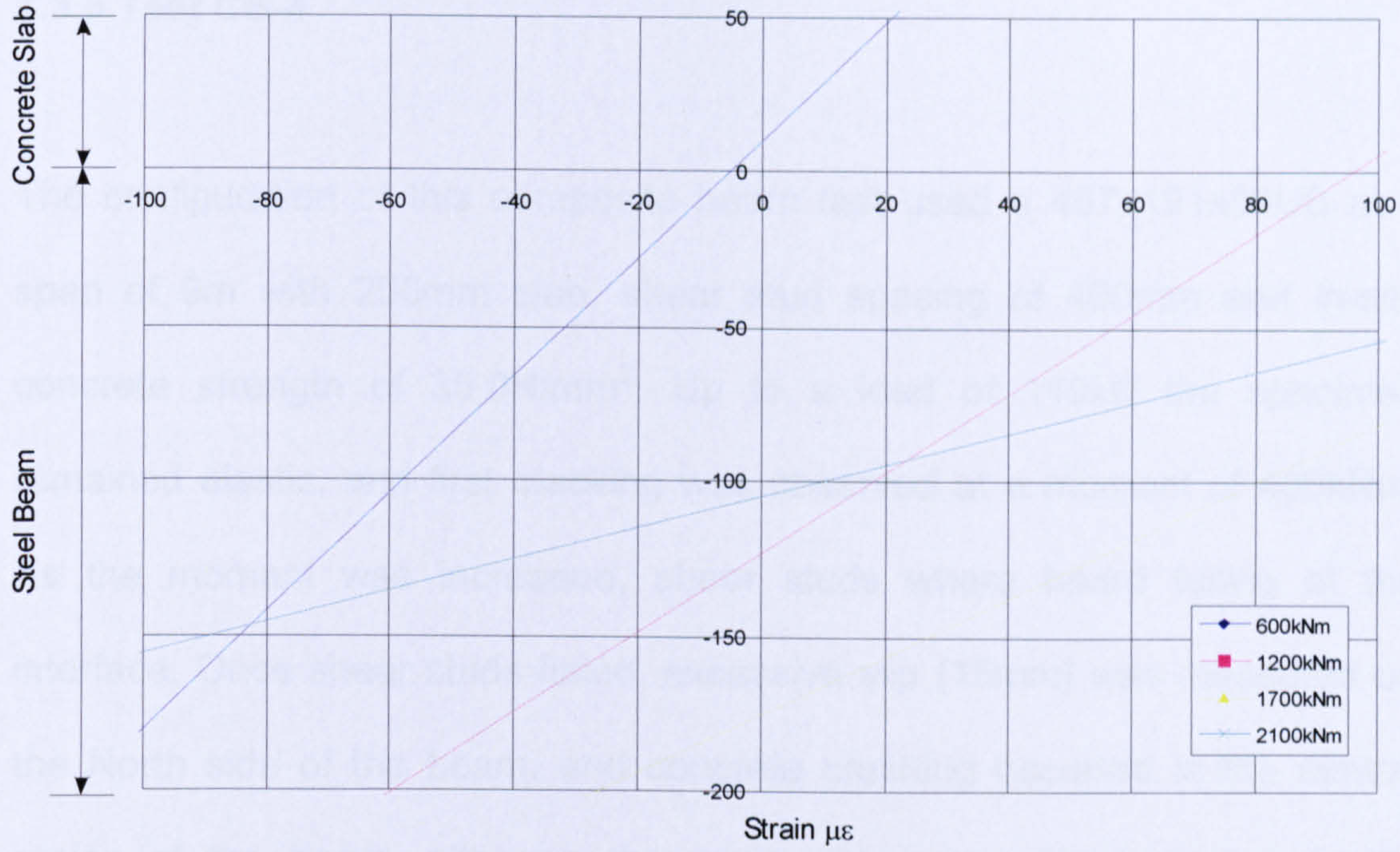

Figure 4.30: Strain Distribution for Test CB-3

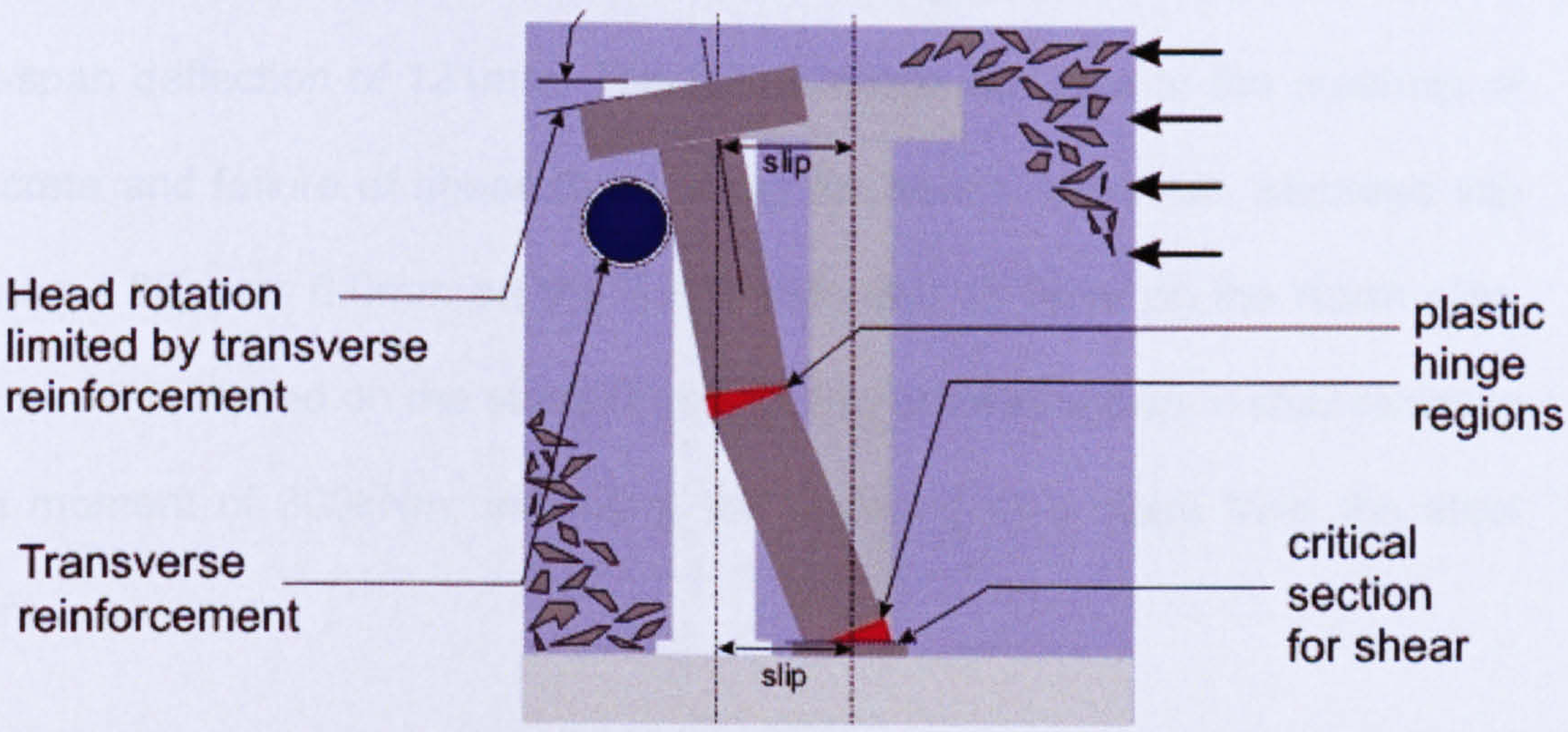

Figure 4.31: Transverse bar limiting rotation of stud

4.3.6 Test CB-4

The configuration of this composite beam test used a 457x191x89UB at a span of 9m with 200mm slab, shear stud spacing of 400mm and in-situ concrete strength of 35.0N/mm^2. Up to a load of 110kN the specimen remained elastic, and first cracking was observed at a moment of 400kNm. As the moment was increased, shear studs where heard failing at the interface. Once shear studs failed, excessive slip (15mm) was measured on the North side of the beam, and concrete crushing occurred in the central region of the beam, although the composite beam demonstrated ductile behaviour. The neutral axis remained in the slab throughout the test, and the steel did not yield.

The maximum load reached was 310kN (Bending moment = 930kNm), with a mid-span deflection of 121mm. The failure mode was due to the crushing of concrete and failure of shear studs along the beam. Maximum recorded slip (Figure 4.35) was 6.0mm on the South side and 15.0mm on the North side. The strain recorded on the studs (Figure 4.36) showed a loss in stud capacity at a moment of 300kNm, indicating the shearing of a studs from the steel beam.

The beam specimen was then dismantled to investigate the mode of failure, which was found to be concrete crushing and shear failure in the mid-span region of the beam with shear studs on the steel beam shearing off. Figures 4.32 and 4.33 show regions of the slab dismantled along the beam.

Figure 4.34 shows the moment vs. deflection curve of test CB-4, the beam remained elastic up to 330kNm; however the beam was able to carry further moment, although shear studs were failing and there was an increase in strain on the transverse reinforcement after studs failed. Figure 4.37 shows the strain measured on the transverse reinforcement with increased strain as studs are lost from the connection.

As failure in connection occurred the neutral axis moved towards the compression zone of the beam, finishing 160mm above the interface in the concrete slab. Figure 4.38 shows the position of neutral axis and the strain distribution for test CB4 is shown in Figure 4.39.

Figure 4.32: Moment vs. Slip at Interface of CB-4

Figure 4.33: Moment vs. Strain on Shear Studs of CB-4

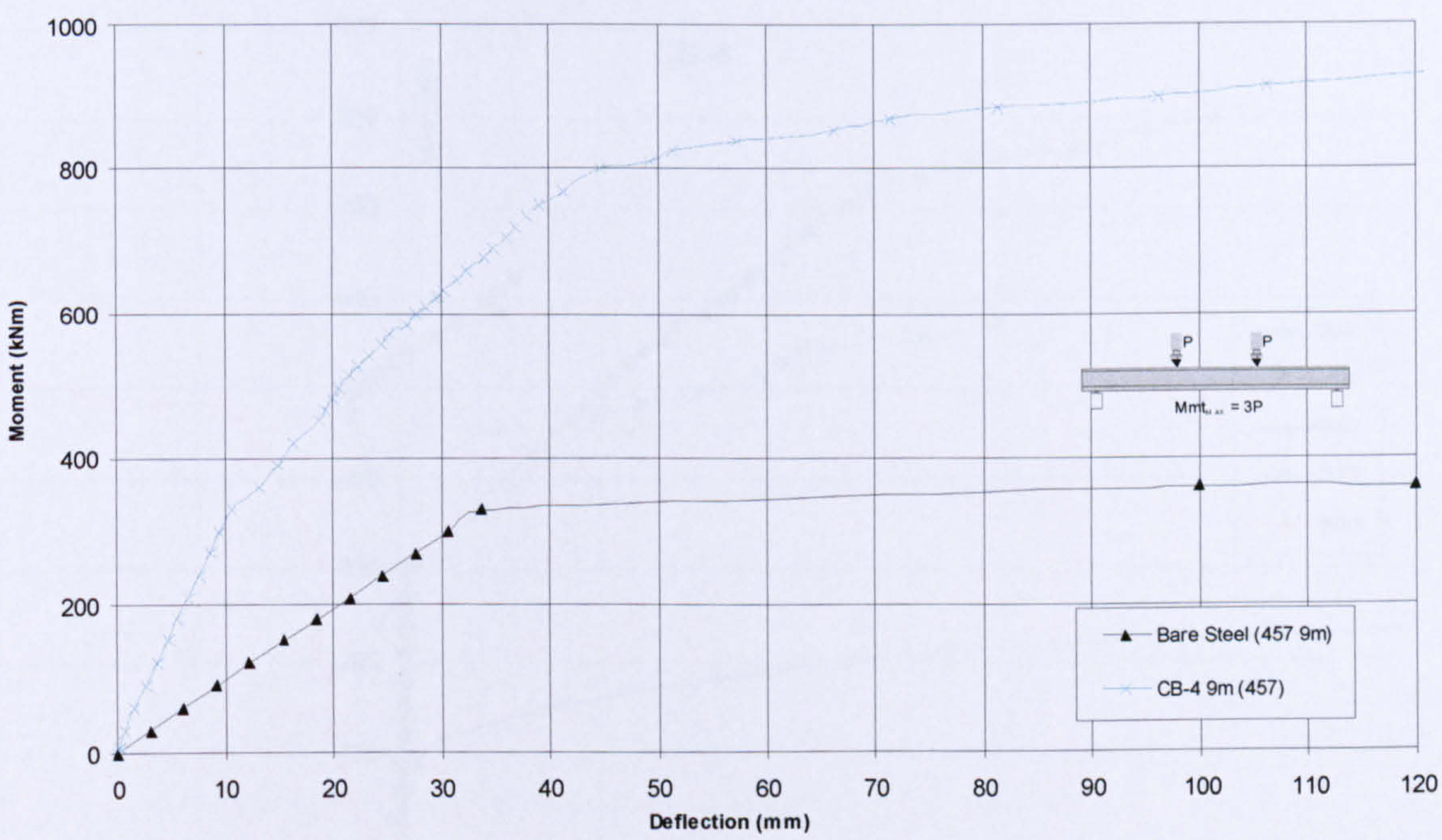

Figure 4.34: Moment vs. Mid-span deflection of CB-4

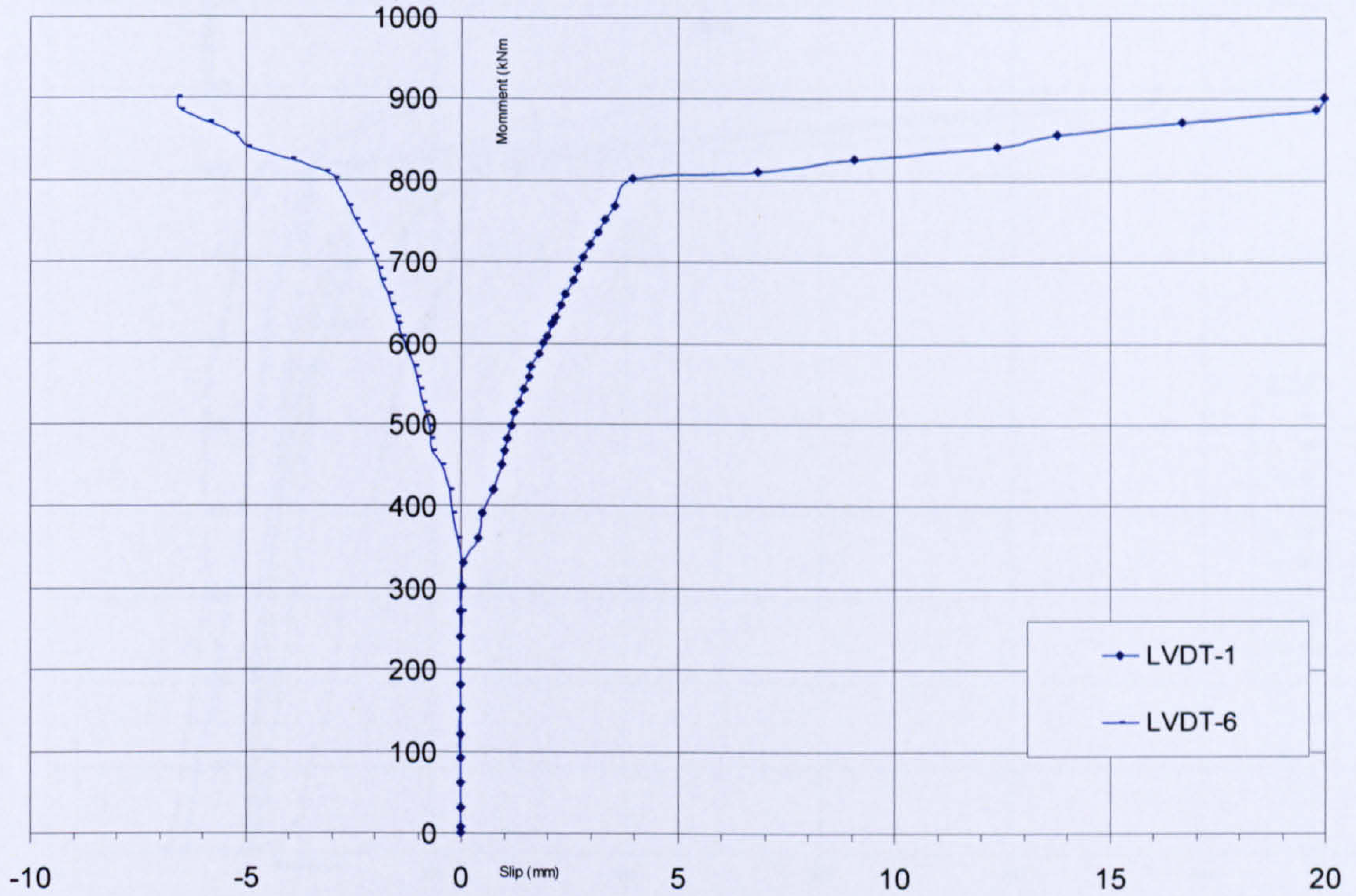

Figure 4.35: Moment vs. Slip at Interface of CB-4

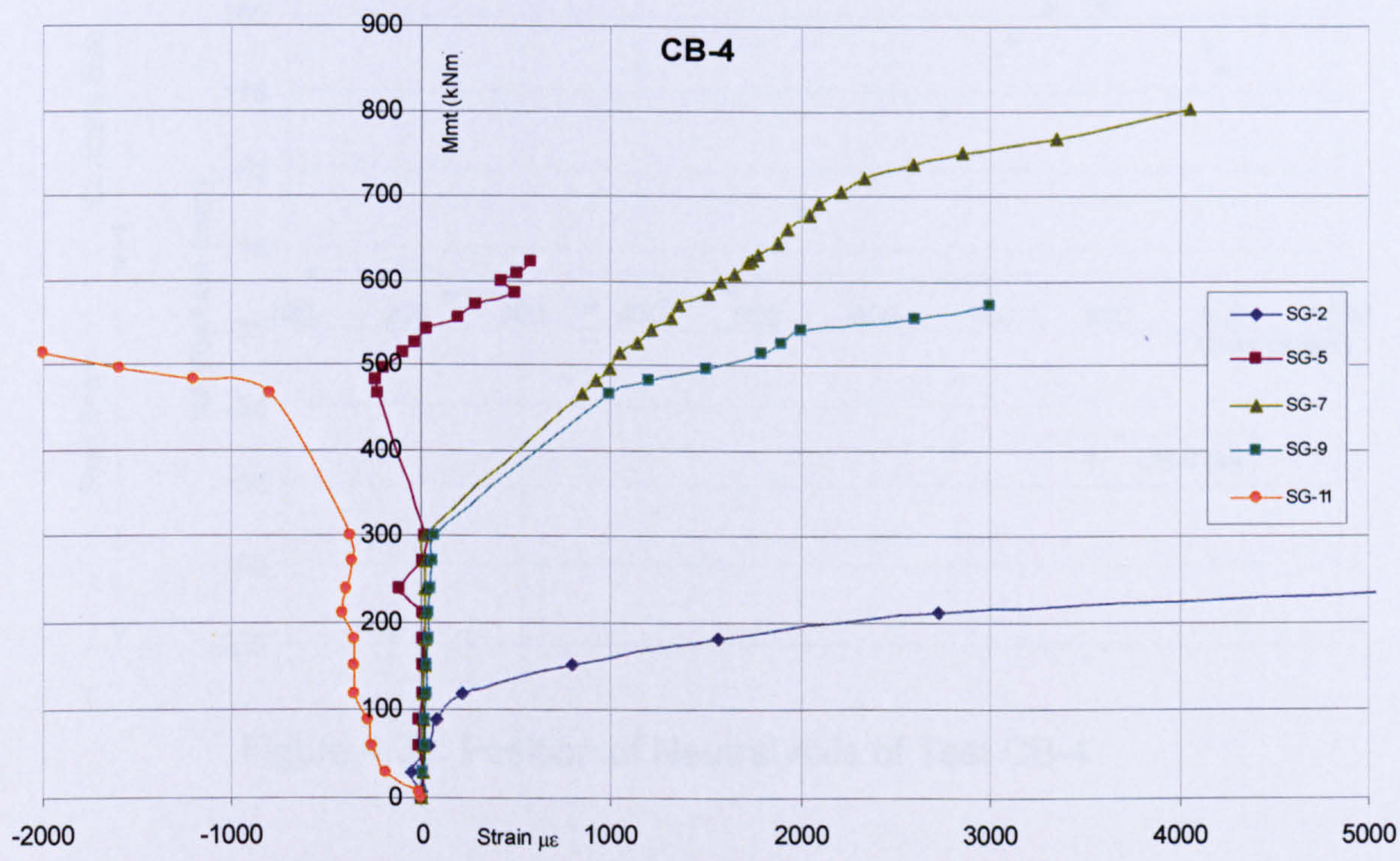

Figure 4.36: Moment vs. Strain on Shear Studs of CB-4

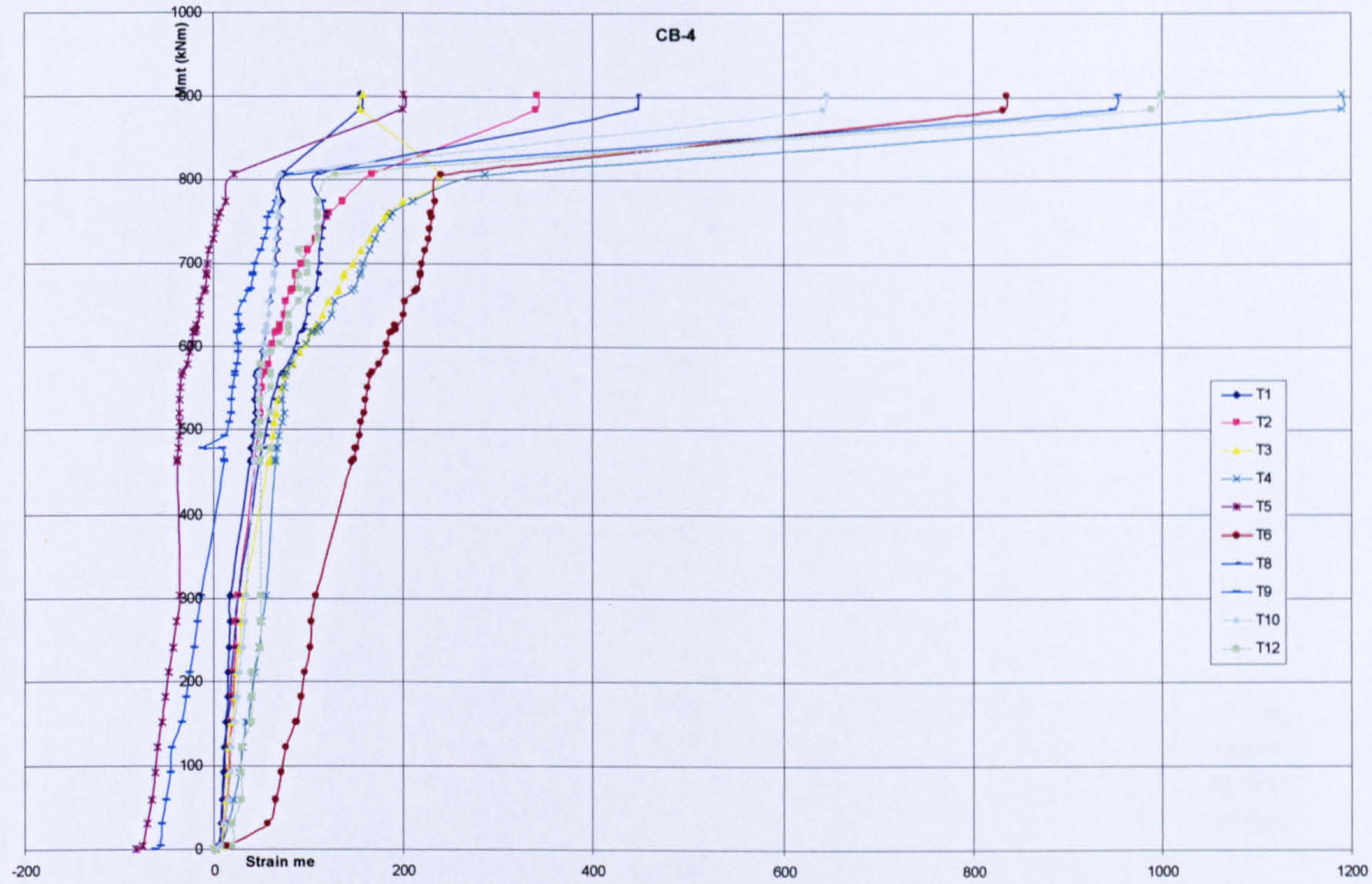

Figure 4.37: Moment vs. Strain on Transverse Reinforcement of CB-4

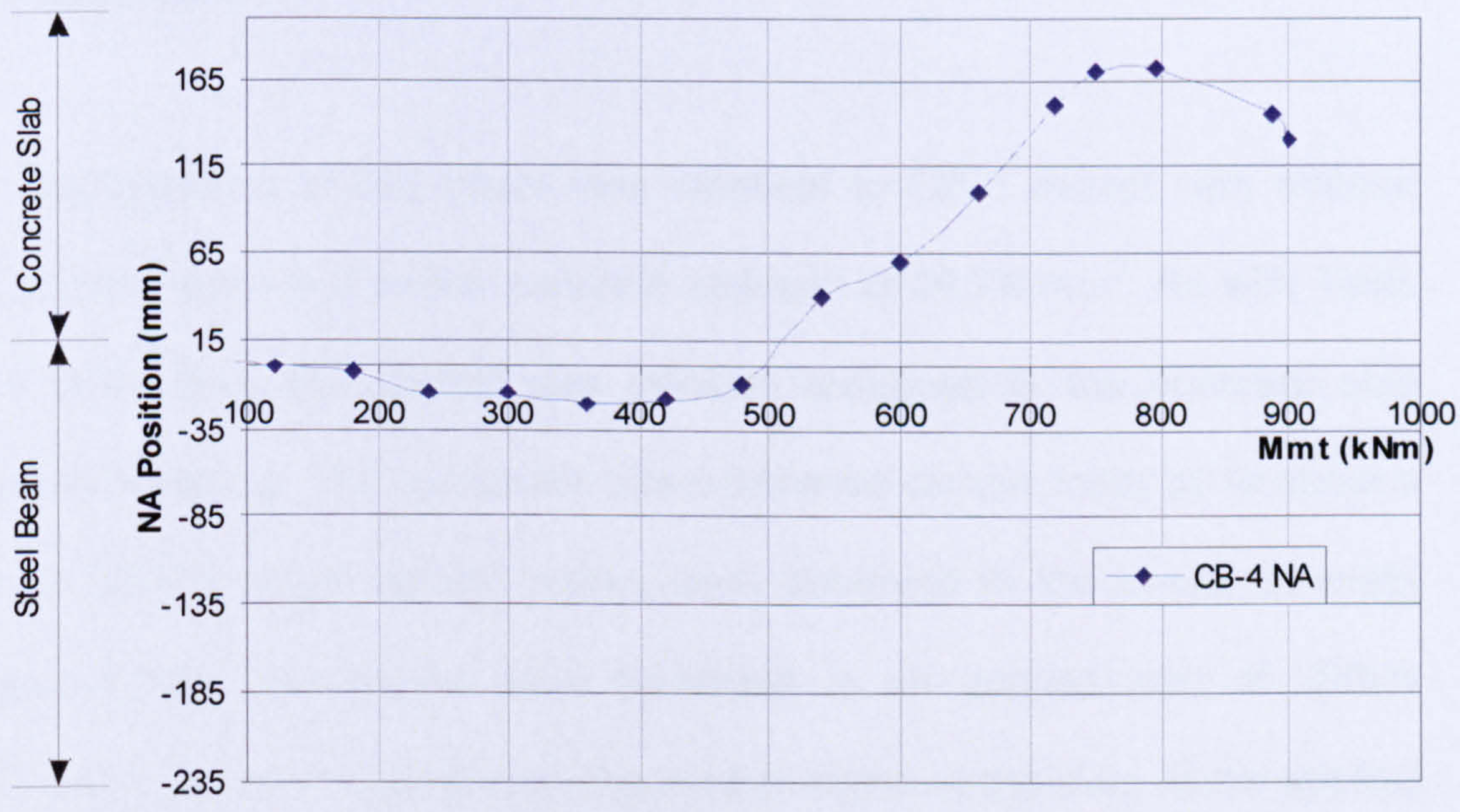

Figure 4.38: Position of Neutral Axis of Test CB-4

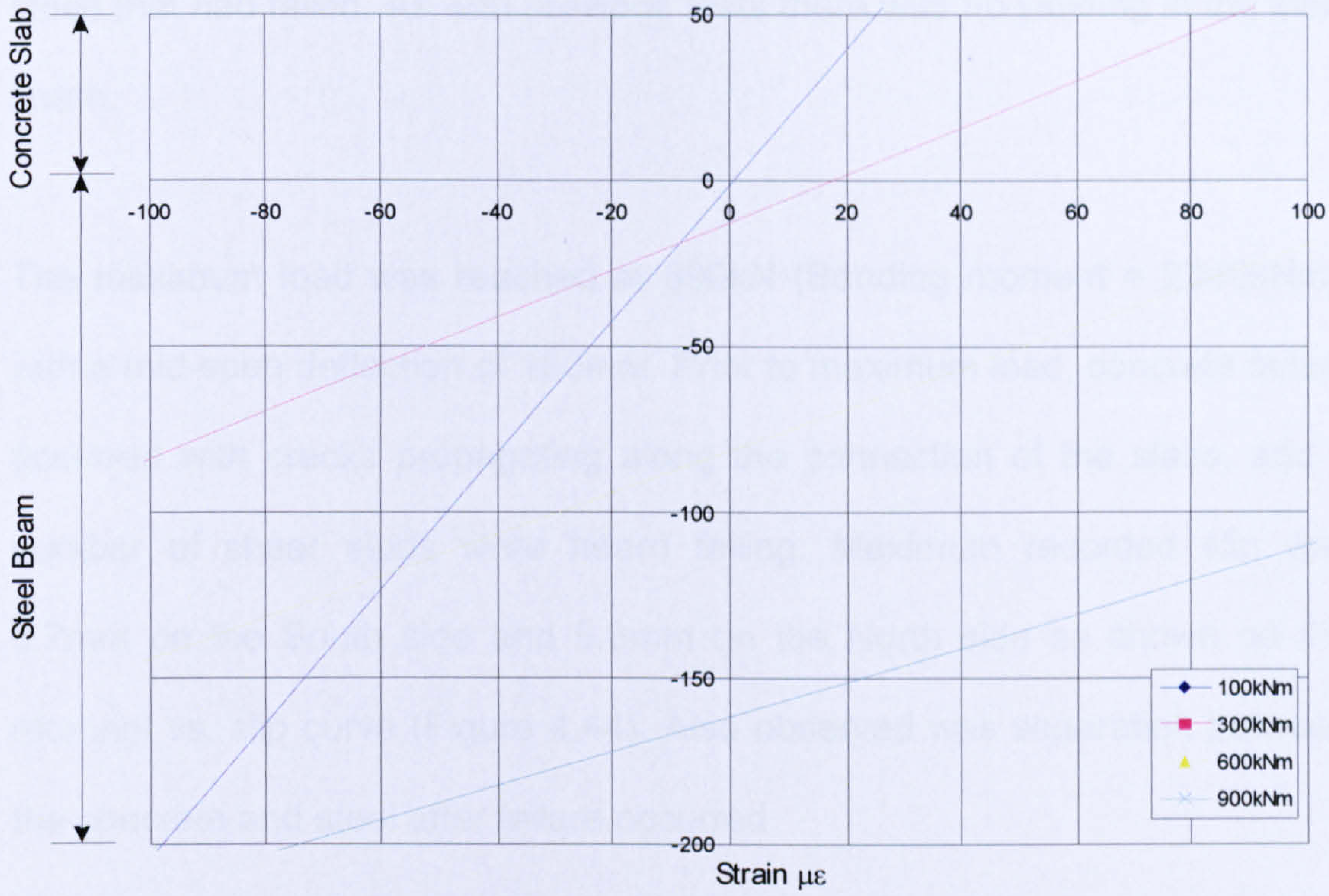

Figure 4.39: Strain Distribution for Test CB-4

4.3.7 Test CB-5

The configuration of this beam was identical to CB-3 except with 400mm hollow-core slabs and in-situ concrete strength of 30.7N/mm^2. As with Tests CB-3 and CB-4, the neutral axis position remained in the concrete slab throughout testing. The composite beam behaved almost linear up to about a load of 250kN, when tensile cracks were observed in the in-situ concrete (Figure 4.40). First cracks were observed at an applied load of 320kN (Bending moment = 1920kNm) in the central region of the slab. At the applied load of 340kN (Bending moment = 2040kNm), excessive cracking in the concrete slabs around the mid-span of the beam was seen on the underside of the hollow-core slabs (Figures 4.41 and 4.42). Failure occurred at a moment of 2340kNm, this was due to crushing of concrete around the shear studs that had failed. As with previous tests there was no yielding in the steel beam.

The maximum load was reached at 390kN (Bending moment = 2340kNm), with a mid-span deflection of 150mm. Prior to maximum load, concrete failure occurred with cracks propagating along the connection of the slabs, and a number of shear studs were heard failing. Maximum recorded slip was 8.7mm on the South side and 5.8mm on the North side as shown on the moment vs. slip curve (Figure 4.44). Also observed was separation between the concrete and steel after failure occurred.

After the experiment, the beam specimen was dismantled to investigate the mode of failure. This was found to be concrete crushing around the mid-span region of the beam with studs failing along the steel beam. Figure 4.42 shows the moment vs. deflection curve of test CB-5, the beam remained elastic up to 1750kNm. Figure 4.45 shows the strain measured on studs along the beam; there was an increase in strain on the studs at the ends of the beam after cracks on the underside of the slab was observed. The strain measured on the transverse reinforcement (Figure 4.46) increased after a moment of 1750kNm was reached. After this point, the stiffness of the beam decreased when the load was increased. As expected the beam had an increased stiffness and behaved in a ductile manner when compared to the other composite beams tested.

The cracking in the underside of the hollow-core slab is a consequence of crushing of concrete in the concrete section. This causes the neutral axis to move towards the compression zone, allowing tensile force to develop in the hollow-core slab. The position of neutral axis and strain distribution for test CB5 is shown in Figures 4.47 and 4.48.

Figure 4.40: Tensile cracks in In-situ concrete of CB-5

Figure 4.41: Excessive cracking on underside slab of CB-5 (West)

Figure 4.42: Excessive cracking on underside slab of CB-5 (East)

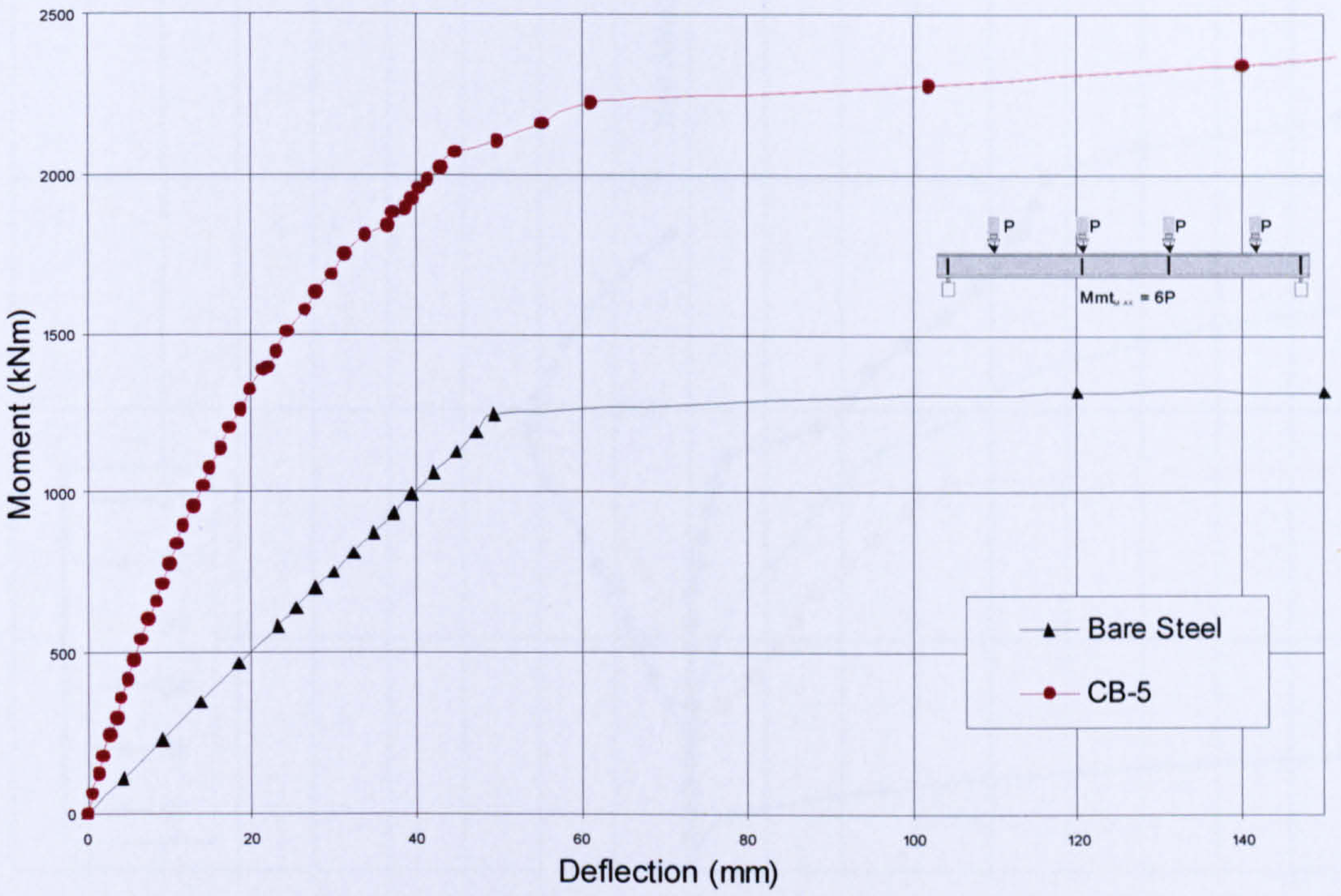

Figure 4.43: Moment vs. Mid-span deflection of CB-5

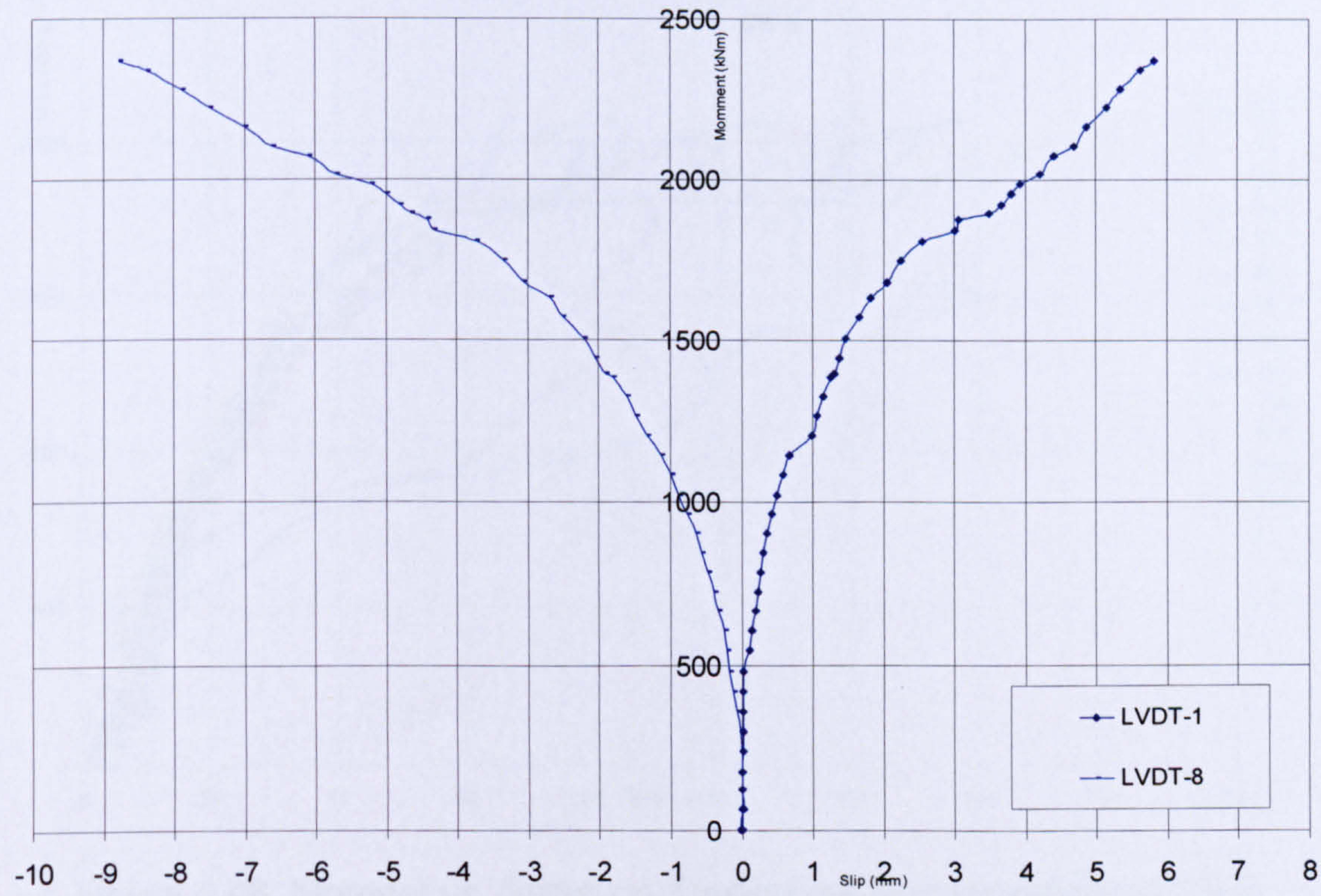

Figure 4.44: Moment vs. Slip at Interface of CB-5

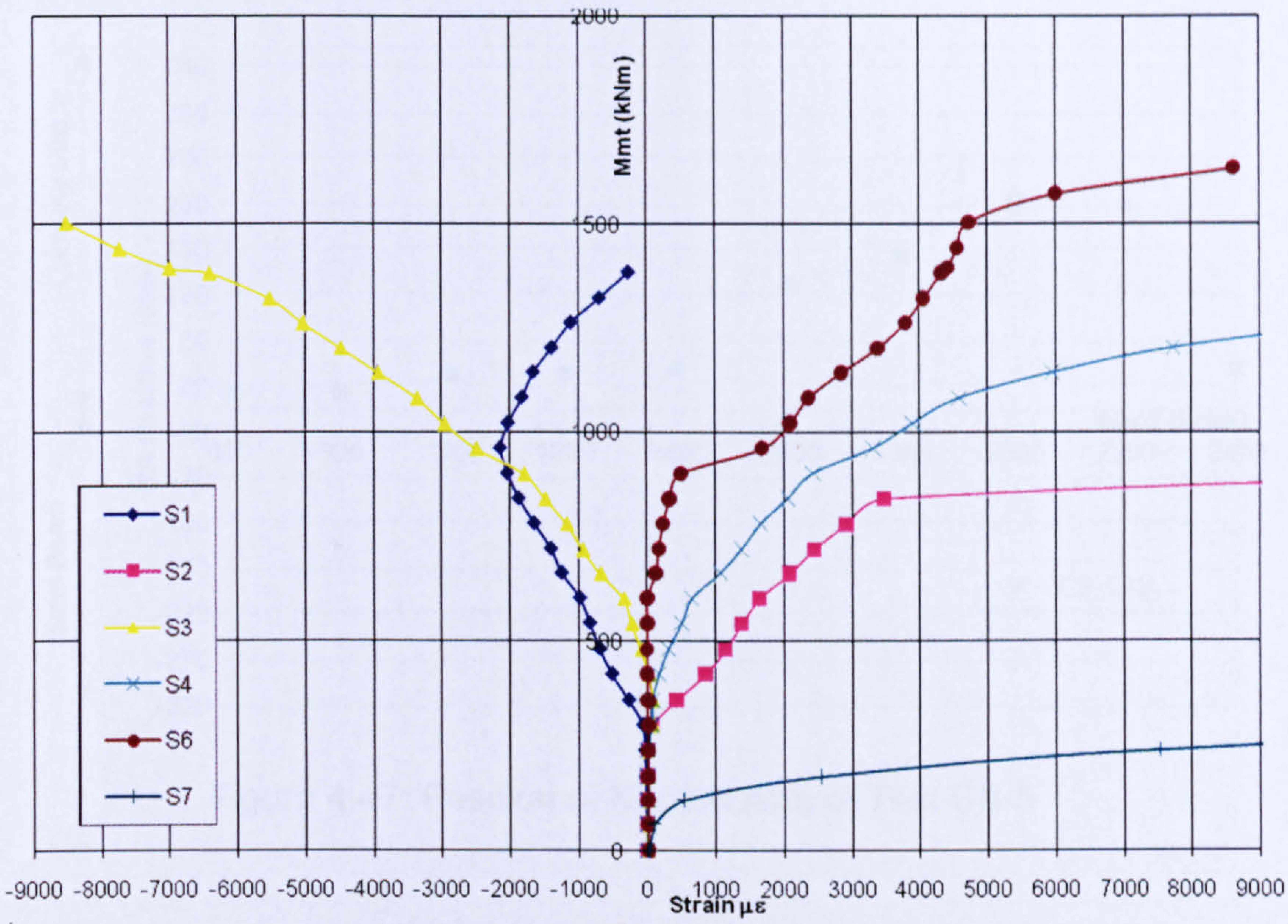

Figure 4.45: Moment vs. Strain on Shear Studs of CB-5

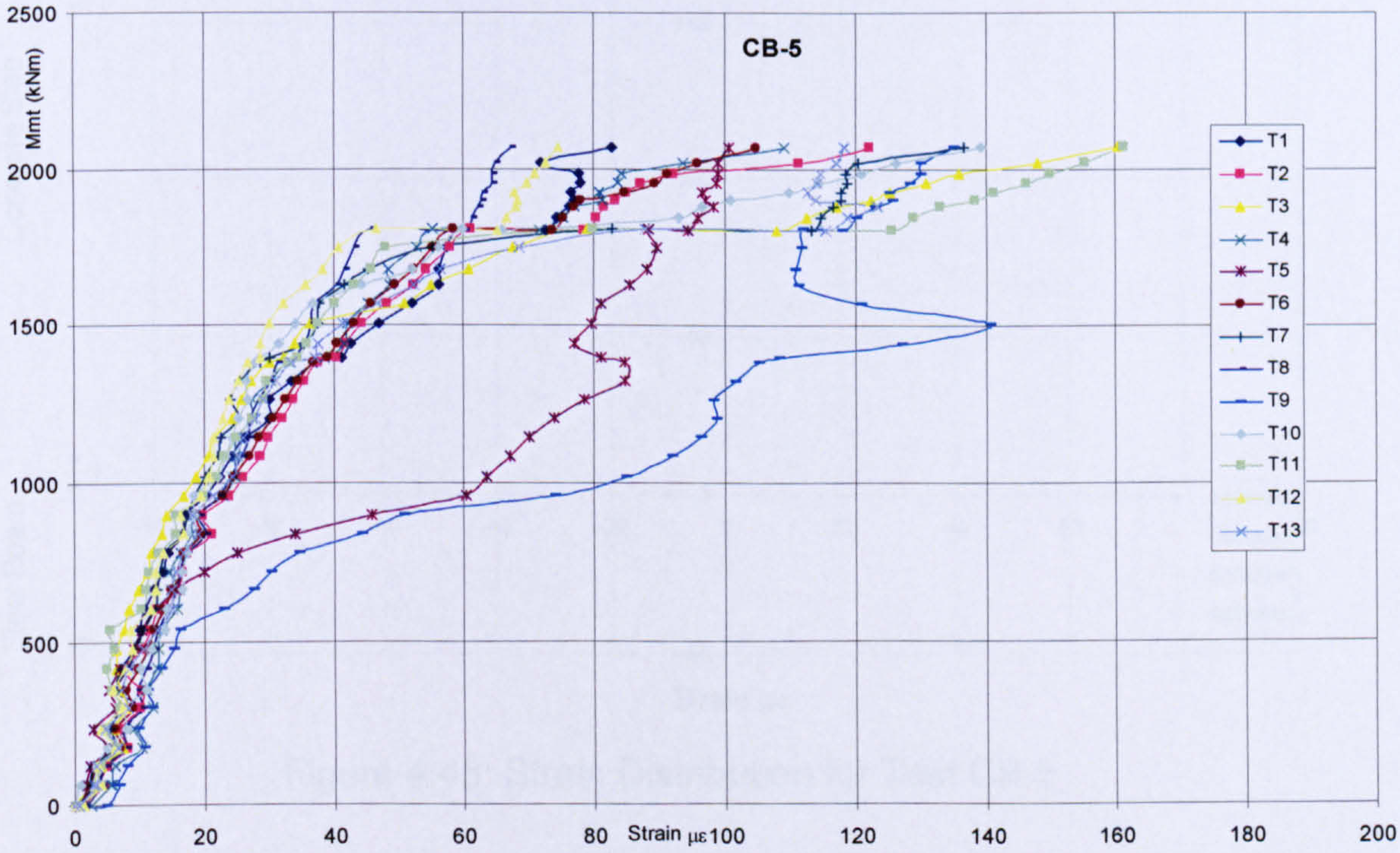

Figure 4.46: Moment vs. Strain on Transverse Reinforcement of CB-5

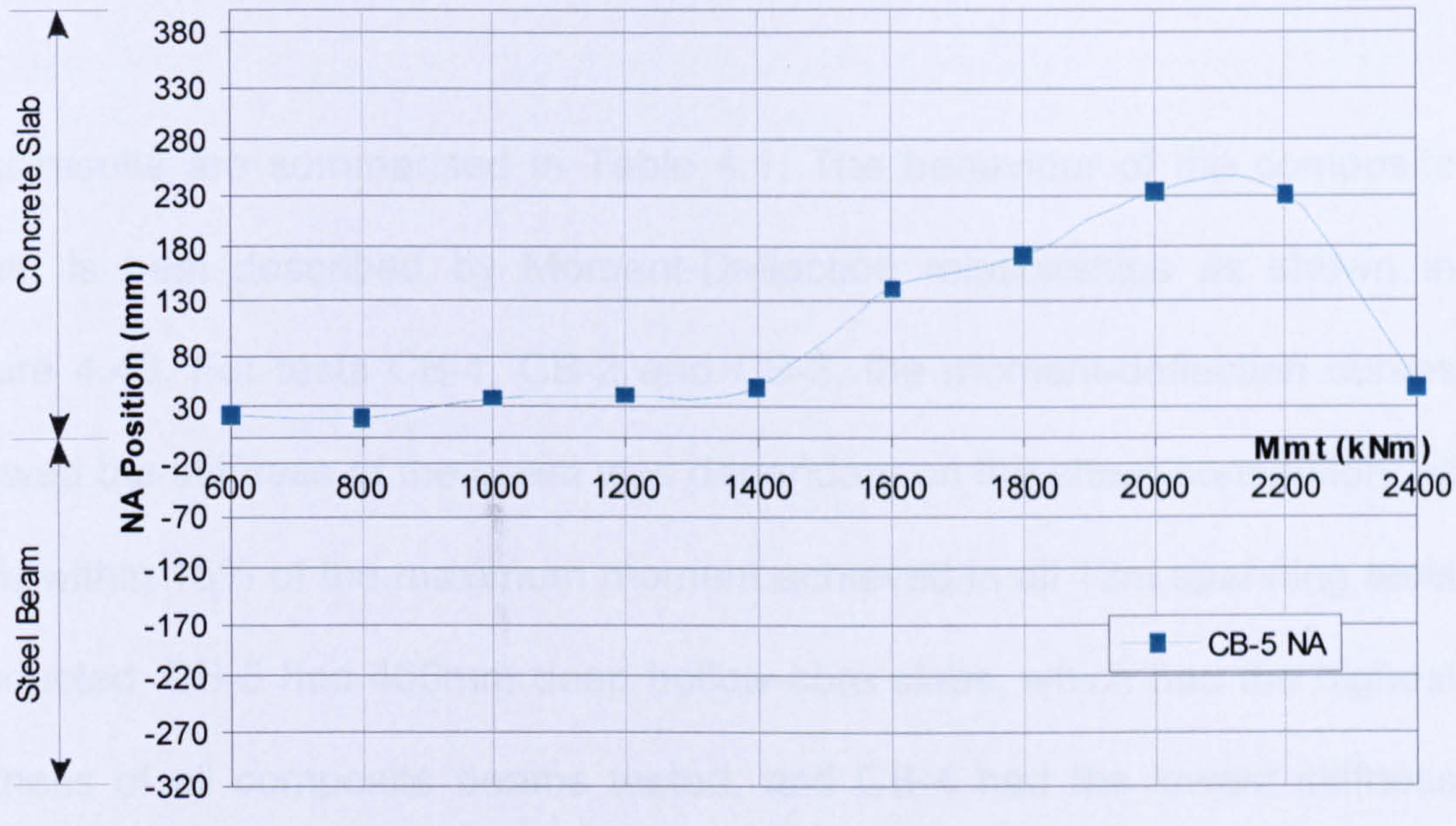

Figure 4.47: Position of Neutral Axis of Test CB-5

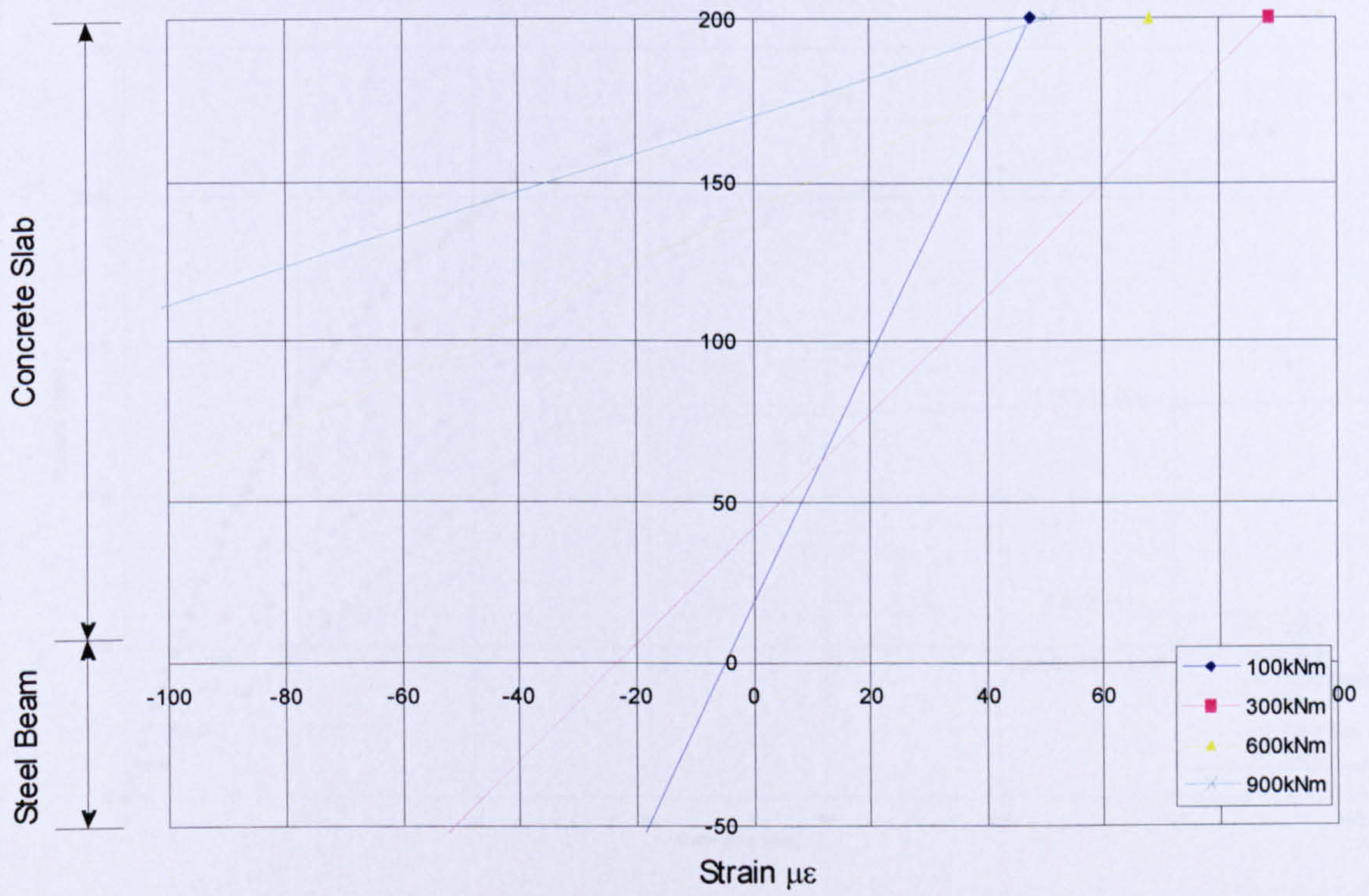

Figure 4.48: Strain Distribution for Test CB-5

4.4 Comparison of Test Results

Test results are summarised in Table 4.1. The behaviour of the composite beam is best described by Moment-Deflection relationships as shown in Figure 4.49. For tests CB-1, CB-2 and CB-3, the moment-deflection curves showed the stiffness of the beam was dependant on the shear connection; all were within 15% of the maximum moment achieved in all 12m spanning tests conducted. CB-5 had 400mm deep hollow-core slabs, which had the highest stiffness of all composite beams tested, and CB-4 had the lowest stiffness due to beam size and shorter span.

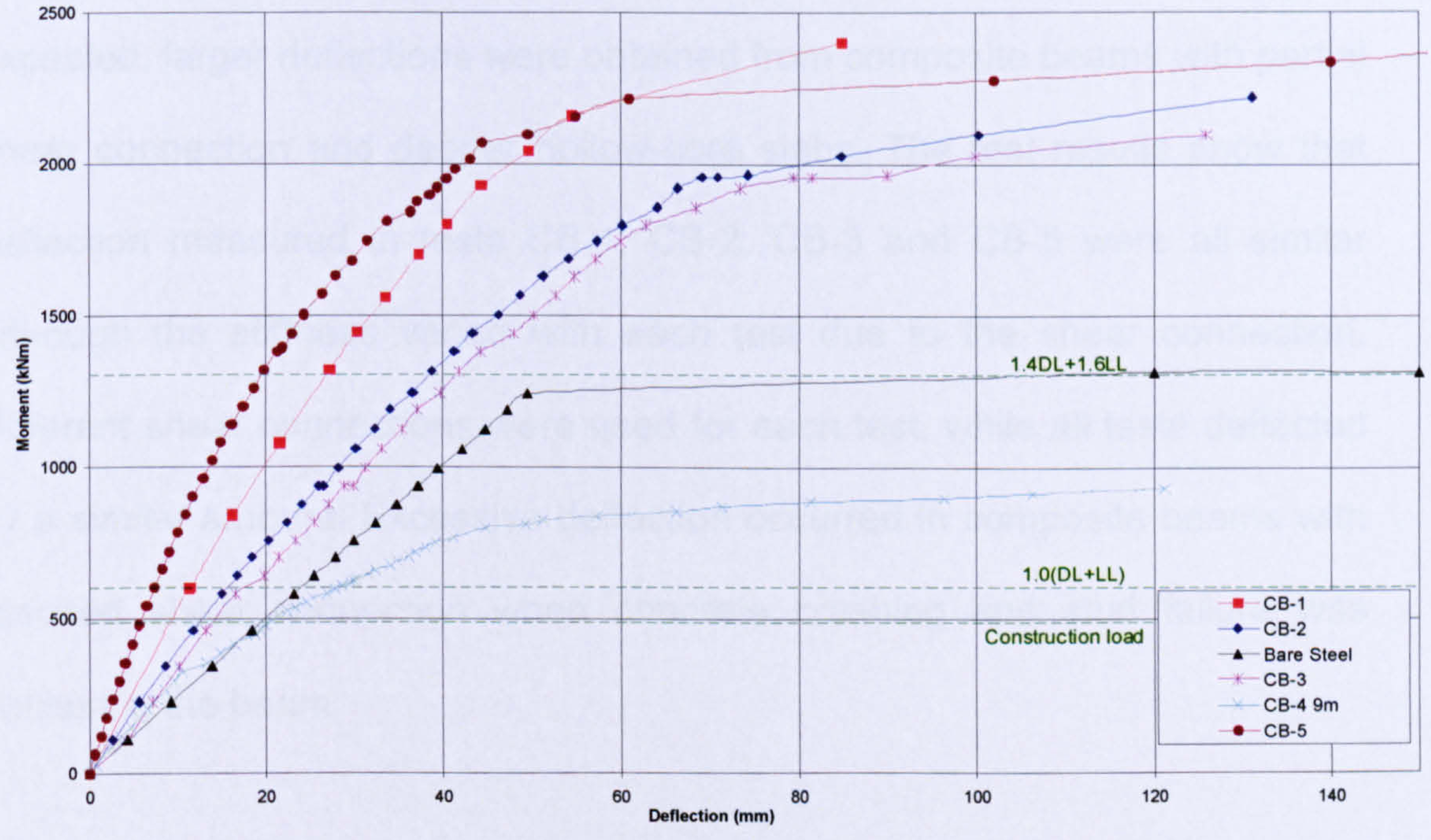

Figure 4.49: Moment vs. Deflection relationships

In the ultimate stage, all tests failed in a ductile manor, either by concrete crushing in the mid-span region of the beam or shear connection failure. There was no yielding of the steel beam, due to the large size of beams used in all tests. CB-1 and CB-2 both failed due concrete crushing in the centre region of the slabs. CB-3, CB-4 and CB-5 failed with a combination of both concrete crushing and shear stud failure. Yielding in steel was only noticed in the Test CB-1, while no yielding or buckling of the beam's flanges and webs was observed in the other tests.

4.4.1 Comparison of Moment – Deflection

Figure 4.49 shows the moment-deflection curves for all tests conducted. As expected, larger deflections were obtained from composite beams with partial shear connection and deeper hollow-core slabs. The test results show that deflection measured in tests CB-1, CB-2, CB-3 and CB-5 were all similar although the stiffness varied with each test due to the shear connection. Different shear connections were used for each test, while all tests deflected by a similar amount. Excessive deflection occurred in composite beams with reduced shear connection when concrete crushing and stud failure was noticed in the beam.

4.4.2 Comparison of End Slip

As expected, larger slip was obtained from composite beams with low shear connection and deeper slabs. The beams with the lowest shear connection

(CB-3 and CB-4) had excessive slip in comparison to the other tests, which did not exceed 6.0mm. Although CB-5 had a low shear connection, slip for this beam was not found to be excessive, due to the 400mm deep concrete slabs used for this test. Excessive slip occurred in beams when studs failed and sheared off, hence the shear connection was reduced.

A comparison between the slip results and push tests can be made, with the load at 6mm slip taken as 102kN (Table 4.1) to calculate the actual shear connection of the composite beam.

4.4.3 Comparison of Strain on Studs

As expected, larger strains were obtained from composite beams with partial shear connection and deeper slabs. Studs placed in the central region of the slab (SG-5, SG-6, SG-7 and SG-8) were found to have larger strain when beam was still elastic. When the beam demonstrated plastic behaviour, larger strain was imposed onto studs at either ends of the specimen (SG-1, SG-2, SG-11 and SG-12) due to the increase in slip. Beam tests with lower shear connection had larger strains induced onto the studs during bending as expected. Studs with the transverse reinforcement placed close behind the stud (in direction of bending) had an increase in strain measured, due to the support provided by the transverse bar.

4.4.4 Comparison of Strain on Transverse Reinforcement

Tests CB-1, CB-2 and CB-3 all had forty nine 16mm reinforcing bars, with a bar spacing at 240mm. CB-4 had thirty one 16mm reinforcing bars at 300mm spacing and CB-5 had thirty seven 16mm bars at 300mm spacing. Strains measured in all tests were relatively low. There was an increase in strain realised in beam tests with forty nine bars (CB-1, CB-2 and CB-3), while strains measured in the tests (CB-4 and CB-5) with thirty one and thirty seven had a smaller measurement of strain due to the reduced number of reinforcing bars. Stresses developed in the reinforcing bars were less than 25% of the yield stresses, suggesting that the bars were not fully mobilised.

4.4.5 Position of Neutral Axis

The positions of the neutral axis for all beam specimens are shown in Figure 4.50. The neutral axis position for all beam specimens began in the concrete slab, except for Test CB-1, where the neutral axis was in the top flange of the steel beam. In Test CB-2 the neutral axis was 97mm above the steel/concrete interface. The neutral axis for CB-1 and CB-2 then drops into the steel web when cracking occurs in the concrete. Test CB-3 followed a similar position to CB-1 and CB-2, but the neutral axis remained in the concrete, at failure the position of the neutral axis was approximately 22mm above the interface. The neutral axis of CB-4 started in the top flange of the steel beam and moved up into the concrete, finishing 130mm above the interface. The neutral axis of CB-5 behaved similarly to the neutral axis of

CB-4, starting 23mm above the interface and then moving up as the studs failed, to a maximum of 229mm above the interface. At failure load the neutral axis of CB-5 drops down to 49mm above the interface. it is shown that composite beams with the neutral axis in the concrete provided adequate moment capacity with ductile failure.

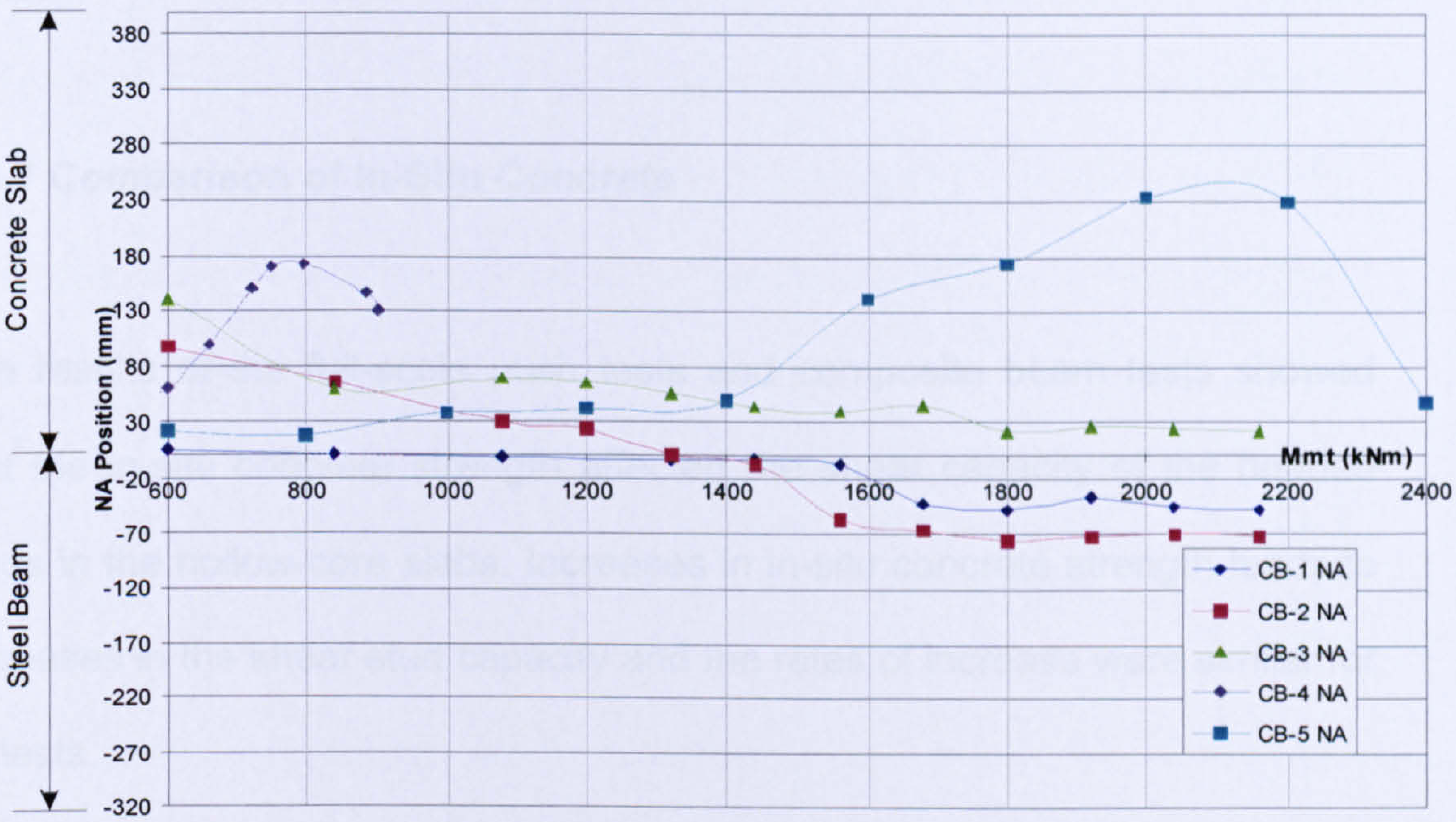

Figure 4.50: Position of Neutral Axis of all Tests

4.4.6 Comparison of Failure Modes

Three modes of failure were observed during the testing of the composite beams, both of which were shear connection failure:

1. Concrete crushing (CC) as occurred in CB-1 and CB-2.
2. Fracture of shear studs (SF) as occurred in CB-3, CB-4 and CB-5.
3. Combination of concrete crushing (CC) and shear stud failure (SF) as occurred in CB-3, CB-4 and CB-5.

In Tests CB-1 and CB-2, concrete crushing occurred with no fracture of shear studs. In tests CB-3, CB-4 and CB-5 concrete crushing and fracture of shear studs occurred. There was no yielding in the steel beam, due to the large size of steel and stiffened web region. The purpose of the composite beam tests was to investigate the design of composite beams with the neutral axis in the concrete slab, which was found to have sufficient moment capacity when tested.

4.4.7 Comparison of In-Situ Concrete

The results of the full-scale push tests and composite beam tests showed that the in-situ concrete strength affected the shear capacity of the headed studs in the hollow-core slabs. Increases in in-situ concrete strength leads to increases in the shear stud capacity and the rates of increase were similar for all tests.

4.5 Effect of Different Variables

Discussed in this section is the effect of different variables that were looked at in the five full scale composite beam tests performed. These include the degree of shear connection, amount of transverse reinforcement and slab depth.

4.5.1 Effect of Degree of Shear Connection

Composite beams with high shear connection (CB-1 at 150mm stud spacing) were found to have a high stiffness as expected, although the failure was sudden due to concrete crushing. With the reduction in the stud spacing (CB-2 at 300mm and CB-3 at 400mm), the composite beams were found to behave more ductile but with a reduced stiffness with greater shear forces being induced on to the studs. This was confirmed in Test CB-3 with the failure of studs along the beam. In tests CB-4 and CB-5, the stud spacing was kept at 400mm, with a variation in span and slab depth. Although these tests had a low shear connection capacity, both beams behaved in a ductile manner with stud failure occurring after the moment capacity of the composite beam was reached.

4.5.2 Effect of Transverse Reinforcement

Tests CB-1, CB-2 and CB-3 all had four core openings in each precast slab with a total of forty nine transverse bars placed along the 12m spanning beam, while Tests CB-4 and CB-5 had three core openings in each precast slab with a total of thirty one transverse bars placed along a 9m span for CB-4 and thirty seven bars placed along a 12m span for CB-5. In all tests there was no yielding of bars. The transverse bars which were gauged had a relatively small strain recorded, although the beam tests with additional transverse bars (CB-1, CB-2 and CB-3) had an increase in strain recorded, due to the shear load transfer between more reinforcing bars. There was also an increase in strain realised on the bars placed behind the studs in the direction of bending acting against the slip of the shear studs.

4.5.3 Effect of Precast Slab Depth

The only difference between Tests CB-3 and CB-5 was the depth of precast slab, with CB-3 having 200mm deep slabs and CB-5 having 400mm slabs. The results show that using deeper slabs, a higher stiffness and moment capacity could be obtained. The deeper slabs induced higher strains into the studs and consequently stud failure in the composite connection may occur.

4.6 Conclusions

Five full scale bending tests were carried out and the experimental behaviour of each test is fully described in this chapter. Three modes of failure were observed in the shear connection: (1) Concrete crushing in the mid-span region of the beam, (2) Fracture of shear studs along the shear connection of the beam and (3) Combination of concrete crushing and stud failure. Composite beam tests conducted showed adequate moment capacity and stiffness is acquired from this form of construction. From the analysis of the test results, the following conclusions can be made:

1. Composite beams with the neutral axis position in the concrete slab perform adequately in plastic design.

2. Three modes of failure occurred at the connection of the composite, either through concrete crushing and fracture of shear stud or both.

3. Reduction of the shear connection provided a more ductile failure with small loss in the moment capacity of the composite beam.

4. Designing using partial shear connection shows the shear connectors have control of failure mode, depending on concrete parameters.

The results of these tests are used in Chapter 5, with an analytical study of the composite beam. The effective width is calculated and the composite moment is found and compared with test data. In Chapter 6 comparison is made with the design equations for this form of construction.

Chapter 5

Analytical Study

Chapter 5: Analytical Study

5.1 Introduction

In the previous chapter, the results of five simply supported composite beams subjected to bending were presented. The beams were subject to loading and the level of shear connection, slab depth and span was varied in the tests. From the beam tests carried out, partial shear connection design was found to be advantageous in terms of strength and ductility.

The development of an analytical based model to study the behaviour of composite beams under bending moment is described herein. This simple model considers the concept of partial interaction, allowing for slip at the steel-concrete interface. The material properties of all main components were incorporated and the inherent equilibrium and compatibility principles were satisfied. The results from the analysis showed good agreement with the experimental results of the five composite beams tested.

5.1.1 Background

Composite beams designed with full shear connection (FSC) are defined as the strength of the shear stud connectors being greater than the fully yielded strength of the reinforcing steel. The definition of FSC also implies that the bending resistance of the composite beam would not increase even if additional connectors are provided (Johnson and Molenstra 1991). Otherwise it is termed as partial shear connection (PSC), where the reinforcement is now partially stressed since it is governed by the strength of the shear connection.

Shear stud connectors attach the concrete slab and steel beam together, and are important in the development of composite action for flexure and to distribute the significant longitudinal shear forces acting along the interface. The longitudinal shear forces are transmitted through the shear connectors and considering that the concrete was cracked in tension, the load transfer system was possible. This suggested that there were no detrimental effects to the behaviour of the shear connectors (Bradford et al 2003).

One of the key objectives of the experimental study was to investigate the scope of using partial shear connection (PSC) design. The results from experiments have demonstrated that composite beams designed with low shear connection, up to as low as 25% possessed considerable ductility whilst maintaining high levels of moment resistance at ultimate. The failure mode of the beams was governed by concrete crushing and fracture of the shear stud connectors. This occurred after large deformations and presented a ductile mode of failure.

This chapter is intended to complement the results obtained from the experimental work carried out, in order to study the behaviour of long span composite beams in bending. The formulation of an equilibrium based model using the cross-sectional analysis to simulate the response of composite beams is described in this chapter. The model satisfies inherent equilibrium and compatibility principles and includes the material stress-strain properties of the main components.

Rigid-plastic analysis is employed to determine the strength of the composite beam under bending at the ultimate load using the yielded strength of all materials. An implicit assumption in the analysis is that premature failure of the materials does not occur, either through local buckling of steel elements, failure of shear connectors and crushing of the concrete (Oehlers and Bradford 1995). The current methods in practice seem to have conservative predictions on the ultimate strength of the beams; hence an improvement was made based on observations from experimental and analytical results.

5.2 Analytical Model

The following section describes the formulation of the analytical model used to simulate composite beams subject to bending using cross-sectional analysis.

5.2.1 Basic Assumptions

The analytical model is two-dimensional and is based on the following assumptions:

1. Plane sections remain plane for the entire cross-section under bending.
2. No uplift or vertical separation occurs between the steel and the concrete slab.
3. The strain distribution throughout the depth of the cross-section is linear, implying that there is one neutral axis in the cross-section.
4. The strain and stress distributions do not vary across the width of the cross-section.
5. The shear connectors are considered as discrete elements with uniform spacing of studs. The slip strain distribution of each stud is assumed to have linear distribution.
6. The load-slip characteristics for the stud are based o experimental push test results.
7. Concrete has some strength in tension based on existing experimental models.

5.2.2 Equilibrium and Compatibility

Figures 5.1 and 5.2 present a typical cross-sectional illustration of strain, stress, force and moment distribution at a cross-section of the composite beam in the linear elastic range, while Figure 5.3 shows the cross-section in the linear plastic range. The notation represents each of the force components in the concrete, flanges and web of the steel as illustrated. The following presents the two important conditions of equilibrium that were satisfied at all cross-sections of the beams.

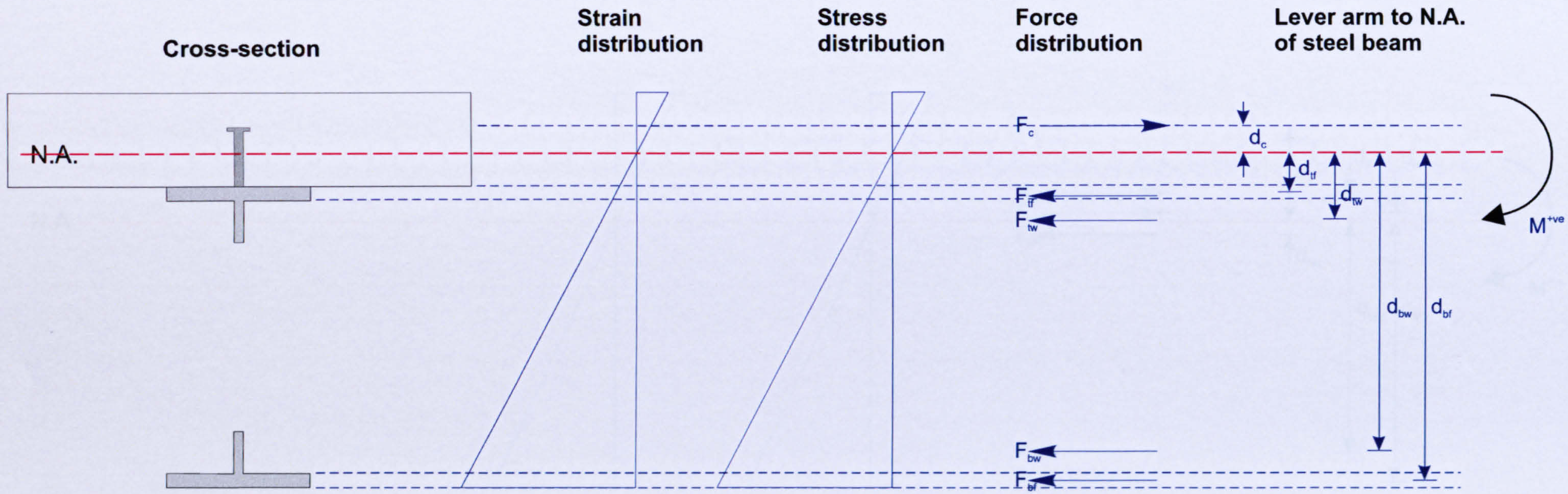

Figure 5.1: Typical linear elastic behaviour of composite beam under bending moment with neutral axis in concrete

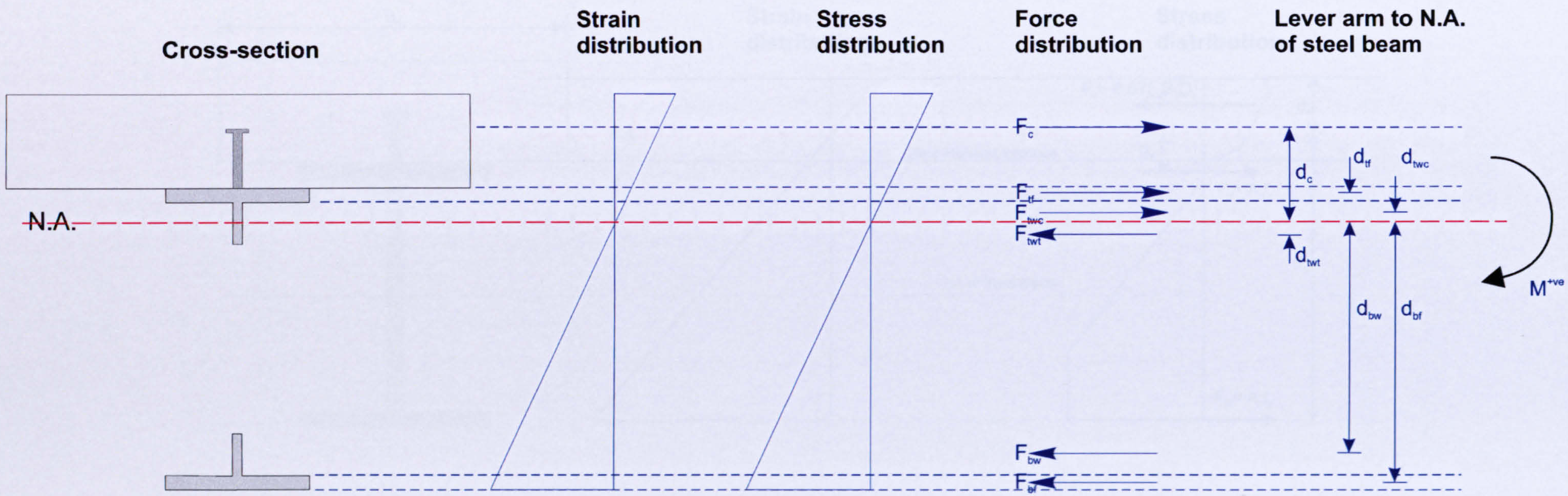

Figure 5.2: Typical linear elastic behaviour of composite beam under bending moment with neutral axis in steel

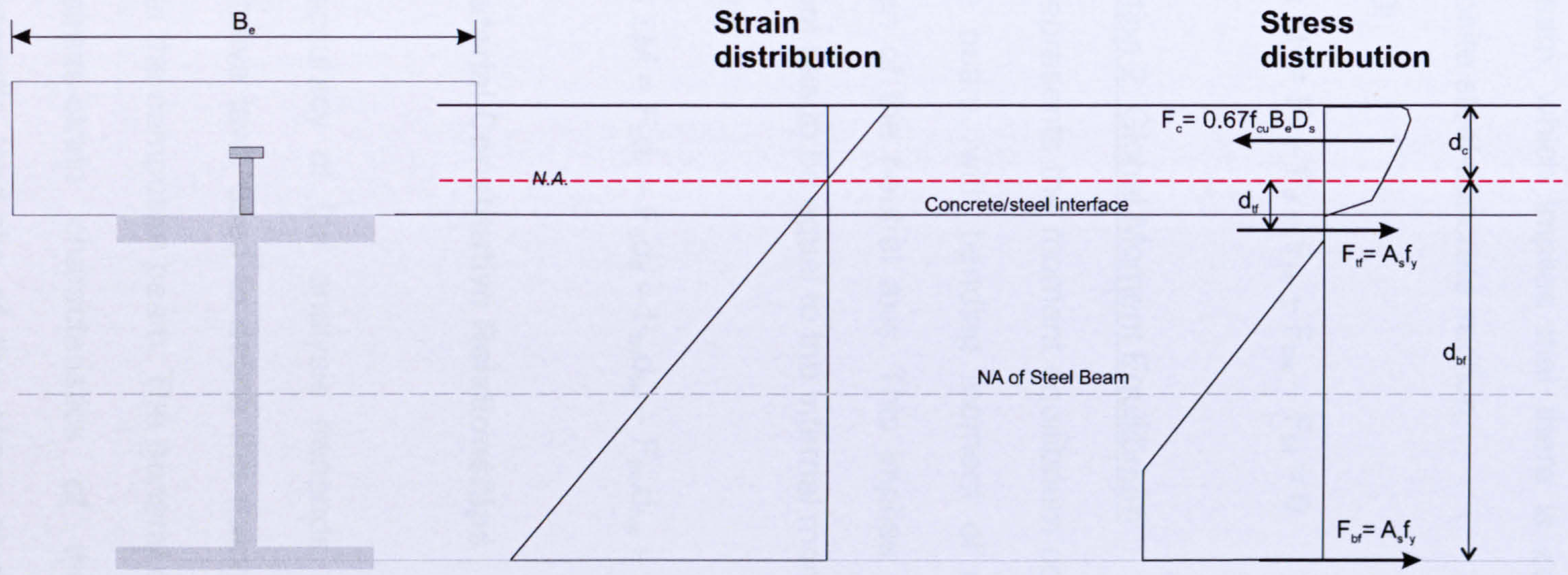

Figure 5.3: Typical linear plastic behaviour of composite beam under bending moment

Condition 1: Global Force Equilibrium

This represents the force equilibrium condition of the entire cross-section of the beam, which implies that there is zero net axial force acting on the composite steel-concrete section.

$\Sigma F = 0$;

where $\Sigma F = F_c - F_{tf} - F_{tw} - F_{bw} - F_{bf} = 0$ (5.1)

Condition 2: Global Moment Equilibrium

This represents the moment equilibrium condition of the entire cross-section of the beam, with bending moment of each component taken from the position of the neutral axis. This implies that the applied external bending moment has to be equal to the internal moment of the composite section.

$\Sigma M = 0$;

where $\Sigma M = F_c d_c - F_{tf} d_{tf} - F_{tw} d_{tw} - F_{bw} d_{bw} - F_{bf} d_{bf} = 0$ (5.2)

5.3 Material Constitutive Relationships

The accuracy of the analysis depends strongly on the accuracy of the constitutive laws used to define the mechanical behaviour of the materials used in the composite beam. The general constitutive laws used to represent the stress-strain characteristics of the relevant materials and the characteristic load-slip of the shear stud connectors is described in the following section.

5.3.1 Concrete

The effective width, B_{eff} is defined in general to allow for none uniform distribution of stress due to shear lag. Figure 5.4a shows the typical horizontal longitudinal stress contours of the composite slab. Considering the cross-section A-A in Figure 5.4b, it is assumed that the concrete element is narrower such that the rectangular stress block of area $B_{eff} \times \sigma_{max}$ is equal to the area under the curvilinear stress block σ_x over the width l. This is equivalent to integrating the rigorously calculated horizontal longitudinal stress σ_x in the concrete slab over the width l, and dividing by the peak value of the stress σ_{max} (Lam 1998).

Hence

$$B_{eff} = \frac{\int_{bl}^{br} \sigma_x dx}{\sigma_{max}} \qquad (5.3)$$

where b_r = half the transverse spans of the slab on the right of the steel beam.

b_l = half the transverse spans of the slab on the left of the steel beam.

x = coordinate transverse to the centreline of the steel.

It is still important to proportion the concrete element to incorporate the non-linear effects of shear lag. In simple T-beam theory, based primarily on the engineering assumption that plane sections remain plane after bending, the idealised T-beam consists of the steel element with a certain width of slab referred to as effective breadth that is stressed uniformly.

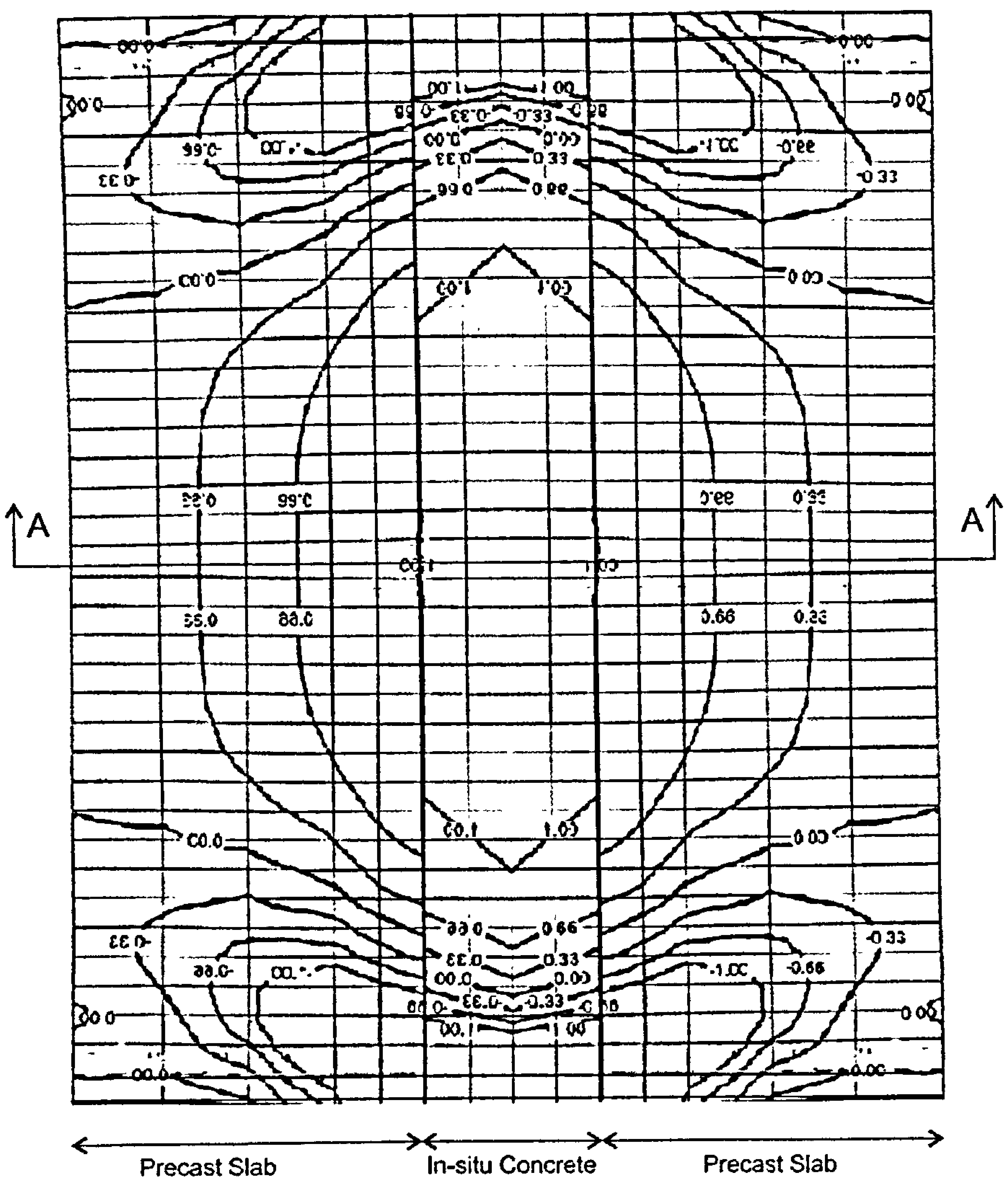

Figure 5.4a: Typical stress contours of concrete

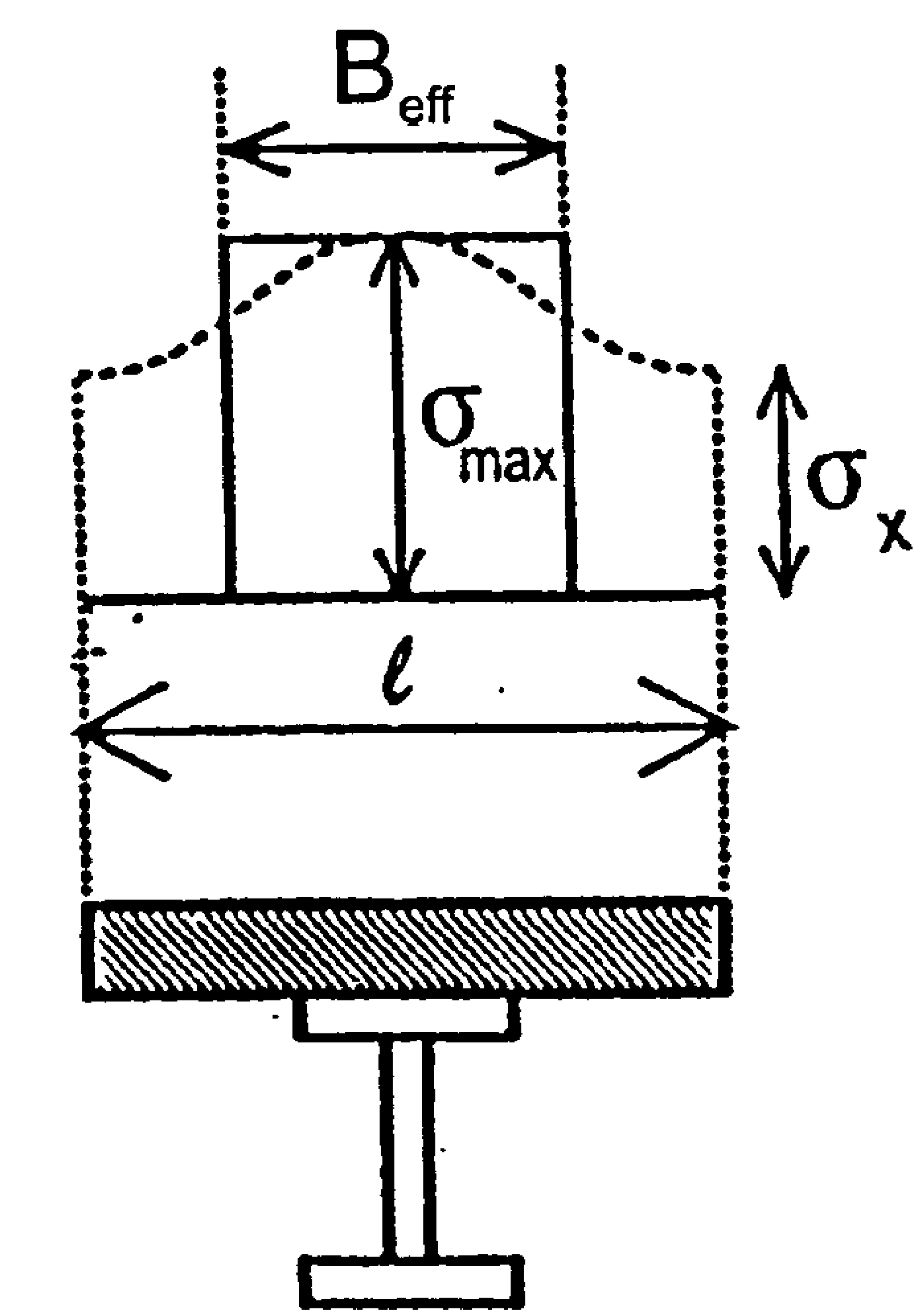

Figure 5.4b: Effective width B_{eff} of composite section (Section A-A)

Figure 5.4: Typical stress contours of concrete and effective width of composite section

For the force in concrete, the strain profile of the beam was calculated using strain gauges placed on the top and bottom flanges of the steel beam. Taking equilibrium of forces ($F_s = F_c$), the effective width was determined using the equation below:

$$\mathbf{F_c = 0.67f_{cu}B_{eff}d} \tag{5.4}$$

where f_{cu} = Strength of concrete

B_{eff} = Effective width

d = depth of concrete from neutral axis

The calculation spreadsheets in Appendix B show the calculation of the effective width using the strain profile of the composite beams tested. Using the force in steel and calculating the force in concrete with the effective width gained from the analysis, the moment capacity of the tested beams were found.

5.3.2 Steel

Figure 5.5 shows the generalised stress-strain curves for the steel beam section. The values were obtained from material tests, details of which are reported in Chapter 3.

Structural steel beams are generally hot-rolled sections, where their stress-strain behaviour is elastic for a certain region followed by a well defined yield plateau before developing strain hardening and plasticity. Simple linear lines were deemed sufficiently accurate to represent the stress-strain relationship in both tension and compression.

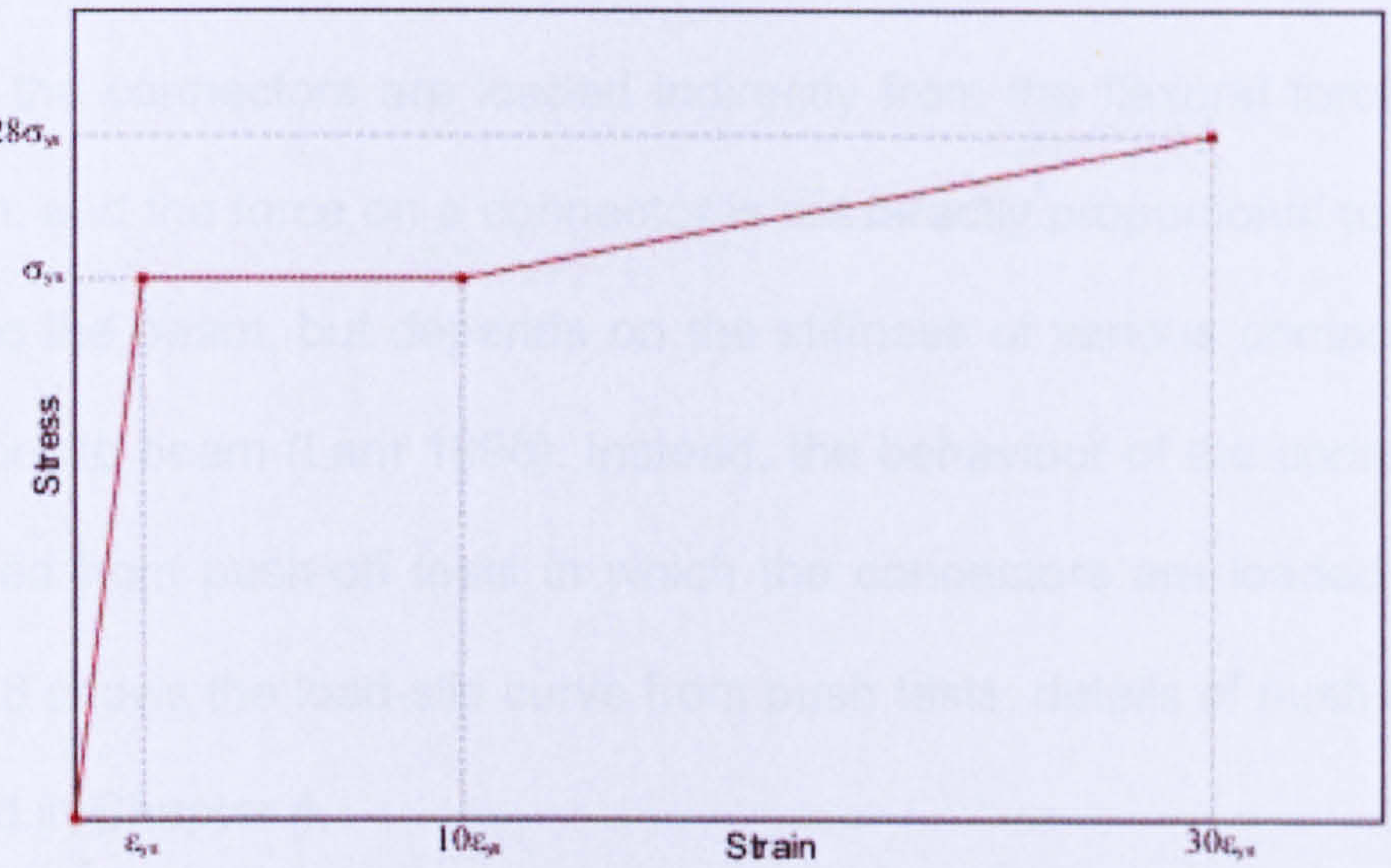

Figure 5.5: Stress-Strain model curve for structural steel

5.3.3 Shear Stud Connectors

The connectors most commonly used in composite beams are headed studs, as the 19mm diameter studs used in the experiments conducted. The presence of these connectors embedded in the concrete slab and welded to the steel flange provides the link that enables composite action between the slab and the steel beam. The shear connectors are not only responsible for transferring shear forces at the slab-beam interface but also function to prevent vertical separation at the interface. The behaviour of the composite beam is therefore highly dependent on the shear stud connectors, particularly the amount of connection provided.

Due to the complexity of the dowel action, the strength and ductility of shear connectors are always determined experimentally. It is difficult to determine the behaviour of the shear connectors from composite beam tests. This is because the connectors are loaded indirectly from the flexural forces within the beam, and the force on a connector is not directly proportional to the load applied to the beam, but depends on the stiffness of various components of the composite beam (Lam 1998). Instead, the behaviour of the connectors is determined from push-off tests in which the connectors are loaded directly. Figure 5.6 shows the load-slip curve from push tests; details of push tests are described in Chapter 4.

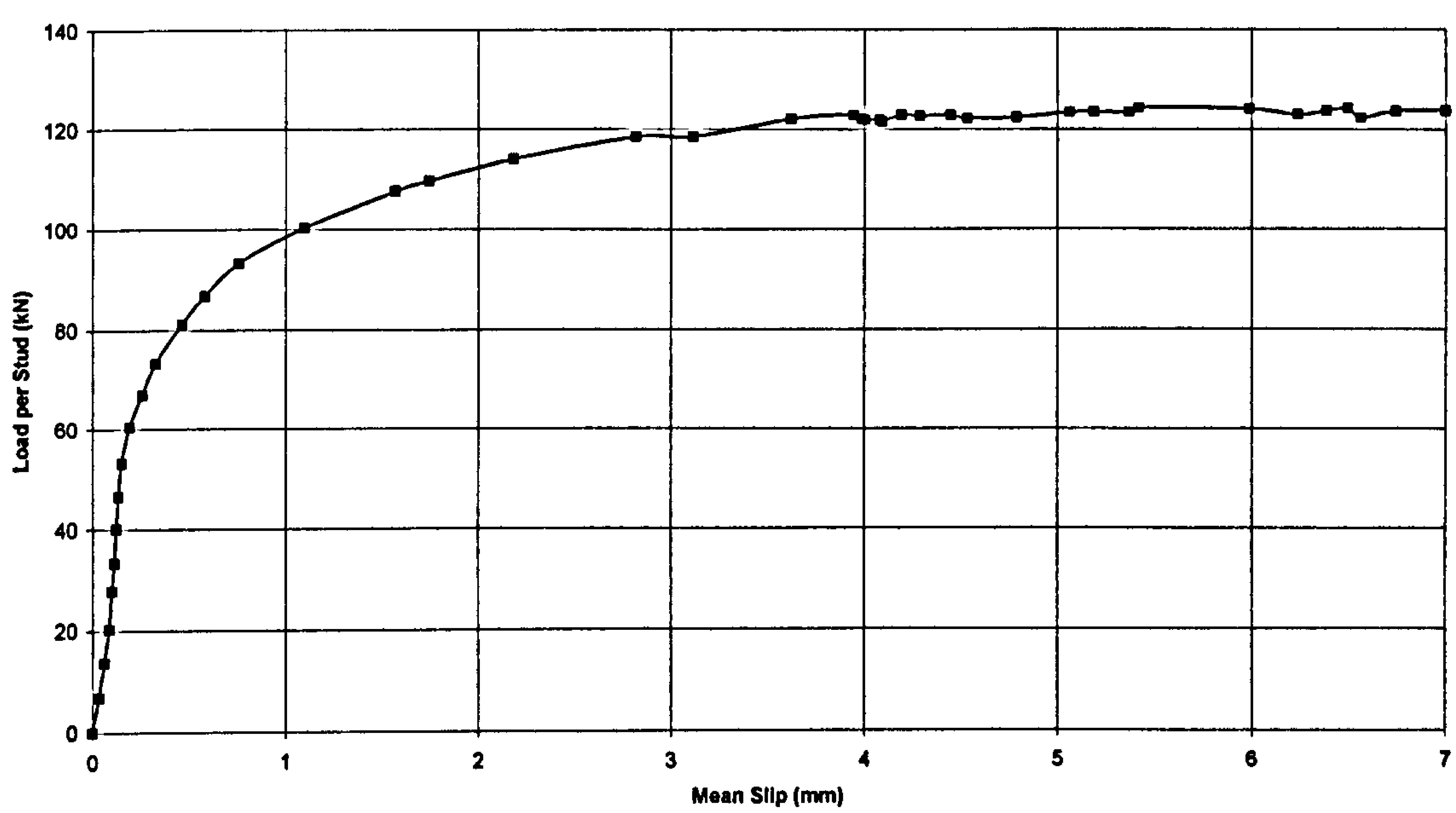

Figure 5.6: Load-Slip curve of shear connector

From the push test results in Chapter 4, the shear connector capacity was obtained and used to calculate the shear capacity of the connections for the conducted composite beam tests.

5.4 Failure Criteria

Failure was considered to have occurred due to one of the following causes, a) crushing of concrete in compression, b) fracture of shear connection due to excessive slip, taken as the slip at 6mm as obtained from the push tests and c) fracture of structural steel, when ultimate strain is reached.

The phenomenon of local buckling represents another failure mode which is critical for beams, where the beam flange buckles under high compressive stresses or strains. Due to the large size and stiffened web of steel beams used in experiments, the possibility of local buckling in the steel is reduced. Therefore failure was controlled predominately by the connection of the beam.

5.5 Discussion of Results

From the results of the tests conducted, the strain in the steel was established and the effective width of the composite beam is calculated. By using the force and moment equilibrium technique, the composite moment of the beam was gained and compared with the actual moment for all tests. The composite moment was calculated in the analysis using the following equations:

For full shear connection:

$$M_{comp} = F_s\left(\frac{D}{2} + D_s - \frac{F_s}{F_c} \times \frac{D_s}{2}\right) \qquad (5.5)$$

For partial shear connection:

$$M_{comp} = F_s\left(\frac{D}{2}\right) + F_{con} \times \left(D_s - \frac{F_{con}}{\frac{F_c \times D_s}{2}}\right) - \left[\frac{(F_s - F_{con})^2}{F_{flange} \times \left(\frac{T}{4}\right)}\right] \tag{5.6}$$

where F_s = Force in steel

F_c = Force in concrete

F_{con} = Force of shear connection

F_{flange} = Force in steel top flange

D = depth of steel beam

D_s = depth of concrete slab

Table 5.1 shows the effective width (B_{eff}), composite moment (M_{comp}) and shear connection (SC) calculated from the analytical study. The values shown are when failure occurred in the beam.

Equation 5.5 was used in the analysis of tests CB-1 and CB-2 due to their relatively high shear connection. From the calculations for Test CB-1, the composite moment calculated was slightly higher than the moments during the experiment. Although as the beam got closer to failure the moments calculated were almost identical to the experiment and the effective width was found to be L/16. For Test CB-2 the composite moment calculated matched closely to the moments during the experiment and the effective width was found to be L/13.

Equation 5.6 was used in the analysis of tests CB-3, CB-4 and CB-5 due to their partial shear connection. In these tests the moment reached during testing was almost the same as the calculated composite moment. The effective widths found in these tests were L/19, L/10 and L/9 for CB-3, CB-4 and CB-5.

5.6 Conclusions

From the analytical study performed on the beam test results, it has been shown that long span composite beams with precast hollow-core slabs have a reduced effective width when designed with partial shear connection with little reduction in moment capacity. With the position of the neutral axis in the concrete of the composite beam, the failure mode was found to be ductile and is likely to occur in the connection. It was established that the effective width in these beams is much smaller than current design suggests.

In Chapter 6 results from the analytical study was used to compare with current design equations to show favourable comparisons for the use of partial shear connection in long span composite beams with precast hollow-core slabs.

Test Specimen	B_{eff} (mm)		M_{comp} (kNm)	M_{exp} (kNm)	M_{comp} / M_{exp}	Design Shear Connection (%)	Exp. Shear Connection (%)
CB-1	732	L/16	2091	2160	0.97	68.1	84.5
CB-2	910	L/13	1418	1920	0.74	34.1	51.0
CB-3	629	L/19	1681	1800	0.93	25.6	62.0
CB-4	910	L/10	795	800	0.99	37.6	28.2
CB-5	1319	L/9	2001	2196	0.91	25.6	17.7

Table 5.1: From analytical study at failure

Chapter 6

Design of Composite Beam

Chapter 6: Design of Composite Beam

6.1 Introduction

From the beam test results and analytical study carried out in previous chapters, the shear stud capacity, effective width and composite moment was determined. In this chapter, comparisons are made with design equations and the competence of the composite beam tests is revealed. By using the different design equations currently in use for this form of construction, evaluation of composite beams with the neutral axis in the concrete slab is made.

6.2 Design of Effective Width

For designing the effective width, there are currently three design equations available, as shown below:

$$b_{eff} = \left(\frac{25}{f_{cu}}\right)^2 \times \left(\frac{0.4}{f_t^{'}}\right) \times 1000 + 300 \qquad (6.1)$$

where: f_{cu} = concrete cube strength of in-situ concrete (N/mm^2)

f_t' = effective tensile strength (N/mm^2)

Equation 6.1 from Lam et al (2000) is derived from research conducted into composite beams with hollow-core slabs. It was the first equation proposed to calculate the effective width of such composite beams.

$$b_{eff} = \left(\frac{\sqrt{f_{cu}}}{40}\right) \times \left(\frac{32 \times \phi}{500}\right) \times \left(\frac{f_y}{460}\right) \times 1000 + 2.5g \qquad (6.2)$$

where: f_{cu} = concrete cube strength of in-situ concrete (N/mm^2)

ϕ = diameter of reinforcement (mm^2)

f_y = characteristic strength of reinforcement (N/mm^2)

g = gap between ends of precast slabs (mm)

Equation 6.2 is modified in comparison to 6.1, with the inclusion of the diameter of reinforcement, characteristic strength of reinforcement and gap between ends of precast slabs.

$$b_{eff} = \left(\frac{\phi}{16}\right) \times \left(\frac{f_y}{460}\right) \times \left(\frac{300}{s}\right) \times \left(\frac{40}{f_{cu}}\right) \times 1000 + 2.5g \qquad (6.3)$$

where: ϕ = effective tensile strength (N/mm^2)

f_y = characteristic strength of reinforcement (N/mm^2)

s = reinforcement bar spacing (mm)

f_{cu} = concrete cube strength of in-situ concrete (N/mm^2)

g = gap between ends of precast slabs (mm)

Equation 6.3 is the latest effective width equation modified by Bison Concrete Ltd. The equation is modified to take into account the reinforcement bar spacing in the concrete slabs.

The effective width is calculated using the three equations for each of the composite beams tested. Table 6.1 shows effective widths calculated using the three equations for each beam test. From the calculations, it can be seen that equation 6.2 is the nearest match to the actual effective widths found for the beams tested.

Test	B_{eff1} Eqn. 6.1	B_{eff2} Eqn. 6.2	B_{eff3} Eqn. 6.3	B_{eff4} EC 4 (L/4)	B_{eff} from experiments	
	(mm)	(mm)	(mm)	(mm)	(mm)	
CB-1	444	1087	1300	2925	732	L/11
CB-2	444	1087	1300	2925	909	L/13
CB-3	444	1087	1300	2925	528	L/19
CB-4	480	1087	1200	2250	909	L/10
CB-5	480	1087	1200	2925	1319	L/9

Table 6.1: Effective width calculation for each beam test

6.3 Design of Shear Stud Capacity

From the six push tests carried out using hollow-core slabs, the results corresponded well with the design equations shown below.

$$P_{RD} = 0.29\alpha\beta\lambda d^2 \times \frac{\sqrt{\omega f_{cp} E_{cp}}}{\gamma_v} \tag{6.4}$$

$$P_{RD} = 0.8 f_u \times \frac{\pi d^2}{4\gamma_v} \tag{6.5}$$

where: α = 0.2 (h/d + 1) < 1.0.

β = gap width factor and is given as 0.5 (g/70 + 1) < 1.0, and g > 30mm (5mm aggregate + stud dia. + 5mm aggregate).

λ = transverse reinforcement factor (grade 460).

d = diameter of headed shear stud.

ω = transverse joint factor = 0.5(w/600 +1) < 1.5.

w = width of hcu.

f_{cp} = average concrete cylinder strength = 0.8 x average cube strength of the insitu and precast concrete (N/mm^2).

E_{cp} = average value of elastic modulus of the insitu and precast concrete (N/mm^2).

λ_v = partial safety factor (normally taken as 1.25 at ultimate accordance to EC4.

f_u = ultimate tensile strength of the headed stud material.

The slip measured in the beam test experiments with low shear connections agreed well with results gained from the push tests. For beams designed with partial shear connection, the ductility of the shear stud is an important issue. The parameters affecting the stud capacity are the transverse reinforcement, in-situ concrete, the gap between the slabs and the depth of slab.

6.4 Design of Composite Moment Capacity

As mentioned in Chapter 5, the composite moments of each test were calculated in the analysis using the following equations:

For full shear connection:

$$M_{comp} = F_s\left(\frac{D}{2} + D_s - \frac{F_s}{F_c}\frac{D_s}{2}\right) \qquad (6.6)$$

For partial shear connection:

$$M_{comp} = F_s\frac{D}{2} + F_{con} \times \left(D_s - \frac{F_{con}}{F_c}\frac{D_s}{2}\right) - \left[\frac{(F_s - F_{con})^2}{F_{flange}} \times \left(\frac{T}{4}\right)\right] \qquad (6.7)$$

where F_s = Force in steel

F_c = Force in concrete

F_{con} = Force of shear connection

F_{flange} = Force in steel top flange

D = depth of steel beam

D_s = depth of concrete slab

Using the Bison software for the design of composite beams, the conditions for each test (beam and slab sizes, span, loading points, number of studs and load at failure) were input into the program and the composite moment capacity of the section was found. The results from the program for CB-1, CB-2, CB-3, CB-4 and CB-5 are shown in Figures 6.1, 6.2, 6.3, 6.4 and 6.5

and summarised in Table 6.2. The results corresponded well with the moments calculated for all tests.

Test	M_{comp} from Experiments	M_{comp} from Bison Design
	(kNm)	(kNm)
CB-1	2091	2180
CB-2	1418	1979
CB-3	1681	1655
CB-4	795	710
CB-5	2001	2180

Table 6.2: Composite moments from analysis and Bison software

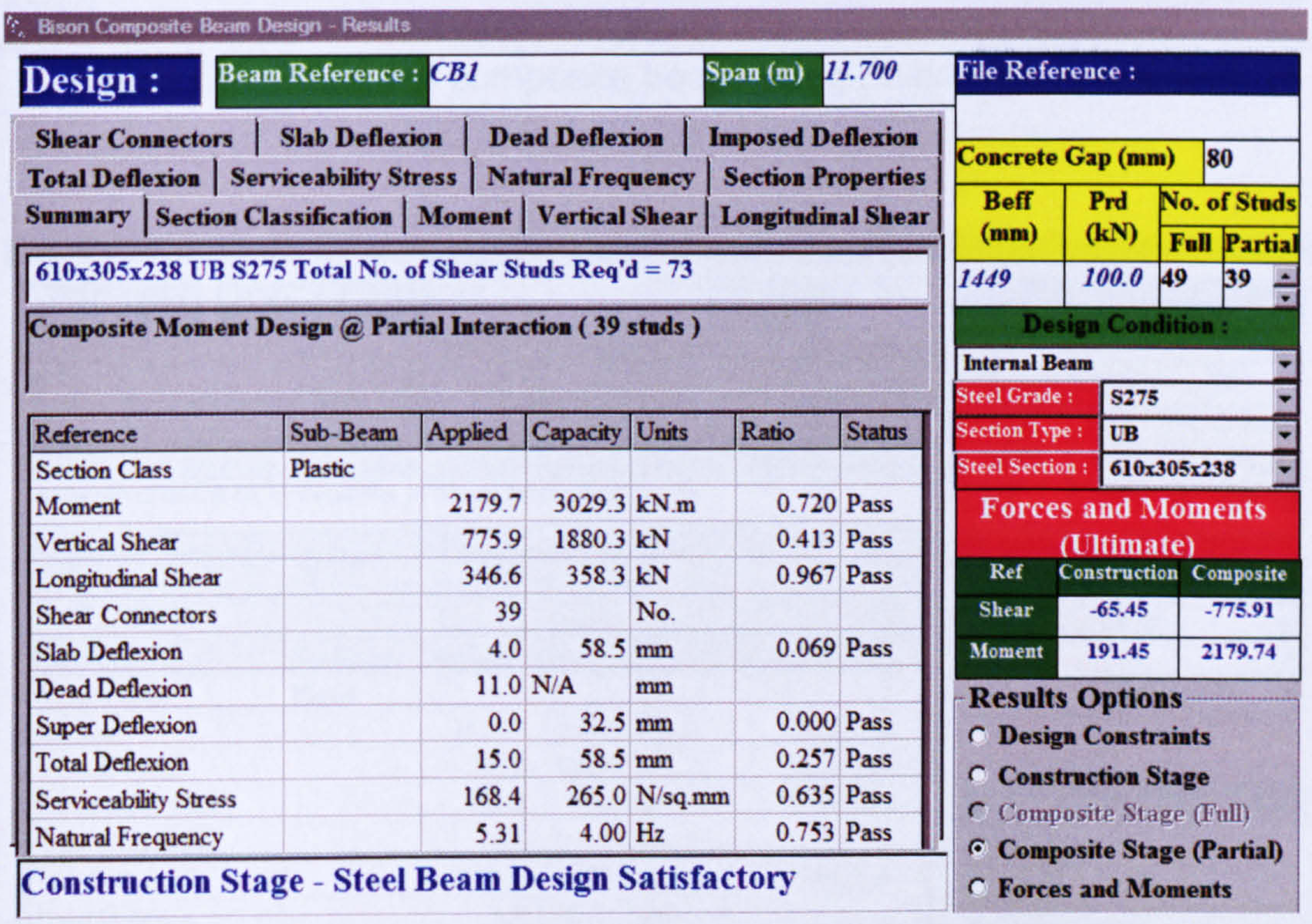

Figure 6.1: Design of composite beam using Bison software (CB-1)

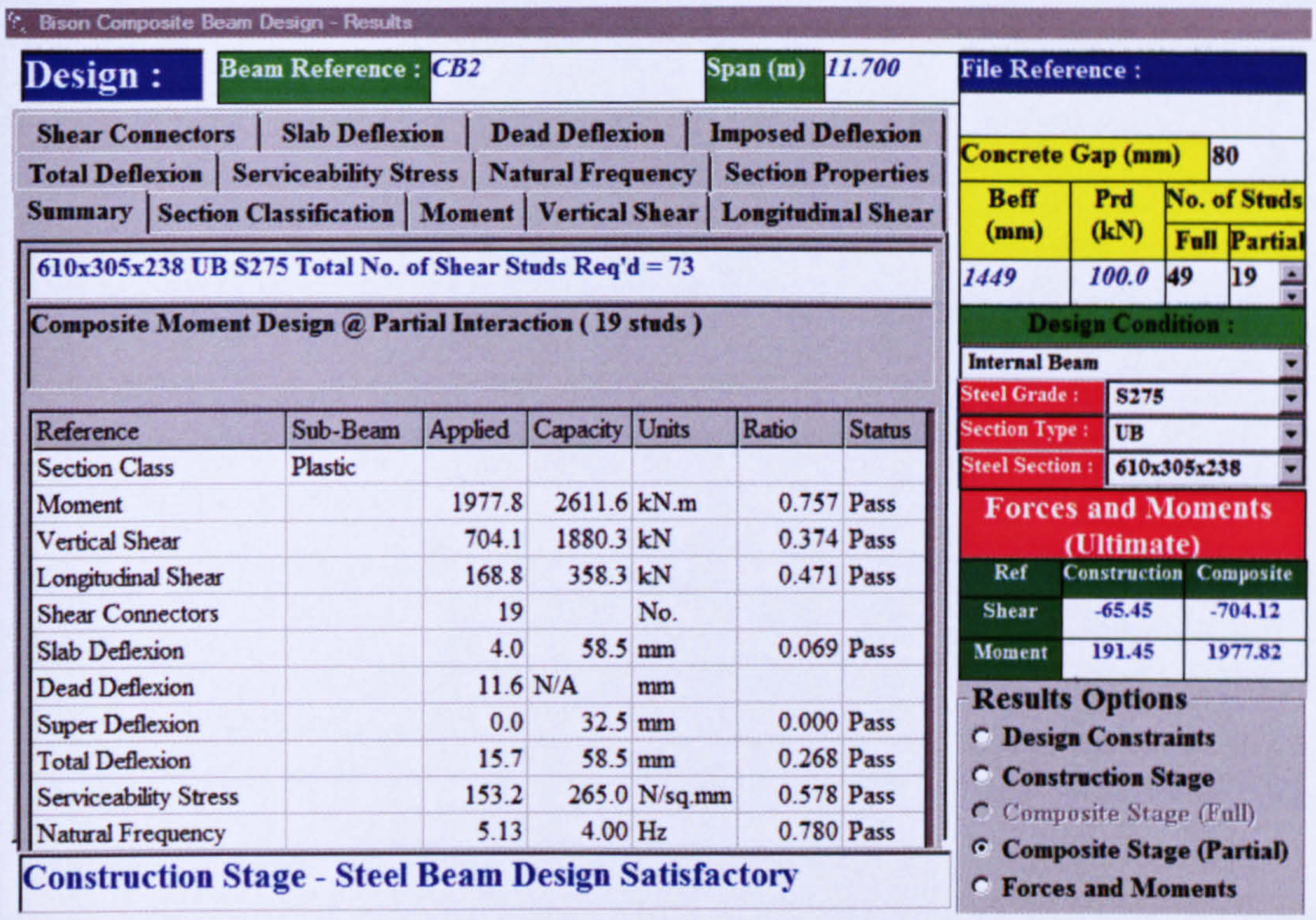

Figure 6.2: Design of composite beam using Bison software (CB-2)

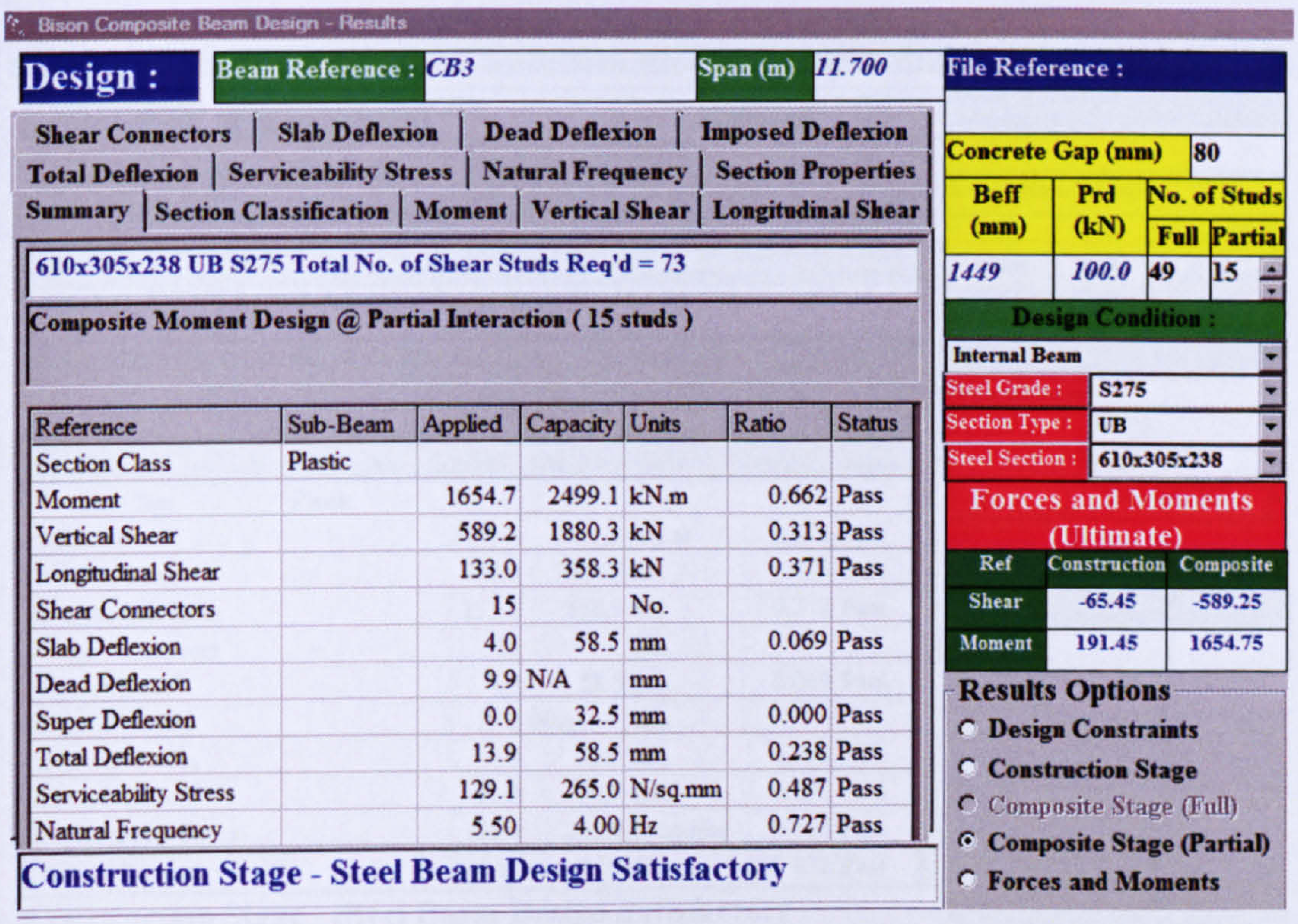

Figure 6.3: Design of composite beam using Bison software (CB-3)

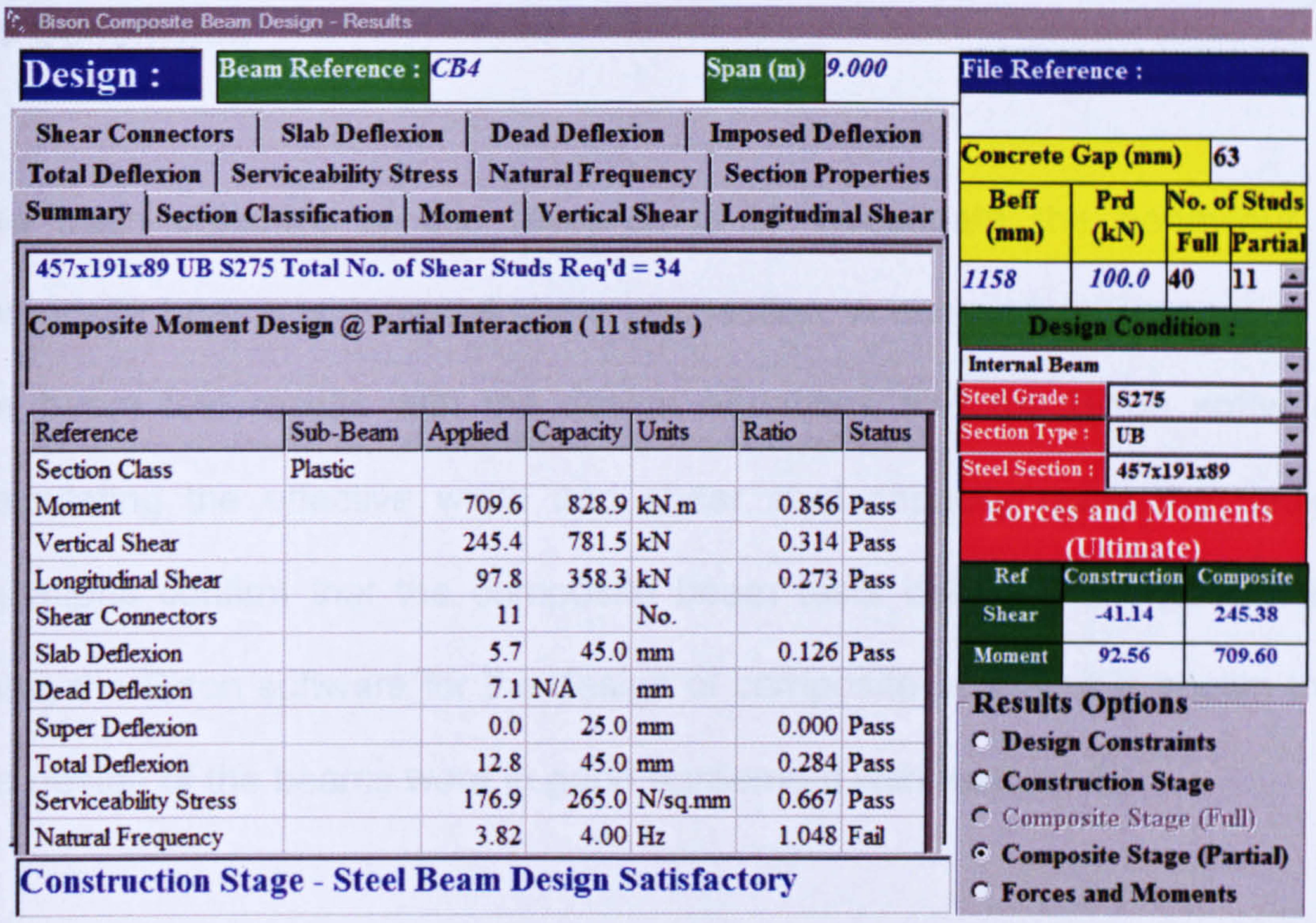

Figure 6.4: Design of composite beam using Bison software (CB-4)

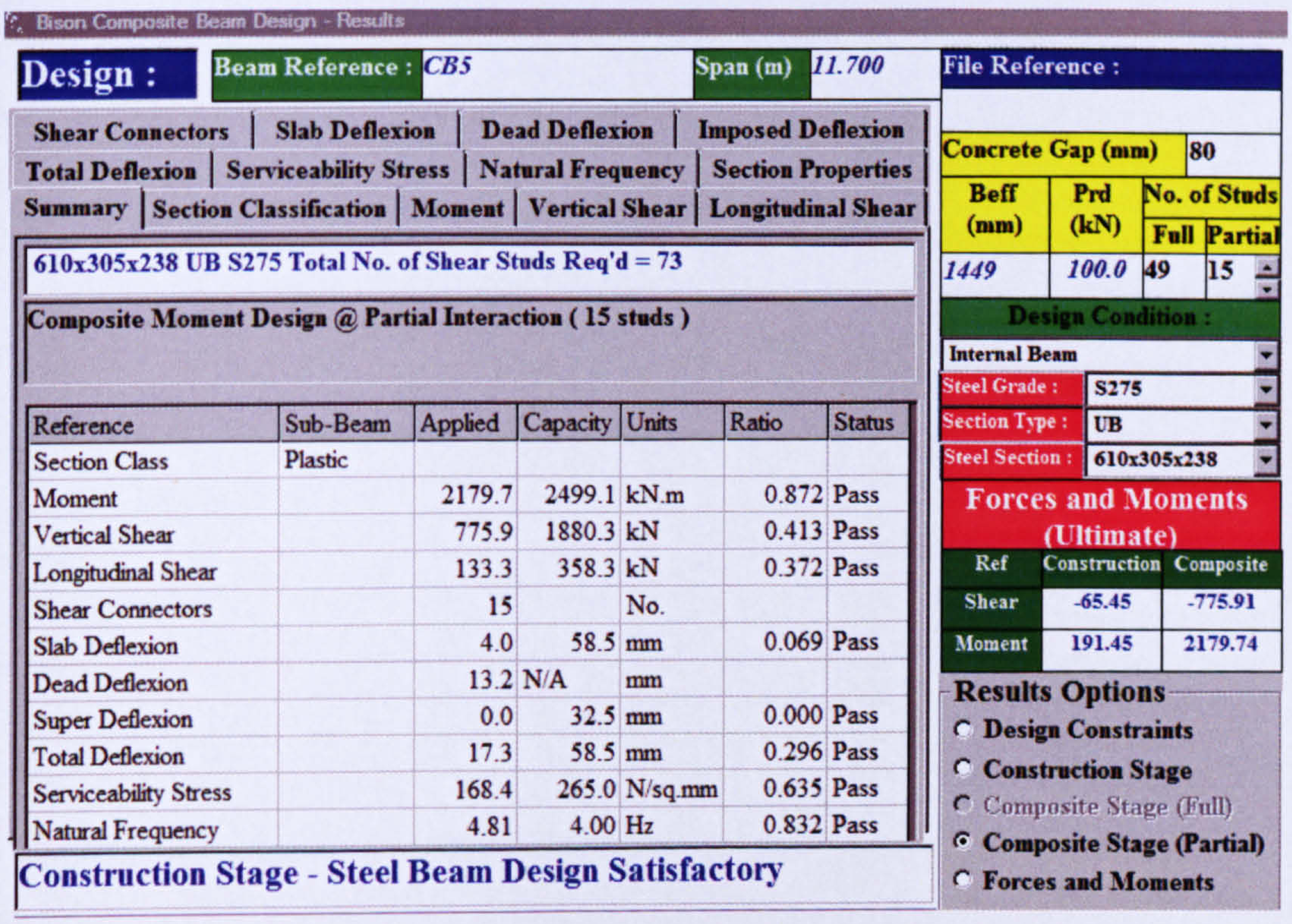

Figure 6.5: Design of composite beam using Bison software (CB-5)

6.5 Conclusion

The main objective of this research is to investigate the behaviour of composite beams with partial shear connection. A comparison was made of the beam test results with the design equations and the Bison software. Calculating the effective width and shear stud capacity using the design equations confirm that the composite beam tests behaved adequately. By using the Bison software for the design of composite beams, it is shown that the design of the beams were in good agreement with test results.

Chapter 7

Conclusion and Future Work

Chapter 7: Conclusion and Future Work

7.1 Conclusions from Research Work

The behaviour of long span composite beams with precast hollow-core slabs has been investigated by a combination of experimental and analytical study, and the following conclusions can be extracted from this research:

1. Long span composite beams with precast hollow-core slabs behave similarly to short span beams of the same composite construction.

2. Long span composite beams designed with partial shear connection showed similar behaviour with full shear connection beams, with only a slight reduction in ultimate strength.

3. The effective width of long span composite beams was found to be smaller than current design suggests.

4. Long span composite beams with partial shear connection and the position of neutral axis in the concrete slab had no premature failure.

5. Three modes of failure occurred at the connection of the composite beam, either through concrete crushing and fracture of shear stud or both.

6. Reduction of the shear connection provided a more ductile failure with little loss in the moment capacity of the composite beam.

7. Increasing the slab depth will increase the moment capacity of the composite beam.

8. Shear connectors have control of the failure mode in long span composite beams using partial shear connection.

7.2 Proposed Future Work

Further work needed for a complete understanding of long span composite beams with hollow-core slabs is as follows:

1. To study the behaviour of long span composite beams with semi-rigid connections.

2. To establish a finite element model of long span composite beams, so parametric studies can be carried out.

3. Further research is required into the behaviour of the whole frame of buildings using composite construction.

References

References

Aglan A A and Redwood R G (1974) '*Web Buckling in Castellated Beams'*. Institution of Civil Engineering (London), Vol. 57, June 1974, Pg 307-320.

Ahmed, M, Bradford M A, Nguyen N T and Oehlers D J (1997) '*Partial Interaction in Composite Steel and Concrete Beams with Full Shear Connection'*. Journal of Constructional Steel Research, Vol. 41, No. 2/3, Pg 235-248.

Allen D N, De G and Severn R T (1961) '*Composite Action between Beams and Slabs under Transverse Load'*. The Structural Engineer, May 1961, Pg 149-154.

Amadio, C and Fragiacomo, M (2002) '*Effective Width Evaluation for Steel-Concrete Composite Beams'*. Journal of Constructional Steel Research, Vol. 58, Pg 373-388.

Bild, S and Sedlacek, G (1993) '*A simplified method for the determination of the Effective Width due to Shear Lag Effects'*. Journal of Constructional Steel Research, Vol. 24, Pg 155-182.

Bower, J E (1968) '*Ultimate Strength of Beams with Rectangular Holes'*. ASCE Journal of Structural Engineering 94: ST6 June 1968, Pg 1315-1337.

Bradford, M.A, Loh, H.Y and Uy, B (2003) '*The behaviour of composite beams in hogging moment regions*'. School of Civil and Environmental Engineering, The University of New South Wales, Sydney.

Bradford, M A and Oehlers, D J (1999) '*Elementary Behaviour of Composite Steel and Concrete Structural Members'*. Butterworth-Heinemann, Oxford.

BS 4449 (1998) *'Carbon Steel Bars for the reinforcement of Concrete.'* British Standards Institution, London.

BS 5950 – Part 1 (1990) *'Code of practice for design in simple and continuous construction: hot rolled sections, British Standard: Structural Use of Steelwork in Building'.* British Standards Institution, London.

BSI 881 (1983) *'Method of Determination of Compressive Strength and Tensile Splitting Strength'.* British Standards Institution, London.

BS EN 10002 – Part 1 (2001) *'Metallic materials: Tensile testing – Part 1: Method of test at ambient temperature'.* British Standards Institution, London.

Cairns, R, Kim, B and Wright, H D (2001) *'The Behaviour of through-deck welded shear connectors: an experimental and numerical study'.* Journal of Constructional Steel Research, Vol. 57, Pg 1359-1380.

Cho, S H and Redwood, R (1993) *'Design of Steel and Composite Beams'.* Journal of Constructional Steel Research, 25(1-2), Pg 23-41.

Darwin, D and Donahey, R C (1986) *'Performance and Design of Composite Beams with Web Openings'.* University of Kansas Center for Research, SM Report No. 18, Kansas.

Darwin, D and Donahey, R C (1988) *'Web Openings in Composite Beams with Ribbed Slabs'.* ASCE Journal of Structural Engineering 114: 3 March 1988, Pg 518-534.

Darwin, D and Donahey, R C (1988) *'LRFD for Composite Beams with Unreinforced Web Openings'.* ASCE Journal of Structural Engineering 114: 3 August 1988, Pg 535-552.

Darwin, D (1990) *Design Guide 2: 'Design of Steel and Composite Beams with Web Openings'.* American Institute of Steel Construction, Chicago.

Darwin, D and Lucas, W K (1990) *'LRFD for Steel and Composite Beams with Web Openings'.* ASCE Journal of Structural Engineering 116: No. 6, June 1990, Pg 1579-1593.

Darwin, D (2000) *'Design of Composite Beams with Web Openings'.* Prog. Structural Engineering Materials 2000; 2: Pg 157-163, John Wiley & Sons Ltd, Kansas.

Davies, C (1975) *'Steel-Concrete Composite Beams for Buildings'.* George Godwin Limited, London.

Darwin, D and Donahey (1986) R C *'Performance and Design of Composite Beams with Web Openings'.* University of Kansas Center for Research, SM Report No. 18, Kansas.

Donoghue, C M (1982) *'Composite Beams with Web Openings: Design'.* ASCE Journal of Structural Engineering 108: No. 12, December 1982.

Elliott, K S, Lam, D and Nethercot D A (2000) *'Parametric study on composite steel beams with precast hollow core floor slabs'.* Journal of Constructional Steel Research, 54, Pg 283-304.

Eurocode 4: Design of composite sreel and concrete structures – Part 1.1. Common rules and rules for buildings, ENV 1994-1-1: 2005.

Fabsec Limited (2002) *Design of Fabsec 'Beams in Non-Composite and Composite Applications (including Fire)'.* Fabsec Ltd, Leeds.

Johnson, R P (1994) *'Composite Structures of Steel and Concrete'.* Second Edition, Blackwell Scientific Publications, Oxford.

Johnson, R.P and Molenstra, N (1991) *'Partial shear connection in composite beams for buildings*'. Proceedings of the Institute of Civil Engineers, London, 79(2), pp679-704.

Lam, D, Elliott K.S, Nethercot D.A (1998) ,*Push off tests on shear studs with hollow-cored floor slabs'*. The Structural Engineer, Vol. 76, No. 9, pp167-174, May 1998.

Lam, D, Elliott K.S and Nethercot D.A (2000) *'Designing composite steel beams with precast concrete hollow-core slabs'*. Institute of Civil Engineers, Vol. 140, pp139-149, London.

Lam, D (1998) *'Composite Steel Beams using Precast Concrete Hollow Core Floor Slabs'*. PhD Thesis. Nottingham, UK: University of Nottingham, March.

Lam, D (2002) *'Composite Steel Beams with Precast Hollow-Core Slabs: Behaviour and Design'*. Prog. Structural Engineering Materials 2002; 4. John Wiley & Sons Ltd.

Lam, D (2006) *'Capacities of Headed Stud Shear Connectors in Composite Steel Beams with Precast Hollow-Core Slabs'*. Journal of Constructional Steel Research, School of Civil Engineering, University of Leeds, Nov 2006.

Lam, D (2007) *'Capacities of Headed Stud Shear Connectors in Composite Steel Beams with Precast Hollow-Core Slabs'*. Leeds, UK: University of Leeds, 2007.

Liew, J Y R and Uy, B (2003) *'The Civil Engineering Handbook, Section 6: Structural Engineering'*. Chapter 51: Composite Steel-Concrete Structures, CRC Press LLC, Florida.

Lupien R and Redwood R G (1978) *'Steel Beams with Web Openings reinforced on one side'*. Canadian Journal of Civil Engineering 05, No. 4 1978, Pg 451-461.

Morris, L J and Plum, D R (1996) *'Structural Steel work Design to BS5950'*. Second Edition, Longman, Essex.

Nethercot, D A (2001) *'Limit States Design of Structural Steelwork'.* Third Edition, Spon Press, London.

Newmark, N M, Siess, C P and Viest, I M (1951) *'Test and Analysis of Composite Beams with incomplete interaction'.* Proceedings of the Society for Experimental Stress Analysis. Vol. 9, No. 1. Pg 75-92.

Oehlers, D.J and Bradford, M.A (1995) *'Composite steel and concrete structural members: fundamental behaviour.'* Pergamon Press, Oxford.

OneSteel Market Mills (2001) *'Composite Structures Design Manual – Design Booklet DB1.2, Design of the Shear Connection of Simply Supported Composite Beams'.* OneSteel Manufacturing Ltd and The University of Western Sydney, Sydney.

Redwood, R G and Shrivastava, S C (1980) *'Design Recommendations for Steel Beams with Web Holes'.* Canadian Journal of Civil Engineering 07, No. 1 1980, Pg 642-650.

SCI Publication 100 (1990) *'Design of Composite and Non-Composite Cellular Beams'.* The Steel Construction Institute, Berkshire.

SCI Publication P351 (2007) *'Precast concrete floors in steel framed buildings'.* The Steel Construction Institute, Ascot.

Appendix A

Steel Beam and Slab Specification Drawings

One 12m beam with two 15mm thick full depth stiffeners and 19x125mm studs @ 400 c/c.

Description of stud spacing

Stud size	Initial distance from end	C/C
19 x 125mm	400mm	400mm

29 No. 19 x 125mm headed stud @ 400 c/c.

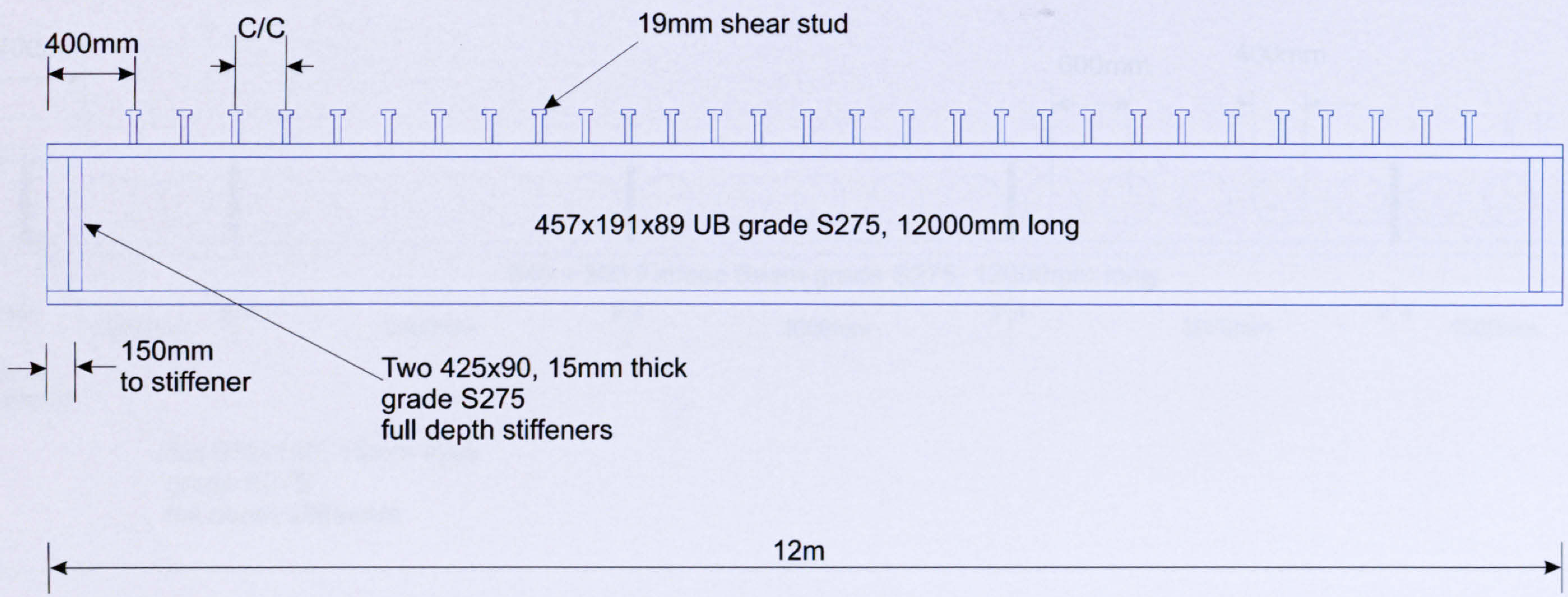

A. Murad

457 BEAM SPECIFICATION

Not to Scale

10/4/03
Page: 1/4

Three 12m beam with six 15mm thick
full depth stiffeners and 19x125mm
studs @ 200 c/c.

Description of stud spacing

Stud size	Initial distance from end	C/C
19 x 125mm	400mm	200mm

57 No. 19 x 125mm headed stud @ 200 c/c.

Description of hole diameter and spacing

Hole diameter	Centre spacing	Initial distance from end
400mm	600mm	400mm

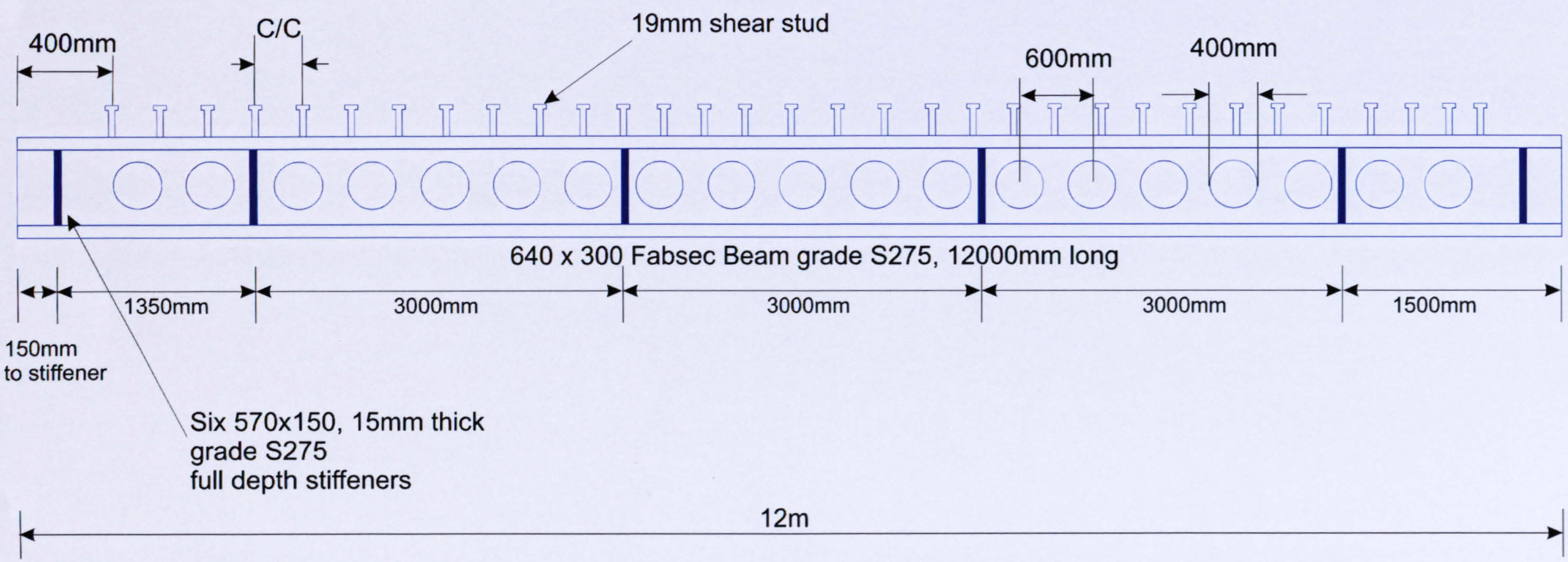

A. Murad

Fabsec BEAM SPECIFICATION

Not to Scale

10/4/03
Page: 2/4

Two 12m beam with six 15mm thick full depth stiffeners and 19x125mm studs @ 150 c/c.

Description of stud spacing

Stud size	Initial distance from end	C/C
19 x 125mm	300mm	150mm

77 No. 19 x 125mm headed stud @ 150 c/c.

Description of hole diameter and spacing

Hole diameter	Centre spacing	Initial distance from end
400mm	600mm	300mm

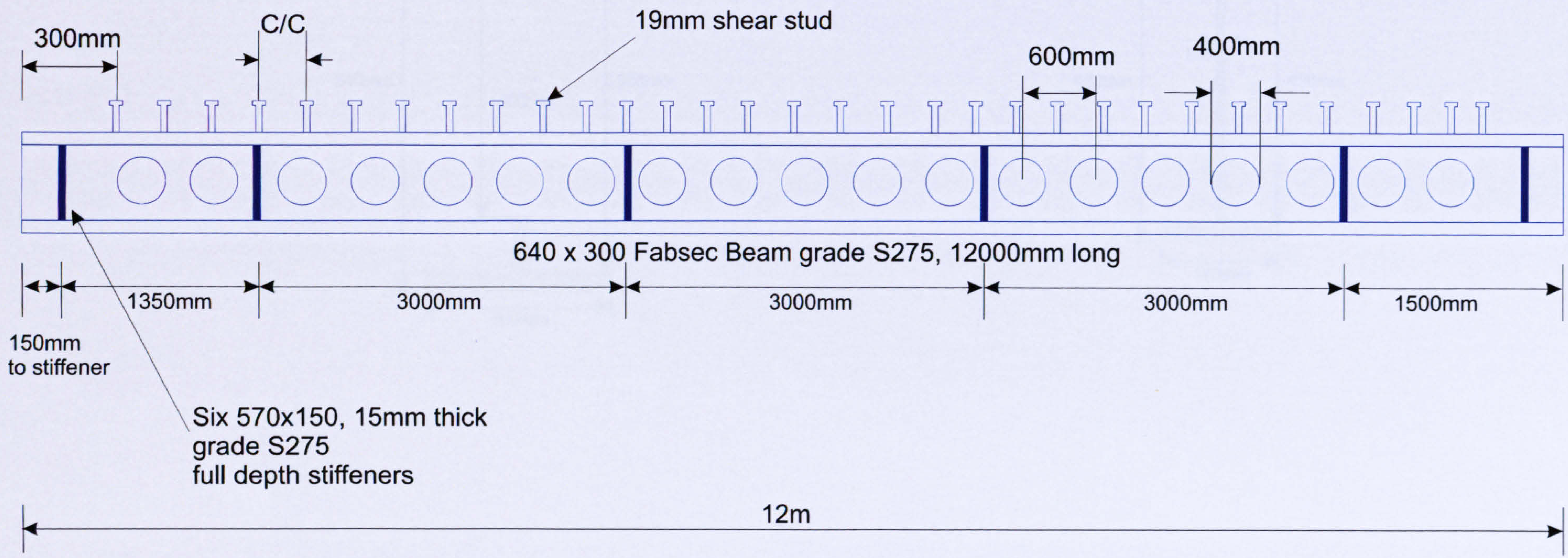

A. Murad

Fabsec BEAM SPECIFICATION

Not to Scale

10/4/03
Page: 3/4

640 x 300 Fabsec Steel Beam with Web Openings

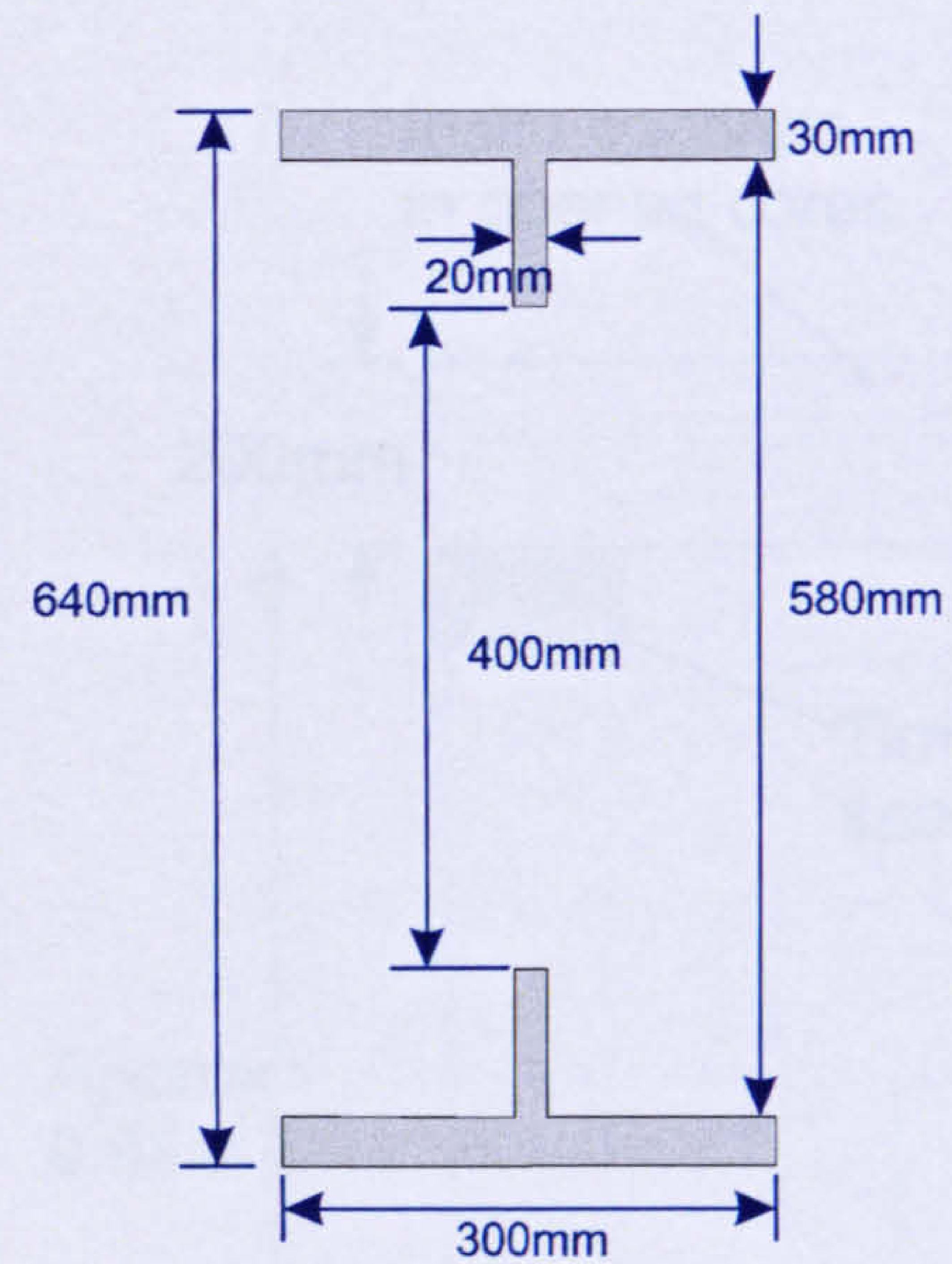

457x191x89 UB

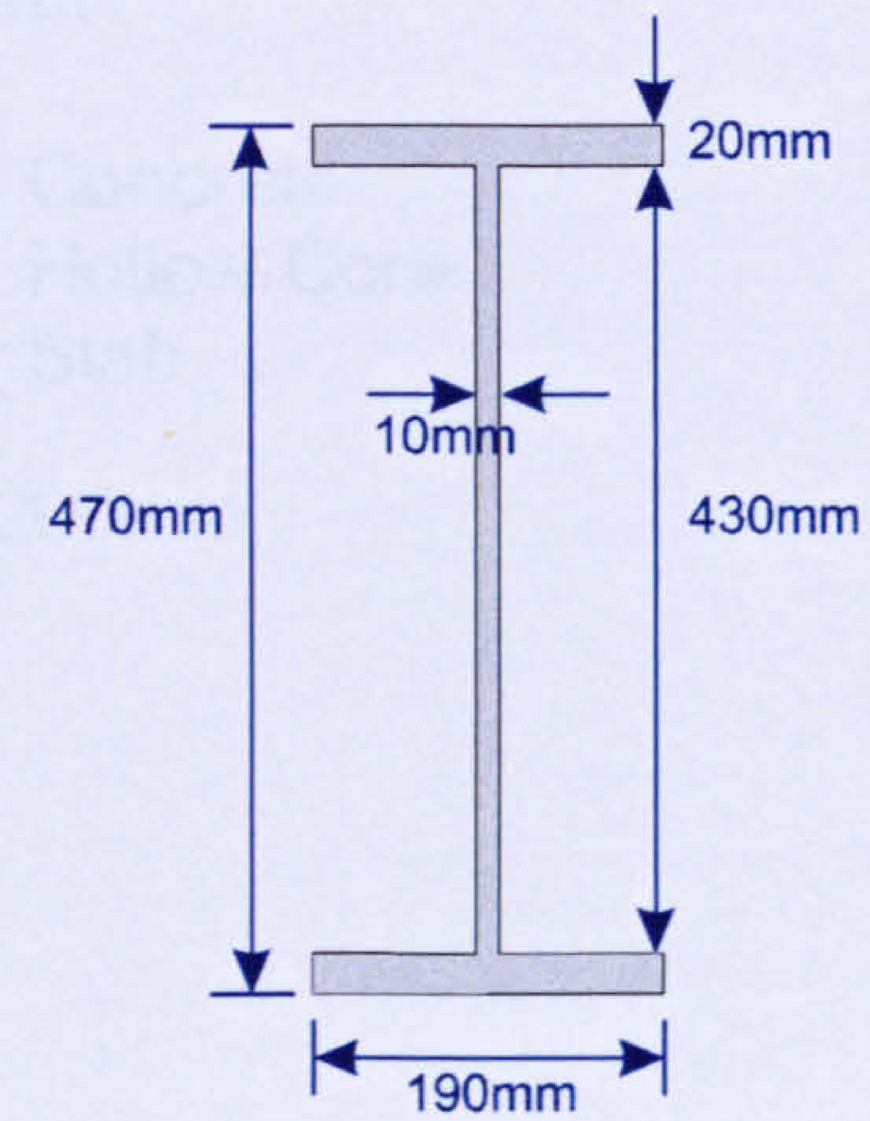

A. Murad

I Section beam dimensions

10/4/03
Page: 4/4

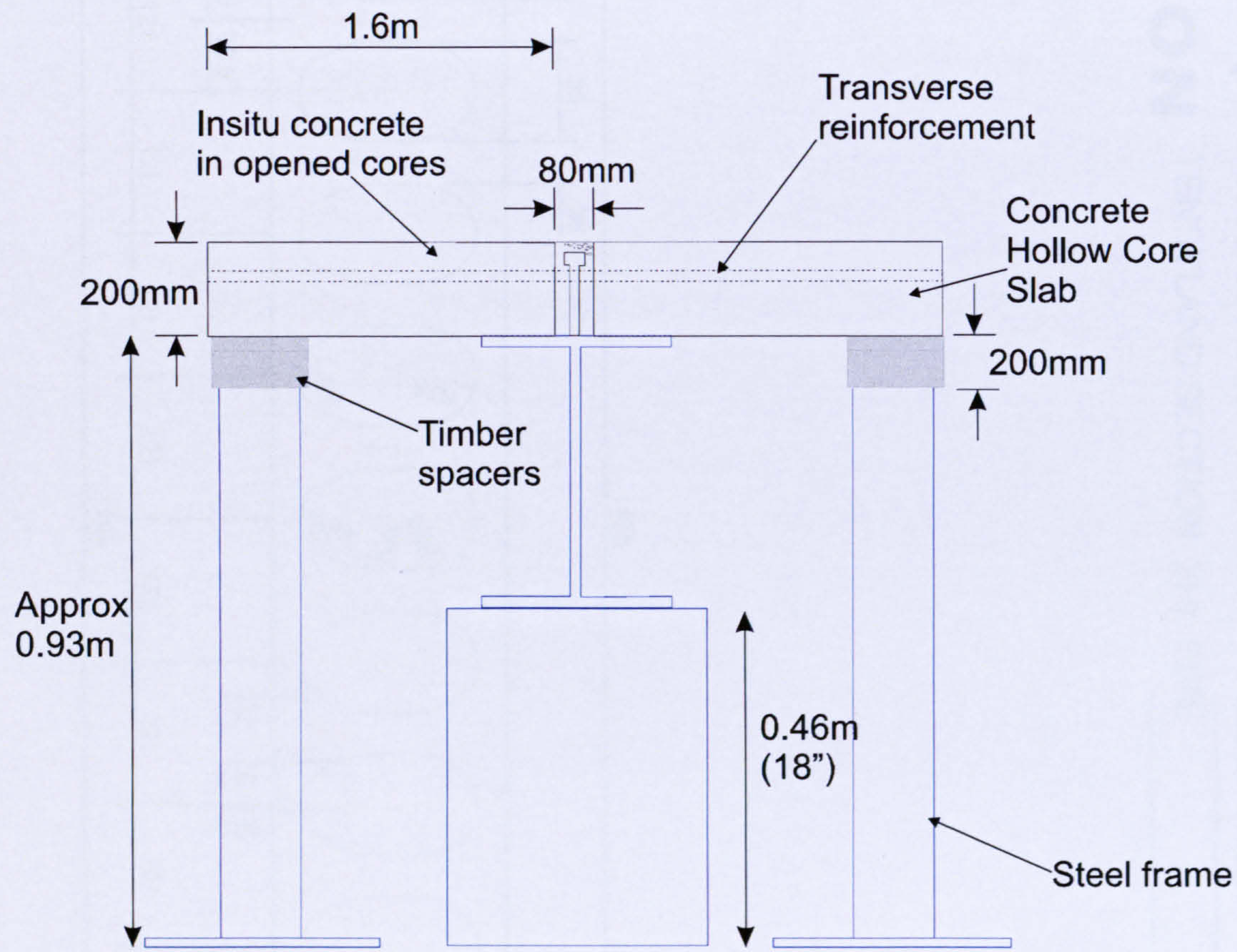

Composite beam

Not to Scale

BISON

TECHNICAL INFORMATION SHEET **SHEET** 330/200 **REV.** B

1200 x 200 DEEP P/S UNIT **DATE** AUGUST 1995

TENSYLAND SECTION 2Hr. FIRE

BISON

TECHNICAL INFORMATION SHEET **SHEET** 321/13 **REV.** A

STANDARD FLOORING & ROOFING **DATE** March 2002

TENSYLAND UNITS

END SLOTS

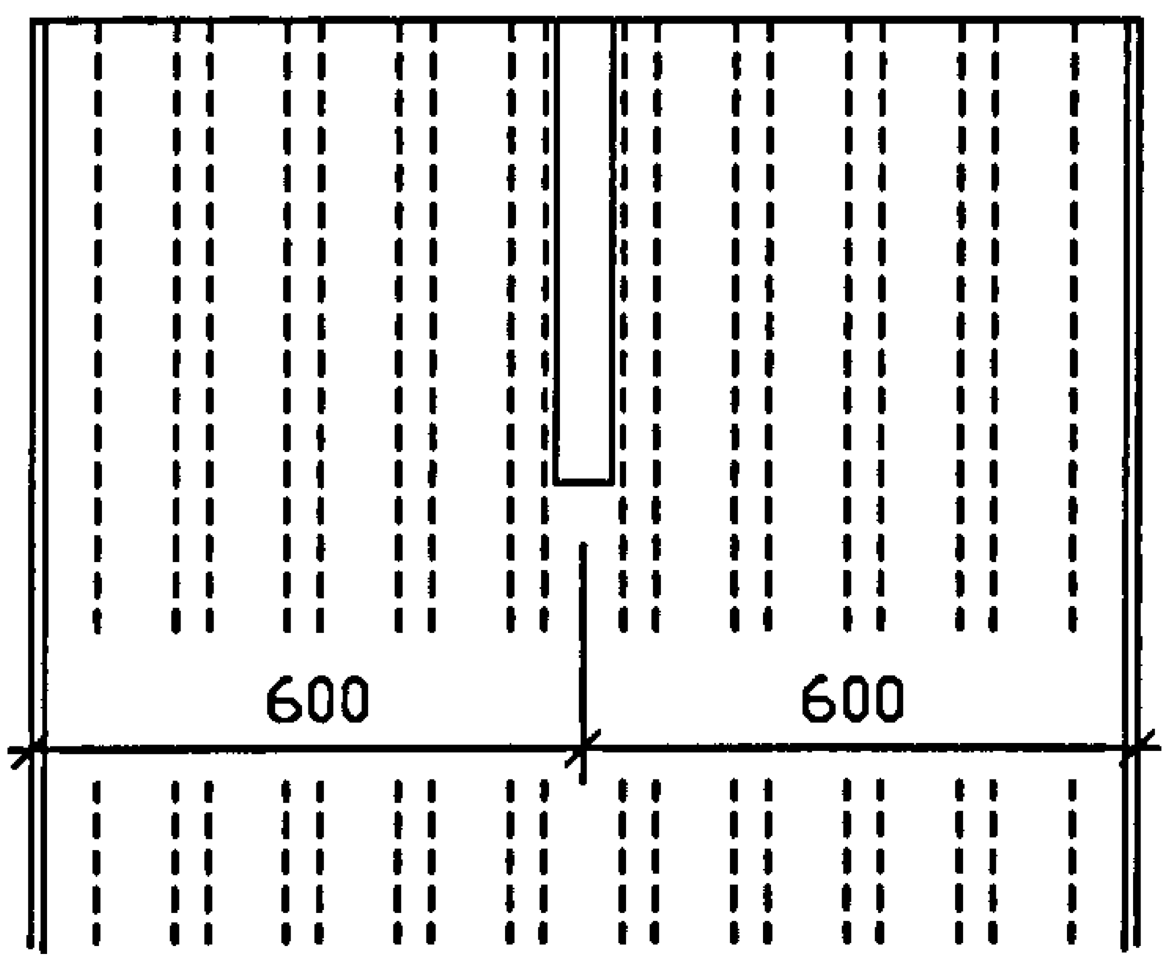

ES1

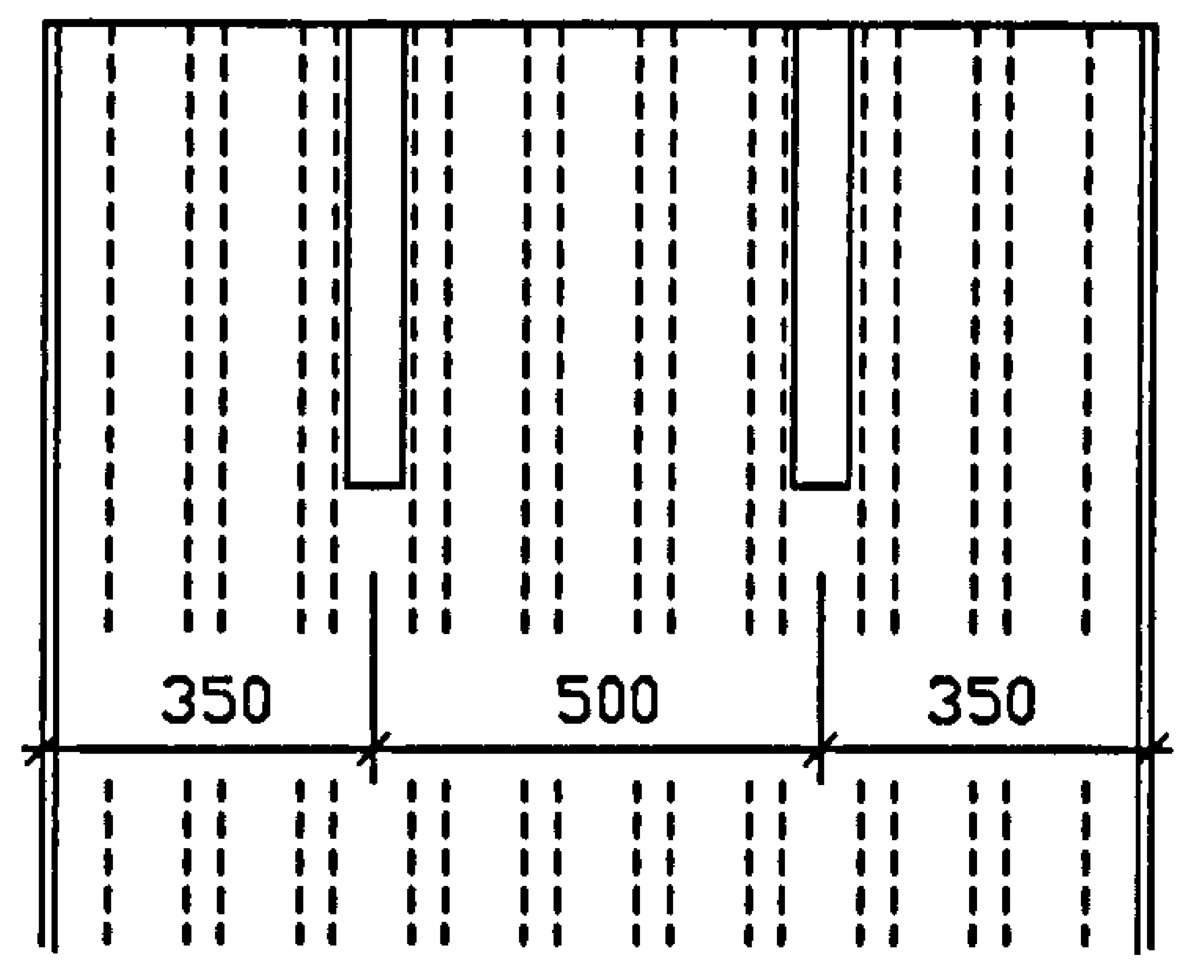

ES2

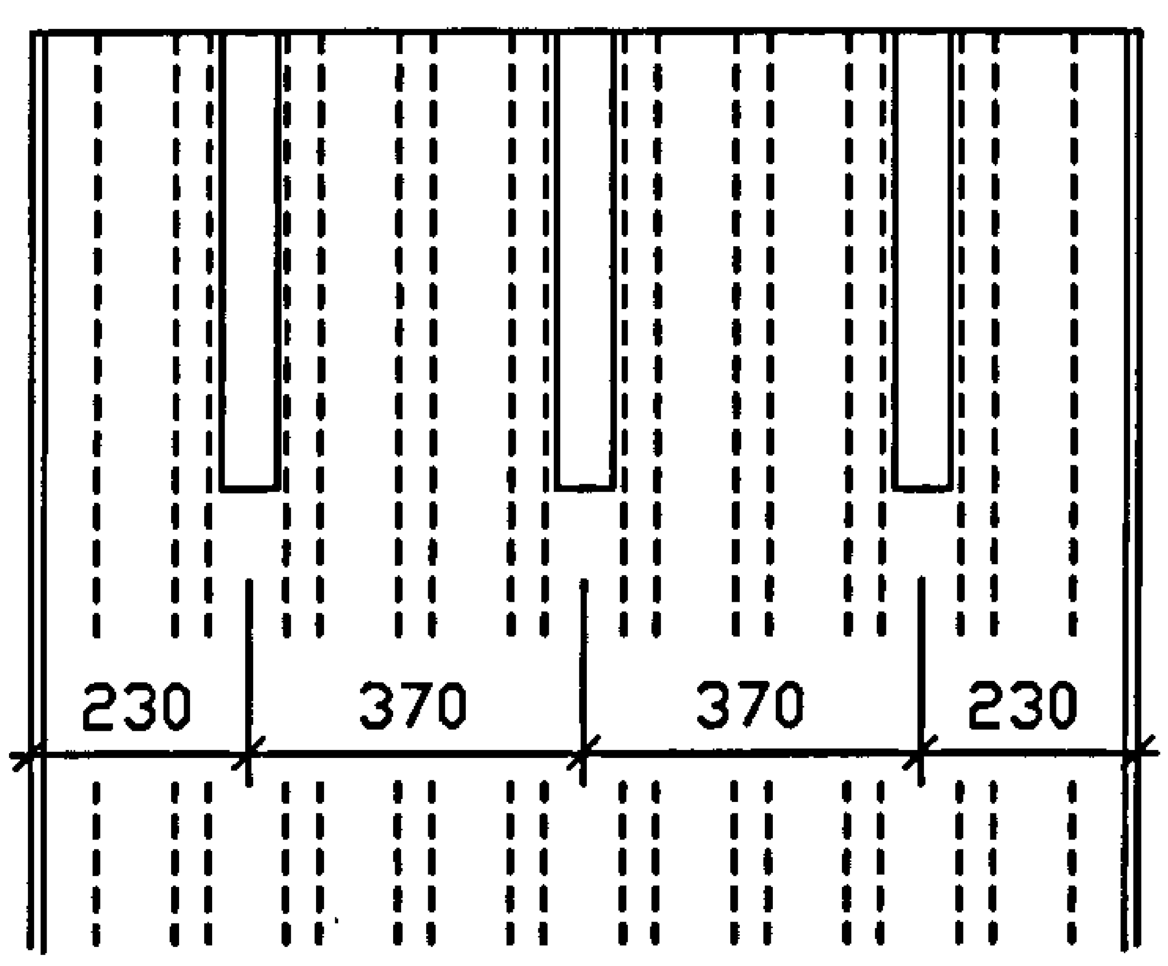

ES3

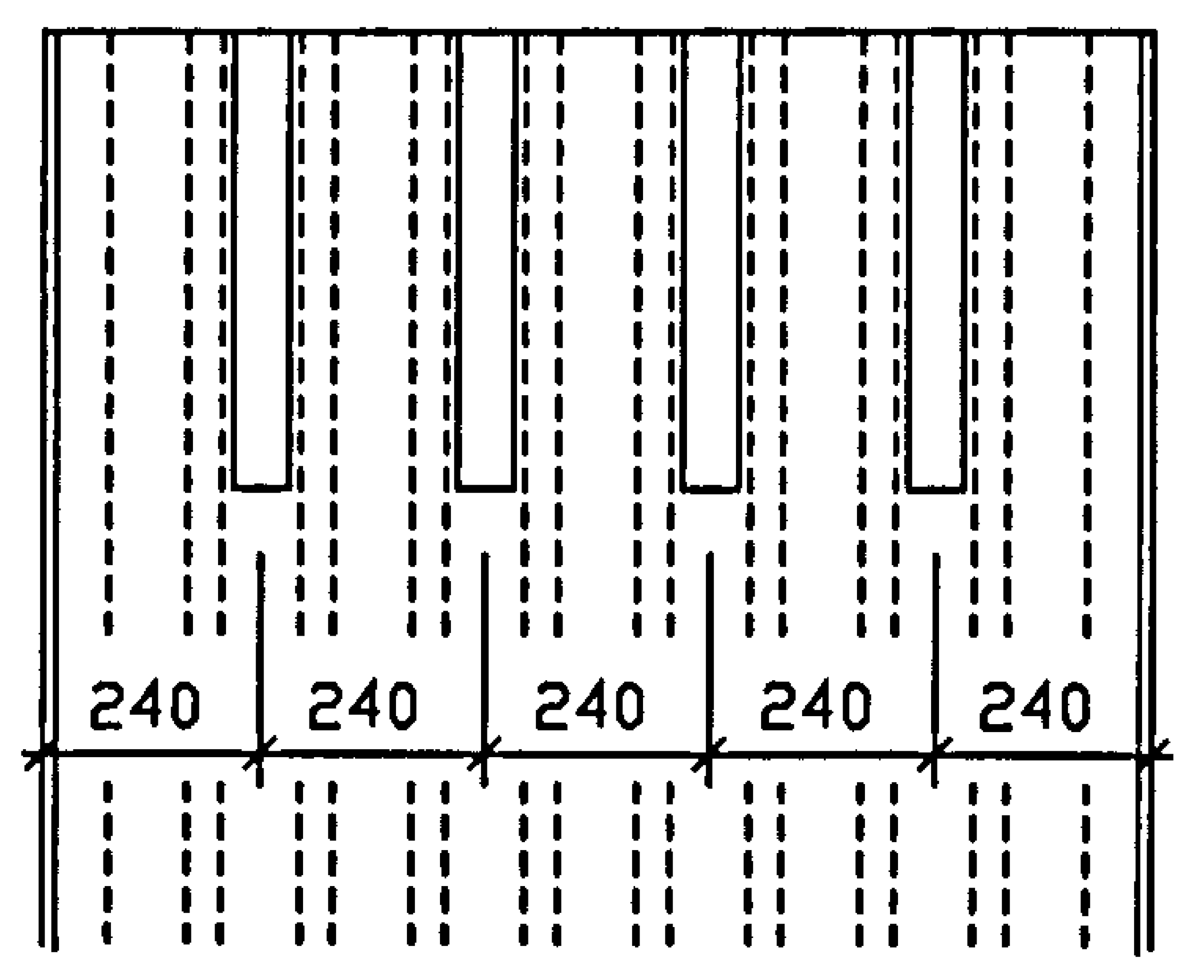

ES4

STANDARD END SLOTS FOR 150 - 250 DEEP TENSYLAND UNITS

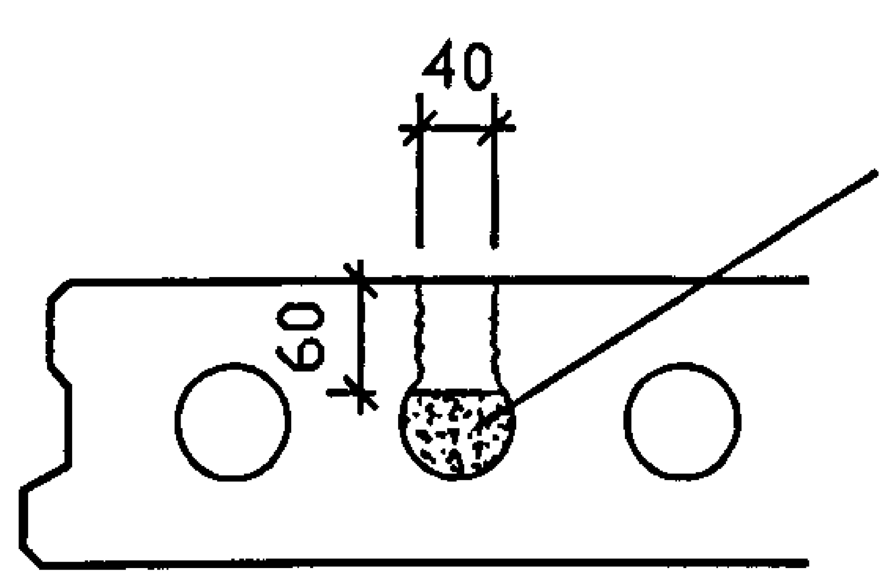

Top concrete compacted
into core space over
length of slots.

NB. Concrete to be removed from core where composite steel beam design is used in conjunction with a sound or other hollowcore slab.

DETAIL OF LIMITED END SLOTS
AVAILABLE WITH SOUND SLABS

ALL SLOTS ARE 500mm LONG.
ANY OTHER FORM OF E.S. END TO BE ORDERED AS ES.SP.

Xref tim

BISON

TECHNICAL INFORMATION SHEET **SHEET** 321/10 **REV.** E

SPECIAL ENDS & SIDE POCKETS **DATE** March 2002

TENSYLAND UNITS 150-250 mm DEEP

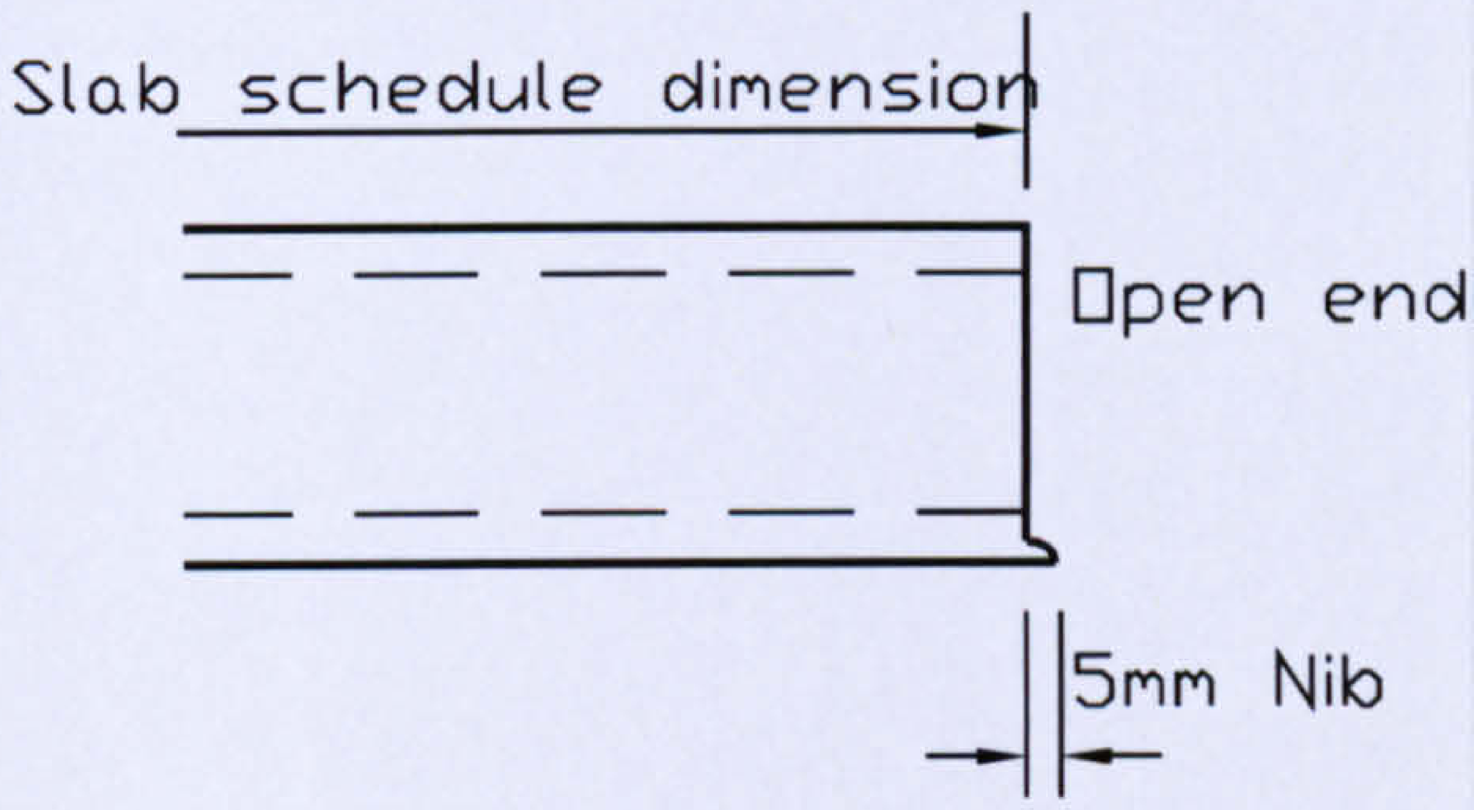

SQ. (Square End)

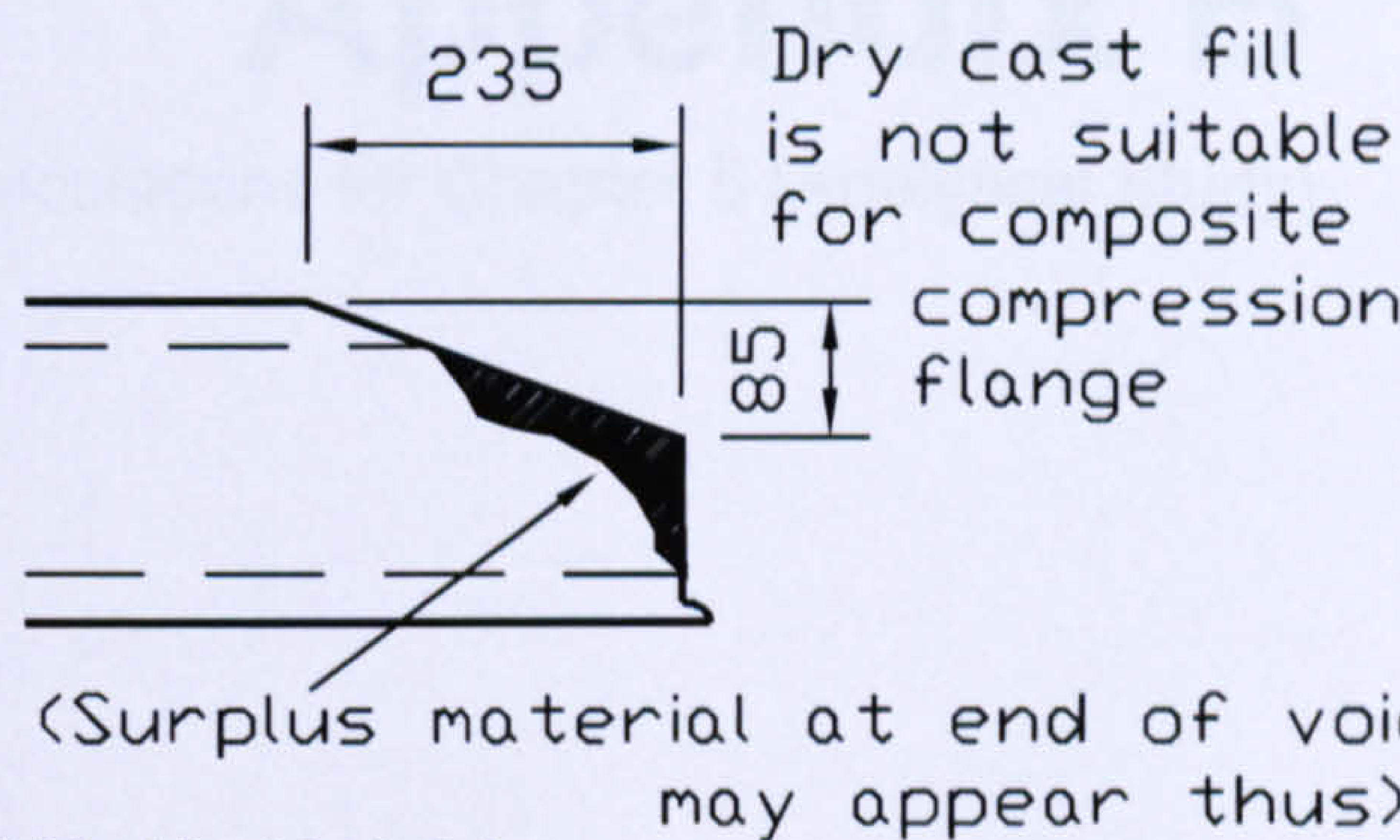

AN. (A. Notch)

(Not applicable to less than 150 deep)

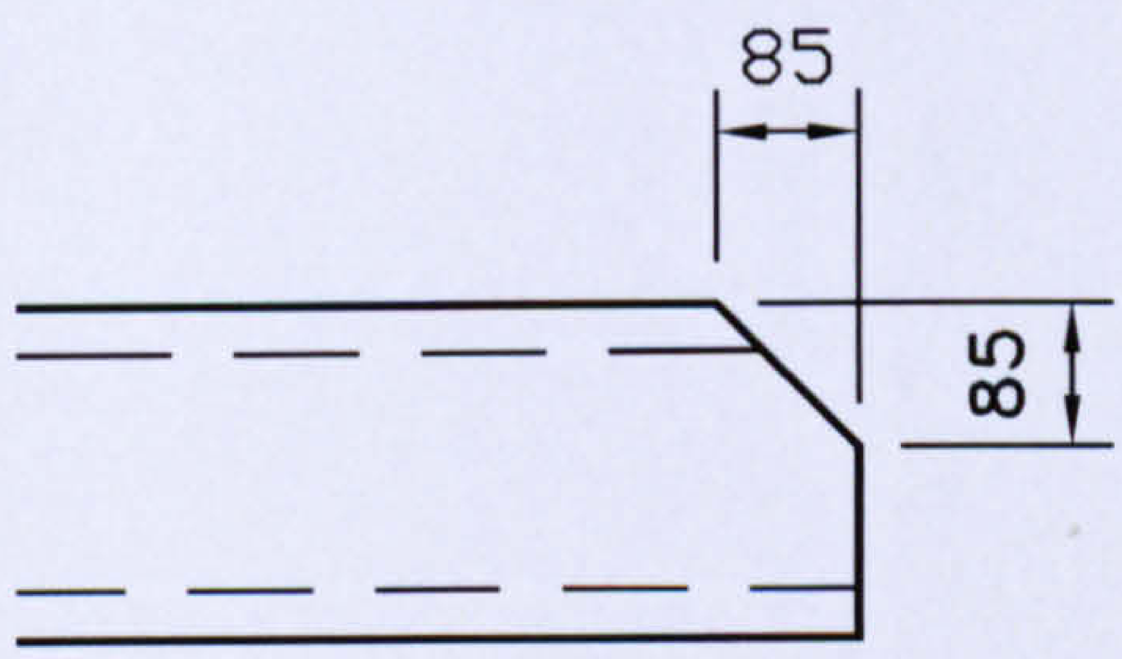

EN. (E Notch)

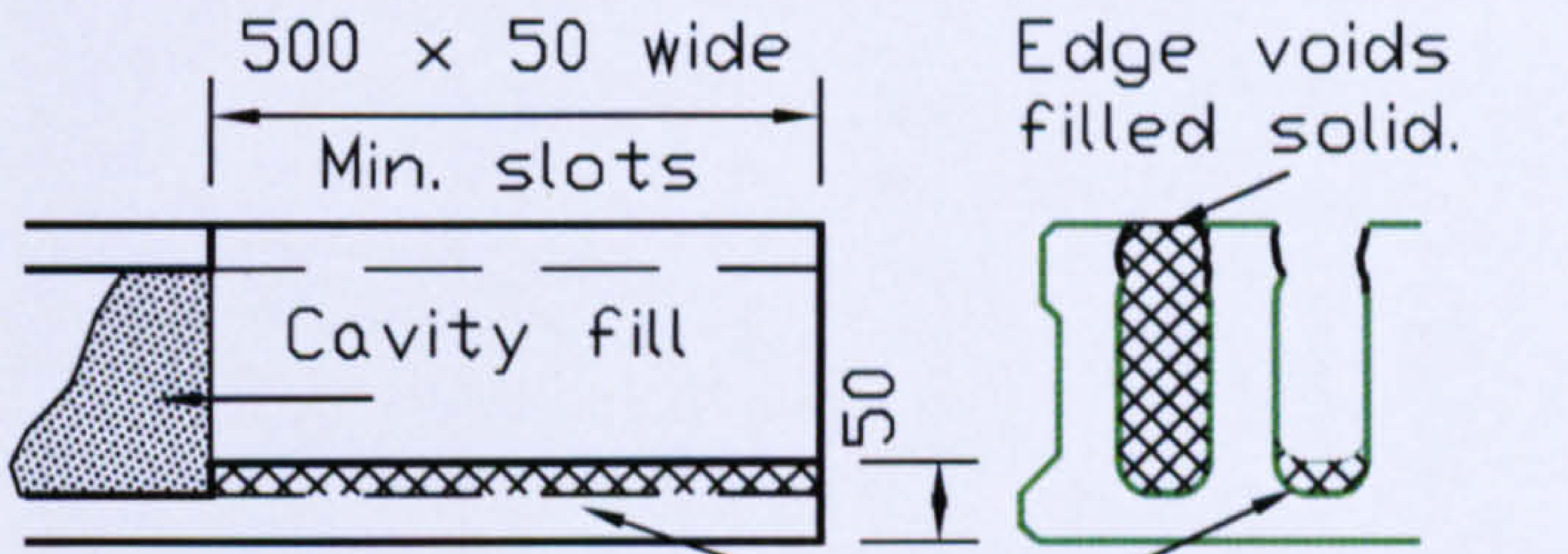

Note top concrete compacted into soffit over slot length.
(See 321/12 & /13 for slot ctrs.)

ENS1
E Notch plus 1no. slot

ENS2
E Notch plus 2no. slots etc.

(See 321/12)

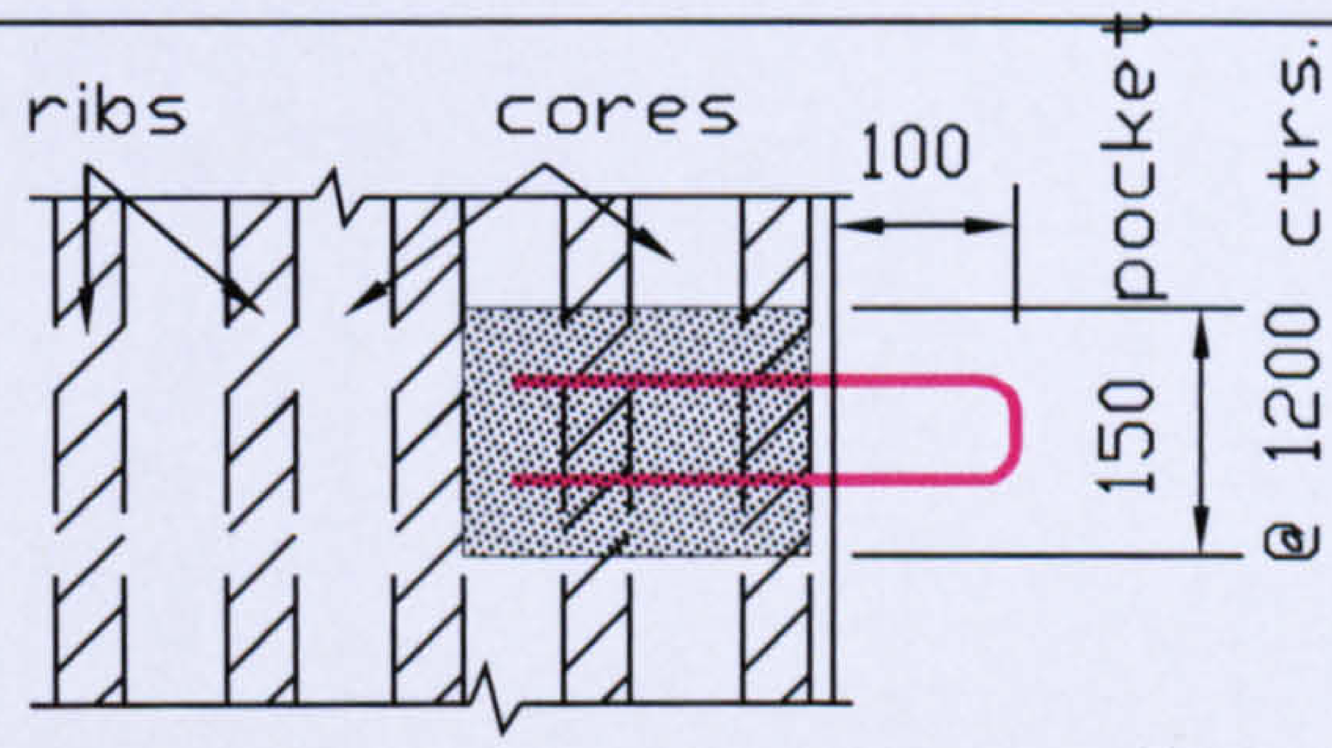

PLAN

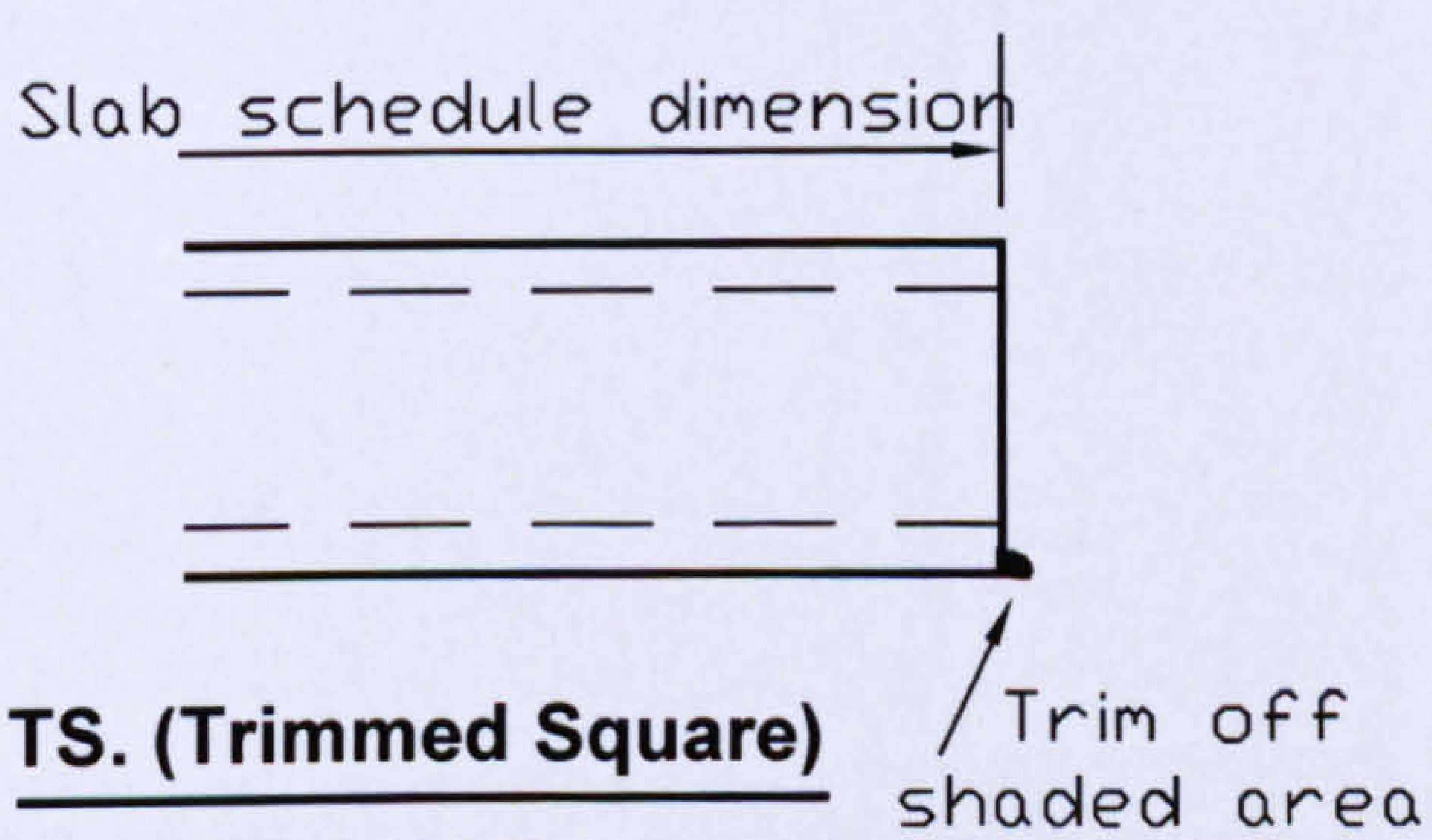

TS. (Trimmed Square)

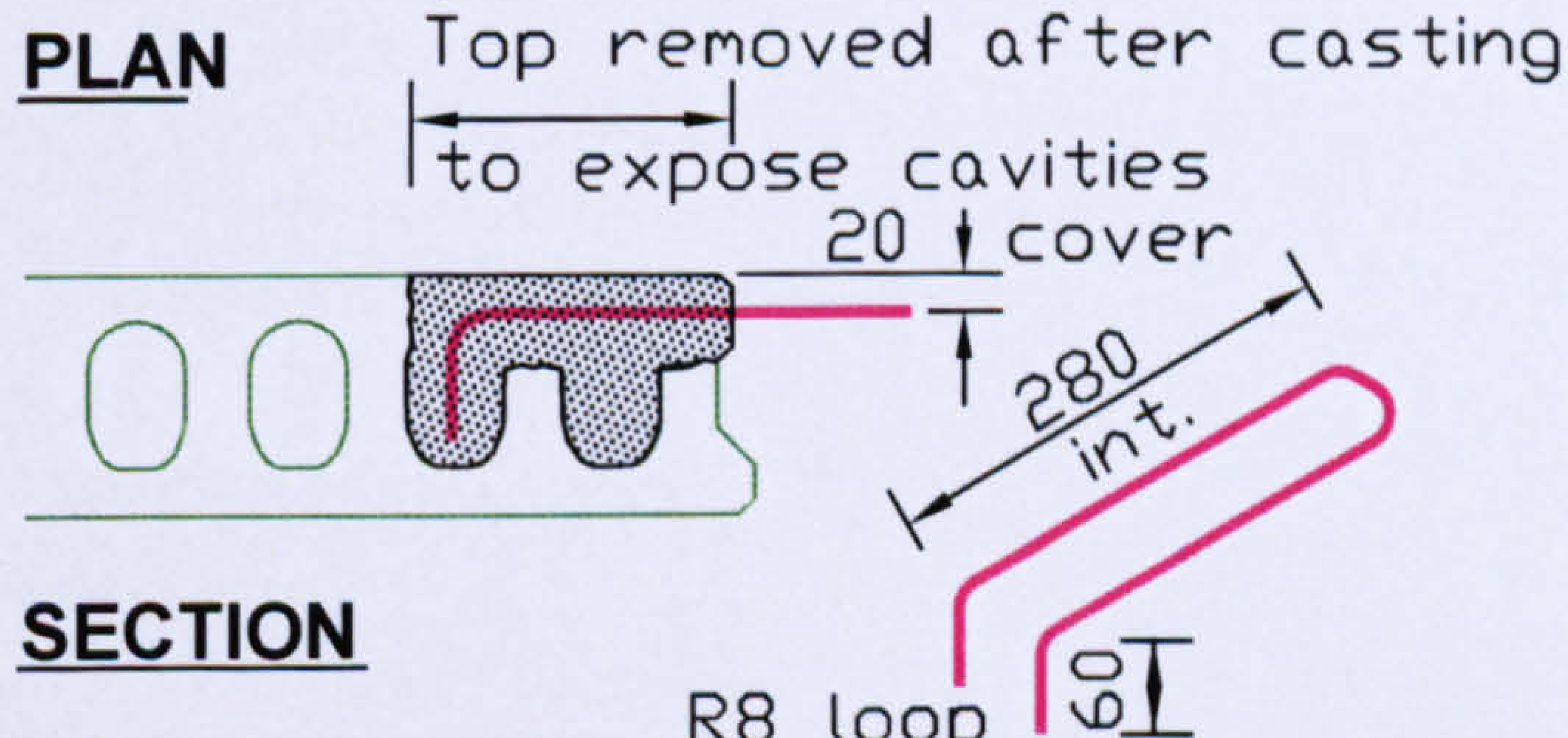

SECTION

SP. (Side pocket)

Closed ends

To be avoided where possible.
If they must be provided, it must be appreciated that the concrete is not compacted.

See T.I. SHEET 321/11 regarding Weep Holes in Tensyland slabs

In wallframe construction the size of the loop bar must be designed to pass round the lifter/leveller at the appropriate centres.
Handling stresses in reduced width slabs over 4m long should be checked and any special instructions issued.

Xref tim

Appendix B

Calculations for Chapter 5 (Analytical Study)

Effective Width Calculations

From Strain measured on Beam

CB-1		y =	320	245	-245	-320
	Load (kN)	Eqn. Of Strain	Strain at TF	Strain at TW	Strain at BW	Strain at BF
	100	-1.77x + 316.9	-3.50	81.24	698.41	791.63
	140	-1.264x + 319.3	-1.11	117.56	982.17	1112.71
	180	-0.958x + 321	2.03	154.31	1264.16	1431.68
	220	-0.756x + 320.9	2.38	200.79	1646.80	1865.05
	240	-0.675x + 321.3	3.85	226.07	1845.72	2090.16
	260	-0.610x + 310.1	-32.46	213.44	2002.00	2272.49
	280	-0.549x + 275.6	-161.75	111.48	2086.19	2386.74
	300	-0.514x + 271.5	-188.72	103.11	2210.70	2531.71
	320	-0.481x + 289.3	-127.65	184.20	2443.78	2786.82
	340	-0.447x + 279.8	-179.87	155.70	2582.91	2952.04
	360	-0.442x + 276.9	-195.02	144.34	2597.69	2971.00
	400	-0.357x + 341.7	121.57	541.74	3615.52	4077.70

Effective Width Calculation

CB-1								F_{TF}	F_{Tw}	F_{BW}	F_{BF}	F_{STEEL}	
	Load (kN)	Mmt (kNm)	Position of NA (mm)	e_1	e_2	e_3	e_4	$e_1.E.A_{TF}$	$e_2.E.A_{TW}$	$e_3.E.A_{BW}$	$e_4.E.A_{BF}$		**B_{eff}**
				Strain at TF	Strain at TW	Strain at BF	Strain at BW						
NA in Con	100	600	635.9	3.50	81.24	698.41	791.63	6462.7	29978.6	257712.1	1460552.0	1754705.5	**272.81**
	140	840	639.0	1.11	117.56	982.17	1112.71	2043.5	43380.9	362419.9	2052942.0	2460786.3	**382.58**
	180	1080	641.2	2.03	154.31	1264.16	1431.68	3746.2	56942.1	466475.9	2641440.6	3168604.9	**492.63**
	220	1320	643.0	2.38	200.79	1646.80	1865.05	4392.9	74092.9	607668.8	3441022.6	4127177.1	**641.66**
	240	1440	643.7	3.85	226.07	1845.72	2090.16	7106.7	83421.3	681070.1	3856350.7	4627948.8	**719.52**
NA in Steel	260	1560	632.5	32.46	213.44	2002.00	2272.49	59886.9	393801.6	680400.0	3402000.0	4536088.5	**705.24**
	280	1680	597.1	161.75	111.48	2086.19	2386.74	298426.2	205672.1	680400.0	3402000.0	4586498.4	**713.07**
	300	1800	592.2	188.72	103.11	2210.70	2531.71	348180.9	190243.2	680400.0	3402000.0	4620824.1	**718.41**
	320	1920	602.7	127.65	184.20	2443.78	2786.82	235515.6	339848.2	680400.0	3402000.0	4657763.8	**724.15**
	340	2040	593.5	179.87	155.70	2582.91	2952.04	331852.3	287275.2	680400.0	3402000.0	4701527.5	**730.96**
	360	2160	591.4	195.02	144.34	2597.69	2971.00	359816.7	266314.5	680400.0	3402000.0	4708531.2	**732.05**
	400	2400		121.57	541.74	3615.52	4077.70	224294.1	999504.2	680400.0	3402000.0	5306198.3	**824.97**

Total Area of Steel =	21600	B =	300	A_{TF} =	9000	D	640
f_{cu} =	48	T =	20	A_{TW} =	1800		
D_s =	200	t =	30	A_{BW} =	1800		
p_y =	378	E =	205	A_{BF} =	9000	L	11700

All dimensions in N - mm unless stated

CB-1

$Span/B_{eff}$		F_c (kN) $0.67f_{cu}B_eD_s$	F_s (kN)	$M_{comp} = F_s\,(D/2 + D_s - F_s/F_c.D_s/2)$ kNm	M_{exp} kNm	M_{comp} / M_{exp}
42.89		1728.52	1754.71	734.32	600	1.22
30.58		2424.06	2460.79	1029.80	840	1.23
23.75		3121.31	3168.60	1326.01	1080	1.23
18.23		4065.58	4127.18	1727.16	1320	1.31
16.26		4558.87	4627.95	1936.73	1440	1.34
16.59		4468.39	4536.09	1898.28	1560	1.22
16.41		4518.04	4586.50	1919.38	1680	1.14
16.29		4551.86	4620.82	1933.74	1800	1.07
16.16		4588.24	4657.76	1949.20	1920	1.02
16.01		4631.36	4701.53	1967.52	2040	0.96
15.98	L/16	4638.25	4708.53	1970.45	2160	0.91
14.18						

Capacity of stud	102
No. Of studs	39

From Strain measured on Beam

CB-2		y =	320	245	-245	-320
	Load (kN)	Eqn. Of Strain	Strain at TF	Strain at TW	Strain at BW	Strain at BF
	100	4.265x + 217.6	48.02	12.85	-238.62	-277.31
	140	3.351x + 185.9	80.04	35.27	-282.89	-332.13
	180	2.584x + 118.3	156.11	98.07	-309.31	-373.17
	200	2.319x + 118.2	174.04	109.36	-344.56	-415.71
	220	2.089x + 119.4	192.05	120.25	-383.76	-462.75
	240	1.888x + 117.9	214.09	134.64	-422.87	-510.26
	260	1.694x + 113.2	218.37	139.18	-416.07	-503.19
	280	1.601x + 124.6	244.10	150.41	-507.88	-610.94
	300	1.421x + 194.6	176.50	70.94	-680.59	-796.71
	320	1.237x + 197.5	198.06	76.80	-786.98	-920.37
	340	1.117x + 214.9	188.18	53.89	-905.80	-1053.52
	360	1.037x + 214.1	204.24	59.59	-973.98	-1133.10

Effective Width Calculation

CB-2

	Load (kN)	Mmt (kNm)	Position of NA (mm)	e_1 Strain at TF	e_2 Strain at TW	e_3 Strain at BF	e_4 Strain at BW	F_{TF} $e_1.E.A_{TF}$	F_{Tw} $e_2.E.A_{TW}$	F_{BW} $e_3.E.A_{BW}$	F_{BF} $e_4.E.A_{BF}$	F_{STEEL}	B_{eff}
NA in Con	100	600	97.2	48.02	12.85	238.62	277.31	88594.6	23706.0	440256.4	511633.9	1064190.8	**515.03**
	140	840	65.9	80.04	35.27	282.89	332.13	147666.1	65078.8	521940.6	612786.7	1347472.2	**499.91**
	180	1080	30.0	156.11	98.07	309.31	373.17	288031.3	180930.0	570679.1	688490.6	1728131.0	**505.75**
	200	1200	24.0	174.04	109.36	344.56	415.71	321104.8	201764.6	635717.5	766991.7	1925578.5	**544.32**
	220	1320	1.0	192.05	120.25	383.76	462.75	354338.9	221859.3	708041.9	853769.6	2138009.7	**534.52**
NA in Steel	240	1440	-7.1	214.09	134.64	422.87	510.26	394994.2	248410.5	780196.6	941438.6	2365039.8	**588.32**
	260	1560	-56.7	218.37	139.18	416.07	503.19	402899.7	256780.4	767652.5	928383.7	2355716.3	**586.00**
	280	1680	-65.3	244.10	150.41	507.88	610.94	450359.8	277499.1	937043.3	1127190.1	2792092.3	**694.55**
	300	1800	-75.1	176.50	70.94	680.59	796.71	325634.1	130876.8	1255690.6	1469923.6	3182125.1	**791.57**
	320	1920	-70.0	198.06	76.80	786.98	920.37	365420.4	141693.6	1451986.7	1698086.1	3657186.7	**909.75**
	340	2040	-73.0	188.18	53.89	905.80	1053.52	347197.0	99435.1	1671203.3	1943741.4	4061576.7	**1010.34**
	360	2160	-74.0	204.24	59.59	973.98	1133.10	376828.4	109952.7	1796998.0	2090561.1	4374340.2	**1088.14**

Total Area of Steel =	21600	B =	300	A_{TF} =	9000	D	640
f_{cu} =	30	T =	20	A_{TW} =	1800		
D_s =	200	t =	30	A_{BW} =	1800		
p_y =	300	E =	205	A_{BF} =	9000	L	11700

All dimensions in N - mm unless stated

CB-2

$Span/B_{eff}$		F_c (kN)	F_s (kN)	$M_{comp} = F_s (D/2 + D_s - F_s/F_c.D_s/2)$	M_{exp}	M_{comp} / M_{exp}
		$0.67f_{cu}B_eD_s$		*kNm*	kNm	
22.72		1390.57	1064.19	471.94	600	0.79
23.40		1349.77	1347.47	566.17	840	0.67
23.13		1365.51	1728.13	679.92	1080	0.63
21.49		1469.66	1925.58	749.01	1200	0.62
21.89		1443.19	2138.01	795.03	1320	0.60
19.89		1588.46	2365.04	877.69	1440	0.61
19.97		1582.20	2355.72	874.23	1560	0.56
16.85		1875.29	2792.09	1036.18	1680	0.62
14.78		2137.25	3182.13	1180.92	1800	0.66
12.86	L/13	2456.32	3657.19	1357.22	1920	0.71
11.58		2727.92	4061.58	1507.30	2040	0.74
10.75		2937.99	4374.34	1623.37	2160	0.75

Capacity of stud	102
No. Of studs	19

From Strain measured on Beam

CB-3	Load (kN)	Eqn. Of Strain	y = 320 Strain at TF	245 Strain at TW	-245 Strain at BW	-320 Strain at BF
	100	-5.225x - 378.3	-400.94	-357.88	-76.54	-33.47
	140	-3.911x - 357.2	-86.06	-28.53	-519.46	-461.93
	180	-1.597x - 420.9	-203.20	-39.84	-855.87	-356.92
	200	-2.734x - 317.8	-79.88	2.41	-699.85	-617.56
	220	-2.497x - 319.9	-89.99	0.12	-768.80	-678.69
	240	-2.172x - 290.4	-62.71	40.88	-843.09	-739.50
	260	-1.929x - 280.7	-55.52	61.12	-934.21	-817.57
	280	-1.699x - 267.9	-40.44	92.00	-1038.08	-905.65
	300	-1.514x - 261.0	-31.70	116.91	-1151.25	-1002.64
	320	-1.409x - 249.4	-9.37	150.32	-1212.35	-1052.66
	340	-1.843x - 337.2	-150.08	-28.00	-1069.78	-947.69

Effective Width Calculation

CB-3

	Load (kN)	Mmt (kNm)	Position of NA (mm)	e_1 Strain at TF	e_2 Strain at TW	e_3 Strain at BF	e_4 Strain at BW	F_{TF} $e_1.E.A_{TF}$	F_{Tw} $e_2.E.A_{TW}$	F_{BW} $e_3.E.A_{BW}$	F_{BF} $e_4.E.A_{BF}$	F_{STEEL}	B_{eff}
NA in Con	100	600	140	400.94	357.88	76.54	33.47	739730.2	132056.1	28241.7	61758.9	961787.0	**797.50**
	140	840	60	86.06	28.53	519.46	461.93	158789.8	52646.9	191680.0	852257.0	1255373.7	**446.12**
	180	1080	70	203.20	39.84	855.87	356.92	374896.6	73513.4	315816.8	658523.6	1422750.4	**544.49**
	200	1200	65	79.88	-2.41	699.85	617.56	147384.1	-4453.9	258246.0	1139392.1	1540568.3	**567.74**
	220	1320	55	89.99	-0.12	768.80	678.69	166027.8	-221.7	283688.1	1252191.2	1701685.5	**583.87**
	240	1440	43	62.71	-40.88	843.09	739.50	115694.8	-75430.9	311101.7	1364382.6	1715748.1	**543.70**
	260	1560	40	55.52	-61.12	934.21	817.57	102436.2	-112765.9	344725.2	1508423.8	1842819.3	**573.02**
	280	1680	45	40.44	-92.00	1038.08	905.65	74603.6	-169731.3	383052.0	1670925.0	1958849.2	**628.74**
	300	1800	22	31.70	-116.91	1151.25	1002.64	58494.1	-215696.8	424813.1	1849874.5	2117484.8	**591.84**
	320	1920	27	9.37	-150.32	1212.35	1052.66	17284.6	-277339.2	447356.8	1942160.4	2129462.6	**612.39**
	340	2040	25	150.08	28.00	1069.78	947.69	276900.2	51656.0	394747.9	1748495.4	2471799.5	**702.71**

Total Area of Steel =	21600	B =	300	A_{TF} =	9000	D	640
f_{cu} =	30	T =	20	A_{TW} =	1800		
D_s =	200	t =	30	A_{BW} =	1800		
p_y =	300	E =	205	A_{BF} =	9000	L	11700

All dimensions in N - mm unless stated

CB-3

Partial

$M_{exp.comp} = Fs.D/2 + F_{con} \times (D_s - F_{con}/F_c \cdot D_s/2) - [(F_s - F_{con})^2 / F_{flange} \times (T/4)]$

$Span/B_{eff}$		F_c (kN) $0.67f_{cu}B_eD_s$	F_s (kN)	F_{con}	F_{flange}				$M_{exp.comp}$	M_{exp} kNm	M_{comp} / M_{exp}
14.67		3205.96	961.79	1530	3618	308	232.98	0.67	540.09	600	0.90
26.23		1793.39	1255.37	1530	3618	402	175.47	0.16	577.03	840	0.69
21.49		2188.85	1422.75	1530	3618	455	199.05	0.02	654.31	1080	0.61
20.61		2282.32	1540.57	1530	3618	493	203.43	0.00	696.42	1200	0.58
20.04		2347.15	1701.69	1530	3618	545	206.27	0.06	750.74	1320	0.57
21.52		2185.67	1715.75	1530	3618	549	198.90	0.07	747.87	1440	0.52
20.42		2303.52	1842.82	1530	3618	590	204.38	0.20	793.88	1560	0.51
18.61	L/19	2527.55	1958.85	1530	3618	627	213.38	0.38	839.84	1680	0.50
19.77		2379.20	2117.48	1530	3618	678	207.61	0.72	884.49	1800	0.49
19.11		2461.81	2129.46	1530	3618	681	210.91	0.74	891.59	1920	0.46
16.65		2824.91	2471.80	1530	3618	791	223.13	1.84	1012.27	2040	0.50

Capacity of stud	102
No. Of studs	15

CB-4 **Effective Width Calculation**

	Load (kN)	Mmt (kNm)	Position of NA (mm)	e_1 Strain at TF	e_2 Strain at W	e_3 Strain at BF	F_{TF} $e_1.E.A_{TF}$	F_W $e_3.E.A_{BW}$	F_{BF} $e_4.E.A_{BF}$	F_{STEEL}	B_{eff}
NA in Steel	100	300	-15	1022.39	912.58	195.17	796442.9	804441.7	152034.7	1752919.3	**436.05**
	120	360	-20	219.47	72.76	1324.62	170963.7	64141.5	1031877.2	1266982.4	**315.17**
	140	420	-18	518.15	101.60	2182.47	403638.7	89563.9	1700147.3	2193349.8	**545.61**
	160	480	-10	203.70	-6.16	1784.63	158683.5	-5426.4	1390224.4	1543481.5	**383.95**
	180	540	40	229.47	-0.31	1960.45	178756.6	-270.1	1527187.9	1705674.4	**530.37**
	200	600	60	159.90	-104.25	2149.89	124564.7	-91900.0	1674763.9	1707428.6	**606.76**
	220	660	100	141.58	-155.86	2382.25	110289.7	-137386.5	1855770.6	1828673.8	**909.79**
	240	720	150	103.11	-234.59	2647.11	80323.2	-206789.3	2062096.4	1935630.3	**1926.00**
	250	750	170	80.85	-298.12	2935.70	62978.6	-262790.6	2286910.4	2087098.4	**3461.19**
	265	795	172	23.89	-383.31	3091.49	18609.8	-337891.7	2408271.0	2088989.1	**3711.78**
	295	885	145	382.71	71.39	2727.93	298129.2	62934.2	2125059.6	2486123.0	**2262.03**

Total Area of Steel =	11286	B =	190	A_{TF} =	3800	D	470
f_{cu} =	30	T =	10	A_W =	4300		
D_s =	200	t =	20				
p_y =	300	E =	205	A_{BF} =	3800	L	9000

All dimensions in N - mm unless stated

CB-4

Partial

$$M_{comp} = F_{con}.D/2 + F_{con} \times (D_s - F_{con}/F_c . D_s/2) - [(F_s - F_{con})^2 / F_{flange} \times (T/4)]$$

Span/B_{eff}		F_c (kN)	F_s (kN)	F_{con}	F_{flange}				$M_{exp.comp}$	M_{exp}	M_{comp} / M_{exp}
		$0.67f_{cu}B_eD_s$								kNm	
20.64		1752.92	1752.92	1122	1368	264	152.58	1.45	414.80	300	1.38
28.56		1266.98	1266.98	1122	1368	264	125.04	0.08	388.63	360	1.08
16.50		2193.35	2193.35	1122	1368	264	167.00	4.20	426.48	420	1.02
23.44		1543.48	1543.48	1122	1368	264	142.84	0.65	405.86	480	0.85
16.97		2132.09	1705.67	1122	1368	264	165.36	1.25	427.78	540	0.79
14.83		2439.18	1707.43	1122	1368	264	172.79	1.25	435.21	600	0.73
9.89	L/10	3657.35	1828.67	1122	1368	264	189.98	1.83	451.82	660	0.68
4.67		7742.52	1935.63	1122	1368	264	208.14	2.42	469.39	720	0.65
2.60		13913.99	2087.10	1122	1368	264	215.35	3.40	475.62	750	0.63
2.42		14921.35	2088.99	1122	1368	264	215.96	3.42	476.22	795	0.60
3.98		9093.35	2486.12	1122	1368	264	210.56	6.80	467.42	885	0.53

Capacity of stud	102
No. Of studs	11

From Strain measured on Beam

CB-5		y =	320	245	-245	-320
	Load (kN)	Eqn. Of Strain	Strain at TF	Strain at TW	Strain at BW	Strain at BF
	100	y = 13.712x - 23.144	90.09	70.40	-58.25	-77.94
	133	y = 8.104x + 1.919	139.03	106.64	-104.98	-137.37
	200	y = 5.7827x - 41.565	218.83	173.44	-123.12	-168.52
	233	y = 4.9069x - 50.609	287.01	228.93	-150.54	-208.62
	266	y = 3.471x - 141.42	531.74	445.31	-119.37	-205.80
	300	y = 2.8571x - 172.86	603.76	511.89	-88.37	-180.25
	333	y = 2.379x - 232.21	905.26	782.31	-20.97	-143.92
	366	**y = 2.2248x - 229.34**	**1111.02**	**959.34**	**-31.67**	**-366.71**
	400	y = 1.262x - 148.75	1485.74	936.01	-305.07	-2171.16

Effective Width Calculation

CB-5

	Load (kN)	Mmt (kNm)	Position of NA (mm)	e_1 Strain at TF	e_2 Strain at TW	e_3 Strain at BW	e_4 Strain at BF	F_{TF} $e_1.E.A_{TF}$	F_{Tw} $e_2.E.A_{TW}$	F_{BW} $e_3.E.A_{BW}$	F_{BF} $e_4.E.A_{BF}$	F_{STEEL}	B_{eff}
NA in Con	100	600	30	90.09	70.40	58.25	77.94	166216.6	25977.4	21493.1	143795.0	357482.2	**48.07**
	133	798	28	139.03	106.64	104.98	137.37	256514.3	196752.2	38738.8	253456.1	745461.3	**99.70**
	200	1200	50	218.83	173.44	123.12	505.55	403736.1	319988.5	45432.5	932730.8	1701887.9	**241.92**
	233	1398	55	287.01	228.93	150.54	834.49	529527.7	422367.4	55549.3	1539628.1	2547072.6	**367.30**
	266	1596	140	531.74	445.31	119.37	823.19	981065.9	821601.7	44046.1	1518778.9	3365492.6	**643.99**
	300	1800	170	603.76	511.89	88.37	721.00	1113941.9	944430.0	32609.6	1330239.1	3421220.6	**740.04**
	333	1998	230	905.26	782.31	20.97	863.51	1670208.9	1443364.7	7736.9	1593172.6	4714483.1	**1379.71**
	366	2196	230	1111.02	959.34	278.45	1320.21	2049840.6	1769981.1	11686.9	676588.4	4508097.0	**1319.31**
	400	2400	55	1485.74	936.01	305.07	2171.16	2741184.6	1726946.3	112571.3	4005784.5	8586486.7	**1238.23**

Total Area of Steel =	21600	B =	300	A_{TF} =	9000	D	640
f_{cu} =	30	T =	20	A_{TW} =	1800		
D_s =	400	t =	30	A_{BW} =	1800		
p_y =	300	E =	205	A_{BF} =	9000	L	11700

All dimensions in N - mm unless stated

CB-5

Partial

$M_{comp} = F_{con}.D/2 + F_{con} \times (D_s - F_{con}/F_c . D_s/2) - [(F_s - F_{con})^2 / F_{flange} \times (T/4)]$

Span/B_{eff}		F_c (kN) $0.67f_{cu}B_eD_s$	F_s (kN)	F_{con}	F_{flange}				$M_{exp. comp}$	M_{exp} kNm	M_{comp} / M_{exp}
243.40		386.47	357.48	1400	3519	448	454.32	2.32	900.00	600	1.50
117.35		801.57	745.46	1400	3519	448	-70.96	0.91	376.13	798	0.47
48.36		1945.01	1701.89	1400	3519	448	-358.46	0.19	89.35	1200	0.07
31.85		2953.13	2547.07	1400	3519	448	427.26	2.80	872.46	1398	0.62
18.17		5177.68	3365.49	1400	3519	448	484.29	8.23	924.06	1596	0.58
15.81		5949.95	3421.22	1400	3519	448	494.12	8.71	933.41	1800	0.52
8.48		11092.90	4714.48	1400	3519	448	524.66	23.41	949.25	1998	0.48
8.87	L/9	10607.29	4508.10	1400	3519	448	523.04	20.59	950.46	2196	0.43
9.45		9955.35	8586.49	1400	3519	448	520.62	110.07	858.55	2400	0.36

Capacity of stud	102
No. Of studs	14

Moment Analysis

CB-1

	Load (kN)	Mmt (kNm)	Position of NA (mm)	e_1 Strain at TF	e_2 Strain at TW	e_3 Strain at BF	e_4 Strain at BW	F_{tf}	F_{tw}	F_{bw}	F_{bf}
NA in Con	100	600	635.9	3.50	81.24	698.41	791.63	6463	150	1289	1461
	140	840	639.0	1.11	117.56	982.17	1112.71	2044	43	362	2053
	180	1080	641.2	2.03	154.31	1264.16	1431.68	3746	57	466	2641
	220	1320	643.0	2.38	200.79	1646.80	1865.05	4393	74	608	3441
	240	1440	643.7	3.85	226.07	1845.72	2090.16	7107	83	681	3856
NA in Steel	260	1560	632.5	32.46	213.44	2002.00	2272.49	59887	79	739	4193
	280	1680	597.1	161.75	111.48	2086.19	2386.74	298426	41	770	4404
	300	1800	592.2	188.72	103.11	2210.70	2531.71	348181	38	816	4671
	320	1920	602.7	127.65	184.20	2443.78	2786.82	235516	68	902	5142
	340	2040	593.5	179.87	155.70	2582.91	2952.04	331852	57	953	5447
	360	2160	591.4	195.02	144.34	2597.69	2971.00	359817	53	959	5481
	400	2400		121.57	541.74	3615.52	4077.70				

Total Area of Steel =	21600	B =	300	A_{TF} =	9000
f_{cu} =	48	T =	20	A_{TW} =	1800
D_s =	200	t =	30	A_{BW} =	1800
p_y =	378	E =	205	A_{BF} =	9000

CB-1

625	565	75	15		M_{steel}			Moments in Steel Compression	Moments in Steel Tension	F_c (kN)	d_c	$M_{concrete}$	M_{comp}	M_{exp}	M_{comp}/M_{exp}
d_{tf}	d_{tw}	d_{bw}	d_{bf}	M_{tf}	M_{tw}	M_{bw}	M_{bf}			$0.67f_{cu}B_ed$					
10.9	70.9	560.9	620.9	70	11	723	113		917	1754.71	100	175.47	1093	600	1.82
14.0	74.0	564.0	624.0	29	3	204	160		396	2460.79	99.5	244.85	641	840	0.76
16.2	76.2	566.2	626.2	61	4	264	207		536	3168.60	99.1	314.01	850	1080	0.79
18.0	78.0	568.0	628.0	79	6	345	270		700	4127.18	98.5	406.53	1107	1320	0.84
18.7	78.7	568.7	628.7	133	7	387	303		830	4627.95	98.15	454.23	1284	1440	0.89
7.5	67.5	557.5	617.5	449	5	412	324		1190	4536.09	96.75	438.87	1629	1560	1.04
27.9	32.1	522.1	582.1	833	1	402	2563	833	2967	4586.50	78.55	360.27	1774	1680	1.06
32.8	27.2	517.2	577.2	1142	1	422	2696	1142	3119	4620.82	76	351.18	1626	1800	0.90
22.3	37.7	527.7	587.7	525	3	476	3022	525	3500	4657.76	81	377.28	2598	1920	1.35
31.5	28.5	518.5	578.5	1045	2	494	3151	1045	3647	4701.53	76.5	359.67	2242	2040	1.10
33.6	26.4	516.4	576.4	1209	1	495	3160	1209	3656	4708.53	75.7	356.44	2091	2160	0.97

CB-2

	Load (kN)	Mmt (kNm)	Position of NA (mm)	e1	e2	e3	e4	F_{tf}	F_{tw}	F_{bw}	F_{bf}
				Strain at TF	Strain at TW	Strain at BF	Strain at BW				
NA in Con	100	600	97.2	48.02	12.85	238.62	277.31	8859	5	88	512
	140	840	65.9	80.04	35.27	282.89	332.13	14767	13	104	613
	180	1080	30.0	156.11	98.07	309.31	373.17	28803	36	114	688
	200	1200	24.0	174.04	109.36	344.56	415.71	32110	40	127	767
	220	1320	1.0	192.05	120.25	383.76	462.75	35434	44	142	854
NA in Steel	240	1440	-7.1	214.09	134.64	422.87	510.26	39499	50	156	941
	260	1560	-56.7	218.37	139.18	416.07	503.19	40290	51	154	928
	280	1680	-65.3	244.10	150.41	507.88	610.94	45036	55	187	1127
	300	1800	-75.1	176.50	70.94	680.59	796.71	32563	26	251	1470
	320	1920	-70.0	198.06	76.80	786.98	920.37	36542	28	290	1698
	340	2040	-73.0	188.18	53 89	905.80	1053.52	34720	20	334	1944
	360	2160	-74.0	204.24	59.59	973.98	1133.10	37683	22	359	2091

CB-2

625	565	75	15		M steel			Moments in Steel		Fc (kN)	d_c	$M_{concrete}$	M_{comp}	M_{exp}	M_{comp}/M_{exp}
d_{tf}	d_{tw}	d_{bw}	d_{bf}	M_{tf}	M_{tw}	M_{bw}	M_{bf}	Compression	Tension	$0.67f_{cu}B_ed$					
112.2	157.2	662.2	722.2	994	1	58	46		1099	1390.57	51.4	71.48	1171	600	1.95
80.9	125.9	630.9	690.9	1195	2	66	53		1315	1349.77	67.05	90.50	1406	840	1.67
45.0	90.0	595.0	655.0	1296	3	68	56		1424	1365.51	85	116.07	1540	1080	1.43
39.0	84.0	589.0	649.0	1252	3	75	62		1393	1469 66	88	129.33	1522	1320	1.15
16.0	61.0	566.0	626.0	567	3	80	67		717	1443.19	99.5	143.60	860	1440	0.60
7.9	67.9	557.9	617.9	312	3	87	73		475	1588.46	103.55	164.48	640	1560	0.41
41.7	18.3	508.3	568.3	168	1	78	528	168	607	1582.20	128.35	203.08	810	1680	0.48
50.3	9.7	499.7	559.7	227	1	94	631	227	725	1875.29	132.65	248.76	974	1800	0.54
60.1	0.0	489.9	549.9	196	0	123	808	196	931	2137.25	137.55	293.98	1225	1920	0.64
55.0	5.0	495.0	555.0	201	0	144	942	201	1086	2456.32	135	331.60	1418	2040	0.70
58.0	2.0	492.0	552.0	201	0	164	1073	201	1237	2727.92	136.5	372.36	1610	2160	0.75
59.0	1.0	491.0	551.0	222	0	176	1152	222	1328	2937.99	137	402.50	1731	2161	0.80

CB-3

	Load (kN)	Mmt (kNm)	Position of NA (mm)	e_1 Strain at TF	e_2 Strain at TW	e_3 Strain at BF	e_4 Strain at BW	F_{TF} $e_1.E.A_{TF}$	F_{Tw} $e_2.E.A_{TW}$	F_{BW} $e_3.E.A_{BW}$	F_{BF} $e_4.E.A_{BF}$	F_{STEEL}
NA in Con	100	600	140	400.94	357.88	76.54	33.47	739730.24	132056.10	28241.74	61758.95	961787.02
	140	840	60	86.06	28.53	519.46	461.93	158789.82	52646.89	191679.98	852256.97	1255373 66
	180	1080	70	203.20	39.84	855.87	356.92	374896.61	73513.43	315816.83	658523.58	1422750.45
	200	1200	65	79.88	-2.41	699.85	617.56	147384.05	4453.91	258246.01	1139392.10	1540568.25
	220	1320	55	89.99	-0.12	768.80	678.69	166027.83	221.67	283688.15	1252191.23	1701685.54
	240	1440	43	62.71	-40.88	843.09	739.50	115694.75	75430.94	311101.66	1364382.60	1715748.07
	260	1560	40	55.52	-61.12	934.21	817.57	102436.24	112765.94	344725.19	1508423.79	1842819.28
	280	1680	45	40.44	-92.00	1038.08	905.65	74603.59	169731.31	383051.97	1670924.96	1958849.21
	300	1800	22	31.70	-116.91	1151.25	1002.64	58494.06	215696.83	424813.08	1849874.50	2117484.81
	320	1920	27	9.37	-150.32	1212.35	1052.66	17284.60	277339.25	447356.85	1942160.40	2129462.60
	340	2040	25	150.08	28.00	1069.78	947.69	276900.16	51656.00	394747.91	1748495.39	2471799.46

CB-3

625	565	75	15		M steel			Moments							
d_{tf}	d_{tw}	d_{bw}	d_{bf}	M_{tf}	M_{tw}	M_{bw}	M_{bf}	Compression	Tension	F_c (kN) Exp	d_c	$M_{concrete}$	M_c	M_{exp}	M_{comp}/M_{exp}
														kNm	
155	215	705	765	115	28	20	47		210	3205.96	30	96.18	306	600	0.51
75	135	625	685	12	7	120	584		723	1793.39	70	125.54	848	840	1.01
85	145	635	695	32	11	201	458		701	2188.85	65	142.28	843	1080	0.78
80	140	630	690	12	1	163	786		961	2282.32	67.5	154.06	1115	1200	0.93
70	130	620	680	12	0	176	851		1039	2347.15	72.5	170.17	1209	1320	0.92
58	118	608	668	7	9	189	911		1116	2185.67	78.5	171.57	1288	1440	0.89
55	115	605	665	6	13	209	1003		1230	2303.52	80	184.28	1415	1560	0.91
60	120	610	670	4	20	234	1120		1378	2527.55	77.5	195.88	1574	1680	0.94
37	97	587	647	2	21	249	1197		1469	2379.20	89	211.75	1681	1800	0.93
42	102	592	652	1	28	265	1266		1560	2461.81	86.5	212.95	1773	1920	0.92
40	100	590	650	11	5	233	1137		1386	2824.91	87.5	247.18	1633	2040	0.80

CB-4

	Load (kN)	Mmt (kNm)	Position of NA (mm)	e1	e2	e3	F_{TF}	F_W	F_{BF}	F_{STEEL}
							$e_1.E.A_{TF}$	e3.E.ABW	e4.E.ABF	
				Strain at TF	Strain at W	Strain at BF				
NA in Steel	100	300	-14.663	1022.391388	912.58278	195.16651	796442.89	804441.72	152034.709	1752919.32
	120	360	-20	219.4656098	72.763999	1324.6177	170963.71	64141.465	1031877.22	1266982.4
	140	420	-18	518.1497882	101.60392	2182.474	403638.69	89563.858	1700147.25	2193349.8
	160	480	-10	203.7015362	-6.1558157	1784.6269	158683.5	5426.3515	1390224.37	1543481.52
	180	540	40	229.4693632	-0.3063676	1960.4465	178756.63	270.06308	1527187.85	1705674.42
	200	600	60	159.9033149	-104.25414	2149.8895	124564.68	91900.028	1674763.92	1707428.58
	220	660	100	141.5785381	-155.85537	2382.2473	110289 68	137386.5	1855770.63	1828673.81
	240	720	150	103.1106533	-234.58799	2647.1071	80323.199	206789.32	2062096.45	1935630.33
	250	750	170	80.84544254	-298.11757	2935.7001	62978.6	262790.64	2286910.4	2087098.37
	265	795	172	23.88928318	-383.31441	3091.4904	18609.752	337891.65	2408271.04	2088989.14
	295	885	145.3	382.7075421	71.394466	2727.9327	298129.18	62934.221	2125059.59	2486122.98

CB-4

460	235	10		M steel		Moments							
d_{tf}	d_{bw}	d_{bf}	M_{tf}	M_w	M_{bf}	Compression	Tension	F_c (kN) Exp	d_c	$M_{concrete}$	M_c	M_{exp} kNm	M_{comp}/M_{exp}
4.6	220.3	445.3	3.66	88.83	21.41	3.66	110.25	1752.92	114.663	200.99	311.24	300	1.04
10	215	440.0	1.71	6.91	143.58	1.71	150.49	1266.98	120	152.04	302.53	360	0.84
8	217	442.0	3.23	9.74	237.63	3.23	247.37	2193.35	118	258.82	506.19	420	1.21
0	225	450.0	0.00	0.61	197.83	0.00	198.44	1543.48	110	169.78	368.23	480	0.77
50	275	500.0	8.94	0.04	241.47		250.44	2132.09	60	127.93	378.37	540	0.70
70	295	520.0	8.72	13.59	275.40		297.70	2439.18	40	97.57	395.27	600	0.66
105	330	555.0	11.58	22.72	325.70		360.00	3657.35	5	18.29	378.29	660	0.57
160	385	610.0	12.85	39.90	397.78		450.53	7742.52	50	387.13	837.66	720	1.16
180	405	630.0	11.34	53.34	455.61		520.28	13913.99	70	973.98	1494.26	750	1.99
182	407	632.0	3.39	68.92	481.31		553.62	14921.35	72	1074.34	1627.96	795	2.05
155.3	380.3	605.3	46.30	12.00	406.76		465.06	9093.35	45.3	411.93	876.99	885	0.99

CB-5

	Load (kN)	Mmt (kNm)	Position of NA (mm)	e_1 Strain at TF	e_2 Strain at TW	e_3 Strain at BW	e_4 Strain at BF	F_{TF} $e_1.E.A_{TF}$	F_{Tw} $e_2.E.A_{TW}$	F_{BW} $e_3.E.A_{BW}$	F_{BF} $e_4.E.A_{BF}$	F_{STEEL}
NA in Con	100	600	30	90.09	70.40	58.25	77.94	166216.6	25977.4	21493.1	143795.0	357482.2
	133	798	28	139.03	106.64	104.98	137.37	256514.3	196752.2	38738.8	253456.1	745461.3
	200	1200	50	218.83	173.44	123.12	505.55	403736.1	319988.5	45432.5	932730.8	1701887.9
	233	1398	55	287.01	228.93	150.54	834.49	529527.7	422367.4	55549.3	1539628.1	2547072.6
	266	1596	140	531.74	445.31	119.37	823.19	981065.9	821601.7	44046.1	1518778.9	3365492.6
	300	1800	170	603.76	511.89	88.37	721.00	1113941.9	944430.0	32609.6	1330239.1	3421220.6
	333	1998	230	905.26	782.31	20.97	863.51	1670208.9	1443364.7	7736.9	1593172.6	4714483.1
	366	2196	230	1111.02	959.34	278.45	1320.21	2049840.6	1769981.1	11686.9	676588.4	4508097.0
	400	2400	55	1485.74	936.01	305.07	2171.16	2741184.6	1726946.3	112571.3	4005784.5	8586486.7

CB-5

625	565	75	15	M steel				Moments							
d_{tf}	d_{tw}	d_{bw}	d_{bf}	M_{tf}	M_{tw}	M_{bw}	M_{bf}	Compression	Tension	F_c (kN) Exp	d_c	$M_{concrete}$	M_c	M_{exp}	M_{comp}/M_{exp}
45	105	595	655	7	3	13	94		117	386.47	135	52.17	169	600	0.28
43	103	593	653	11	20	23	166		220	801.57	136	109.01	329	798	0.41
65	125	615	675	26	40	28	630		724	1945.01	125	243.13	967	1200	0.81
70	130	620	680	37	55	34	1047		1173	2953.13	122.5	361.76	1535	1398	1.10
155	215	705	765	152	177	31	1162		1522	5177.68	80	414.21	1936	1596	1.21
185	245	735	795	206	231	24	1058		1519	5949.95	65	386.75	1906	1800	1.06
245	305	795	855	409	440	6	1362		2218	11092.90	35	388.25	2606	1998	1.30
245	305	795	855	502	540	9	578		1630	10607.29	35	371.26	2001	2196	0.91
70	130	620	680	192	225	70	2724		3210	9955.35	122.5	1219.53	4430	2400	1.85

Appendix C

Publication related to PhD Research

Murad A and Lam D (2005) *'Experimental Study of Long Span Composite Beams with Precast Hollow-Core Slabs'.* Eurosteel 2005 - Fourth European Conference on Steel and Composite Structures, Masstrcht, June 8 - 10, 2005.

EXPERIMENTAL STUDY OF LONG SPAN COMPOSITE BEAMS WITH PRECAST HOLLOW-CORE SLABS

A Murad
Research Student
School of Civil Engineering,
University of Leeds
cenamu@leeds.ac.uk

Dr D Lam
Senior Lecturer
School of Civil Engineering,
University of Leeds
d.lam@leeds.ac.uk

ABSTRACT

Experiments of long span composite beams are presented in this paper. The composite beam consists of I-section steel beams with circular web openings and precast concrete hollow-core slabs. The beam test specimen is setup as simply supported, to investigate the behaviour of the composite construction. The evaluation of test results will cover the behaviour of the specimen observed during the tests, and also the performance and behaviour of all composite components (precast hollow-core slab, transverse reinforcing bars, shear stud connector and the steel beam with web openings). In addition to a comparison and appraisal of the test results, the various parameters that influence the behaviour and modes of failure of the composite beams are discussed.

1. INTRODUCTION

The use of long span composite beams in multi-storey buildings is common nowadays. By using long span steel beams with precast hollow-core slabs, fewer columns are needed in a building therefore allowing for column free space. Web openings in the steel beams are useful for passing utilities (sprinkler pipes and air-conditioning ducts etc.) through, and also the reduction in building height can provide major cost savings. These savings include; saving on cladding costs, fewer columns leading to faster speed of erection and reduction in number of columns and their foundations.

The conventional steel beams with web openings are known as cellular or castellated beams, they are manufactured by using a solid steel beam and burning along the web to form openings in the web. While Fabsec beams are fabricated differently to cellular beams, they are fabricated by automatic welding of profiled steel plates used to form the flanges and web of the section, i.e. the web of the beam has the openings cut into it, and then the flanges are welded to the web to form the I-section beam. In the majority of these structures, the concrete slab is designed to act non-compositely with the steel. During the past decade the design techniques for openings in composite beams with metal decks flooring have reached a level of maturity. [1]

Precast concrete hollow-core slabs may be designed to act compositely with steel beams. The slabs are produced with regular circular or elongated cores. The use of precast concrete hollow-core slabs in composite construction uses the same principle as metal decks flooring, but without the need of pouring the concrete floor. The slabs are cast in the factory, and can be placed directly on site. The only in-situ concrete needed is to cast the joint between the steel beam, precast slab and transverse reinforcement. (Figure 1)

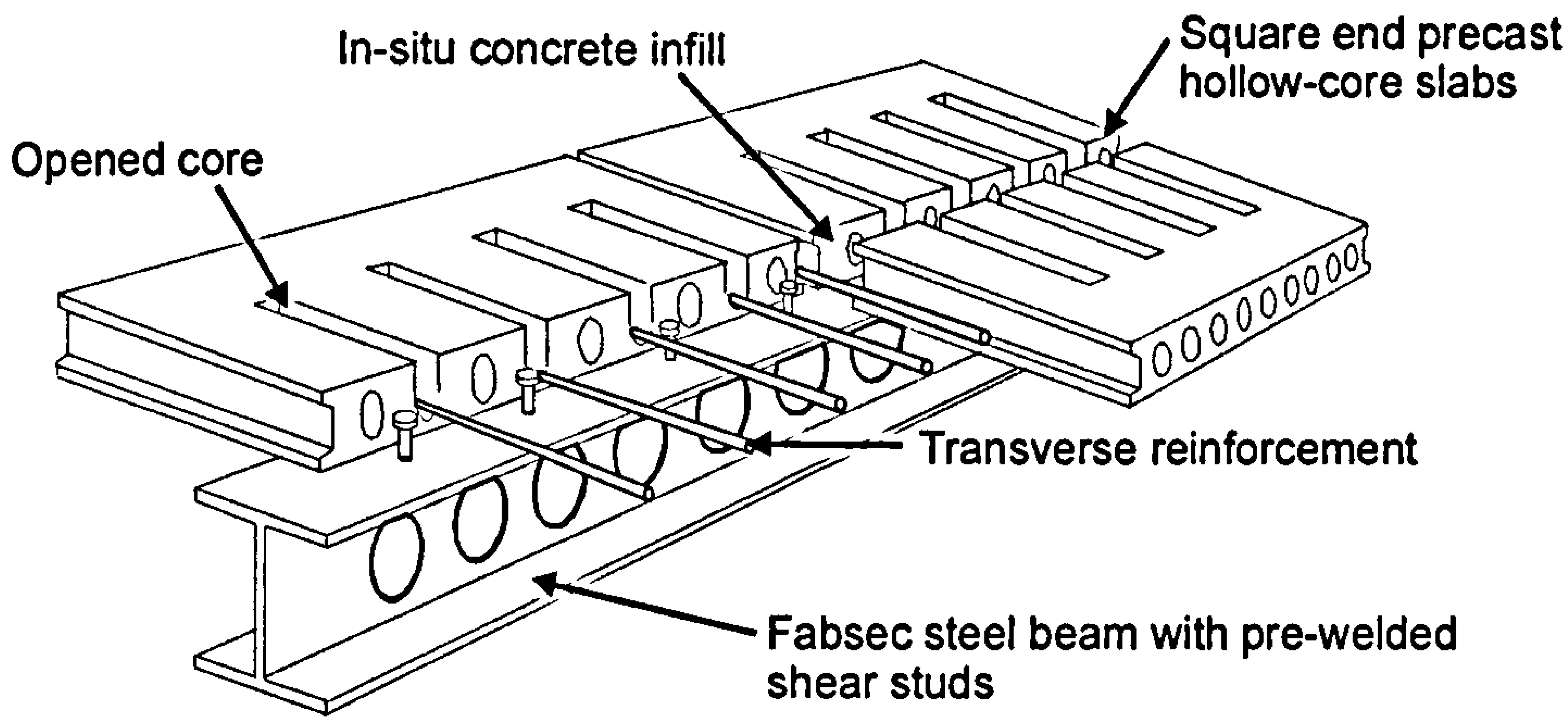

Figure 1: Composite Beam with Precast Hollow-Core Slabs

Composite steel beams with precast concrete hollow-core slabs, as shown in Figure 1 are commonly used in long span multi-storey steel framed buildings. The slabs are placed on the top flanges of universal beams (UBs). The main advantages of this form of construction are that precast concrete slabs can span up to 15m without propping and the erection of 1.2m wide precast concrete units is simple and quick. Shear studs are pre welded onto beams before delivery to site, thereby offering the savings associated with shorter construction time. [2]

The hollow-core slabs have longitudinal voids for the placement of transverse reinforcement bars. The slabs depth ranges from 150 to 400mm, with the performance limited to a maximum span/depth ratio of around 50, although 35 is more usual for office loading conditions. The horizontal compressive forces are transferred through the slab and joint between the units being filled with in-situ concrete (Figure 1). The compressive strength of the infill may vary from 20-40N/mm^2, although 30N/mm^2 is normally used in design. [2]

Experimental tests [3], together with a parametric study conducted by Lam et al. found that an increase in transverse reinforcement significantly increases the moment capacity but, as ductility is reduced, a brittle failure of the composite beam is found due to crushing failure of the concrete slab. In addition, increases in slab thickness lead to increases in moment capacity, though slab failure might occur due to direct tensile force in the slab. [4]

The advantages of long span composite beams are the increased moment capacity and stiffness with shallower floor depths. Research conducted show that the use of hollow-core slabs with steel beams is as competent as metal decking used with steel beams for multi-storey buildings. The concept of using steel beams with web openings and precast hollow-core slabs have potential benefits in the design of multi-storey buildings.

This paper presents the experimental results obtained from tests done on two 12m full scale composite beam specimens. Fabsec steel beams are used with Bison precast concrete slabs. The only difference in the beam specimens is the shear connection (shear studs on the steel beam), where Beam 1 (CB-1) has shear studs at 150mm spacing and at 300mm spacing for Beam 2 (CB-2).

2. SPECIMEN AND TEST SETUP

The beam designs are based on a multi-storey composite frame building, which are commonly constructed in the UK. Office loading was assumed according to the British Standard BS5950, with live load taken as 5.0kN/m^2 and the superimposed dead load taken as 1.5kN/m^2. The design of the steel beams with web openings was based on SCI Publication [5]. The SCI design guide gave the size of beam as 610x305x238 with 400mm web openings for a castellated steel beam. Using the beam size from the castellated beam design, the steel beams were specified for fabrication by Fabsec Ltd. The equivalent steel beams fabricated were 640x300 Fabsec steel beams with 20mm web and 30mm flange thickness, with varying shear connection consisting of a single row of 19mm diameter headed shear studs pre-welded to the top flange of the steel beam. The precast hollow-core concrete slabs were 200mm in depth and are used for both test specimens.

2.1 TEST ARRANGEMENT

The test arrangement of the composite beam comprised of a 12m 640x300 Fabsec beam with 400mm diameter web openings together with twenty 200mm deep x 1200mm wide precast slabs. The slabs are connected through 125x19mm shear studs placed along the full length of the beams. The beam is loaded at four symmetrical points over an 11.7m simply supported span, as shown in Figure 2. The only differences between the specimens are the shear connection and in-situ concrete strength.

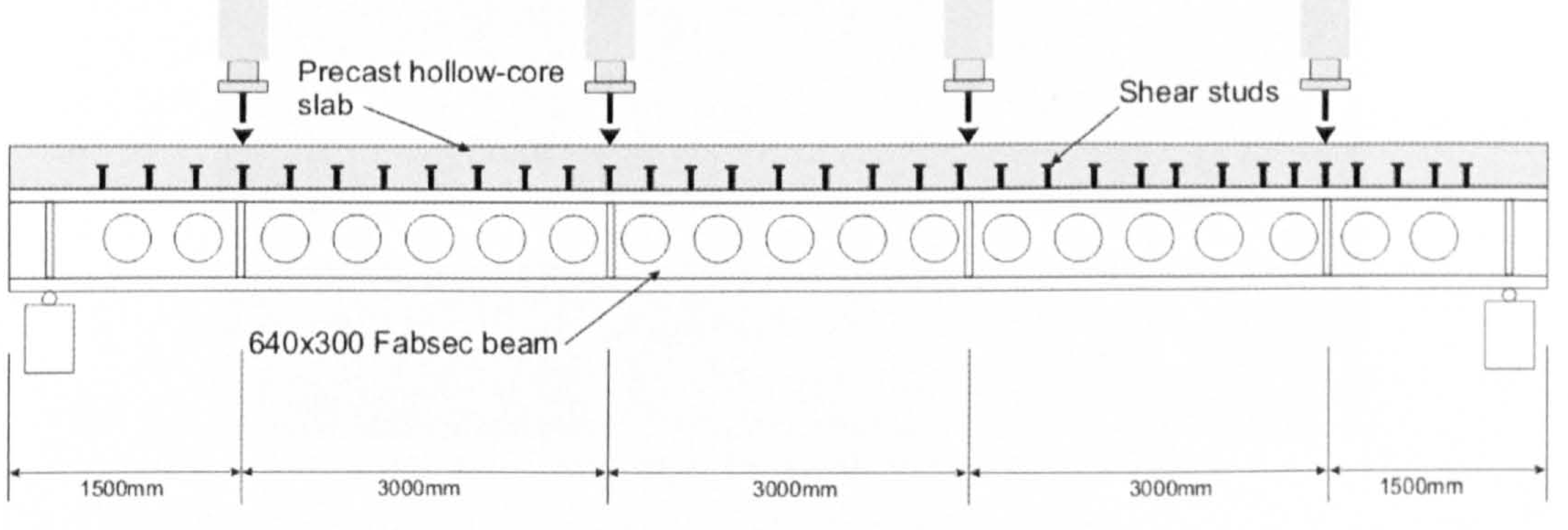

Figure 2: Composite beam specimen test arrangement

The precast hollow-core slabs are placed on to the top flange of the steel beam, ten slabs on either side of the beam. The slabs are 1600mm wide and 1200mm long. In addition, a total of forty nine 16mm diameter (T16) by 1100mm long transverse reinforcement bars are placed across the 600mm slots in the slabs. The 80mm gap between the slabs and the slots for the transverse bars are filled with in-situ concrete. The in-situ concrete had a slump of 80mm (workability), so the concrete could flow into the gaps between the steel beam and slab to form the composite connection as shown in Figure 3 and 4.

Figure 3: Composite beam specimen before casting

Figure 4: Composite beam specimen after casting

The main components of the test rig consist of four 500kN hydraulic loading jacks. A single electrical pump was used for all the jacks, so loading was applied simultaneously to the composite beam. To improve distribution of load, a 300x300mm square steel plate was placed between the hydraulic jacks and precast concrete surface. The details of the test specimens are shown in Table 1.

Beam Specimen	In-situ concrete cube strength (N/mm^2)	Stud spacing (mm)	Beam Span (m)	Slab depth (mm)
CB1	48	150	12	200
CB2	30	300	12	200

Table 1: Composite beam specimen tests

2.2 INSTRUMENTATION

Electrical resistance strain gauges were used to measure strain; on shear studs, the top and bottom of the beam flange, around the centre opening of the beam (Figure 5), and at the centre of transverse reinforcing bars. Linear voltage displacement transducers (LVDTs) were used to measure the slip between the concrete slab and steel beam, as well as bending deflection. A total of thirteen LVDT's were used on each test, with eight LVDT's placed at the interface of the steel/concrete and five LVDT's placed at the top of the bottom flange of the steel beam to measure the vertical deflection. Load is applied simultaneously until the mode of failure was reached. All the data from the instrumentation are recorded into the data logger.

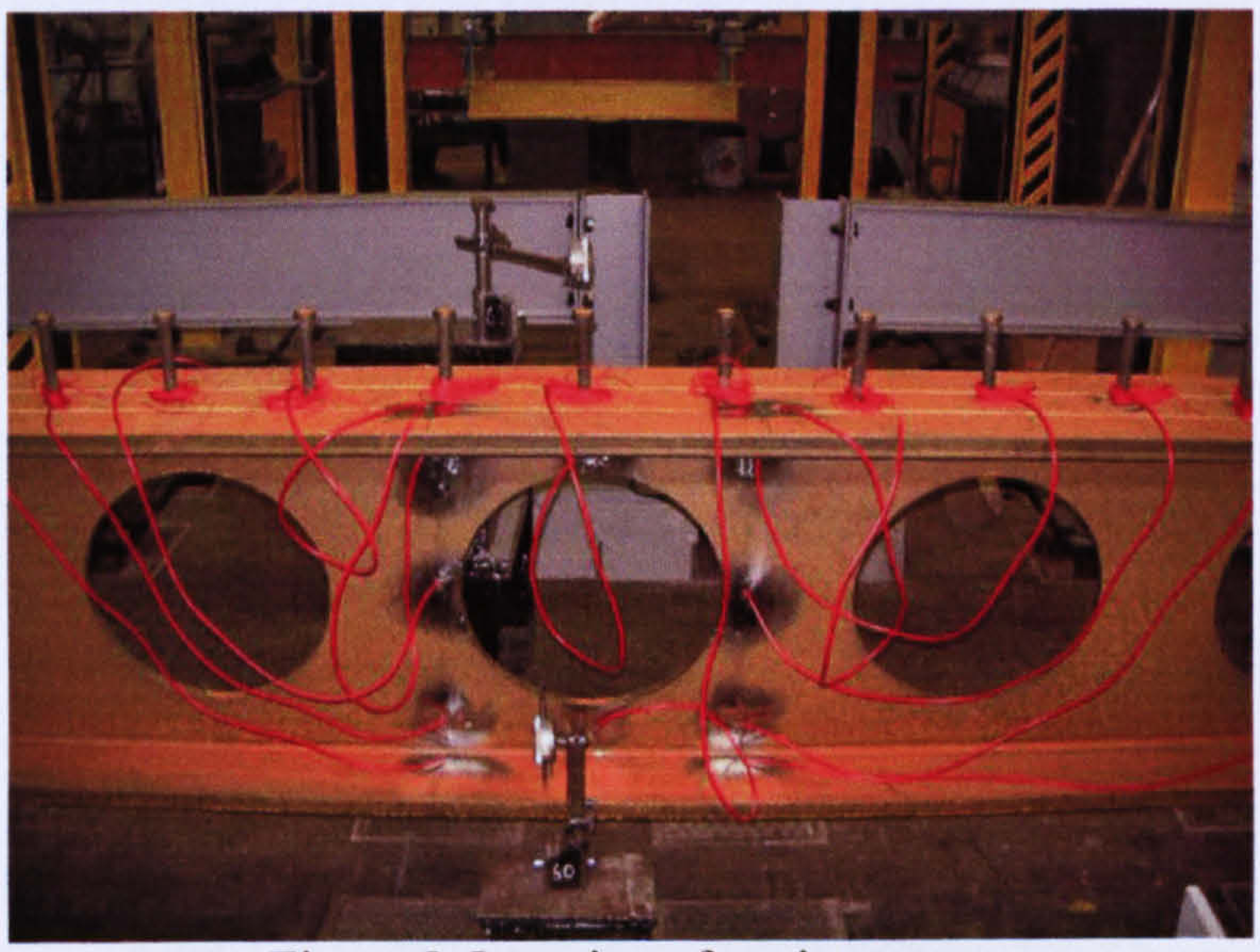

Figure 5: Location of strain gauges

3. TEST RESULTS

The results of the composite beam tests are given in Table 2 and the moment vs. deflection curves are given in Figure 6, where the increases in moment capacity and flexural stiffness of the composite beam compared to the bare steel UB are shown.

The elastic neutral axis of the composite beam is normally designed to lie closely to the interface between the steel and concrete. As the moment is increased, the concrete flange of the composite beam begins to reach the ultimate compressive stress and the position of width of a simply supported beam to be *L/4*. This was not the case in either of the composite beam specimens, where the effective width of CB-1 was found to be closer to *L/5* and *L/7* for CB-2. It would suggest that the effective width is governed not only by the span of the beam but also other parameters for this type of composite construction.

4. CONCLUSIONS

After conducting two long span composite beam tests, it has been shown that precast hollow-core slabs can be used compositely with steel beams. The composite beam has an increase in both flexural strength and stiffness. The only extra costs with these composite beams are the welding of shear studs on to the steel beam.

From the effective width calculations, it can be seen that the design of long span composite beams can be further utilised by considering the reduction in the effective width of the beam. The failure mode of the beams were found to be ductile and can be controlled by the shear stud spacing, in-situ concrete infill for the composite connection and the quantity of transverse bars. A further four composite beams are to be tested, with varying span, shear connection and slab depth.

ACKNOWLEDGEMENT

The authors would like to acknowledge the support provided by the EPSRC; Fabsec Ltd. and Watson Steel for supplying the steel specimens and Bison Concrete Products Ltd. for supplying the precast hollow-core slabs. Also appreciated is the skilled assistance provided by the technical staff in the School of Civil Engineering at Leeds University.

REFERENCES

[1] Darwin, D, *Design of Composite Beams with Web Openings.* Prog. Structural Engineering Materials, Vol. 2 (2), 2000, pp. 157-163.

[2] Lam, D (2002) *Composite Steel Beams with Precast Hollow-Core Slabs: Behaviour and Design.* Prog. Structural Engineering Materials, Vol. 4 (2), 2002, pp. 179-185.

[3] Lam, D, *Composite Steel Beams using Precast Concrete Hollow Core Floor Slabs.* PhD Thesis. Nottingham, UK: University of Nottingham, March 1998.

[4] Lam, D, Elliott, K S and Nethercot D A, *Parametric study on composite steel beams with precast hollow core floor slabs.* Journal of Constructional Steel Research, Vol. 54 (2), 2000, pp. 283-304.

[5] SCI Publication 100, *Design of Composite and Non-Composite Cellular Beams.* The Steel Construction Institute, UK, 1990.

the neutral axis moves towards the steel web. When the stress of the slab reached approximately $0.67f_{cu}$, cracking and then spoiling of the concrete began and the ultimate strength of the section was then fully reached. As the moment is further increased, the load carried by the composite beam remains approximately constant and then crushing of the concrete slab occurred. The failure in tests CB-1 and 2 was due to the crushing of concrete in the hollow-core slabs.

Test specimen	Max. Load in Test (kN)	Deflection at Max. Load (mm)	Max. Mmt in Test (kNm)	Max. recorded slip (LHS)	Max. recorded slip (RHS)	Failure Mode
CB-1	400	85	2400	4.6	4.2	CC
CB-2	367	131	2200	4.5	3.7	CC

CC – concrete crushing

Table 2: Beam test results

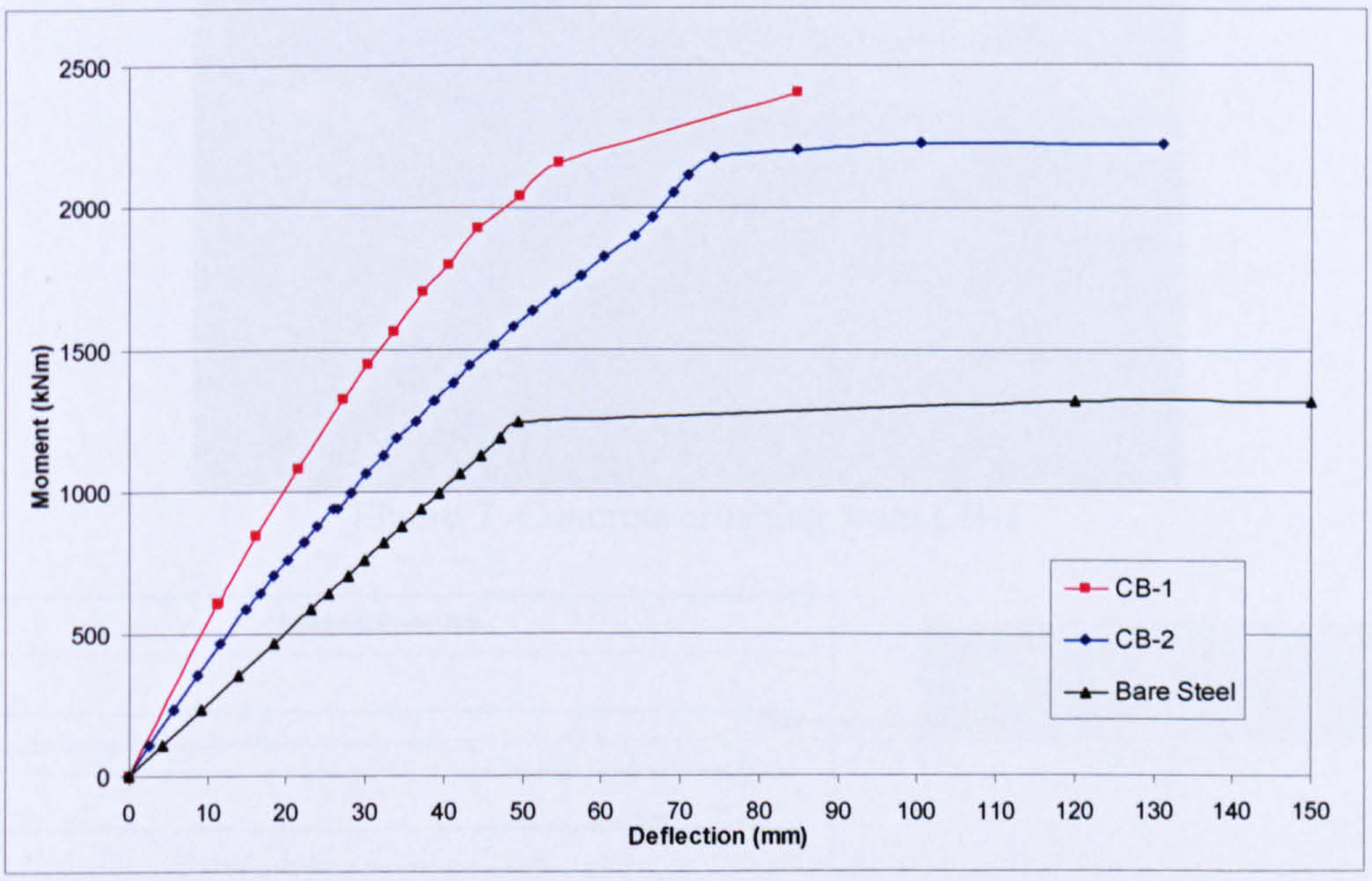

Figure 6: Moment vs. mid-span deflection curves

In test CB-1, the first cracks were observed at an applied moment of 1440kNm. This moment is about 0.58 times the ultimate moment capacity of the composite beam and may be taken as working load. The cracking caused the neutral axis to move downwards into the web of the steel beam (Figure 8), which resulted in further cracking in the precast slab. The deformation of the beam remained linear up to 1500kNm, when tensile cracks were observed on the underside of the hollow-core slabs. At the applied moment of 2040kNm, excessive cracking in the concrete slabs around the mid-span region of the test specimen was seen. Sudden failure occurred at a moment of 2280kNm, this was due to crushing of concrete around the shear studs in the mid-span region (Figure 7).

In test CB-2, hairline cracks between the in-situ concrete and precast slabs were observed before testing was started. The deformation was linear up to 900kNm, where further cracks between the in-situ concrete and precast slabs were observed. The reduced shear connection caused the neutral axis to be in the steel beam, indicating a reduced effective width of the concrete slab. The position of the neutral axis moved from 90mm to 190mm below the steel/concrete interface (Figure 8), which suggest further reduction of the effective concrete section. At an ultimate moment of 2150kNm, which was 5% less than reached in test CB-1, crushing of the concrete in the mid-span region occurred and spoiling of concrete from the precast slab was observed. Due to the partial shear connection of CB-2, the beam was found to be more ductile under bending.

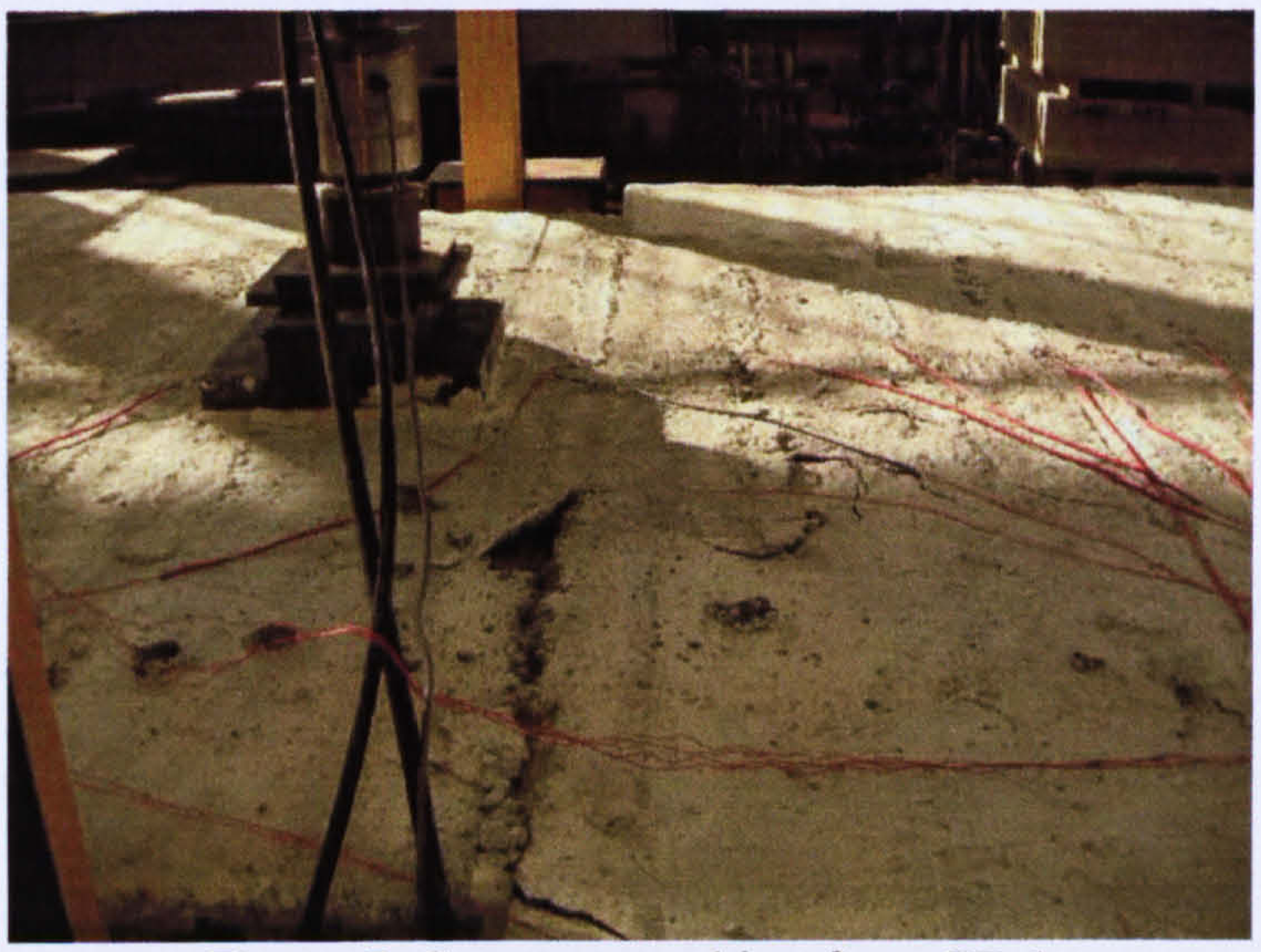

Figure 7: Concrete crushing from CB-1

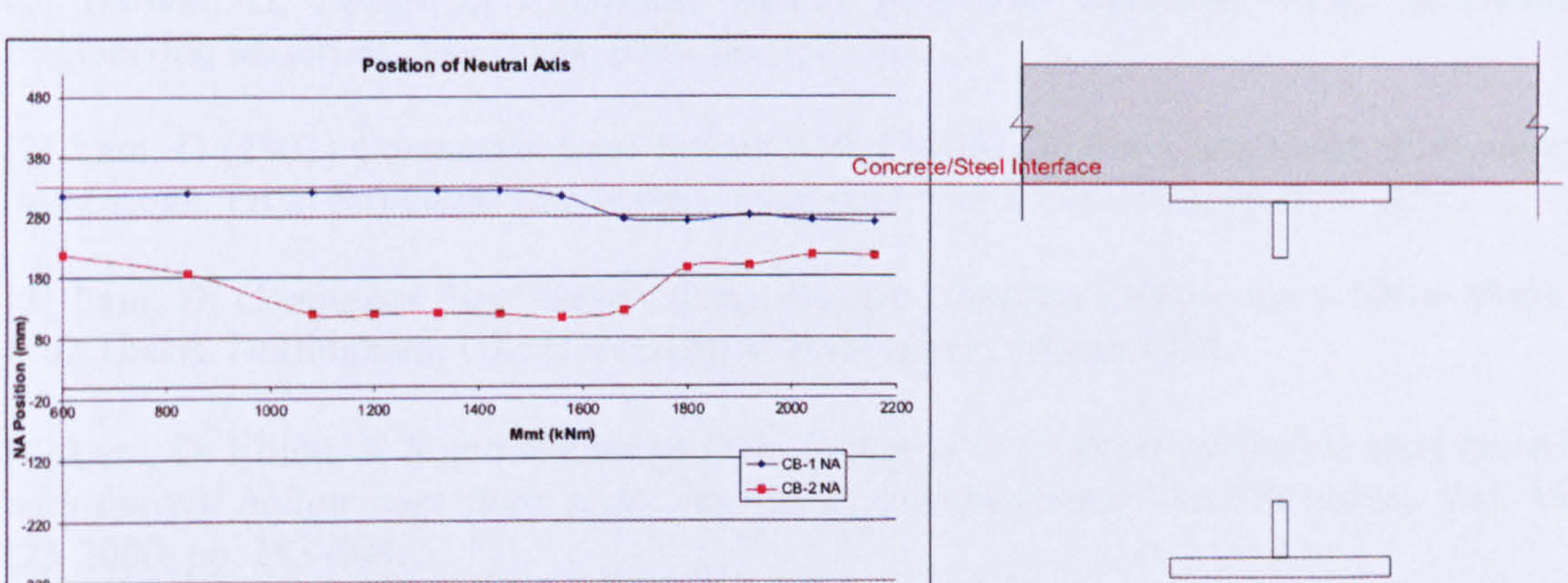

Figure 8: Position of neutral axis

Using the data obtained from the strain gauges placed on the top and bottom flanges and around the centre opening of the steel beam, the strain profile for the beam was found. From the calculations, the effective width of the composite specimen CB-1 and CB-2 was found to be 2600mm and 1700mm respectively. Current design codes take the effective